Catalytic Partial Oxidation of Pyrolysis Oils

A THESIS
SUBMITTED TO THE FACULTY OF THE GRADUATE SCHOOL
OF THE UNIVERSITY OF MINNESOTA
BY

David Carl Rennard

IN PARTIAL FULFILLMENT OF THE REQUIREMENTS
FOR THE DEGREE OF
Doctor of Philosophy

Regents Professor Lanny D. Schmidt, Advisor

August, 2009

Acknowledgements

This work would not have been possible without the direct and indirect contributions of many people. First and foremost, I would like to thank my advisor, Professor Schmidt, for his support and leadership. In addition to his input in all facets of this work, his ability to maintain a sense of the bigger picture and how research can find a niche has been enormously inspirational.

I could not have contemplated a PhD without the inspiration and instruction of my teachers. I'd like to thank all of them at the University of Minnesota, Harvard, Central, Lewis and Clark, and Harrison.

I am very grateful to the people who sponsored this research. Thanks especially to 3M for awarding me a Fellowship, and to the Institute for Renewable Energy and the Environment at the University of Minnesota, the National Renewable Energy Laboratory, the Department of Energy, and the Corn Growers Association of Minnesota. Thank you to the publishers of my papers, the American Chemical Society and Wiley-VCH, who have allowed me to reprint sections in chapters 2, 3, and 4.

I'd also like to thank all past members of the Schmidt Group for building up a knowledge base and for constructing and maintaining much of the experimental equipment used in this work. In particular, I am indebted to Bradon Dreyer for always finding time to talk through an experimental issue or show me how to fix a problem, to Paul Dauenhauer for guidance in choosing an experimental path of my own, to Nick Degenstein for teaching me how to utilize hardware to conduct experimental research, and to Greg Panuccio and James Salge for helping me with my first project. I'd like to express my gratitude to Raimund Horn for teaching me how to think outside of the box and find new experimental approaches to understand a phenomenon. Thanks also to Anders Bitsch-Larsen for reminding me that experiments can have a mind of their own, and Ken Williams for inspiring me to pave my own way in my research.

I am also deeply indebted to current members of the group, and would like to thank Brian

Michael for many enlightening discussions as well as for sharing an astounding knowledge of chemical engineering and experimentation, and Josh Colby for broadening my understanding of complex phenomena. I am also especially grateful to the coauthors of my published work, Jacob Kruger and Sarah Tupy, who helped me develop and trouble-shoot ideas and gather data, without which this thesis would have been impossible. Thanks also to Mark Huberty, Jason Walker, David Nare, Christine Balonek, Reetam Chakrabarti, Hui Sun, and Michael Skinner for making the lab in Amundson Hall an enjoyable place to work. I would also like to thank Wieslaw Suisinski for his help with the fast photography experiments and Professor Caretta for his tutelage and lively discussions.

Thanks to all of my friends in Minneapolis who have taught me so much and kept me entertained and relatively sane for the past four years. And to my family, who have made vacations worthwhile, and who have taught me so much and kept me entertained for my whole life.

I'd especially like to thank Kate Williams for putting up with me while I earned my PhD. My gratitude for her support and companionship cannot be adequately expressed here.

Dedication

This work is dedicated to my Dad, for teaching me to love science, and to my Mom, who has always been a paragon for her ability to keep everything in perspective.

ABSTRACT

The industrial revolution brought about an energy intensive society heavily dependent on fossil fuels. As western society begins to understand the ramifications of fossil fuel dependence, including energy security issues, global warming, and cost considerations, other countries are industrializing. The rapid consumption of fossil fuels is causing governments to question whether other energy sources might be more sustainably developed, resulting in energy independence and reduced emissions.

Many renewable resources can be developed to offset electricity use, but liquid fuels require another metric. Fuels are energy dense and portable, driving remote power applications including the transportation industry. Liquid carbon-based fuels are the most concentrated conventional energy carrier, and biomass is the only renewable source of fixed carbon.

However, biomass is also a diffuse resource that requires significant chemical processing before it can be used as a liquid fuel in existing infrastructure. One vector for upgrading biomass to liquid fuels involves a two step process. First, biomass undergoes fast pyrolysis, rapid heating in the absence of oxygen that depolymerizes lignocellulose, resulting in high yields of a liquid called pyrolysis oil. This oil has higher energy density than raw biomass, and can be transported to a central facility for further chemical treatment. Second, the bio oil is upgraded to biofuels.

Advances in the production of bio oil have continued for thirty years, resulting in commercial application of the technology. However, bio oil upgrading is still in the research phases. One promising route is the conversion of pyrolysis oil to synthesis gas, a mixture of CO and H_2. Synthesis gas is used industrially as C_1 building blocks in the refining industry. Syngas can be purified to H_2 to be utilized in hydrocracking or ammonia production. It can be converted to liquid fuels such as alkanes via the Fischer-Tropsch process utilizing Fe based catalysts, or methanol over a CuZnO catalyst, or dimethyl ether.

Industrially, syngas is produced by steam reforming over Ni, a high temperature process which has residence times on the order of $\tau = 1$ second. Pyrolysis oil cannot be vaporized, and low heat rates result in the production of char. As such, large quantities of steam are required to process pyrolysis oils to syngas, requiring attendant heat loads and energy costs. However, syngas can also be produced by partial oxidation, an exothermic process which releases heat

and, in the presence of a catalyst, occurs on the order of τ = 1 millisecond. Catalytic partial oxidation (CPO) has high heat rates which typically avoid the production of char.

This thesis explores the CPO of pyrolysis oils to syngas and chemicals. First, an exploration of model compounds and their chemistries under CPO conditions is considered. Then CPO experiments of raw pyrolysis oils are detailed. Finally, plans for future development in this field are discussed.

In Chapter 2, organic acids such as propionic acid and lactic acid are oxidized to syngas over Pt catalysts. Equilibrium production of syngas can be achieved over Rh-Ce catalysts; alternatively mechanistic evidence is derived using Pt catalysts in a fuel rich mixture. These experiments show that organic acids, present in pyrolysis oils up to 25%, can undergo CPO to syngas or for the production of chemicals. As the fossil fuels industry also provides organic chemicals such as monomers for plastics, the possibility of deriving such species from pyrolysis oils allows for a greater application of the CPO of biomass. However, chemical production is highly dependent on the originating molecular species. As bio oil comprises up to 400 chemicals, it is essential to understand how difficult it would be to develop a pure product stream.

Chapter 3 continues the experimentation from Chapter 2, exploring the CPO of another organic functionality: the ester group. These experiments demonstrate that equilibrium syngas production is possible for esters as well as acids in autothermal operation with contact times as low as τ = 10 ms over Rh-based catalysts. Conversion for these experiments and those with organic acids is >98 %, demonstrating the high reactivity of oxygenated compounds on noble metal catalysts. Under CPO conditions, esters decompose in a predictable manner: over Pt and with high fuel to oxygen, non-equilibrium products show a similarity to those from related acids. A mechanism is proposed in which ethyl esters thermally decompose to ethylene and an acid, which decarbonylates homogeneously, driven by heat produced at the catalyst surface.

Since bio oil cannot be vaporized, the successful prevaporization experiments detailed in Chapters 2 and 3 was exchanged for reactive flash volatilization. Chapter 4 details the catalytic partial oxidation of glycerol without preheat: droplets of glycerol are sprayed directly onto the top of the catalyst bed, where they react autothermally with contact times on the order of $\tau \approx 30$ ms. The reactive flash volatilization of glycerol results in equilibrium syngas production over Rh-Ce catalysts. In addition, water can be added to the liquid glycerol, resulting in true autothermal reforming. This highly efficient process can increase H_2 yields and alter the H_2 to CO ratio, allowing for flexibility in syngas quality depending on the purpose.

Mechanistic conclusions can also be drawn from the decomposition products of glycerol under CPO conditions. Gas phase experiments identify acetaldehyde, acrolein, and hydroxyacetone as the main glycerol thermal decomposition products. These experiments are described by theoretical modeling. The presence of another dominant species in the catalytic partial oxidation of glycerol indicates the relevance of surface chemistry: dehydrogenation of alcohols can lead to stable intermediate products which are observable at the reactor effluent. A mechanism is proposed to explain these products consistent with previous experiments in the catalytic partial oxidation of oxygenates.

As glycerol is a byproduct of biodiesel transesterification, the conversion of glycerol to syngas and syngas to methanol - a reactant in biodiesel esterification - is industrially relevant aside from bio oil considerations. The stability of the reactor design and noble metal catalyst - Rh is an expensive metal - is essential to plans for industrial application. Chapter 5 details the results of a time on stream experiment, in which optimal syngas conditions are chosen. Although conversion is 100% for 450 hours, these experiments demonstrate the deactivation of the catalyst over time. Deactivation is exhibited by decreases in H_2 and CO_2 production accompanied by a steady increase in CO and temperature. These results are explained as a loss of water-gas shift equilibration. SEM images suggest catalyst sintering may play a role; EDS indicates the presence of impurities on the catalyst. In addition, the instability of quartz in the reactor is demonstrated by etching, resulting in a hole in the reactor tube at the end of the experiment. These results suggest prevaporization may be desirable in this application, and that quartz is not a suitable material for the reactive flash volatilization of oxygenated fuels.

In Chapter 6, pyrolysis oil samples from three sources - poplar, pine, and hardwoods - are explored in the context of catalytic partial oxidation. Lessons derived from the tests with model compounds are applied to reactor design, resulting in the reactive flash vaporization of bio oils. Syngas is successfully produced, though deactivation due to coke and ash deposition keeps H_2 below equlibrium. Coke formation is observed on the reactor walls, but is avoided between the fuel injection site and catalyst by increasing the proximity of these in the reactor design. Low temperatures are maintained in the fuel delivery system utilizing a water-jacketed nebulizer, which allows for the delivery of bio oil into a furnace at 800 ^{o}C. The addition of methane to the reactor environment enhances reactor performance, likely by promoting transport of gaseous fuel to the catalyst to sustain reaction. In several configurations, the catalytic partial oxidation of bio oil to syngas is achieved autothermally with contact times of $\tau = 30$ ms.

Contents

Acknowledgements **i**

Dedication **iii**

Abstract **iv**

List of Tables **xii**

List of Figures **xiii**

1 Introduction **1**

1.1 Summary 1

1.2 Motivation 2

1.2.1 Energy Security 2

1.2.2 Increasing Energy Demand 3

1.2.3 Climate Change and Intergovernmental Cooperation 4

1.2.4 Role of the Government 5

1.3 Biomass Pyrolysis Oil 6

1.4 Gasification 9

1.5 Catalytic Partial Oxidation 10

2 CPO of Organic Acids **15**

2.1 Summary 15

2.2 Introduction 16

2.2.1 Chemistry of C_1 Products 17

2.2.2 Non-Equilibrium Acid Chemistry 18
2.3 Experimental 22
2.4 Results 26
2.5 Discussion 29
2.5.1 Equilibrium Products and Surface Chemistry 29
2.5.2 Non-Equilibrium Products and Homogeneous Chemistry 31
2.6 Conclusions 35

3 CPO of Ethyl Esters **36**
3.1 Summary 36
3.2 Introduction 37
3.2.1 Background on Esters 37
3.2.2 Chemical Uses 41
3.2.3 Equilibrium Products of CPO of Ethyl Esters 42
3.2.4 Non-Equilibrium Products 45
3.3 Experimental 50
3.4 Results 50
3.4.1 Equilibrium Products from Esters: CO, CO_2, H_2, H_2O, CH_4 52
3.4.2 Non-Equilibrium Products: Ethylene, Acetylene, Acetaldehyde 52
3.4.3 Temperature Controlled Uncoated Foam Experiments 57
3.5 Discussion 57
3.5.1 Equilibrium Products and Surface Chemistry 59
3.5.2 Non-Equilibrium Products and Homogeneous Chemistry 60
3.6 Conclusions 64

4 CPO of Glycerol **65**
4.1 Summary 65
4.2 Introduction 66
4.2.1 Catalytic Partial Oxidation 67
4.2.2 Synthesis Gas 68
4.2.3 Non-Equilibrium Products 70
4.3 Experimental 71
4.3.1 Catalyst Preparation 71

4.3.2 Reactor Design and Conditions . . . 71
4.3.3 Isothermal Decomposition over Uncoated Foams . . . 74
4.3.4 Product Analysis . . . 74
4.3.5 Data Analysis and Equilibrium Calculation . . . 76
4.4 Results . . . 76
4.4.1 Rhodium Ceria . . . 76
4.4.2 Platinum . . . 80
4.5 Discussion . . . 81
4.5.1 Syngas Production and Steam Reforming . . . 81
4.5.2 Thermal Decomposition and Non-Equilibrium Chemicals . . . 83
4.6 Conclusion . . . 85

5 CPO of Glycerol: Time On Stream 88
5.1 Summary . . . 88
5.2 Introduction . . . 88
5.3 Experimental . . . 90
5.4 Data Analysis . . . 95
5.4.1 Transient Analysis via Accelerated Aging Experiment . . . 95
5.4.2 Aging Experiment . . . 98
5.5 Discussion . . . 99
5.5.1 Thermal Deactivation: Sintering . . . 103
5.5.2 Poisoning . . . 105
5.5.3 System Management . . . 108
5.5.4 Effect of Diluent on Reactive Flash Volatilization . . . 108
5.6 Conclusion . . . 109

6 CPO of Pyrolysis Oil 110
6.1 Summary . . . 110
6.2 Introduction . . . 111
6.2.1 Catalytic Gasification . . . 111
6.3 Experimental . . . 114
6.4 Data Analysis . . . 116
6.4.1 Autothermal Operation . . . 119

6.4.2 Thermodynamic Calculations 122
6.5 Discussion 126
6.6 Conclusions 130

7 Future Work **131**
7.1 Fast Photography of CPO of Liquid Fuels 131
7.2 Spatially Resolved CPO of Pyrolysis Oil Model Compounds 133
7.3 Investigation of the Effect of Inorganic Impurities on Noble Metal Catalysts in a CPO Reactor 137
7.4 Analysis of Chemistry of CPO Model Compounds 142
7.4.1 Organic Functional Groups 142
7.4.2 Anisole and Phenol: Effect of Aromatics 142

References **144**

Appendix A. Glossary and Acronyms **163**
A.1 Glossary 163
A.2 Acronyms 167

Appendix B. Safety Protocol for the Time on Stream Apparatus **169**
B.1 Summary 169
B.2 Introduction 169
B.3 Materials Considerations 170
B.4 Regular Precaution and Typical Dangers 171
B.5 Safety Mechanisms 172
B.5.1 Software Safety 172
B.5.2 Hardware Safety 173
B.6 Conceived Errors and Safety Scenarios 174
B.6.1 Catalyst Deactivates: CPO Unsteady 174
B.6.2 Catalyst Deactivates: Catalyst Support Disintegrates 174
B.6.3 Reactor Explosion 175
B.6.4 Power Outage 176
B.7 Catastrophic Failure 177

B.7.1 CO Poisoning 177
B.7.2 Dangerous Explosion 177
B.7.3 Chemical Hazard 177
B.8 False Positive 178
B.9 Standard Operating Procedure 178
B.9.1 Fuel Maintenance 178
B.9.2 Gas Maintenance 178

Appendix C. Deactivation Pictures **180**

List of Tables

1.1 Typical properties of wood pyrolysis bio-oil and heavy fuel oil[1, 2] 8
4.1 Species expected from the CPO of glycerol 75
5.1 Conditions for the CPO of glycerol in the time-on stream reactor, selected for maximum stability and ease of analyis 93
5.2 Impurities in USP glycerol batch as determined by the manufacturer 106
6.1 A survey of the major contents of bio oil, roughly listed according to the water-soluble cellulosic portion and the water insoluble lignin derived fraction. 112
6.2 Elemental analysis performed at NREL on the pyrolysis oils yielded these results for defining a “mole” of each oil. 116
6.3 Experimental and theoretical yields from the CPO of three different bio oils in various reactor configurations and under various conditions 125
7.1 Inorganic impurities introduced to noble metal catalyst via reactive flash volatilization in a qualitative study. 139
A.1 Acronyms 167

List of Figures

1.1 Hubbert's Peak: a Gaussian Fit for Oil Consumption 3
1.2 Ceramic foam monoliths coated with noble metals. Three pore sizes are depicted: 80 ppi, 45 ppi, and 20 ppi. The 45 ppi foam also has a hole bored into it to accommodate a capillary for spatial sampling. 11
1.3 Catalytic Autothermal Reforming is 1000 times faster than steam reforming, allowing for downscaling of reactors. 11
1.4 Catalytic Partial Oxidation is typically autothermal, operating at temperatures over 600 ^{o}C, which causes the catalyst to incandesce. 12
2.1 Sketch of acetic acid, propionic acid, and lactic acid 17
2.2 Pyrolysis of lactic acid decarbonylates via 3 membered ring. 20
2.3 Proposed two-step mechanism for decarbonylation of lactic acid via the keto-enol tautomerization. 20
2.4 The lactic acid dimer thermally decarbonylates 21
2.5 α-keto acid thermal decarboxylation. 22
2.6 Reactor used for acid and ester catalytic partial oxidation experiments with fuel prevaporization zone. 24
2.7 Conversion and Temperature data from CPO of propionic acid and lactic acid. . 27
2.8 Selectivity to major projects from the CPO of propionic acid and lactic acid . . 28
2.9 Adsorbed acids form carboxylate species. The first step in adsorption breaks the O–H bond of the acidic hydrogen atom. 31
2.10 4-center mechanism for decarboxylation of formic acid. 32
2.11 4-center mechanism for the dehydration of acetic acid 32
2.12 5-center mechanism for dehydration of Propionic Acid. 33
2.13 Possible 6-center mechanism for decarboxylation of Propionic Acid 33

2.14 Proposed mechanism for the decomposition of lactic acid and propionic acid involving decarbonylation and dehydration to observed species. 34
3.1 Sketch of ethyl propionate and ethyl lactate, which differ by a hydroxyl group (-OH) on the α' carbon. 37
3.2 Cellulose is an oxygenated polymer with C–O–C–O groups similar to esters. From U. Tschirner presentation, September 2006. 38
3.3 Lignin is an aromatic polymer with oxygenated bridges. From U. Tschirner presentation, September 2006. 39
3.4 Adsorption conformations of the carbonyl (C=O) group. The η^1 conformation adsorbs via free electrons on the O; the η^2 via the π bond. 43
3.5 6-Membered metallocycle of adsorbed ethyl lactate 44
3.6 6-membered ring decomposition of esters. 47
3.7 Pyrolysis of β'-OH esters. 48
3.8 5-Membered ring transition, followed by 3 membered ring, for pyrolysis of a methyl ester. 48
3.9 Conventional 6 membered intermediate for pyrolysis of ethyl lactate producing lactic acid and ethylene. 49
3.10 Conversion and temperature data from the CPO of ethyl propionate and ethyl lactate over Rh and Pt catalysts 51
3.11 Selectivity to syngas species from the CPO of ethy lactate and ethyl propionate over Rh and Pt catalysts 53
3.12 Selectivity to combustion products from the CPO of ethyl lactate and ethyl propionate over Rh and Pt catalysts 54
3.13 Selectivity to methane from the CPO of ethyl lactate and ethyl propionate over Rh and Pt catalysts 55
3.14 Non-equilibrium products from the CPO of ethyl propionate and ethyl lactate over Rh and Pt catalysts 56
3.15 Experiments over uncoated monoliths suggest gas phase chemistry produces many of the non-equilibrium products in the thermal decomposition of ethyl lactate and ethyl propionate. 58
3.16 Proposed mechanism for the decomposition of ethyl lactate and ethyl propionate under CPO conditions 61

3.17 Comparison of ethylene and acetaldehyde production from ethyl lactate and ethyl propionate over Rh-Ce shows that ethyl propionate produces twice the ethylene of ethyl lactate, while ethyl lactate produces acetaldehyde instead. . . 62
4.1 Photo & schematic of catalytic partial oxidation of glycerol 69
4.2 Reactor setup for the Reactive Flash Volatilization of liquid fuels using a nebulizer and without preheat 73
4.3 Products, conversion, and temperature data from the CPO of glycerol over Rh-Ce WC catalysts 78
4.4 Product species from autothermal reforming of glycerol experiments over Rh-Ce catalysts 79
4.5 Conversion, temperature, and product species from the CPO of glycerol over Pt, showing high selectivity to non-equilibrium species 82
4.6 Gas phase dehydration mechanisms of glycerol predict acetaldehyde, acrolein, and acetol 86
4.7 Proposed mechanism for the dehydrogenation of poly-ols. Glycerol or perhaps hydroxyacetone adsorbs in the η^1 conformation. The molecule dehydrogenates on the catalyst and desorbs as an aldehyde or ketone. 87
5.1 Configuration of the reactor system for the time-on-stream experiment. All gas flows, temperatures (T) and pressure (P) are monitored and controlled by the LabView interace. 91
5.2 Design of the CPO reactor for sturdy, long term use. Quartz-stainless unions and seals are chosen to minimize materials issues over the course of the experiment. 94
5.3 Temperature and selectivity to H_2 data from a 375 hour glycerol CPO test show deactivation of the catalyst. Flags indicate transient experiments. 96
5.4 Selectivity to carbon species from the 375 hour time on stream CPO test of glycerol. CO increases steadily over the course of the experiment. 97
5.5 Temperature and selectivity to H_2 from the 450 hour time on stream experiment. Deactivation and loss of H_2 production occur in the first 100 hours. Flags indicate thermal events. 100
5.6 Selectivity to carbon species from the 450 hour time on stream CPO of glycerol experiment 101

5.7 Molar flowrates of CO, CO_2 and H_2 show the product relationship in the decay of catalytic activity. Adiabatic equilibrium calculations are depicted at 490 hours. 102
5.8 SEM images of fresh and used catalyst from the 450 hour experiment. The unused catalyst displays high surface area films of Rh and Ce. The used catalyst shows boulders with crystallites, suggesting sintering and a loss of active metal surface sites. 104
5.9 Red ash was deposited upstream of the reactors for both the 375 hr (left) and 450 hr (right) experiments. Etching is also apparent in the quartz swirls below the ash deposit for both reactors. 105
5.10 Deactivated catalysts used in the CPO of glycerol: unused, used for over 375 hours, and used for 450 hours. 107
6.1 Reactor setup for several of the CPO of bio oil experiments. The furnace is replaced by insulation for autothermal runs. 115
6.2 Data from the CPO of pine pyrolysis oil inside a furnace 118
6.3 Data from the CPO of pine oil with the addition of water for reforming and elimination of coke 118
6.4 Catalytic partial oxidation of 80 wt% hardwoods, 20 wt% methanol in a furnace with 700 ^{o}C preheat 119
6.5 Autothermal CPO of a 50-50 wt% solution of methanol and poplar bio oil . . . 120
6.6 Autothermal Partial Oxidation of a 50-50 wt% poplar oil-methanol solution with 0.1 SLPM CH_4 addition 121
6.7 Reactor configuration to test the need to water-cool the nebulizer with a jacketed system. Bio oil is sprayed upwards; the nebulizer spraying from a pool of water. 122
6.8 Autothermal Partial Oxidation of a 50-50 wt% poplar oil-methanol solution with 0.1 SLPM CH_4 123
6.9 Dry effluent concentrations from the catalytic partial oxidation of pine oil with 0.15 SLPM methane (79% pyrolysis liquid by carbon content) 124
6.10 Autothermal catalytic partial oxidation of pine pyrolysis oil with a methane cofeed (74% oil, 26% CH_4 by C). Greater methane addition stabilizes the reactor, but the improvement diminishes with CH_4 increase. GHSV $\approx$ 27000 hr^{-1}, $\tau \approx$ 39 ms. 124

7.1 Setup for fast photography experiments with liquid fuels using temperature control. 132
7.2 A droplet of glycerol introduced to an 80 ppi Rh-Ce catalyst at >500 ^{o}C film-boils, causing it to skitter across the foam over 44 ms 134
7.3 A droplet of poplar pyrolysis oil exhibits Leidenfrost Film boiling and the self-cleaning nature of the hot Rh-Ce surface. 135
7.4 Reactor setup for the spatial resolution of products and temperatures in the CPO of pyrolysis oil model compounds 138
7.5 Ash accumulates on top of the catalyst in the CPO of controlled ash doped ethanol as well as pyrolysis oil. 140
C.1 Photo of catalyst foam monoliths that have lost mechanical stability 181
C.2 Photo of a completely coked reactor after the CPO of 50-50 wt% poplar pyrolysis oil and methanol, which ran autothermally for a short while before shutting down due to coke formation. 181
C.3 Photo of a coked Rh-Ce 20 ppi catalyst used in the CPO of pyrolysis oil with water addition. 182
C.4 Photo of a clean reactor area after the CPO of pine pyrolysis oil in a furnce . . 183
C.5 Ash accumulation from pyrolysis oil is apparent in this reactor. The pyrex annulus is used to insulate the jacketed nebulizer from the hot furnace, shown here from the CPO of 50 wt% pine pyrolysis oil, 50 wt% methanol. All of this ash is upstream of the catalyst, suggesting that this type of ash accumulation can be eliminated with reactor design. 184
C.6 Rh-Ce catalyst used in the CPO of 50 wt% poplar pyrolysis oil with methanol shows the deposition of a glass due to introduced impurities. 185
C.7 Photo of molten FiberFrax deposited on the catalyst in an exothermic burnoff of coke deposited during bio oil CPO 185
C.8 Close-up of the quartz etching in the reactor from the 450 hour time on stream test of the RFV of glycerol. Red ash deposit is visible above the smoky bubbling of the reactor. 186

Chapter 1

Introduction

1.1 Summary

As a fundamental asset to the economy and modern society, energy is an essential commodity. With increases in population and technology diffusion, management of the energy resources of the world is becoming an ever greater challenge. Fossil fuel dependence brings a barrage of adverse consequences: burning stored fixed carbon emits greenhouse gases linked to global warming; fossil fuels are not distributed equitably or with any consideration to geopolitical borders, resulting in energy security issues for dependent states; and fossil fuels are inherently a fixed resource - as they are depleted, basic laws of supply and demand will explode prices. For these reasons, governments are taking an active role in identifying alternatives to fossil fuels.

Biomass, the only other source of fixed carbon, is high in oxygen content, diffuse, and low density. Upgrading biomass to liquid fuels is possible, but economic considerations require either new technologies or processes that operate on different scales than traditional chemical conversion processes. One route for biomass to fuels is through a two step process: local densification via pyrolysis to an energy containing liquid which can be more readily transported, followed by scaled conversion of this pyrolysis liquid to fuels and chemicals. While the first step has been thoroughly researched for thirty years, upgrading pyrolysis oils is still a nascent field.

Pyrolysis oils can be upgraded by catalytic partial oxidation. CPO has been applied to many constituents in pyrolysis oils and has found success in every attempt at converting fuels into synthesis gas. This gas can be burned, used as a H_2 source, or converted into synthetic fuels

using well established technologies.

1.2 Motivation

Few issues transcend the boundaries between national security, climate change, and economic policy. Energy is such an issue. Our society depends on energy to make the materials we use, to grow the foods we eat, to drive the businesses that provide for us.

1.2.1 Energy Security

Because our economies and homes are powered by energy, we become highly dependent on our fuel source. As President Bush said in his 2006 State of the Union Address:

> Keeping America competitive requires affordable energy. And here we have a serious problem: America is addicted to oil, which is often imported from unstable parts of the world. The best way to break this addiction is through technology. [3]

Recent political events such as the War on Terror and the War in Iraq have underscored how energy can be a geopolitical tool, highly related to national security. The merging of the two concepts is made vivid by the term "energy security." Retaining energy supplies or preventing the enemy from utilizing them is a frequent military objective.

> That terrorists and their ilk are interested in attacking energy-related targets is hard to dispute. A review of data compiled by the National Memorial Institute for the Prevention of Terrorism, or MIPT, indicates that terrorist groups mounted at least 330 attacks against oil and gas facilities around the world during the period 1990-2005. Most of these incidents occurred in eight countries: Iraq, Russia, Columbia, Ecuador, Philippines, Turkey, Pakistan and Algeria. Since the American invasion of Iraq insurgents have systematically attacked the country's oil export terminal at Basra, various oil pipelines traversing Iraq, and the electrical power grid. These actions have been a serious complicating factor in restoring Iraqi oil production to their pre-war levels.[4]

Natural gas plants and oil lines are military concerns because of the scarcity of supply and the reliance of society on these forms of energy. However, the powerful forces of ever increasing demand and fixed supply require that oil and gas become yet more precious.

1.2.2 Increasing Energy Demand

In 1956, Marion King Hubbert, a geophysicist, modeled the consumption of a nonrenewable resource to produce the famous Hubbert Peak. The basic premise of Hubbert's calculation is that demand increases exponentially, consuming a fixed resource. Production initially maintains pace with demand until new discoveries are outstripped by demand growth. At this point, demand continues to increase while reserves deplete, no longer able to keep pace.

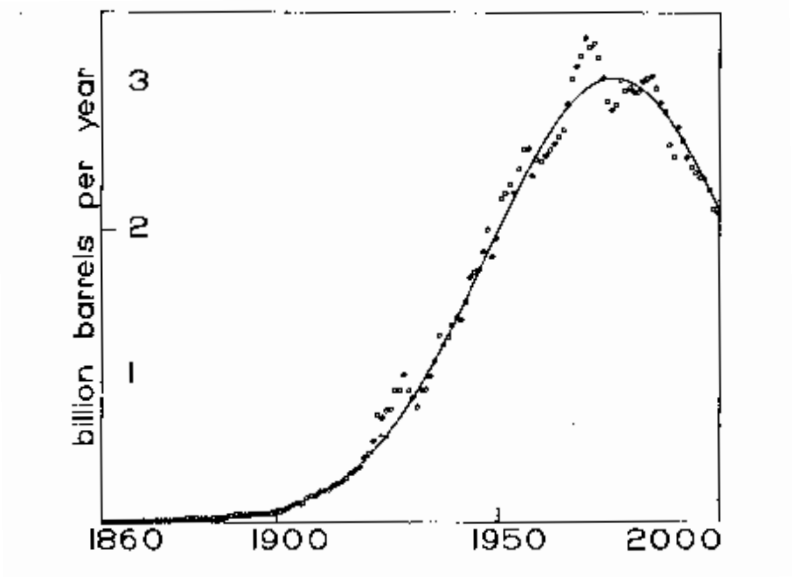

Figure 1.1: A Hubbert's Peak fit to a Gaussian.[5] The dots show annual production of U. S. crude oil, including Alaska and off-shore sources.

This curve has been applied to the US oil deposits with striking precision (see Figure 1.1), but the complications in obtaining data for world supplies make such a precise application difficult. Recent modeling suggests the peak production should occur between 2010 and 2025.[6] Peak oil production will eventually occur as demand outstrips supply for the world's oil deposits. At this point, the price of a barrel of oil will increase dramatically with demand.

In May of 2009, the Energy Information Administration released the International Energy Outlook, projecting global consumption of liquid fuels to increase from 2006 to 2030 by 25%.[7] During the same period, reliance on unconventional fuels is predicted to increase from 3.8% to 12.6%. By contrast, OPEC produced conventional fuels, which provided 40% of global liquid fuels in 2006, are projected to still provide 40% of global fuel demand in 2030.

The message of these data is clear: based on the assumptions of the EIA study, energy security will still be an issue in 20 years, and the source of liquid fuels will very slowly shift to alternatives. These alternatives comprise extra heavy oil, oil sands, shale oil, coal or gas to liquids, and biofuels. The study indicates that high oil prices and government mandates will likely play a large role in shaping these numbers:

> Although production of unconventional petroleum liquids, such as Canadas oil sands and Venezuelas extra-heavy oil, is limited somewhat by environmental concerns and investment restrictions, production of unconventional nonpetroleum liquids, such as biofuels, coal-to-liquids (CTL), and gas-to-liquids (GTL), is spurred by sustained, relatively high prices both in the reference case and in the high oil price cases. Development of nonpetroleum liquids production also will depend on country-specific programs or mandates.[7]

Government mandates may thus determine the energy portfolio in the coming years.

1.2.3 Climate Change and Intergovernmental Cooperation

Two months later, in July of 2009, the Group of Eight (G8) countries, comprising Canada, France, Germany, Italy, Japan, Russia, the United Kingdom, and the United States convened and adopted a document titled “Responsible leadership for a sustainable future.”[8] The leaders agreed on a need to decrease global emissions by 50% by 2050, adopting a goal of reduction by 80% or more for developed countries, in order to keep the global temperature rise below 2 ^{o}C above pre-industrial levels. To this end, G8 leaders agreed to push for more private and public funding for developing new renewable energy technology:

> The key role of major economies in driving innovation was stressed and Leaders launched a Global Partnership to further such efforts. There was agreement on substantially increasing public investments in R&D, with a view to doubling them

> by 2015. Underlining the role of the private sector and of international cooperation, Leaders committeed to remove barriers and create incentives to accelerate deployment, diffusion and transfer of low-carbon technologies.[8]

The G8 used this opportunity to set agenda items in advance of the meeting of the United Nations Framework Convention on Climate Change (UNFCCC) in Copenhagen in December of 2009. At this conference, the UNFCCC will attempt to draft the next stage after the Kyoto Protocol, which expires in 2012. The Kyoto Protocol was enacted to counter increases in global temperature due to the green house effect.

In 2007, the Intergovernmental Panel on Climate Change released its fourth "Assessment Report" on climate change.[9] The report found that greenhouse gases, notably CO_2, had increased in the atmosphere since the industrial revolution. It further concluded that human activity was the most likely reason for this increase and the associated increase in the average temperature of the earth: climate change is anthropogenic.

Greenhouse gases are predominantly the result of the use of fossil fuels. Since these fuels power modern society, contemporary culture has a pressing need for an alternative energy source. Renewable biofuels do not produce net CO_2 because they are part of the carbon cycle: crops grow by absorbing CO_2 from the atmosphere. Fuel crops can even sequester carbon by increasing topsoil, thus acting as a net carbon sink.[10]

The EIA study, the close ties to energy security, the efforts of intergovernmental organizations like the G8 and UN, and the threat of climate change underscore the importance of the role of government in approaching the energy crisis.

1.2.4 Role of the Government

In 1980, in response to the high prices of the second oil shock, President Carter won a major political victory by passing an energy package including $20 billion for federally subsidized synthetic fuel plants, to be followed by as much as $68 billion.[11] The Synthetic Fuels Corporation Act lasted five years; the corporation was disbanded during the Reagan administration when oil prices stabilized.[12]

Similarly, policy incentives led to enormous growth in the wind industry in California, followed by a dry period when the incentives were unavailable. These trends demonstrate the importance of a strong, clear signal for steady development.[13] In 2009, as tax credits for

hybrid vehicles set in 2006 are expiring,[14] the Cash for Clunkers (CARS) law is going into effect.[15]

With strong policy incentives that persist for a timeframe on par with intergovernmental objectives, progress can be made, resulting in a shift from fossil fuels to renewable fuels. This sort of policy would price the externality of CO_2 emissions into the cost of fuels, thus shifting behavior by causing consumers to evaluate their options. The Clean Air Act, which passed in the House of Representatives on May 21, 2009, attempts this by implementing a carbon standard: a cap and trade system that would operate through 2020.[16]

To achieve such decreases in carbon emissions will require new technology. In order to stimulate the development of renewables and clean energy technology, the federal stimulus package provides $1.2 billion in funding for research in these areas.[17]

This sort of combination of policy drivers will promote the development of renewable fuels. Through good policy and sound engineering, contemporary society can find alternatives to fossil fuels while maintaining our energy intensive standard of living. However, such development takes place in the laboratory - not in the office. As such, the rest of this thesis will focus on the research and development of novel renewable fuels technologies.

1.3 Biomass Pyrolysis Oil

The concerns detailed above about energy independence, carbon standard, global warming, and peak oil all indicate a need to find alternatives to petroleum to satisfy our fuel needs. However, the benefits derived from a hundred years of infrastructural investment are not the only reasons to consider alternatives that look very much like petroleum. Carbon-based fuels have exceptionally high energy density. As liquid fuels, they are easily stored and transferred from the refinery to the pump to the automobile. They are familiar and an entire fleet of vehicles in every country in the world already makes use of them. They are an entrenched technology and will not be easily replaced. In addition, alternatives put forward for automotive transportation often involve liquid carbon fuels: fuel cell cars can store hydrogen via liquid fuels, making use of an on-board reformer.[18, 19, 20, 21] Electric cars by themselves require long charging times, and as such, plug-in hybrid electrics appear to offer the best of both worlds.

For these reasons, an alternative source of carbon-based fuels is required. Biomass represents the only source of renewable fixed carbon. Estimates indicate that the US has enough

biomass to offset up to 30% of its petroleum consumption through the use of biomass without major changes to food production.[22]

However, converting biomass to liquid fuels is not trivial. Biomass is a distributed resource: it is land-intensive, has high oxygen and water content, and low energy density. Whereas petroleum refining benefits from an economy of scale because high energy petroleum can be shipped and pumped, the low density of hay bales and wood chips require some form of local densification before they can be upgraded on a large scale. For this reason, current biomass models are associated with smaller, village-sized refineries, such as ethanol plants. To reduce the costs of second-generation bio-fuels, alternative technologies are required that will allow biomass to benefit from economies of scale.

One such method of biomass densification is fast pyrolysis, which benefits from years of research and is an industrially demonstrated technology.[23, 24] Fast pyrolysis is a process in which solid particles of biomass are rapidly heated to form a complex liquid mixture, "bio-oil."[25] More specifically, liquids are maximized (≈80 wt% of the original dry wood) by heating biomass to around 500 ^{o}C with fast heating rates for around 1 second.[25] These residence times are a compromise between decomposing lignin, which requires long heating times, and avoiding secondary reactions. The process also produces char and gases which can be burned to provide the heat for the process. The liquid provides an energy-dense intermediate that could become a major biorefinery feedstock analogous to crude oil, as depicted in Table 1.1.

Pyrolysis liquids have higher energy density than biomass: they are still oxygenated and contain water, but they can be pumped or shipped more efficiently to be upgraded at a central facility, thereby benefiting from economy of scale.[26, 27] In addition, pyrolysis represents a chemical step that can be combined with ash removal: at less than 1%, pyrolysis oils contain much less ash than their original biomass source, the ash being removed with the heavy tars and solids during filtration. Pyrolysis oils vary greatly by feedstock and method of preparation and, as such, require further upgrading to convert them to usable fuels compatible with existing infrastructure. A single bio oil can contain over 400 species.[28]. Some of the major species are depicted in Table 6.1.

The next processing step would be to upgrade bio-oil to a stream of building-block chemicals (such as ethylene) or synthesis gas (H_2 + CO) for production of synthetic fuels such as ethanol, alkanes, or dimethyl ether.

Table 1.1: Typical properties of wood pyrolysis bio-oil and heavy fuel oil[1, 2]

Physical Property	Bio-oil	Heavy fuel oil
Moisture content (wt%)	15-30	0.1
pH	2.5	-
Specific gravity	1.2	0.94
Elemental Composition (wt%)		
C	54-58	85
H	5.5-7.0	11
O	35-40	1.0
N	0-0.2	0.3
Ash	0-0.2	0.1
HHV (MJ/kg)	16-19	40
Viscosity (at 50 ^{o}C) (cP)	40-100	180
Solids (wt%)	0.2-1	1
Distillation residue (wt%)	up to 50	1

Several options can be considered for further upgrading pyrolysis oils. The oils can be co-introduced into conventional petroleum feeds; they can be separated and used for their chemical content, or they can be upgraded directly.

1.4 Gasification

Perhaps the most versatile mechanism for upgrading pyrolysis oils is gasification, the conversion to synthesis gas (syngas). This syngas can then be converted to fuel alkanes or alcohols, eg/ by the Fisher Tropsch Synthesis, or it can be converted to a carbon neutral H_2 source for use in other refining steps or the production of ammonia. As such, the two-step process of local pyrolysis and either local or on-site gasification provide a novel carbon and hydrogen vector for use in refining and the production of second generation biofuels.

Gasification technology is over a hundred years old. Autothermal reforming (ATR) of coal was used to produce "town gas" to light streets. Research into gasification of coal is almost as old, though these technologies are being rediscovered to meet high pollution standards and increase power generation efficiency. Catalytic steam reforming is a common industrial technique of reforming hydrocarbons. Gasification, steam reforming, and ATR all produce synthesis gas (or "syngas"), a mixture of CO and H_2, which can be burned for fuel value, purified to H_2 for use in a fuel cell, or converted into synthetic fuels

During World War II, two German scientists developed a process for converting syngas to alkanes in order to process Germany's coal to liquid fuels. The Fischer-Tropsch process utilizes an Fe catalyst and has been well studied for over 60 years. Alternatively, syngas can be used to produce methanol over CuZnO catalysts, or dimethyl ether, a diesel fuel and propane gas substitute.

Gasification is still being applied industrially for the production of power[29, 30] and synthetic fuels.[31] According to the EIA, the net share of global consumption of biofuels and synthetic gasoline (derived from coal and natural gas) is projected to be 6.9% of the entire liquid fuel industry in 2030.[7]

Given the low ash content of bio oils, catalysts can be used in their gasification to enhance selectivity to desired products and control reaction conditions.

1.5 Catalytic Partial Oxidation

Research in the Schmidt Group shifted to the examination of autothermal Catalytic Partial Oxidation (CPO) with the discovery of the conversion of methane to syngas by Hickman and Schmidt in 1992.[32] CPO of methane is given in Equation 1.1.

$$CH_4 + 0.5O_2 \rightarrow 2H_2 + CO_2 \qquad \Delta H = -36\frac{kJ}{mol} \tag{1.1}$$

This process can be generalized to the reacting of virtually any hydrocarbon over a noble metal catalyst, such as rhodium (Rh), nickel (Ni), or platinum (Pt), in the presence of O_2. This reaction produces syngas as well as CO_2, H_2O, and for larger hydrocarbons, olefins such as ethylene.[33] Selectivity to these products depends on the reaction conditions, and is tunable to equilibrium syngas or high selectivity to olefins.

Olefins, unsaturated monomers such as ethylene and propylene, are used as basic building blocks in chemical processing, such as plastics manufacture. As such, olefins are commodity chemicals with higher value than fuels.

Catalytic chemistry can be promoted with small pore catalysts which increase the likelihood of surface interaction.[34] Homogeneous chemistry can be promoted with larger pores, allowing reactants to pass through the catalyst.[35] Heat produced at the surface promotes homogeneous chemistry, allowing for fast heat transfer and immediate product quench upon exiting the catalyst bed. Thus, another experimental parameter in CPO is the pore size of foam monolith catalysts. Figure 1.2 depicts coated and uncoated 80 pores per linear inch (ppi), 45 ppi, and 20 ppi foam monoliths.

As CPO is exothermic, driving reactions to proceed >600 ^{o}C, the catalyst is hot enough to incandesce. [Figure 1.4] CPO chemistry is fast, with residence times measured in milliseconds in a continuous flow reactor. Contact time, the time that a flowing packet of vaporized reactants at reaction temperature can interact with a catalyst, is defined as

$$\tau = \frac{\epsilon \times V}{\left(\frac{T_{rxn}(K)}{291K}\right) Q} \tag{1.2}$$

where T_{rxn} refers to the reaction temperature in Kelvin, Q is the volumetric flow rate of reactants; ϵ is the void fraction of the catalyst (eg, where gas can flow), and V is the total volume of the catalyst.

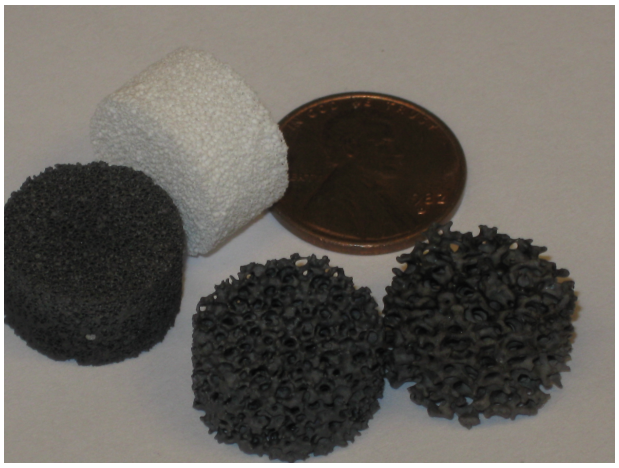

Figure 1.2: Photo of catalyst monoliths. The white foam is a bare 80 ppi 99% Al_2O_3 1% SiO_2 support. Counterclockwise: an identical 80 ppi ceramic catalyst loaded with 2.5 wt% Rh and Ce, a 45 ppi 1 wt% Rh-Ce coated foam catalyst, and a 20 ppi Rh-Ce coated catalyst. Incidentally, the 45 ppi Rh-Ce catalyst also had a hole bored into it to accommodate a capillary for the spatial resolution of acetaldehyde CPO, described in Chapter 7.

Figure 1.3: A commercial steam cracker requires contact times on the order of $\tau \approx 1$ second. The millisecond reaction time of CPO means that this plant can be scaled to approximately the size of the truck parked in front. Photo from [36]

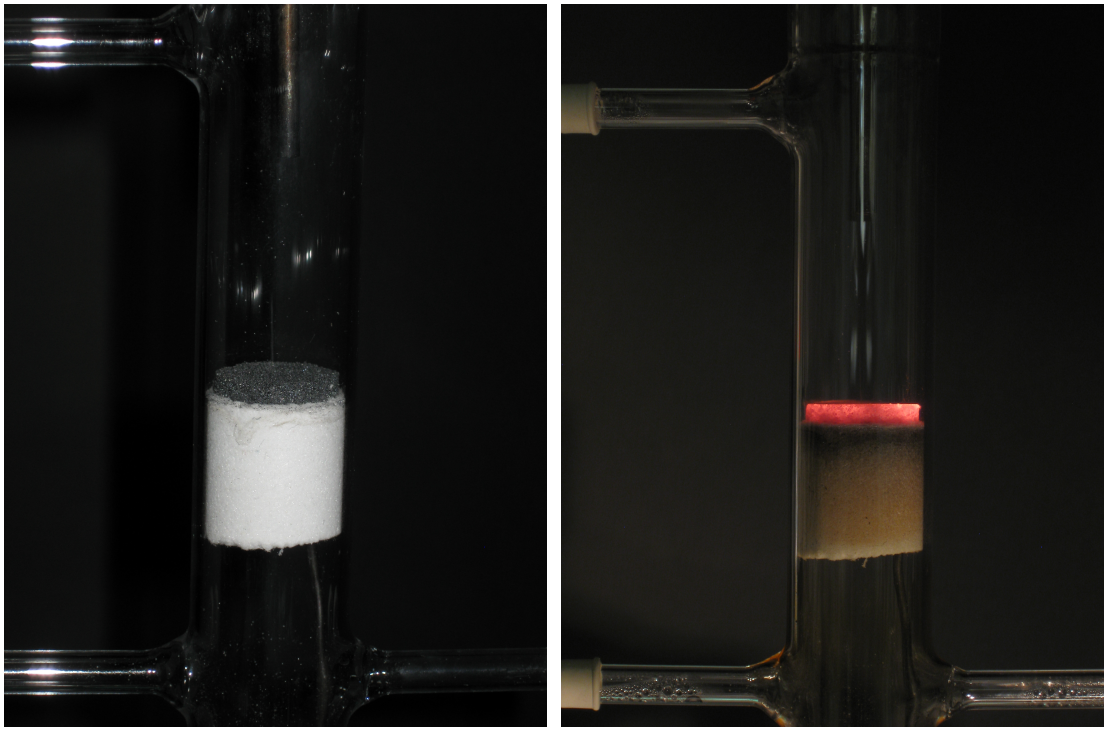

Figure 1.4: Autothermal CPO reactor. On left, the reactor is shut off. On right, fuel is converting to syngas and the exothermic reaction is hot enough (>600 ^{o}C) to cause incandescence.

CPO is autothermal: oxidation of the fuel provides its sufficient heat to produce synthesis gas. This chemistry has high efficiencies and high throughputs, and can achieve even greater efficiency when combined with steam to yield autothermal reforming.[20] Efficiency is essential if biomass is ever to compete with fossil fuels. High throughputs are an advantage because they can decrease reactor size, which can add flexibility to plant scaling and reduce capital costs. [Figure 1.3]

CPO of larger alkanes was demonstrated to be feasible: prevaporizing volatile compounds allowed these alkanes to react as well as methane or ethane.[37, 38, 39, 40, 35] Oxygenated compounds can also be introduced to a catalyst using this setup, demonstrating that renewable fuels can be converted to syngas by CPO.

The CPO of ethanol to form synthesis gas is particularly well studied.[18, 41] Partial oxidation occurs by dehydration of the hydroxyl group to form adsorbed alkoxide species. These species then decarbonylate and desorb as CO and H_2. On Rh, ethanol forms a metallocycle via the β-carbon, and decompose completely into CO and H_2.[42, 43, 44]

Biodiesel is the first molecule containing the ester moiety to be examined for autothermal CPO.[45] It is a natural choice after conventional diesel fuel.[46] Biodiesel proved to be a flexible feed and exhibited high selectivity to syngas at low C/O and produced many olefins at higher C/O. The ester linkage was preserved and produced oxygenated olefins at 6% selectivity.

Carbohydrates have also been successfully converted to syngas. The first three carbohydrates, methanol, ethylene glycol, and glycerol, were all converted into synthesis gas by catalytic partial oxidation with high conversion and low selectivity to side reactions.[47] All of these fuels were prevaporized, allowing good mixing and transport of reactants to the catalyst. As CPO of methane over Rh is transport limited in O_2, this prevaporization allowed equilibrium production of syngas in millisecond contact times, using only a few mm of catalyst.[48]

Recently, a few nonvolatile liquid fuels have been converted to syngas by CPO. Soy oil and sugar water produced syngas, and soy oil generated enough heat to operate autothermally, while glucose and water required some methane cofeed in order to sustain autothermal reaction.[49] Solids such as cellulose and wood chips are also remarkably well behaved under CPO conditions.[50, 51]

At syngas stoichiometry, oxygenated biofuels produce CO and H_2 with very high conversion. The high oxygen content in these fuels increases their sticking coefficient, which results in high surface reactivity.[47]

However, bio-oils produced by fast pyrolysis can be considerably complex: they contain up to 400 different organic compounds with various oxygenated functional groups.[52] Therefore, an understanding of the catalytic reforming of bio-oils must be based on simple, representative feedstocks. The research described above has examined the catalytic reforming of many of the important functional groups occurring in bio-oil including alcohols,[18, 53] polyols,[47] ethers,[54], aromatics[55] methyl esters,[45] and oils and C_6 sugars.[49] Missing functionalities from this list include higher esters, organic acids and functionalized aromatics.

Subsequent chapters in this thesis will explore the CPO of pyrolysis oil. Chapter 2 discusses CPO of organic acids, present in high concentrations in bio oils, and chemically active as feedstock. Chapter 3 addresses the importance of functionality to discover how important it is to consider all of the approximately 400 different types of compounds in pyrolysis liquids. Chapter 4 explores the chemistry of the aqueous phase of bio oil - the cellulosic fraction which is typically decomposed to acids or poly-ols, such as glycerol and ethylene glycol. Chapter 5 details a time-on stream experiment using glycerol as a model compound to discover what problems must be addressed before scaling CPO technology to pilot plants. The upgrading of three different bio oils is described in Chapter 6, which explores novel reactor designs for handling this promising but challenging liquid. Future plans are described in Chapter 7.

Chapter 2

CPO of Organic Acids

2.1 Summary

Pyrolysis oils comprise up to 25% organic acids. Furthermore, organic acids have high oxygen content, making them excellent representatives of biomass as a whole. This chapter examines the catalytic partial oxidation of three different organic acids. Acetic acid, propionic acid, and lactic acid are examined over Pt catalysts under oxygen deficient conditions to probe the chemistry of acids in the CPO environment. Propionic acid is further explored over Rh-Ce for comparison. Acetic acid does not react when introduced as a liquid directly onto the catalyst in the reactive flash volatilization method. Propionic acid and lactic acid react to syngas over noble metal catalysts, producing non-equilibrium products when starved for O_2 over Pt. Propionic acid exhibits high selectivity to ethylene under these conditions; by contrast, lactic acid exhibits high selectivity to acetaldehyde, producing almost no ethylene. These differences in products reveal a mechanism that is sensitive to the particular functional chemistry of the original molecule. With autothermal operation and high flowrates, contact times are on the order of τ = 10 ms: as a result, intermediate products reveal chemical transitions far from equilibrium when rapidly quenched at the catalyst backface. A mechanism is proposed in which lactic acid decarbonylates (loses CO) and dehydrates (loses H_2O) to acetaldehyde, and propionic acid

decarbonylates and dehydrates to ethylene.

2.2 Introduction

Pyrolysis oils contain up to 25% organic acids (see Table 6.1.[28, 23], resulting in a pH of around 2.5.[1] The active acid content in bio oil is one of the reasons oils change over time.[28] Processing pyrolysis oils will require an understanding of the chemistry and materials compatibilities of such acids.

Pyrolysis breaks down polymer chains so that the resultant molecules are relatively small. As carbon chain lengths grow, the number of possible permutations and chemical reactions increases. Thus, to best understand a given functional group, small carbon chains are essential. For all of these reasons, common model compounds for pyrolysis oils are small organic acids.[56, 57, 58, 59, 60]

Formic acid, the simplest organic acid, is difficult to analyze in a GC and is unstable when heated. Furthermore, decomposition of formic acid results in syngas, which reveals nothing about the mechanism of decomposition, and makes it impossible to discern whether products are formed homogeneously or catalytically.

Acetic acid is the next logical choice, and can decompose homogeneously. However, the decomposition of acetic acid results in ketene or C_1 products. While the former is of interest, its instability makes it also difficult to analyze; the latter present the same difficulties as formic acid.

In this chapter, the catalytic partial oxidation of acetic acid, propionic acid, and lactic acid will be discussed. The larger C_3 acids will reveal some characteristic decomposition methods which allow mechanistic conclusions to be drawn from the catalytic partial oxidation of these acids.

Organic acids offer a further advantage for consideration as representative of biomass: the internal C:H:O ratio can match that of carbohydrates. Etymologically, carbo-hydrate refers to a compound with a stoichiometric carbon-water ratio. Acetic acid and lactic acid, for example, follow $C_x(H_2O)_x$: x=2 for acetic acid and 3 for lactic acid. As biomass is built from polymeric carbohydrates, the CPO of these molecules demonstrates the greatest thermodynamic challenge for an autothermal reactor processing bio-derived feedstock. Acetic acid, propionic acid, and lactic acid are depicted in Figure 2.1.

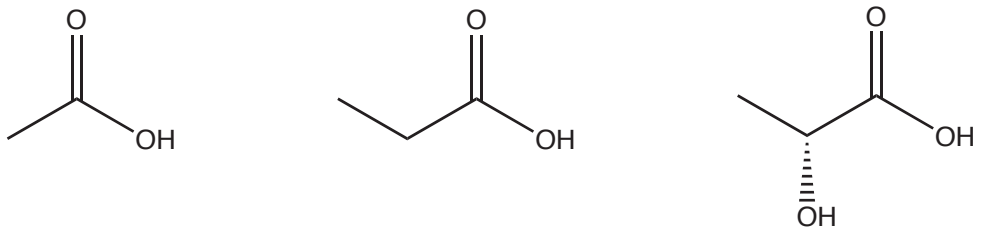

Acetic Acid Propionic Acid Lactic Acid

Figure 2.1: Sketch of acetic acid, propionic acid, and lactic acid. Acetic acid contains only two carbons; other than C_1 products, it can only form ketene from thermal decomposition. Propionic acid has one carbon more in its acid group. Lactic acid is identical to propionic acid with the inclusion of an OH group on the α' carbon.

2.2.1 Chemistry of C_1 Products

Because of their high internal oxygen content, the conversion of C_2 and C_3 organic acids to syngas is endothermic. In two of these three examples (Equations 2.1 and 2.3), it is improper to refer to this chemical reaction as "partial oxidation" because no O_2 is added. The rearrangement of acetic acid to syngas is given in Equation 2.1 and requires about 200 kJ/mol.

$$CH_3COOH \rightarrow 2CO + 2H_2 \qquad \Delta H^o \approx 210\frac{kJ}{mol} \tag{2.1}$$

Similarly, the conversion of propionic acid and lactic acid to syngas are given in Equations 2.2 and 2.3, respectively. Propionic acid, the least oxidized of the three, requires the addition of half a molecule of O_2 and, as a result, is less endothermic than the rearrangement of acetic acid or lactic acid.

$$CH_3CH_2COOH + 0.5O_2 \rightarrow 3CO + 3H_2 \qquad \Delta H^o \approx 180\frac{kJ}{mol} \tag{2.2}$$

Partial oxidation to syngas occurs at a C/O = 3 for propionic acid. Lactic acid, with the same internal C/O ratio, requires no O_2 for stoichiometric syngas production.

$$CH_3CHOHCOOH \rightarrow 3CO + 3H_2 \qquad \Delta H^o \approx 250\frac{kJ}{mol} \tag{2.3}$$

The energy required to maintain high temperature autothermal operation comes from the production of some complete combustion products, H_2O and CO_2, as indicated by Equations 2.4, 2.5, and 2.6. Thus, autothermal operation requires the production of syngas containing some CO_2 and/or H_2O. Acetic acid, the smallest of the three, is the least exothermic because it produces the least number of combustion products.

$$CH_3COOH + 2O_2 \rightarrow 2CO_2 + 2H_2O \qquad \Delta H^o \approx -840\frac{kJ}{mol} \tag{2.4}$$

Again, as propionic acid is the least oxidized of the three, its combustion is most exothermic, releasing 1400 kJ/mol (Equation 2.5).

$$CH_3CH_2COOH + 3.5O_2 \rightarrow 3CO_2 + 3H_2O \qquad \Delta H^o \approx -1400\frac{kJ}{mol} \tag{2.5}$$

Lactic acid, 50% larger, but having the same internal oxidation state as acetic acid, releases approximately 50% more energy per molecule combusted, as depicted in Equation 2.6.

$$CH_3CHOHCOOH + 3O_2 \rightarrow 3CO_2 + 3H_2O \qquad \Delta H^o \approx -1300\frac{kJ}{mol} \tag{2.6}$$

This exothermic chemistry maintains operation at temperatures greater than 600 ^{o}C, permitting complete conversion to equilibrium products in ≈10 milleseconds. The exothermicity of complete oxidation can provide some energy for endothermic chemistry. For the production of syngas, combustion of one mole of acetic acid can drive the rearrangement of four moles to syngas. Thus, autothermal operation cannot yield a selectivity to CO greater than 80% (without consuming H_2 in exchange).

2.2.2 Non-Equilibrium Acid Chemistry

Catalytic methods for producing olefins from acids have been known for some time.[61, 62] Acids can yield olefins at high conversion over noble metal catalysts.[63] This reaction produces commodity olefins from renewable feedstocks.

At the high temperatures of autothermal operation, the contribution of gas-phase chemistry cannot be neglected. Evidence for significant gas-phase chemistry under CPO conditions has been observed by increasing the fuel-to-oxygen ratio, such that non-equilibrium intermediates resulting from homogeneous chemistry exit the reactor before being completely reformed on

the catalyst surface.[64] Under these conditions, the slight variation between fuel molecules provides details of the origin of each intermediate, as well as the overall mechanism.

Propionic Acid Decomposition

Propionic acid has been observed to crack to ethylene,[65] perhaps by the mechanism in Equation 2.7.

$$CH_3CH_2COOH \rightarrow C_2H_4 + CO + H_2O \qquad \Delta H^o \approx 150\frac{kJ}{mol} \tag{2.7}$$

While this decomposition indicates decarbonylation (-CO) of the acid, decarboxylation (-CO_2) may compete. In this case, CO_2 and H_2 would replace CO and H_2O in the equation above. The decarboxylation is slightly favored energetically over decarbonylation by 15 to 30 kJ/mol.

Lactic Acid Decomposition

The addition of a hydroxyl group to the α'-propionate carbon should result in different chemistry, indicative of the overall decomposition mechanism. Thermal decomposition of lactic acid has been observed to proceed to acetaldehyde via decarbonylation,[66] perhaps by the reaction shown in Equation 2.8.

$$CH_3CHOHCOOH \rightarrow C_2H_4O + CO + H_2O \qquad \Delta H^o \approx 0\frac{kJ}{mol} \tag{2.8}$$

which results in acetaldehyde rather than ethylene as a homogeneous product. It is noteworthy that the highly oxidized lactic acid molecule undergoes this rearrangement with less energy input than the rearrangement to syngas products. Indeed, the dehydration to acetaldehyde is enthalpically neutral.

These experiments were performed under excess pressure of free-chain radical inhibitors.[66] All reactions were observed to be first order and unimolecular. Modeling of these results suggests dehydration as a rate limiting step. Two main reaction pathways are identified; the dominant reaction proceeds via a three membered ring [Figure 2.2], and a second possibility is a two-step isomerization involving the keto-enol tautomerization, described in Figure 2.3.[67]

In the absence of oxygen, lactide, the dimer cyclic diester of lactic acid, undergoes a double decarbonylation via six membered ring mechanism. This produces CO and acetaldehyde, as

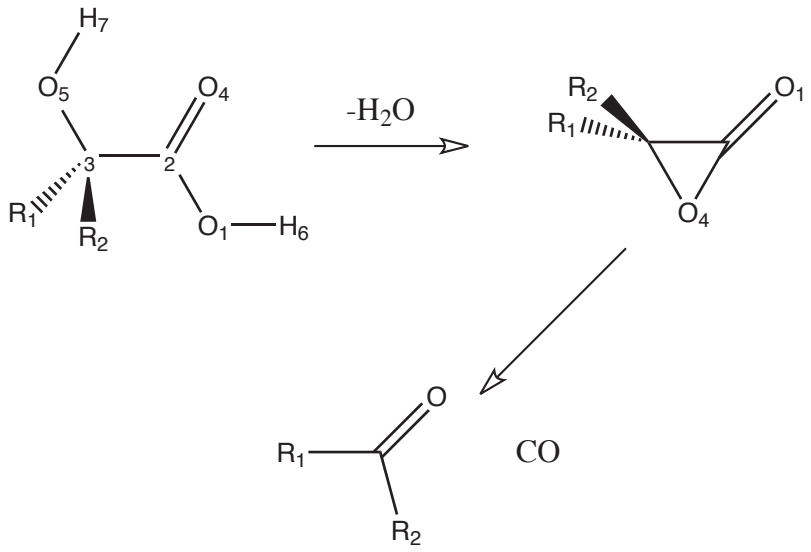

Figure 2.2: Pyrolysis of lactic acid decarbonylates via 3 membered ring [67]

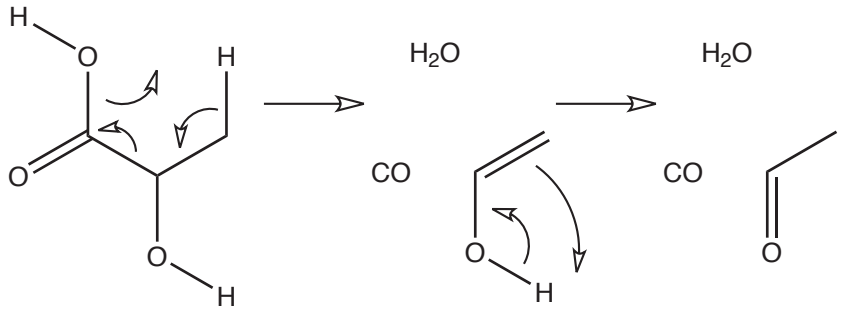

Figure 2.3: Proposed two-step mechanism for decarbonylation of lactic acid via the keto-enol tautomerization.

described in Figure 2.4.[68] Of course, formation of the dimer produces H_2O, so this pathway represents an alternative pathway to the same products described above

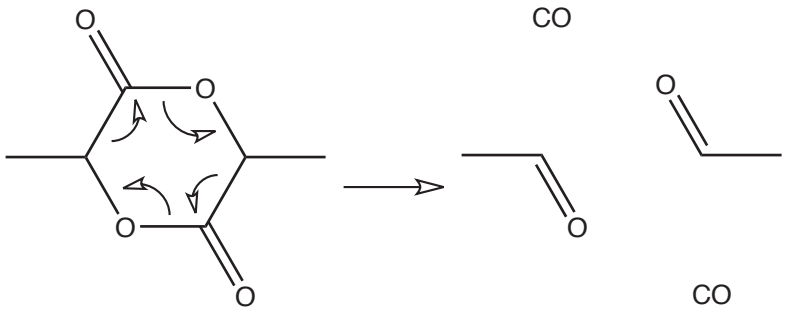

Figure 2.4: The lactic acid dimer thermally decarbonylates[68]

At high temperature and as a product in a milli-second reactor, the formation of these dimers may be difficult. A six-membered transition state is probably concerted and neat, but it may only be descriptive at high lactic acid concentrations. This is perhaps possible in the longer time scaled and catalyst-free pyrolysis conditions, but seems unlikely under catalytic conditions as lactic acid has such a high affinity for the surface.

It is worth noting that, under oxidizing conditions, decarboxylation rather than decarbonylation is favored for the decomposition of an α'-hydroxy acids.[69] The products of such an oxidation are an aldehyde at the hydroxyl group, CO_2, and H_2.[70, 71, 72] It is presumed that these reactions proceed via radical chemistry, which was quenched in the Chuchani experiments detailed above.

Similarly, decarboxylation is favored for the related keto-acid. Thermal decomposition proceeds by a four membered ring transition state. This conformation leads to decarboxylation of α'keto-acids, such as pyruvic acid.[73, 74] The remainder forms a ketone.

In a CPO reactor, O_2 persists for a few millimeters, after which the environment is best described as reducing conditions.[75] Thus, dehydration is likely to dominate decarboxylation for lactic acid decomposition.

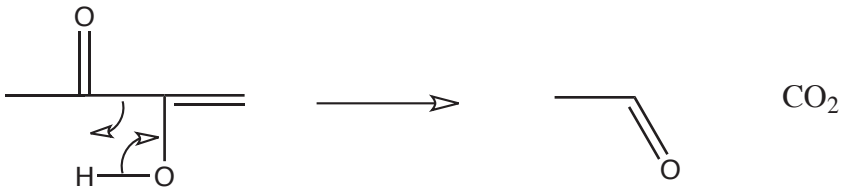

Figure 2.5: α-keto acid thermal decarboxylation [73]

Acetic Acid Decomposition

Acetic acid has no decarbonylation route, as the products would include a CH_2 radical. However, acetic acid could decarboxylate to CH_4 and CO_2.

$$CH_3COOH \rightarrow CH_4 + CO_2 \qquad \Delta H^o \approx -40\frac{kJ}{mol} \tag{2.9}$$

Catalytic partial oxidation experiments with propionic acid were performed over Rh-Ce and Pt coated foam monoliths. Those experiments over Rh-Ce demonstrated that propionic acid reacts readily to syngas over this catalyst. However, experiments performed over Pt demonstrated a product intermediate, ethylene. For this reason, CPO of lactic acid over Pt was explored. These lessons were applied to the CPO of acetic acid over Pt.

2.3 Experimental

Catalysts were prepared by coating noble metals on cylindrical ceramic foam monoliths (92% α-Al_2O_3, 8% SiO_2). The foam monoliths measured 17 mm in diameter and 10 mm in length, and weighed ≈2.2 g before metal loading. Monolith foam density was 80 pores per linear inch (ppi) in all cases except for propionic acid on Pt, which used 45 ppi foams.

Metal loadings were: rhodium and cerium (Rh-Ce 2.5 wt% each), and platinum (Pt 5 wt%). All catalysts were applied using the incipient wetness impregnation technique: Rh was deposited in solutions of $Rh(NO_3)_3$ salt in water, Ce as $Ce(NO_3)_3{\cdot}6H_2O$, and Pt as PtH_2Cl_6. The foams were then allowed to dry in air for six hours. Rh-Ce coated foams were calcined in a furnace for six hours in air at 600 ^{o}C. To prevent loss of Pt loading, Pt catalysts were reduced under N_2 and H_2 at 600 ^{o}C for six hours.

All acids examined are liquid at room temperature and have boiling points between 115 ^{o}C and 150 ^{o}C, so they can be vaporized upstream of the catalyst. Experiments with acetic acid were initially explored using reactive flash volatilization: applying the fuel directly onto the front face of the catalyst without a prevaporization zone or upstream heat shield.

The experimental setup for the CPO of propionic acid and lactic acid is similar to the setup of Deluga et al.[18] A diagram of the reactor is shown in Figure 2.6. Each fuel was placed in a fuel tank pressurized with a blanket of N_2 to 20 PSI. The fuels, acetic acid (99.7% ACS Grade, Sigma Aldrich), propionic acid (>99%, Avocado), and lactic acid (≈65% in water, measured experimentally by closing the carbon balance at low C/O) were sprayed through an automotive fuel injector into a quartz tube 19 mm inner diameter (ID) wrapped in insulation. Varying the duty cycle of the fuel injector (accurate within ±3%) allowed for changes in flow rate. The injector sprayed the fuels in small droplets which facilitated mixing and vaporization. The walls of the reactor were heated externally by wrapped heating tape. A chromel-alumel thermocouple hereafter refered to as upstream was fed through a port 4 cm above the catalyst. This port also enabled upstream samples to be taken to monitor flow rates. A blank monolith wrapped with ceramic paper to hold it in place was placed just above the upstream thermocouple to promote mixing. The upstream temperature was maintained above the boiling point of the injected fuel.

N_2 and O_2 were independently metered by mass flow controllers (accurate to within ±5%). This gas mixture at air stoichiometry was fed through a side port near the fuel injector. The air and vaporized fuel flowed at a rate of 4 SLPM (standard liters per minute, where standard refers to ideal gases measured at the injection site, 18 ^{o}C, 1 atm). This mixture passed over three foam monoliths: a catalyst placed between two heat shields to minimize heat loss, one upstream, which also promoted mixing, and one downstream of the catalyst coated foam monolith. A groove was chiseled in the top face of the downstream heat shield to accommodate a second thermocouple which measured temperatures on the back face of the catalyst ("backface"). This thermocouple was bent to the side of the backface heat shield and trailed downstream where it wound out through a septum at the bottom of the reactor. All three foam monoliths were wrapped in ceramic paper to secure their position, provide extra insulation, and ensure all flow was directed through the foam monoliths.

A port in the reactor positioned 4.0 cm below the backface heat shield and sealed with an NMR septum allowed gas phase samples of the product stream to be obtained by a gas-tight syringe. Product gases then exited through another port into a heated exhaust pipe and

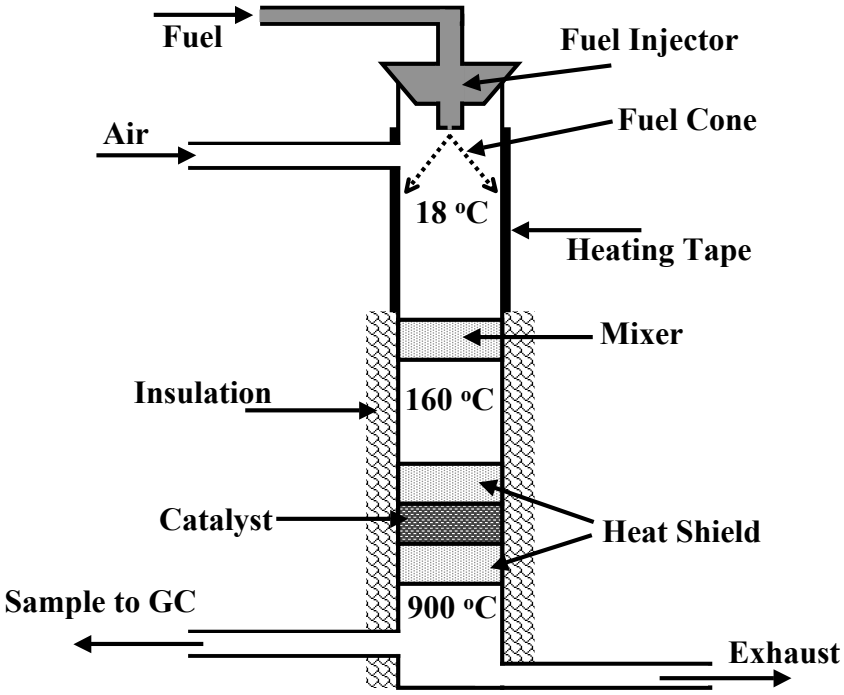

Figure 2.6: Diagram of reactor setup. Fuel and air are fed into the top of a quartz reactor and vaporized by a preheat section. The reaction occurs on a noble metal catalyst that is thermally insulated. Product samples are collected downstream at the bottom of the reactor.

incinerated in a bunsen burner.

The samples were analyzed by gas chromatography (GC). All products and fuels were directly observed except for water, which was derived by balancing oxygen species: oxygen atoms observed in the exit stream were compared with those known to be entering the reactor, and lost oxygen was attributed to water. Balances on atomic carbon typically closed within 10% and balances on atomic hydrogen typically closed to within 5%. For fuel rich experimental trials at C/O > 1.4, carbon balances exceeded 10% error, likely as a result of condensation of reactor effluent within the sampling system.

Experimental runs were at least 10 hours, during which time the reactor experienced several start-ups and shut-downs. Temperatures ranged from 600 ^{o}C to 1200 ^{o}C, limited in the cold regime by poor conversion and in the hot regime by the possibility of sintering the metal loaded on the monolith.

Data is presented in terms of conversion and atomic product selectivities for carbon and hydrogen species. Points are averages of several runs, typically at least three per data point per catalyst. Conversion, X, is defined as the percentage of molar flow of fuel (F_{fuel}) reformed into products. This value is calculated by subtracting the ratio of observed fuel inflow to observed fuel outflow from 100%. Products containing carbon are described by carbon selectivity to the species i, $S_c(i)$. This selectivity is defined as the ratio of the carbons in species i to the total carbon in converted fuel.

$$S_C(i) = \frac{C_i \times F_i}{C_{fuel} \times \left(F^{in}_{fuel} - F^{out}_{fuel}\right)} \tag{2.10}$$

Products containing no carbon (H_2 and H_2O) are analogously described by hydrogen selectivity to j: $S_H(j)$.

$$S_H(j) = \frac{H_j \times F_j}{H_{fuel} \times \left(F^{in}_{fuel} - F^{out}_{fuel}\right)} \tag{2.11}$$

where H_j indicates the number of hydrogen atoms in species j.

Averages at each C/O, defined as the ratio of carbon in fuel to oxygen in air, are represented graphically. Deviations from these averages were pooled among all C/O to calculate error bars which represent one standard deviation.

Equilibrium calculations were performed using Chemkin 3.7. Organic acids, when unavailable in the thermodynamics package, were replaced with a set of molecules with the same

stoichiometry. Isothermal equilibrium calculations were obtained keeping pressure and temperature constant, using the back face temperature measured by the thermocouple.

2.4 Results

Without preheat, the RFV of acetic acid was unsustainable. At very low C/O, the reactor would operate autothermally for a short period (≈20 min). Temperatures never exceeded 700 ^{o}C despite the low C/O.

With preheat and an extra carbon, CPO of propionic acid and lactic acid was able to run autothermally. Conversion at C/O < 1.7 was >98% and >80% at all C/O (Figure 2.7). For C/O = 0.9, autothermal reaction took place at temperatures around 1200 ^{o}C for propionic acid over Rh-Ce, corresponding to a contact time of τ = 7ms. This is almost 400 ^{o}C more than temperatures observed over Pt under the same conditions. Due to the lower temperature, contact times over Pt were τ = 15 ms. Temperatures for both acids over Pt never exceeded 1000 ^{o}C. Temperatures dropped by 100 ^{o}C between 1.1 < C/O < 1.4. Temperatures as low as 400 ^{o}C at C/O = 2.0 were observed. Steady state was obtained for these values, but any higher C/O extinguished the reaction, or any colder temperatures occasionally extinguished the reaction. Deactivation, possibly due to coking, was observed over both catalysts after shutdown and startup. Deactivation manifest by increasing selectivity to olefins and decreasing backface temperatures.

Data from the CPO of propionic acid over Rh-Ce and Pt catalysts are depicted in Figure 2.8 A & B; data from lactic acid in Figure 2.8 C.

Generally, for C/O < 1.2, the partial oxidation of propionic acid proceeds to equilibrium syngas. Selectivity to olefins increased to ≈30% for C/O > 1.5. The production of equilibrium products (C_1 species, H_2 and H_2O) and olefins will be discussed separately.

Selectivity to syngas products was higher over Rh-Ce than on Pt, while olefins had highest selectivity at high C/O on Pt. For propionic acid over Rh-Ce, H_2 selectitivity reached equilibrium values – around 60% – and peaked at C/O = 1.0, below which a decrease in equilibrium decreased H_2 selectivity. H_2 selectivity on Pt was not near equilibrium, even at low C/O, and no peak in H_2 is observed. This indicates leaner C/O may increase hydrogen selectivity on Pt. The highest H_2 selectivity observed was at C/O = 0.9 at ≈26%.

Selectivity to CO from propionic acid on Pt was near 60% which is much closer to equilibrium than Pt selectivity to H_2. Selectivity to CO on Rh-Ce from propionic acid reached the

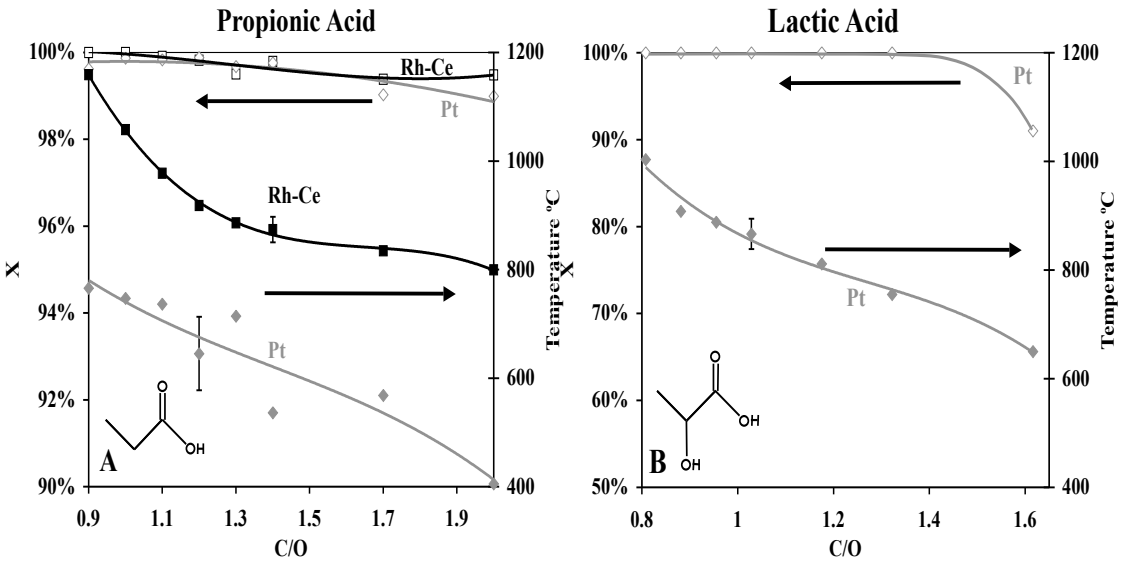

Figure 2.7: Conversion (X) and backface temperatures observed during the CPO at various C/O of propionic acid (Panel A), lactic acid (B). The bottom left corner of each panel depicts the compound. Lactic acid has the same structure as propionic acid with an additional hydroxyl group (OH) on the α' carbon. Rh-Ce (□), Pt (◇) show conversion (left axis); Rh-Ce (■), Pt (◆) show backface temperatures (right axis). Contact times: $\tau \approx 10$ ms. Pt temperatures are lower than the Rh-based catalysts. Temperatures rise at lower C/O as a result of more exothermic oxidative chemistry. Conversion is >98% for C/O < 1.7 and >80% at all C/O.

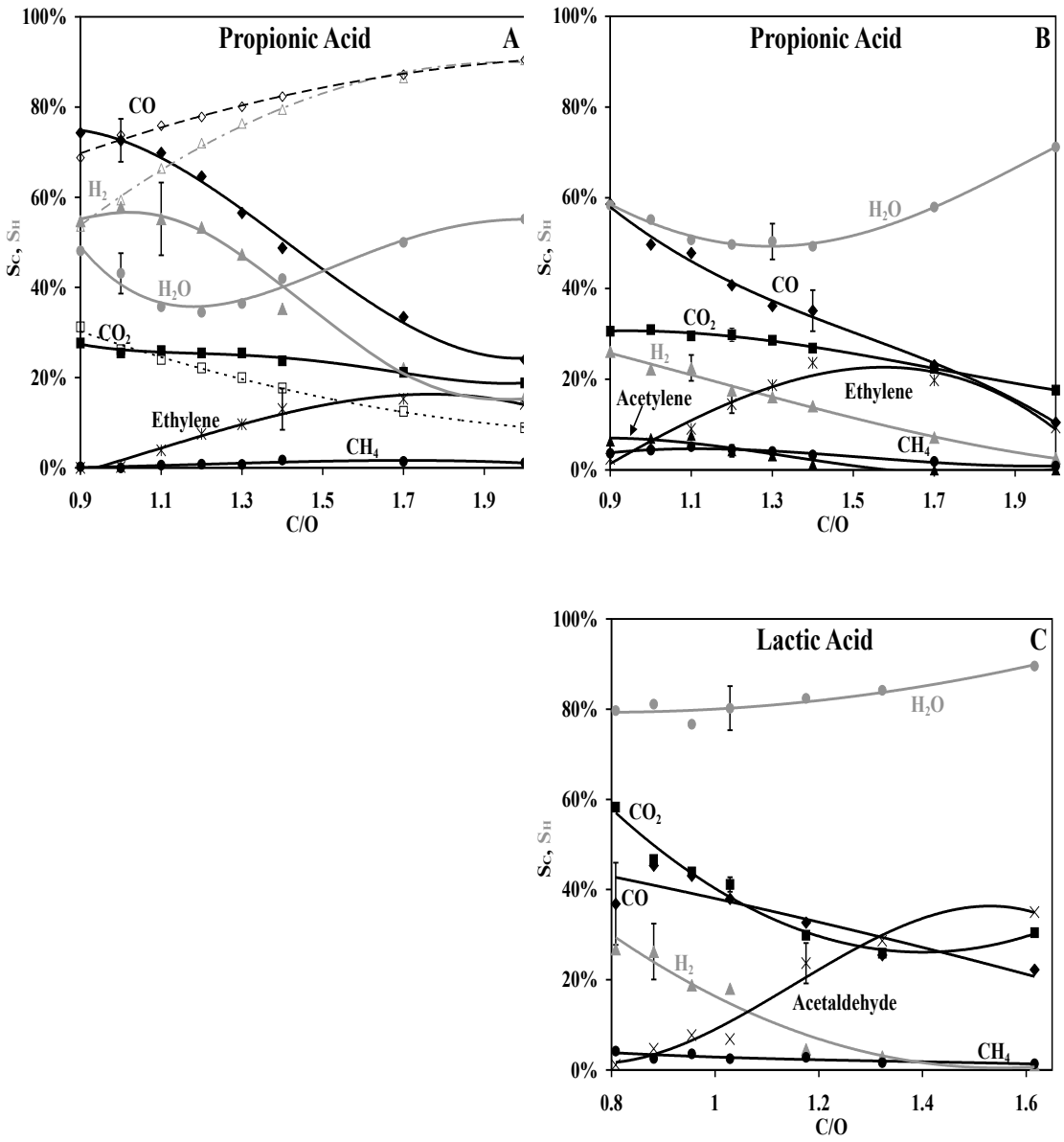

Figure 2.8: CPO of propionic acid over Rh-Ce (Panel A) and Pt (Panel B), and of lactic acid over Pt (Panel C): hydrogen selectivity (S_H to H_2O (●), H_2 (▲)), and carbon selectivity (S_C to CO (◆), CO_2 (■), C_2H_4 (*), C_2H_2 (▲), C_2H_4O (x), CH_4 (●)), the most observed species. Isothermal equilibria are depicted in open symbols and dashed lines for H_2, CO, and CO_2 on Rh-Ce. A ~33% selectivity to CO_2 from propionic acid suggests decarboxylation of the acid; this selectivity decreases with an increase in C/O implying gas phase decarbonylation competes with surface decarboxylation. Lactic acid has a slightly higher selectivity to CO_2 due to its greater internal C/O. Selectivity to acetaldehyde is <1% from propionic acid, but reaches 35% from lactic acid; selectivity to ethylene reaches 20% from propionic acid but <1% from lactic acid.

adiabatic equilibrium at C/O = 1 and followed it closely at lower C/O. The selectivity to CO was essentially level at C/O ≤ 1. It achieved ≈74% selectivity on Rh-Ce.

Pt had higher selectivity to C_2 products than Rh-Ce for both acids. Ethylene was the major olefinic product from propionic acid, but acetylene was also produced. On Rh-Ce, selectivity to acetylene from propionic acid reached ≈2% and on Pt, selectivity to acetlyene reached ≈8% selectivity. On Rh-Ce, ethylene leveled off at 16% and on Pt it peaked at 25%.

No ethylene is observed in the CPO of lactic acid over Pt. Instead, selectivity to acetaldehyde achieves 35% near C/O = 1.6. With a decrease in C/O, acetaldehyde diminishes as selectivity to H_2, CO_2 and CO increase. As for the other fuels studied in this work, selectivity to H_2 does not achieve equilibrium from CPO with a Pt catalyst.

The noteworthy result of these experiments is that propionic acid exhibited less than 1% selectivity to acetaldehyde on both catalysts, while lactic acid exhibited high selectivity (up to 35%) to acetaldehyde. In addition, lactic acid produced <1% selectivity to ethylene, while propionic acid showed a selectivity to ethylene of about 20% (see Figure 2.8) and selectivity to acetylene of ≈7%. Selectivity to CO_2 from lactic acid is higher than for propionic acid at a corresponding C/O, consistent with the higher internal oxygen content of lactic acid. Both acids show selectivity to CO_2 > 30% for C/O < 1.3 and slightly less at higher C/O.

2.5 Discussion

At low C/O, both C_3 acids exhibited high selectivity to synthesis gas. Conversely, at high C/O, selectivity to non-equilibrium products such as ethylene and acetaldehyde increased significantly. The product selectivity is highly tunable between gasification products and non-equilibrium olefinic products.

2.5.1 Equilibrium Products and Surface Chemistry

The selectivity to CO_2 is relatively constant at ≈1/3 for propionic acid over both catalysts (Figures 2.8 A and B), and slightly higher than that for lactic acid over Pt (Figure 2.8C). This is suggestive of an acid reforming mechanism, wherein a particular fraction of the acid forms CO_2. Temperature programmed desorption experiments indicate that acids decarboxylate via adsorbed carbonate species under similar conditions,[43, 76] consistent with a surface mechanism involving decarboxylation of the 3-carbon acids.

Organic acids react readily on the catalytic surface due to the ease with which the acidic hydrogen is cleaved.[43] Consistent with >98% conversion, autothermal reforming temperatures for oxygenates tend to be very hot (>800 ^{o}C) for C/O < 1.3 (Figure 2.7).

The data in Figures 2.8 suggest that acids convert to near equilibrium products similar to other small oxygenated fuels such as ethanol or glycerol,[47, 64] especially at C/O < 1.3, where selectivity to synthesis gas is very near to equilibrium for Rh based catalysts. Propionic acid proceeded to near equilibrium at these C/O.

Organic acids likely adsorb by cleaving the acidic hydrogen to form a surface carboxylate. [77, 43, 78] The carboxylate could form CO_2 which then desorbs. This leaves the rest of the molecule to react in a fashion similar to other fuels such as ethanol, by severing C-C or C-O bonds while reacting with other surface species, depending on the noble metal.[43] Syngas, methane, and combustion products desorb. Additionally, water-gas shift is likely present under these operating conditions providing an alternative surface mechanism to adjust the ratio of CO to CO_2.[79]

In particular, for formic acid, Houtman and Barteau found that Rh catalysts produce mostly CO_2 and H_2, but also some CO and H_2O ($CO:CO_2 \approx 1:3$). On Pt catalysts, formic acid decarboxylates exclusively, forming CO_2. Larger acids are likely to decompose in a manner similar to the decomposition of formic and acetic acid.[76] In the case of larger acids, the β carbon may bond to the metal as well, forming an intermediate oxymetallocyle.[42, 43] This ring allows the entire molecule to be decomposed by breaking C–C bonds. Oxygen then bonds to the carbon atoms and CO desorbs. The presence of CO in the vicinity inhibits CO formation, promoting CO_2 instead.

Acetic acid and propionic acid were examined on Pd(111).[80] Acetic acid was shown to decarboxylate from the adsorbed carbonate without reaction with O adsorbed on the surface. Propionate also decarboxylated, but the higher stability of the longer acid precluded drawing the same conclusion, though the acids behaved very similarly. These results are generalizable to all group VIII metals, and especially Pt.[76] Thus, surface bound propionic acid should decaroboxylate, leaving C_2 species on the surface. H atoms initially bound to these species recombine into H_2 or water to escape. The remaining carbon is deposited on the surface and reacts with adsorbed O species. Similarly, adsorbed lactic acid species should decarboxylate, though they may also adsorb via the additional hydroxyl group. It is likely that, should an oxymetallocycle form, it may make use of these multiple sites for cleaving O-H bonds.

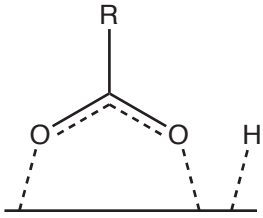

Figure 2.9: Adsorbed acids form carboxylate species. The first step in adsorption breaks the O–H bond of the acidic hydrogen atom.[43]

2.5.2 Non-Equilibrium Products and Homogeneous Chemistry

At C/O > 1.5, selectivity to CO_2 decreases for both acids (Figure 2.8). This phenomenon is accompanied by increases in olefins and aldehydes, probably products of gas-phase chemistry. Thus, with an increase in C/O, surface chemistry decreases in favor of gas phase chemistry, and surface decarboxylation decreases in favor of a gas phase decarbonylation mechanism. Evidence of deactivation due to coke adsorption on the surface at high C/O further indicates that surface sites may be occupied, thus promoting gas phase chemistry.

Since the surface chemistry produces mostly syngas and combustion products, olefin production is explained primarily through homogenous chemistry.

Homogeneous chemistry has been invoked to explain the production of olefins from the CPO of alkanes.[35] Acids also undergo thermal decomposition homogeneously, as several studies have shown. Formic Acid thermally decomposes in two competing channels: decarbonylation and decarboxylation.[81]

$$HCO_2H \rightarrow CO_2 + H_2 \tag{2.12}$$

$$HCO_2H \rightarrow CO + H_2O \tag{2.13}$$

Decarboxylation is an electrophilic substitution reaction.[82] Taylor suggests that, as the decarboxylation reaction is first order, it can proceed by a 4-centered transition state. [See Figure 2.10]

This reaction dehydrogenates the acid, leaving behind CO_2.[83] Radicals are not involved in this chemistry.

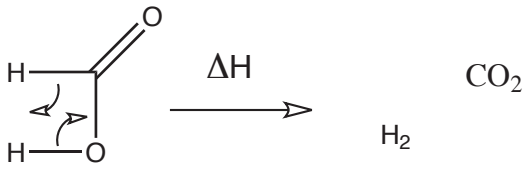

Figure 2.10: 4-center mechanism for decarboxylation of formic acid. ΔH represents heat.[83]

The thermal decomposition of acetic acid was similarly observed to have two competing pathways.[84, 85]. For acetic acid, however, dehydration proceeds to a ketene via 1,1-ethenediol.[86]

$$H_3CCOOH \rightarrow CO_2 + CH_4 \tag{2.14}$$

$$H_3CCOOH \rightarrow H_2CC(OH)_2 \rightarrow H_2CCO + H_2O \tag{2.15}$$

Others omit the middle step and propose that the second reaction proceeds in much the same way as described for the decarboxylation of formic acid, through a 4-membered ring transition state.[83] [See Figure 2.11]

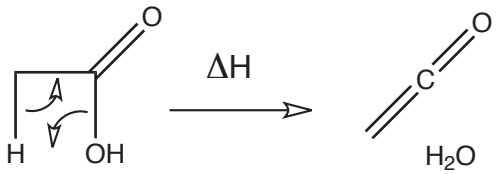

Figure 2.11: 4-center mechanism for dehydration of acetic acid. Again, ΔH denotes that heat is the only input to the reaction.[83]

Propynoic acid, the smallest acetylenic carboxylic acid, also undergoes thermal unimolecular decarboxylation and decarbonylation in competition. Due to the high linearity of the triple bond, these reactions occur in three and four centered transition states. Decarboxylation is energetically favored.[87]

The four membered rings described for acetic and propynoic acid are strained, and while the reaction could be concerted, the possibility of forming five and six membered rings is important for the larger and more flexible propionic acid.

Taylor suggests that propionic acid thermally decomposes via a 5-membered ring transition state. The products are water, ethylene, and CO.[83]. [See Figure 2.12]

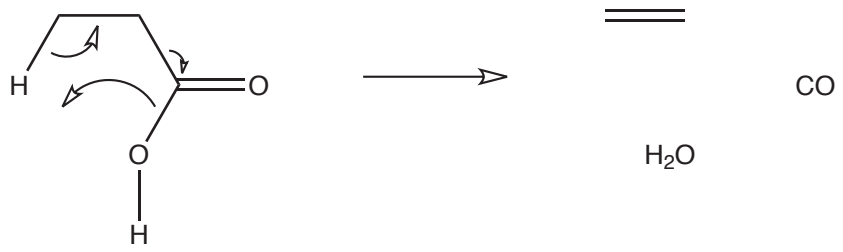

Figure 2.12: 5-center mechanism for dehydration of Propionic Acid.[83]

This decarbonylation does not completely explain the products observed from thermal decomposition of propionic acid, and it is not the only possible conformation for a concerted reaction; decarboxylation can also occur via a six-membered transition state (See Figure 2.13). Alternatively, the high distribution of products in acid decomposition could indicate radical chemistry independent of a concerted mechanism.[88] Indeed, when radical chemistry is disallowed, acids were observed as unreacting, final products in pyrolysis experiments at temperatures up to 650 ^{o}C.[89]

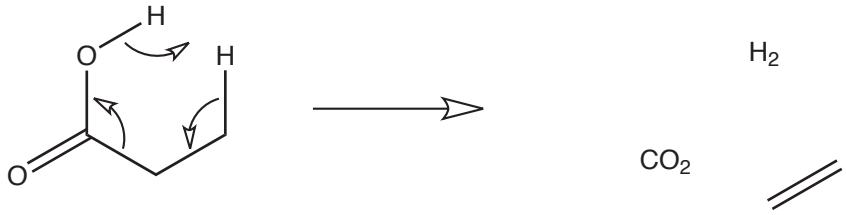

Figure 2.13: Possible 6-center mechanism for decarboxylation of Propionic Acid

In homogenous pyrolysis experiments with propionic acid, Doolan, Mackie and Reid observed high selectivity to ethylene, acetylene, and CO and modeled the reaction.[65] Due to the high selectivity to acetylene, they concluded methyl ketene is an unstable intermediate, which then decomposes to either acetylene or ethylene and CO. The presence of a ketene is consistent with analysis for acetic acid. The workers suggest propionic acid decomposes via free radical processes at high temperatures. The products for such decomposition are ethylene,

acetylene, CO, and H_2O. The authors rule out a unimolecular decarboxylation, and conclude that unimolecular dehydration is also unlikely.

The cracking of propionic acid and lactic acid into ethylene and acetaldehyde explain the high C/O results over Pt. Propionic acid has been shown to decompose in the gas phase to ethylene, CO, and H_2O.[65] Similarly, lactic acid is known to thermally decarbonylate and dehydrate to acetaldehyde.[66] These studies suggest a possible mechanism whereby acids decarbonylate and dehydrate to a resulting chemical: ethylene in the case of propionic acid, and acetaldehyde in the case of lactic acid. This mechanism is depicted in Figure 2.14. Furthermore, the dehydration associated with this reaction explains the high selectivity to water observed in Figure 2.8B and C.

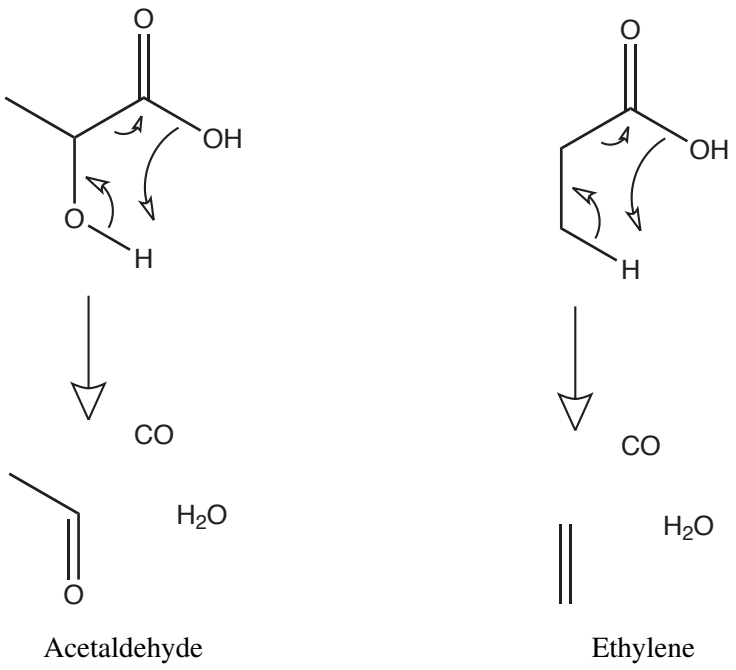

Figure 2.14: Possible mechanism of the decomposition of lactic acid (left) and propionic acid (right). The acid decarbonylates (perhaps through a free radical process[65]) to produce either acetaldehyde in the case of lactic acid, or ethylene in the case of propionic acid. Dehydration produces a molecule of water and CO as byproducts.

By tuning the C/O ratio, it is possible to eliminate olefin production or to achieve high selectivity to predictable olefins depending on the structure of the acid. Based on the stoichiometric thermal decomposition shown in Equation 2.7, the maximum selectivity to ethylene and acetylene from propionic acid is 67%. Similarly, the maximum selectivity to acetaldehyde from ethyl lactate is 67% (Equation 2.8).

2.6 Conclusions

Reactive flash volatilization does not appear to be conducive to the catalytic partial oxidation of acetic acid over Pt. On the other hand, small carbon-chain acids such as lactic acid and propionic acid can be converted by autothermal catalytic partial oxidation at millisecond contact times over Rh and Pt catalysts. Products can be easily tuned to equilibrium synthesis gas or olefins by adjusting the C/O ratio and noble metal choice. Rhodium based catalysts show higher selectivity to synthesis gas while Pt catalysts show higher selectivity for olefins and aldehydes. The reaction occurs at high temperatures with nearly complete conversion over a broad range of C/O. Both acids produce high selectivity to synthesis gas at C/O < 1.3, with few other products as predicted by equilibrium. These results suggest that bio-oils and more complex biomass will be capable of autothermal CPO to synthesis gas under similar conditions.

Organic acids decarbonylate, thus forming an olefin or aldehyde, or react on the surface to form combustion products or synthesis gas. The types of chemicals formed by thermal decomposition of acids depend strongly on the structure of the original molecule. Lactic acid differs from propionic acid by the presence of a hydroxyl group; this hydroxyl group on the acid portion of the molecule produces acetaldehyde instead of ethylene. In this manner, high yield of predictable olefins can be obtained from renewable feeds.

Chapter 3

CPO of Ethyl Esters

3.1 Summary

The catalytic conversion of esters into synthesis gas or chemicals could permit optimal utilization of organic intermediates such as pyrolysis bio-oils. To examine the ester moiety in catalytic partial oxidation, two esters, ethyl lactate and ethyl propionate were compared. Autothermal millisecond operation was examined over platinum and rhodium based catalysts supported on alumina foam monoliths. Conversions >98% were observed for both fuels. The addition of cerium or lanthanum was found to increase the selectivity to synthesis gas. At higher fuel to oxygen ratios, non-equilibrium species such as ethylene and acetaldehyde were observed. Ethyl propionate produced twice as much ethylene as ethyl lactate, but very little acetaldehyde. The additional hydroxyl group in ethyl lactate produced acetaldehyde such that the ratio of ethylene to acetaldehyde was ≈1:1. To test whether decomposition to non-equilibrium products occurs over noble metals, experiments were repeated in a furnace with uncoated ceramic foams. The results provide evidence that homogeneous decomposition of esters to intermediate acids can contribute to the overall CPO process. Products are highly tunable between synthesis gas and olefins by varying the fuel-to-oxygen ratio and catalyst. These products are highly dependent on the chemical structure of the original species, suggesting that, although equilibrium can be achieved at millisecond contact times, intermediate dehydration steps occur in the reactor environment.

3.2 Introduction

The ester and acid functional groups make up a considerable fraction of bio-oil for which significant experimental study remains.[90]

This chapter examines the catalytic partial oxidation of two ethyl esters, ethyl propionate and ethyl lactate (depicted in Figure 3.1). These esters differ only by a hydroxyl group (-OH) on the α' carbonate carbon, but provide sufficiently similar functionality to reveal details of the complex chemistry defining oxygenate reformation.

Ethyl Propionate is a simple ester of propionic acid and ethanol. Ethyl lactate is a similar ester of lactic acid and ethanol. All three of these constituents have been converted by CPO over noble metal catalysts: ethanol by Deluga et al[18]; propionic acid and lactic acid in Chapter 2.

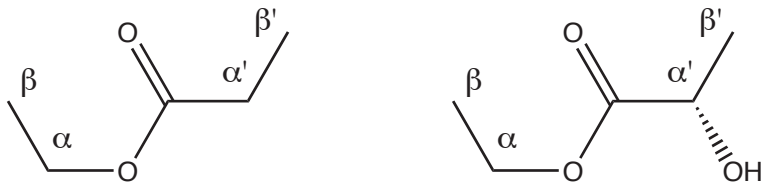

Ethyl Propionate Ethyl Lactate

Figure 3.1: Sketch of ethyl propionate (left) and ethyl lactate (right). Carbons are labeled beginning from the ester group outwards; the carbonate carbons are identified by the '. Ethyl lactate is identical to ethyl propionate with the inclusion of an OH group on the α' carbon.

3.2.1 Background on Esters

The investigation of ester catalytic partial oxidation was chosen for several reasons. First, as ethyl lactate finds more applications as a solvent, waste streams of spent solvent are becoming increasingly available. Many industries will burn off such solvents as a cheap means of disposal. Thus, waste ethyl lactate is a potentially free and growing resource.

Second, much of the current research into processing of biofuels converts low grade biomass

such as lignin and cellulose into various bio-oils. Similar oils such as black liquor are byproducts of the paper mill industry. These oils contain a great variety of oxygenated compounds, including many acids and esters. Esters make excellent model chemicals for more complex bio-oils.

Furthermore, research into CPO of biofuels must necessarily approach more complex mixtures of compounds as more practical biomass is considered. Already, research is underway in the reforming of wood chips and lignin.[50, 51] These types of feed-stock are made of complex polymers consisting of many oxygenated compounds. Here, again, esters and acids offer important insight into the reforming of more complicated structures.

Finally, of the renewable fuels already investigated for CPO, only the ester, biodiesel, had significant selectivity to olefins.[45] To replace fossil fuels, a renewable fuels industry must also produce chemicals. Furthermore, commodity chemicals can fetch higher prices than fuels. An integrated bio-refinery must produce both fuels and chemicals to be competitive. Thus, an investigation into simple esters and their potential for olefins is necessary.

Due to their high oxygen content, esters are excellent candidates for partial oxidation in order to better understand the complexities of low grade plant derived feed stocks, such as cellulose (Figure 3.2) and lignin (Figure 3.3), which are also oxygenated hydrocarbons containing ester linkages and acetal linkages similar to esters. Esters are also excellent index chemicals for understanding the reforming of bio-oils and other higher grade bio-derived feed-stocks.[91]

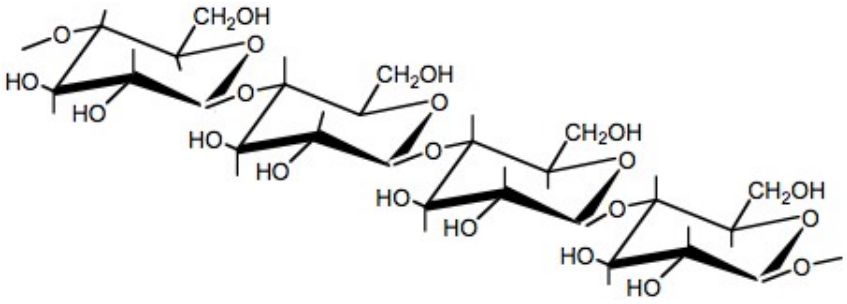

Figure 3.2: Cellulose is an oxygenated polymer with C–O–C–O groups similar to esters. From U. Tschirner presentation, September 2006.[92]

"Ester" comes from Essig-Ather, German for ethyl acetate.[93] Organic esters are sweet smelling, have high vapor pressures, and boiling points similar to water, depending on how large

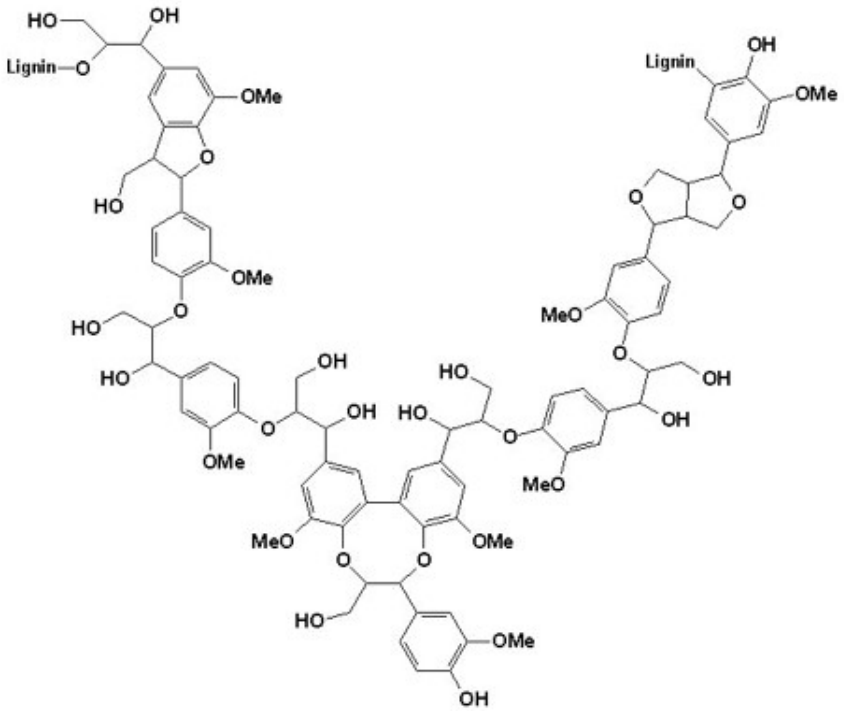

Figure 3.3: Lignin is an aromatic polymer with oxygenated bridges. From U. Tschirner presentation, September 2006.[92]

they are. Small esters have good flow characteristics, low viscosity, and can dissolve a wide variety of chemicals. Esters are highly oxygenated and clean burning. They make excellent organic solvents, can be polymerized, and are easy to synthesize from renewable feedstocks. In short, they are an ideal candidate as a chemical intermediate, chemical product, energy carrier, or liquid fuel from biorefining and are finding industrial application as such.[94]

Esters are naturally occurring. Ethyl lactate, for instance, is found in wine, fruits, and chicken,[93] and is regulated as an easily metabolized food additive.[95, 96] The alcohol used to make ethyl lactate, ethanol, is a broadly known chemical for consumption, and the acid used to make ethyl lactate, lactic acid, is common in dairy products.

Esters can be synthesized in a variety of ways. Typical reactants are carboxylic acids and alcohols - both of which can be renewably derived by fermentation. These reactants are combined by Fischer Esterification or alkylation. Esters are also intermediates in production: they can be used to synthesize other esters by reaction with alcohols.[97]

As demand grows for bio-derived chemicals, ester synthesis and the reagents required - alcohols and acids - are decreasing in price due to new commecial methods and commodities of scale.[98] For example, increased use of ethyl lactate as a commercial solvent has led to research into cheaper production methods. This research is taking place both in industry and the public sector:

> The Argonne process will enable the selling price of lactate esters to be cut in half, from about $1.60 - $2.00/lb to less than $1.00/lb.
>
> At such prices, it would be technically and commercially viable to use lactate esters in various formulations to replace of about 80% of the 3.8 million tons of solvents that are used in the United States each year. It could replace a range of environment-damaging halogenated and toxic solvents, including ozone-depleting chlorofluorocarbons, carcinogenic methylene chloride, and toxic ethylene glycol ethers and chloroform.[99]

In addition, the increased use of poly lactic acid (PLA) has led to cheaper methods of producing the monomer, lactic acid. Similarly, ethanol production is continuously increasing to satisfy the need for a clean burning fuel additive. Thus, the reaction process and the inputs are benefitting from commercialization and scaling. The advent of a comprehensive bio-derived chemical market will further decrease the price of oxygenated chemicals and fuels.[100]

3.2.2 Chemical Uses

Esters such as ethyl lactate are widely applied as organic solvents. Such solvents are "100% biodegradable, easy to recycle, non-corrosive, non-carcinogenic and non-ozone depleting."[101]

Replacing petroleum derived solvents with renewably derived esters stabilizes the price of production while simultaneously providing a better alternative for the environment, both in production and degradation after use.

Esters are making headway in plastics as well. PLA is "the first commodity polymer produced from annually renewable resources."[102] Since developing its first patents for PLA in the early 1990s, Cargill has innovated numerous methods of production.[103] PLA is very versatile, and can be used to make almost anything typically made out of plastics:

> Polylactic acid can be molded, vaccuum formed, blown or extruded to yield products typically made from petroleum-based conventional plastics.
>
> Plastic materials can be made from PLA and formed into grocery bags, pens, television cabinets and toys. So far, researchers haven't found anything made from conventional plastic resins that can't be made from PLA.[104]

Today there are several companies producing PLA plastics in the US and abroad, such as NatureWorks, a subsidiary of Cargill,[105] and BBCA Biochemicals[106] Esters are being used more and more commonly for their polymerization to renewable, biodegradable plastics. However, polymerizing esters is not entirely novel, as polyester has been a common component in the textile industry for decades, thanks to Wallace Carothers of DuPont.[107]

At $1 to $2 per pound (around $8.50 to $17 per gallon), ethyl lactate has yet to be considered as a commodity energy carrier. However, other esters are already used as fuels. Biodiesel is composed of the methyl ester of soy or vegetable oil.[108]

Because of their high oxygen content, esters in biodiesel burn very cleanly and without soot - an important consideration in light of increasing emissions standards. In addition, they have excellent fuel properties. Small esters are also beginning to find commercial application in biodiesel blends. Ethyl lactate, for instance can decrease the flash point of biodiesel without decreasing volatility. These features make small esters excellent choices to meet fuel requirements. Small esters can also decrease the pour point,[109] an important consideration for biodiesel which can gel in cold weather.

3.2.3 Equilibrium Products of CPO of Ethyl Esters

Both of these compounds can be converted to synthesis gas without significant heat generation.

Chemistry

Ethyl propionate is less oxidized than ethyl lactate; it has a greater internal C/O ratio. Converting ethyl propionate to syngas is weakly exothermic and is given by Equation 3.1:

$$C_5H_{10}O_2 + 1\frac{1}{2}O_2 \rightarrow 5CO + 5H_2 \qquad \Delta H^o \approx -100\frac{kJ}{mol} \tag{3.1}$$

Since this reaction is exothermic, autothermal reaction to exclusively syngas products is possible. This requires C/O = $\frac{5}{3}$ = 1.667. By contrast, the partial oxidation of ethyl lactate is given in Equation 3.2, and corresponds to a C/O of 2.5:

$$C_5H_{10}O_3 + O_2 \rightarrow 5CO + 5H_2 \qquad \Delta H^o \approx 80\frac{kJ}{mol} \tag{3.2}$$

This is slightly endothermic due to the higher oxidation state of ethyl lactate. The energy required to maintain high temperature autothermal operation comes from the production of some complete oxidation products, H_2O and CO_2, The combustion of ethyl lactate is depicted in Equation 3.3.

$$C_5H_{10}O_3 + 6O_2 \rightarrow 5CO_2 + 5H_2O \qquad \Delta H^o \approx -2550\frac{kJ}{mol} \tag{3.3}$$

This exothermic chemistry maintains operation at temperatures greater than 600 ^{o}C, permitting complete conversion to equilibrium products in ≈10 milleseconds, and corresponds to C/O ≤ $\frac{5}{12}$ = 0.417. Combustion of one molecule of ethyl lactate provides sufficient enthalpy to drive the partial oxidation of roughly 30 molecules of the same.

Similarly, the complete combustion of ethyl propionate takes place at a C/O ≤ $\frac{5}{13}$ = 0.385 according to Equation 3.4.

$$C_5H_{10}O_2 + 6\frac{1}{2}O_2 \rightarrow 5CO_2 + 5H_2O \qquad \Delta H^o \approx -2700\frac{kJ}{mol} \tag{3.4}$$

Surface Chemistry

The partial and full oxidation chemistries are likely to take place heterogeneously. The ester active group has two oxygens which can bond to a catalytic surface: the ether oxygen bridge and the ketone, each of which have lone pairs that can interact with an electrophilic metal. The strength of the ether bond, O–C, makes its scission a high energy rate limiting step. Reaction is more likely to proceed through the ketone, which has two methods of first contact with the surface. The ketone can adsorbe via the η^1 conformation, Figure 3.4A, through the lone pair electrons on the O. Alternatively, the η^2 conformation, Figure 3.4B involves bonding of the π-bonds on the carbonyl to the surface which is strengthened by backbonding into the π^* orbital, and leads to greater decomposition than the η^1 conformation, which is observed to desorb at low temperatures.[110, 111]

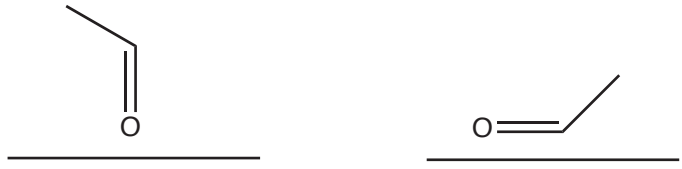

A: η^1 Conformation B: η^2 Conformation

Figure 3.4: Adsorption conformations of the carbonyl (C=O) group. The η^1 conformation adsorbs via free electrons on the O; the η^2 via the π bond.

On oxygen predosed surfaces, back-bonding through the π^* orbital is diminished which decreases the stability of this conformation with respect to η^1.[43] Similarly, in coadsorption experiments with aromatics, η^2 bonding is diminished, though η^1 bonding becomes stronger.[112] Thus, electron distribution on the surface affects the adsorption of the carbonyl and subsequent reaction of the molecule.

Observations indicate that esters adsorb onto Ni(111) at low temperatures through the carbonyl oxygen in the η^1 configuration.[113] The adsorbed species does not cleave to form a carbonate as an adsorbed intermediate, which prevents the decarboxylation pathway described for acids in Chapter 2. Rather, decarbonylation occurs to form CO and alkoxy species. Syngas is the main desorption products of smaller esters (methyl formate, methyl acetate) on Ni(111).

However, CO_2 can be made if oxygen is on the surface and bonds to the available CO.[114, 115] On Ag(110), methyl formate does form a formate species, but only in the presence of surface oxygen, so decarboxylation is a possible route to CO_2 production.[78] For formate esters, the limiting step for heterogeneous ester decomposition was identified as the cleavage of the H–CO bond on the formate group. Heavier formate and propionate esters have a stronger C–CO bond which complicates their decomposition pathways.

For ethyl lactate, the presence of the hydroxyl group alters the electronegativities of carbon atoms which alters C–metal bond strengths.[111] However, the α'-hydroxyl group also provides an alterative site for surface chemistry to initiate. Alcohol adsorption was described in Chapter 1, and in the case of ethanol and higher alcohols on Rh surfaces, can proceed via an oxametallocycle, which have been identified exerimentally.[44] Five membered cycles are very stable, but four membered cycles are possible as well.[116] Six membered rings and higher are proposed as well, and the affinity of the surface for oxygen indicates such a cycle is a likely intermediate.[117]

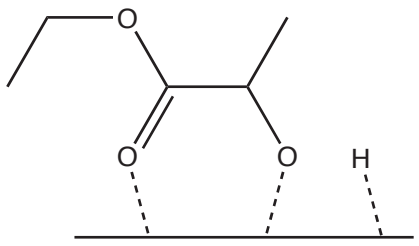

Figure 3.5: 6-Membered metallocycle of adsorbed ethyl lactate

Adsorption for ethyl lactate probably initiates via two main competing sites, on the alcohol and on the ester aldehyde. As substitution groups increase metallocycle stability, the ester carbonyl is a good candidate to initiate reaction.[116] In either case, the other site can then adsorb, forming a six membered ring with two surface metal atoms, and the ester can decompose simultaneously from each side. For the acid portion of the ester, another metallocycle in the manner of ethanol could be formed. However, decomposition is very rapid and the molecule need not have multiple cycles simultaneously.

Ethyl lactate can dehydrogenate to ethyl pyruvate by catalytic oxygenation. This process requires low temperatures, 250 – 300 ^{o}C, and Ag-Pd/SiO_2 catalysts.[118] A reverse process is

also documented: hydrogenation of ethyl pyruvate to ethyl lactate. This latter process occurs over Pt/SiO_2 at 10 ^oC.[119] Further discussion on dehydrogenation of fuels in CPO due to heterogeneous chemistry can be found in Chapter 4.

At high temperatures, catalytic products of ethyl lactate are probably exclusively syngas products with some CO_2 and H_2O, due to the high oxygen content in the molecule. Other species, except perhaps methane, do not desorb in any significant quantity.

For esters that pyrolize to acids and olefins, as discussed in the next section, ethylene may not adsorb as frequently as the many oxygenated species competing for surface sites. Lactic acid and propionic acid, on the other hand, may adsorb via the carbonate as the acidic hydrogen is removed at the surface as described in Chapter 2.

3.2.4 Non-Equilibrium Products

At the high temperatures of autothermal operation, the contribution of gas-phase chemistry cannot be neglected. Evidence for significant gas-phase chemistry under CPO conditions has been observed by increasing the C/O ratio, such that non-equilibrium intermediates resulting from homogeneous chemistry exit the reactor before decomposition on the catalyst surface.[64] Under these conditions, the slight variation between fuel molecules provides details of the origin of each intermediate, as well as the overall mechanism.

Homogeneous oxidation of esters does not distribute the oxygen atoms to carbon atoms near the ester group. Rather, 78% of the ester linkage remains bonded to the ester carbon, which decarboxylates.[120] Thus, even in the presence of O_2, it is expected that ester decomposition chemistry can occur homogeneously in CPO conditions.

Decomposition of esters has been studied extensively and proceeds typically through a six-membered ring transition that does not require free radical chemistry[121, 122] as described in Figure 3.6. Competing free-radical processes can explain minor products of ester decomposition.[88] These processes are probably promoted by oxidation. However, shutting down radical chemistry by pyrolysis in the presence of toluene to quench free radicals reveals that the acids and olefins form from esters in a mechanism that does not require radical chemistry.[89] While the possibility of a mechanism explained by radical chemistry was initially proposed,[123] more recent analysis concludes that esters break down into acids and olefins in a semi-concerted process. Decomposition is not perfectly concerted, and the bond movements do create some carbonium ion characteristic.[124] The speed of the relative bond

movements also indicates a direction about which the ester decomposes.

Ethyl Esters

Ester decomposition takes place in the gas phase.[125] Catalysts do not play a major role except for possibly promoting electron transfer within the molecule.[126]

Ethyl esters in particular have been shown to undergo gas phase decomposition to acids and olefins.[83] Indeed, as early as 1883, Kraft explored the possibility of producing olefins from esters.[127] For example, ethyl-acetate unimolecular decomposition was observed to produce ethylene and acetic acid.[85]

Ethyl and higher esters break into their constituent acid and an olefin made from the alcohol group, while methyl esters and esters without β-hydrogens are more thermally stable and may undergo a completely different reaction mechanism.[127, 123]. Their innability to form a 6-membered ring intermediate explains why methyl esters are much more stable than ethyl esters. The presence of a β-hydrogen is essential to the semi-concerted mechanism.[83]

Recent research suggests that the unimolecular decomposition of ethyl propionate to propionic acid and ethylene are fast enough to precede the combustion of the ester.[128]. Furthermore, at high temperatures, unimolecular processes increase disproportionately to other processes. Thus, unimolecular processes are favored as a side reaction under CPO conditions. In addition, experiment and modeling of the combustion of methyl esters, which is not unimolecular, suggest that the presence of oxygen promotes "chaining", which favors olefin production.[129] These observations indicate that gas phase chemistry favors routes that proceed through olefin formation.

The thermal cracking of ethyl propionate, described in Equation 3.5 and Figure 3.6, could produce an intermediate, propionic acid (which could then undergo additional decomposition to ethylene, as described in Chapter 2).

$$C_5H_{10}O_2 \rightarrow CH_3CH_2COOH + C_2H_4 \tag{3.5}$$

Hydroxy Esters

The addition of a hydroxyl group to the α'-propionate carbon should result in different chemical intermediates, indicative of the overall decomposition mechanism. Thermal decomposition of

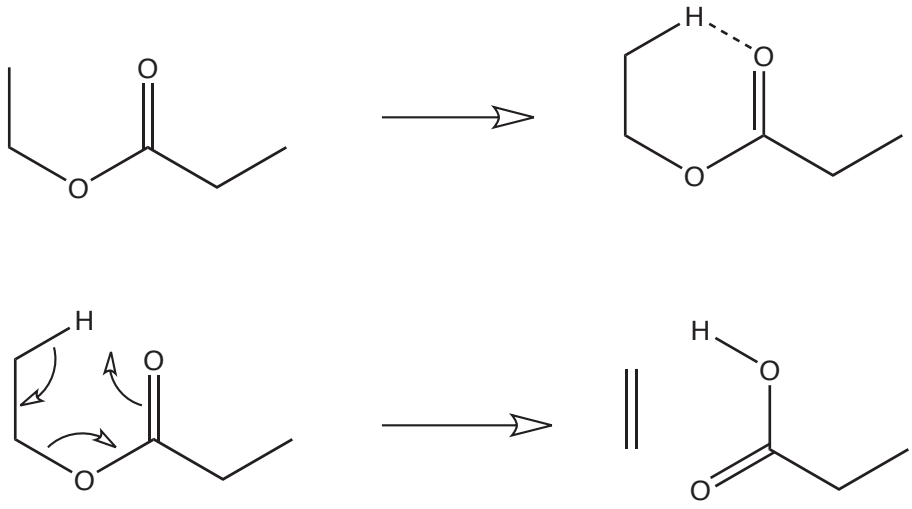

Figure 3.6: 6-membered ring decomposition of esters. Adopted from [130]

ethyl lactate could proceed through a lactic acid intermediate,

$$C_5H_{10}O_3 \rightarrow C_2H_4 + CH_3CHOHCOOH \tag{3.6}$$

which could continue to decompose to acetaldehyde as described in Chapter 2.

While few studies have explored α'-hydroxy esters, many researchers have examined β'-hydroxy esters. The thermal decomposition proceeds via a six membered ring involving the ester ketone and hydroxy group as shown in Figure 3.7, and is faster than the typical decomposition for an ethyl ester.[131, 83, 132]

The well-positioned reactive hydroxyl group promotes this secondary reaction. Six membered rings of the ester ketone and a hydroxy group can proceed to decomposition in other conformations as well. The six-membered transition state is highly favorable for such unimolecular reactions.[133]

Although ethyl lactate does not have a β'-hydroxyl group ideally placed to form a six-membered ring, it does have an α'-hydroxyl group positioned for the less favorable five membered conformation. Hydrogen bond analyses suggest that this five-membered ring does stabilize the molecular arrangement of such esters.[134, 135]. In addition, cyclic conformations

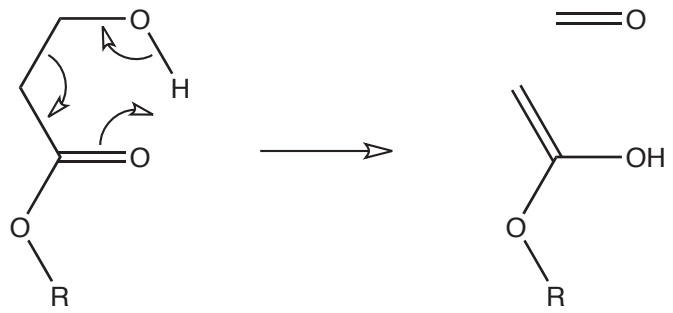

Figure 3.7: Pyrolysis of β'-OH esters.[83]

involving the hydroxy group and the ester linkage oxygen are also observed. While decomposition through either of these arrangements may be less stable than for β'-hydroxy esters, they could still compete with the ethyl ester decomposition described above. Five and three membered rings are proposed for pyrolysis of similar groups. Indeed, in the pyrolysis of α'-keto-esters, five-membered ring transitions are implicated.[73]

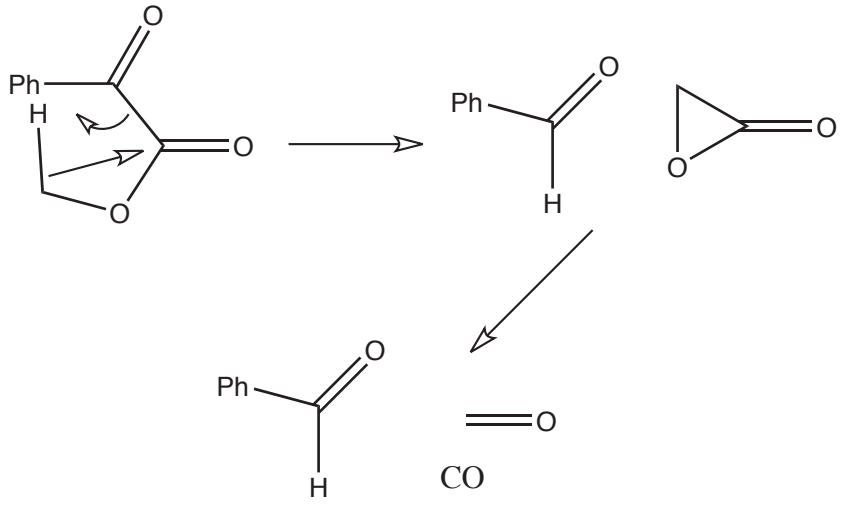

Figure 3.8: 5-Membered ring transition, followed by 3 membered ring, for pyrolysis of a methyl ester.[73]

Alternatively, the ester could decompose via the same six membered ring transition state as described above (and shown in Figure 3.9), a five-membered intermediate being strained in

comparison, and other proposed six membered states being undocumented.

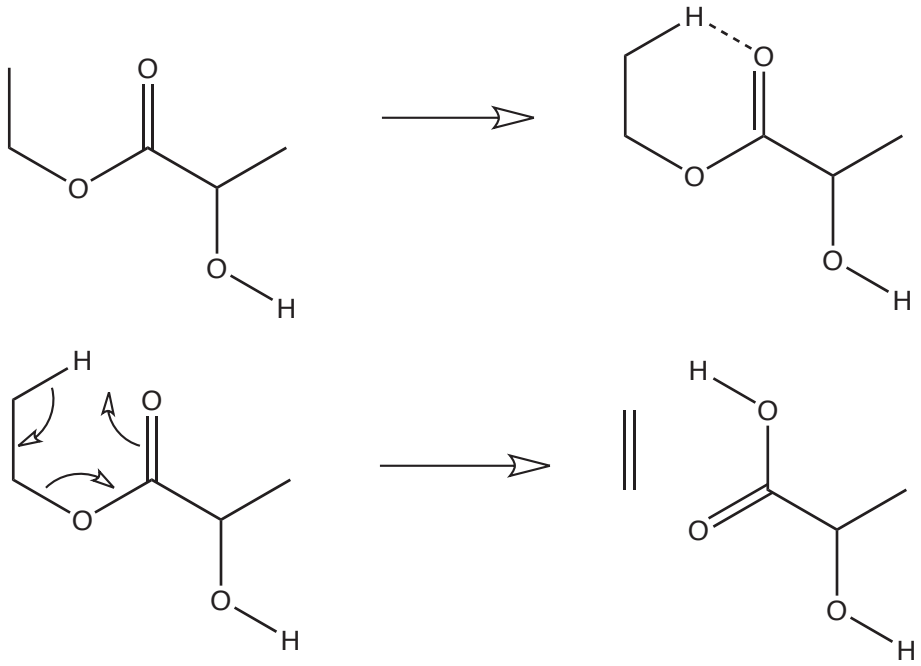

Figure 3.9: Conventional 6 membered intermediate for pyrolysis of ethyl lactate producing lactic acid and ethylene.

The result of such decomposition is lactic acid and ethylene. The expected products should thus be very similar to those observed for ethyl propionate, with the exception that lactic acid will proceed to acetaldehyde while the propionic acid produced ethylene.

These mechanisms were explored with experiments performed on Rh-based catalysts with the addition of Ce or La, which have been shown to increase selectivity to synthesis gas and reduce side-products.[64, 136] Pt catalysts, which have been shown to be selective to olefins,[137] have been considered for comparison. Additionally, the thermal decomposition of the selected esters on blank supports has been examined to provide evidence for the mechanism of gas-phase ester decomposition.

3.3 Experimental

Catalyst preparation is the same as described in Chapter 2. Four different metal loadings were examined: rhodium (Rh 5 wt%), rhodium and cerium (Rh-Ce 2.5 wt% each), rhodium and lanthanum (Rh-La 2.5 wt% each) and platinum (Pt 5 wt%). All catalysts were applied using the incipient wetness impregnation technique: Rh was deposited in solutions of $Rh(NO_3)_3$ salt in water, Ce as $Ce(NO_3)_3{\cdot}6H_2O$, La as $La(NO_3)_3{\cdot}6H_2O$, and Pt as PtH_2Cl_6.

Ethyl lactate (>99%, Nature Works, bp 155 ^{o}C) and ethyl propionate (>99%, Acros, bp 98 ^{o}C) are liquids at room temperature but can be vaporized upstream of the catalyst. The CPO of these fuels made use of the same apparatus as described in Chapter 2, a detailed image of which appears in Figure 2.6.

Experimental runs for the esters were at least 15 hours, during which time the reactor experienced several start-ups and shut-downs. Temperatures ranged from 600 ^{o}C to 1200 ^{o}C, limited in the cold regime by poor conversion and in the hot regime by the possibility of sintering the metal loaded on the monolith.

For experiments over blank alumina foams, the same reactor setup was used except that the catalyst was replaced with an uncoated foam monolith. In addition, heating tape and insulation were replaced with a temperature controlled insulated heating coil. No O_2 was present for these experiments. Due to the longer heating element, contact times for the blank foams are $\tau \approx 0.5$ seconds.

Data is presented in terms of conversion and atomic product selectivities as defined in Chapter 2. Error bars again represent one standard deviation based on pooled averages.

Equilibrium data was calculated using the software package ChemKin 3.7. Heat transfer to the reactor was ignored and pressure set to 1 atm to model adiabatic conditions. Inputs included fuel, N_2, O_2, and input (upstream) temperature, which is taken as an average of all upstream temperatures for a given C/O. Equilibrium products considered were CO, CO_2, H_2, H_2O, CH_4, O_2 and N_2. ChemKin calculated equilibrium products and quantities depicted in the data.

3.4 Results

Conversion at C/O < 1.7 for both esters was >98% and >80% at all C/O. (Figure 3.10) For C/O < 1.1, autothermal reaction took place at temperatures just above 1100 ^{o}C. For ethyl lactate

at C/O < 1.2, Pt exhibited the highest temperatures of the four catalysts, while it had the lowest temperatures of all four catalysts for ethyl propionate at all C/O, reaching 1000 ^{o}C in the most oxygen rich regime. Temperatures dropped by 100 ^{o}C between 1.1 < C/O < 1.4. Temperatures as low as 650 ^{o}C at C/O = 2.5 were observed. For ethyl lactate over a Pt catalyst, temperatures were 200 ^{o}C lower. Steady state was obtained for these values, but any higher C/O extinguished the reaction.

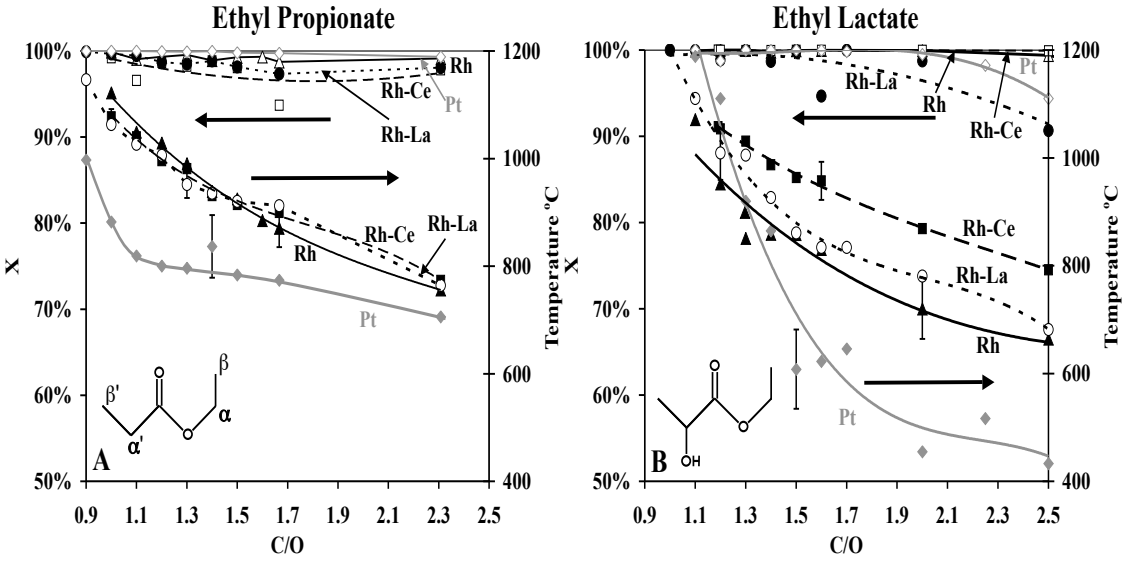

Figure 3.10: Conversion (X) and backface temperatures observed during the CPO at various C/O of ethyl propionate (Panel A), and ethyl lactate (B). The bottom left corner of each panel depicts the compound. Lactic acid has the same structure as propionic acid with an additional hydroxyl group (OH) on the α' carbon. Rh (△), Rh-Ce (□), Rh-La (●), Pt (◇) show conversion (left axis); Rh (▲), Rh-Ce (■), Rh-La (○), Pt (◆) show backface temperatures (right axis). Contact times: $\tau \approx 10$ ms. Pt temperatures are lower than the Rh-based catalysts except at C/O < 1.3 for ethyl lactate. Temperatures rise at lower C/O as a result of more exothermic oxidative chemistry. Conversion is >98% for C/O < 1.7 and >80% at all C/O.

Generally, the partial oxidation of esters proceeded to near equilibrium syngas for C/O < 1.2. Selectivity to olefins increased to ≈30% for C/O > 1.5. The production of equilibrium products

(C_1 species, H_2 and H_2O) and olefins will be discussed separately.

3.4.1 Equilibrium Products from Esters: CO, CO_2, H_2, H_2O, CH_4

For C/O ≤ 1.1, selectivity to CO was ≈80%, which is near equilibrium, for both esters on all Rh catalysts (Figures 3.11 A & B). Selectivity to H_2 was ≈60%, which is within 10% of equilibrium under the same conditions, with Rh-Ce exhibiting the highest selectivities to CO and H_2 (Figures 3.11 C & D). Pt exhibited lower selectivities by up to 20% for CO and as much as 35% for H_2. Syngas production declined at higher C/O for all four catalysts. At C/O ≥ 2.0, selectivity to CO was as low as ≈20%; selectivity to H_2 as low as 10% on all four catalysts for both fuels.

Combustion products did not decline with an increase in C/O as rapidly as syngas products. CO_2 declined gradually from 20% at C/O = 1.1 to 10% at C/O ≥ 2 (Figures 3.12 A & B). Selectivity to H_2O remained relatively consistent at 40% for both esters at all C/O (Figures 3.12 C & D).

Selectivity to methane is shown in Figure 3.13 E and F. Methane production reaches a maximum of 5% for ethyl propionate at C/O = 1.2 and 10% for ethyl lactate at C/O = 1.5.

3.4.2 Non-Equilibrium Products: Ethylene, Acetylene, Acetaldehyde

At C/O > 1.3, Pt produced the highest selectivity to olefins from all fuels, though Rh-La exhibited slightly higher selectivity to ethylene for ethyl lactate with C/O ≥ 1.7 (Figure 3.14 A & B). Ethylene derived from ethyl propionate reaches 35% selectivity on Pt. Ethylene derived from ethyl lactate reaches 22%. At C/O ≤ 1.0, selectivity to ethylene from ethyl propionate is as low as 5% on Rh-La. Selectivity to ethylene from ethyl lactate under the same conditions is <1%.

Selectivity to acetylene reached 8% from ethyl propionate and 2% from ethyl lactate at the high temperatures corresponding to C/O < 1.4. Pt exhibited the highest selectivity to acetylene from both fuels.

Selectivity to acetaldehyde did not exceed 2% at any C/O from ethyl propionate on any of the four catalysts. By contrast, selectivity to acetaldehyde at C/O > 2.0 was >20% on all four catalysts for ethyl lactate. Rh-La exhibited the highest selectivity, nearly 30% at C/O = 2.5.

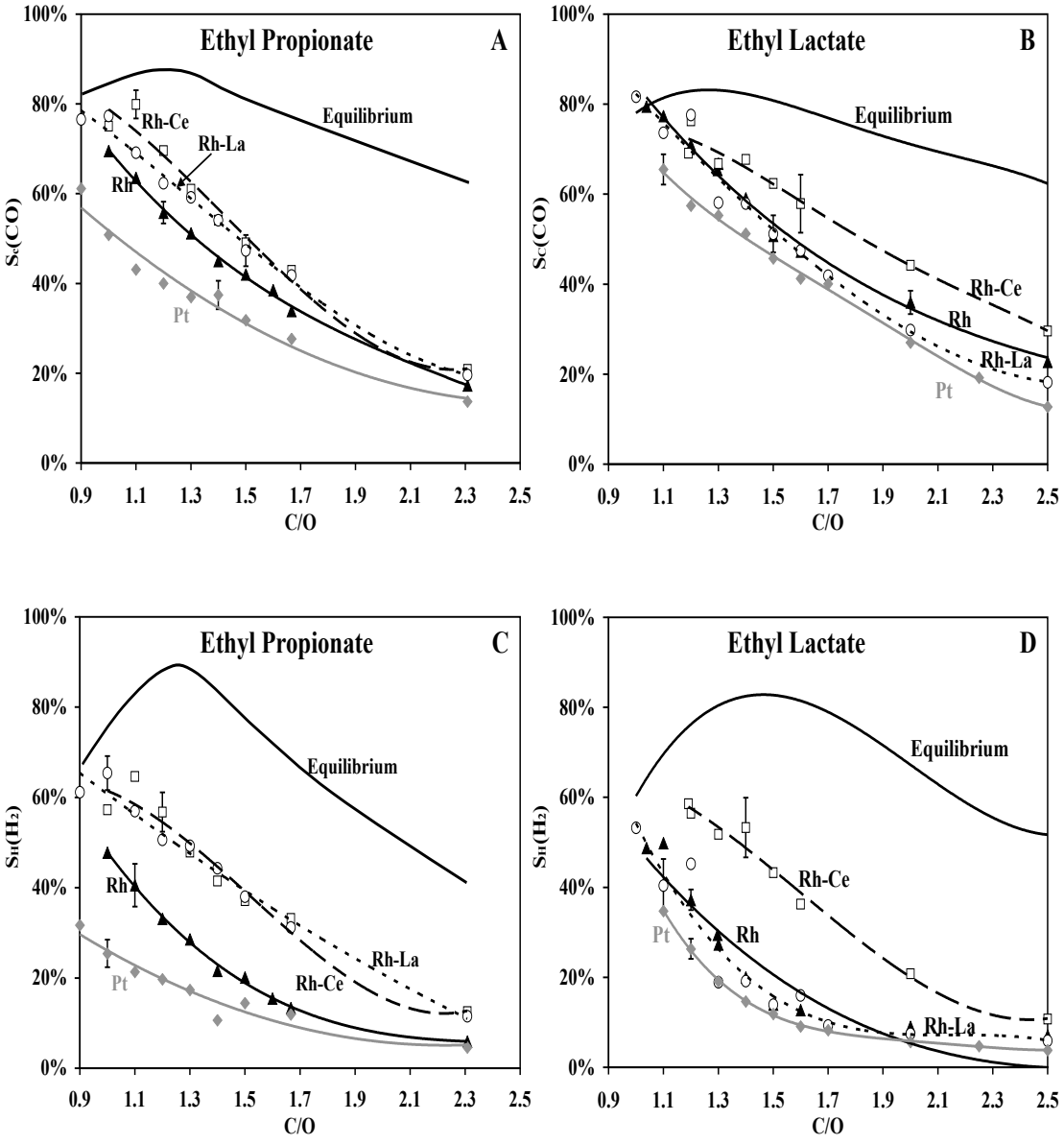

Figure 3.11: Selectivities to syngas products from ethyl propionate (left column) and ethyl lactate (right column) over four catalysts: Rh (▲), Rh-Ce (□), Rh-La (○), Pt (◆). Carbon selectivity to CO (S_c(CO)) is depicted in panels A and B; hydrogen selectivity to H_2 ($S_H(H_2)$) in panels C and D. For C/O < 1.1, Rh-Ce and Rh-La exhibit near-equilibrium selectivities to CO and H_2. At higher C/O > 1.2, selectivity to syngas products decreases away from equilibrium. Pt exhibits consistently lower selectivity to syngas products than Rh-based catalysts.

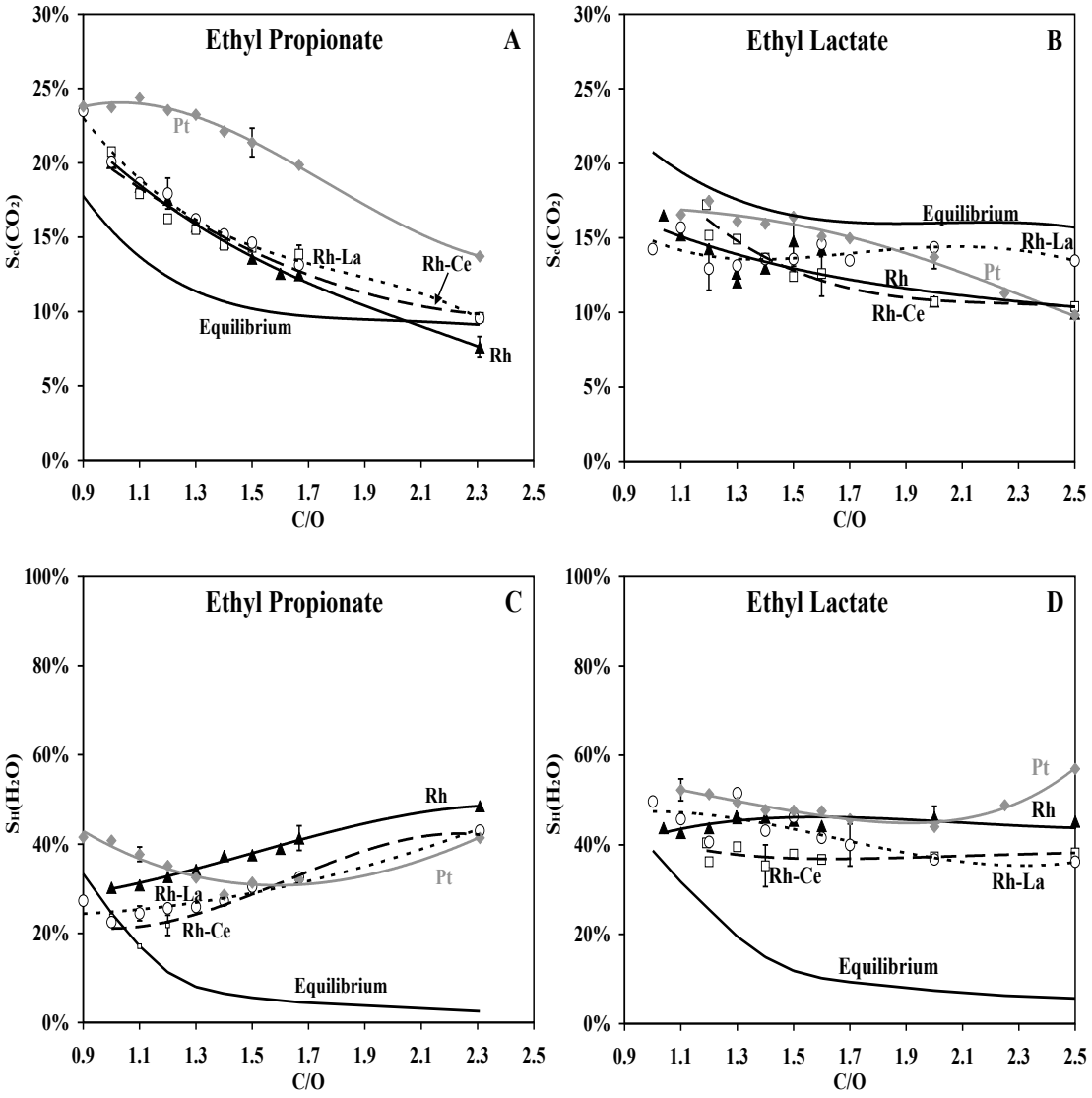

Figure 3.12: CPO of ethyl propionate (left column) and ethyl lactate (right column) selectivities to combustion products over Rh (▲), Rh-Ce (□), Rh-La (○), Pt (◆). Panel A shows carbon selectivity to CO_2 from ethyl propionate. Panel B shows carbon selectivity to CO_2 from ethyl lactate. Panels C and D show hydrogen selectivities to H_2O from ethyl propionate and ethyl lactate, respectively. Pt exhibits the highest selectivities of all catalysts to combustion products for C/O < 1.3 on both fuels.

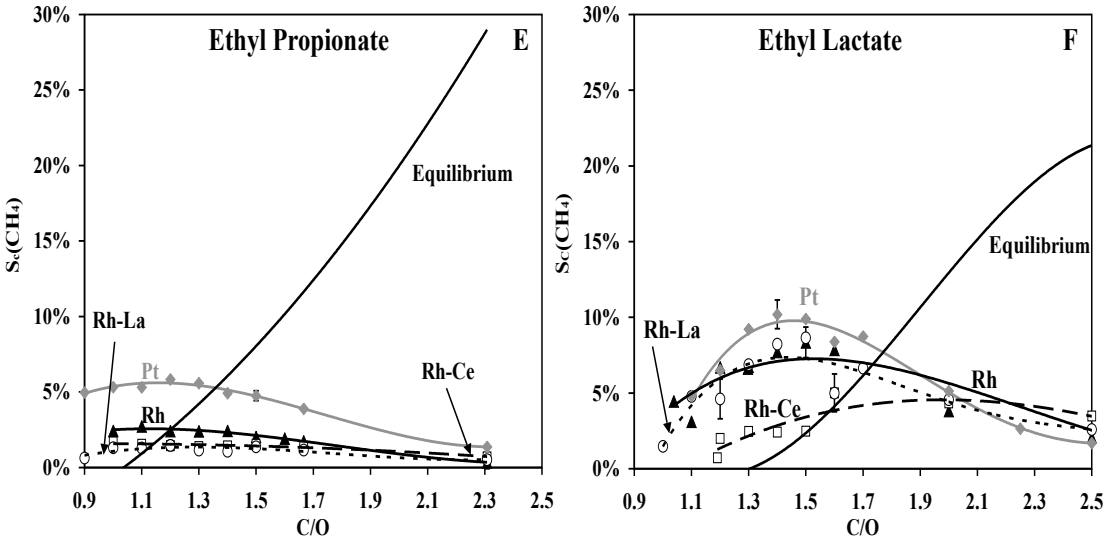

Figure 3.13: CPO of ethyl propionate (left column) and ethyl lactate (right column) selectivities to methane over Rh (▲), Rh-Ce (□), Rh-La (○), Pt (◆). Panels E and F depict carbon selectivity to CH_4 from ethyl propionate and ethyl lactate, respectively. Selectivity to CH_4 peaks at 10% at C/O ≈ 1.4 for both fuels.

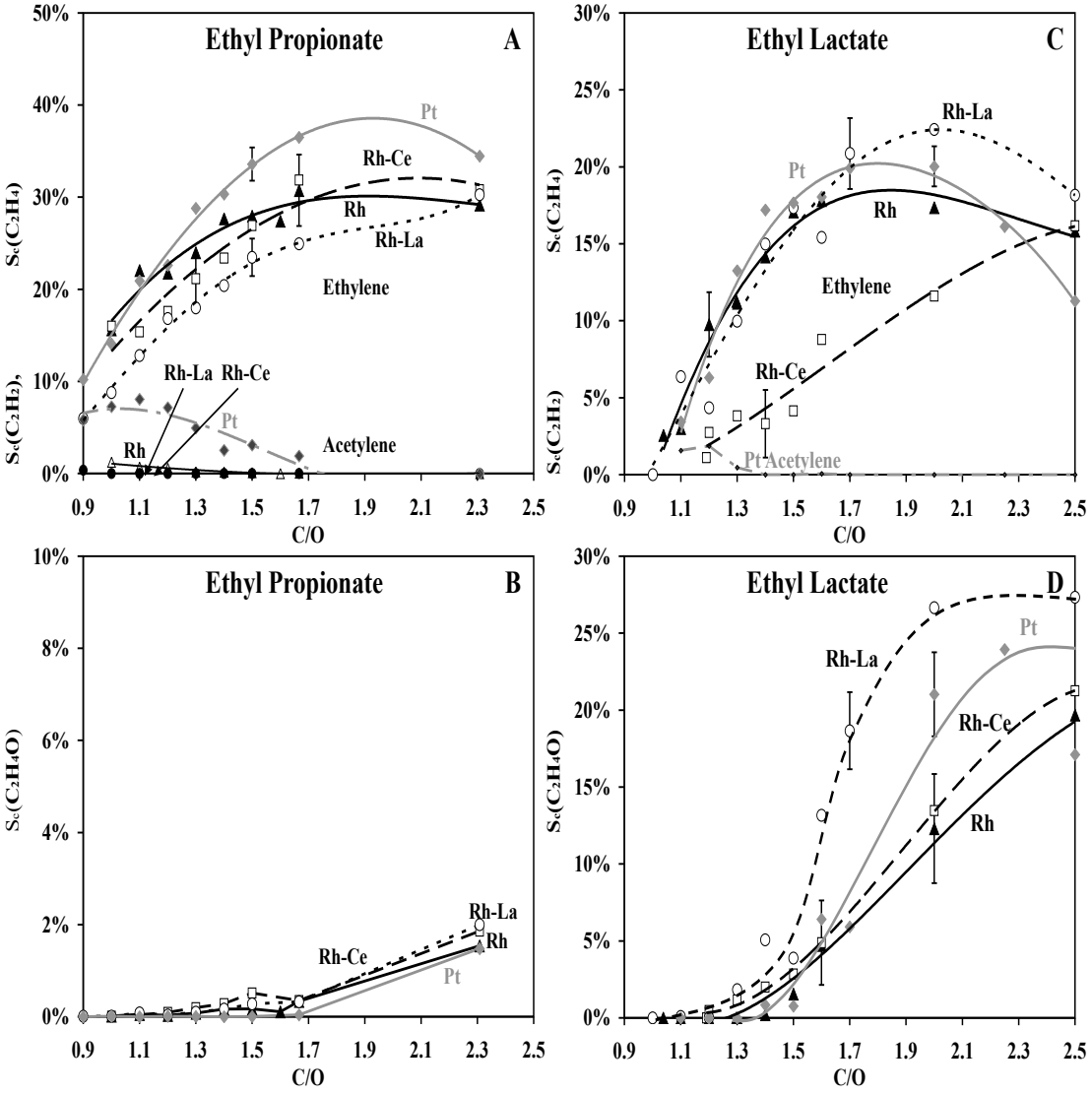

Figure 3.14: Non-equilibrium products from the CPO of ethyl propionate and ethyl lactate. All products are shown as carbon selectivities; ethyl propionate results are depicted in the left two panels and ethyl lactate results in the right two panels for all four catalysts, Rh (▲), Rh-Ce (□), Rh-La (○), Pt (◆) (note the scales for the y axes). Panel (A) shows selectivity to ethylene (C_2H_4) and acetylene (C_2H_2) by reforming of ethyl propionate and panel (B) shows selectivity to these products from ethyl lactate. Panels (C) and (D) depict selectivity to acetaldehyde (C_2H_4O) from ethyl propionate and ethyl lactate. Ethyl propionate produces nearly twice as much ethylene as ethyl lactate (A & B). However, ethyl lactate produces acetaldehyde and ethylene in close to 1:1 ratio (B & D), while ethyl propionate shows negligible selectivity to acetaldehyde (C).

3.4.3 Temperature Controlled Uncoated Foam Experiments

To examine the role of homogeneous chemistry, the catalyst was replaced with an uncoated foam monolith. To provide heat, these experiments were carried out in a temperature controlled furnace between 600 ^{o}C and 950 ^{o}C in an N_2 atmosphere without O_2. Data points in Figure 3.15 each represent a single run, rather than averages of several runs as in the case of the autothermal catalytic experiments. Due to the length of the furnace, the contact time was $\tau \approx 0.5$ seconds, an order of magnitude greater than the contact time for CPO.

Conversion of ethyl lactate was >97% for all temperatures. For ethyl propionate, conversion was >94% for temperatures >670 ^{o}C. Conversion dropped to 69% at 600 ^{o}C.

Selectivities to most observed species - C_1 and C_2 products, H_2 and H_2O - from the temperature controlled experiments are detailed in Figure 3.15 A and B. From ethyl propionate, selectivity to ethylene peaked at 62%, while 10% selectivity to acetylene was observed. No acetaldehyde was observed. In contrast, for ethyl lactate, selectivity to acetaldehyde peaked at 40% and steadily dropped with an increase in temperature, and selectivity to ethylene was approximately 30% throughout the temperature range.

Selectivity to CO from ethyl propionate increased from 5% at 600 ^{o}C to 20% at 750 ^{o}C. For ethyl lactate, CO increased linearly from 22% at 600 ^{o}C to 40% at 925 ^{o}C. This linear increase has approximately the same slope as methane, which increased from 3% to 15%. Ethyl propionate exhibited 10% selectivity to propionic acid. No lactic acid was observed from the reforming of ethyl lactate, but ethanol was observed at temperatures <750 ^{o}C. CO_2 for both experiments was <10% at all temperatures. Very little CO_2 was observed from ethyl lactate.

3.5 Discussion

At low C/O, both fuels produced high selectivity to synthesis gas. Conversely, at high C/O, selectivity to non-equilibrium products such as ethylene and acetaldehyde increased significantly. The product selectivity is highly tunable between C_1 gasification products and non-equilibrium olefinic products.

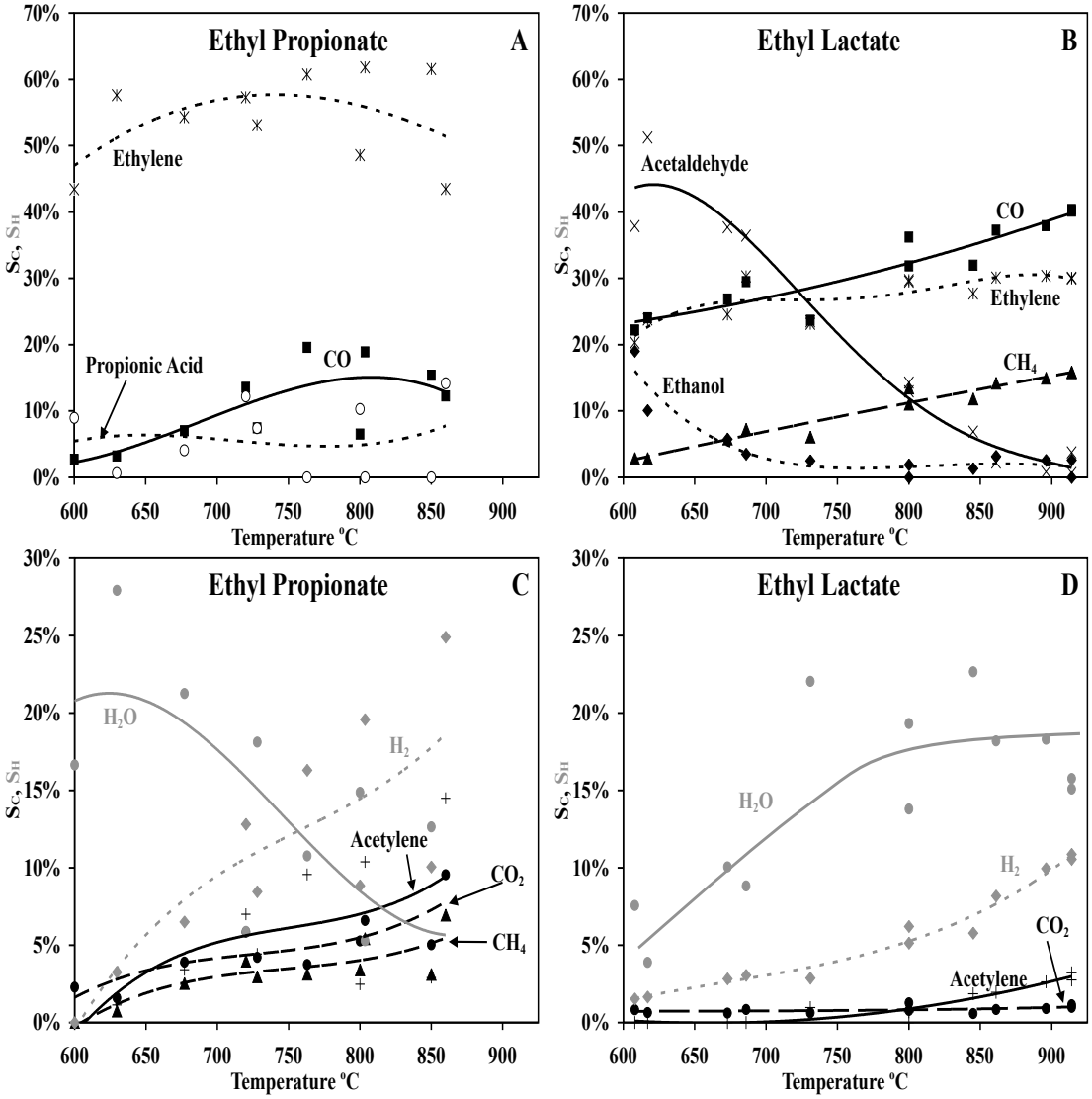

Figure 3.15: Blank foam, temperature controlled experiments for ethyl propionate (left) and ethyl lactate (right) were performed in an N_2 environment. Shown are most observed species: ethylene (∗), acetaldehyde (×), CO (■), ethanol (◆), CH_4 (▲), propionic acid (○), H_2O (●), H_2 (◆), C_2H_2 (+), CO_2 (●). Selectivity to CO_2 is <10%, indicating gas phase decarboxylation is unlikely, while selectivity to CO is near 20%, which suggests gas phase decarbonylation. For ethyl propionate, lower selectivity to CO is accompanied by propionic acid which did not decarbonylate, perhaps due to the low temperatures. For ethyl lactate, selectivity >20% to CO accompanies an increase in methane and a decrease in acetaldehyde, suggesting decomposition of the acetaldehyde.

3.5.1 Equilibrium Products and Surface Chemistry

As shown in Figure 3.10, conversion of both esters was >98% at all C/O ratios examined. This is likely due to the fact that ethyl esters readily thermally decompose in the gas phase even before they interact with the catalyst. The resulting acids react readily on the catalytic surface due to the ease with which the acidic hydrogen is cleaved.[43] Consistent with >98% conversion, autothermal reforming temperatures for oxygenates tend to be very hot (>800 ^{o}C) for C/O < 1.3 (Figure 3.10).

The data in Figures 3.11 suggest that both esters reform to equilibrium products similar to other small oxygenated fuels such as ethanol or glycerol,[47, 64] especially at C/O < 1.3, where selectivity to synthesis gas is very near to equilibrium for Rh based catalysts. The esters examined in this study proceeded to just below equilibrium at these C/O. Adding a washcoat to the catalyst has been shown to increase selectivity to syngas products,[138] though no washcoat was applied for these experiments. With the addition of a washcoat, it is likely that CPO of esters would proceed to equilibrium for C/O < 1.1.

Temperature programmed desorption (TPD) studies of esters on Ni(111) by Zahidi et al suggest that esters adsorb preferentially via the carbonyl group in the η^1 conformation and that they decompose via decarbonylation (lose CO) on the metallic surface.[113] However, Figures 3.12 A and B show 20% selectivity to CO_2 at C/O < 1.3, which is characteristic of a surface mechanism involving decarboxylation (lose CO_2) rather than decarbonylation. This disparity is likely due to the difference in operating conditions.

The conditions of the TPD studies are lower operational temperatures (≈20 ^{o}C) than those observed in autothermal CPO (≈800 ^{o}C), and were studied over different catalysts (Ni(111) rather than Rh or Pt). These reaction conditions are very different from those in the experiments described in this paper. Most importantly, ethyl esters undergo significant thermal decomposition in the gas phase, which can change the reactant prior to adsorbing on the catalytic surface. In contrast, in TPD experiments, the esters are adsorbed at low temperatures and do not thermally decompose. While TPD studies can lend insight into how the esters may adsorb onto the catalytic surface, they do not indicate the gas phase decomposition that can occur under CPO conditions. The observations described in this paper indicate that the main CPO decomposition pathway might be gas phase thermal decomposition of the ester and catalytic decomposition of the remaining products.

If esters decompose thermally before catalytic reaction, then a significant fraction likely

adsorbs as acid by cleaving the acidic hydrogen to form a surface carboxylate.[43] The carboxylate could form CO_2 which then desorbs. This leaves the rest of the molecule to react in a fashion similar to other fuels such as ethanol, by severing C-C or C-O bonds while reacting with other surface species, depending on the noble metal.[43] Syngas, methane, and combustion products desorb. Additionally, water-gas shift is likely present under these operating conditions providing an alternative surface mechanism to adjust the ratio of CO to CO_2.[79]

The selectivity to CO_2 is relatively constant at ≈20% for both fuels (Figures 3.12 A and B), revealing evidence of the ester reforming mechanism. For the five-carbon esters studied in this work, 20% selectivity to CO_2 for most C/O ratios suggests a surface mechanism involving decarboxylation (lose CO_2) of the ester linkage. Temperature programmed desorption experiments indicate that esters prefer to decarbonylate (lose CO) on noble metal catalysts,[113] while acids decarboxylate via adsorbed carbonate species under similar conditions.[43, 76] Since 1 in 5 atoms in the fuel form CO_2 at C/O < 1.3, the surface mechanism may proceed through an acid intermediate that decarboxylates. In the acid CPO experiments, selectivity to CO_2 was about >33% (Figure 2.8), consistent with a surface mechanism involving decarboxylation of the 3-carbon acids.

At C/O > 1.5, selectivity to CO_2 decreases for both esters (Figure 3.12), as it did for both acids in Chapter 2, Figure 2.8). This phenomenon is accompanied by increases in olefins and aldehydes, probably products of gas-phase chemistry. Thus, with an increase in C/O, surface chemistry decreases in favor of gas phase chemistry and surface decarboxylation decreases in favor of a gas phase decarbonylation mechanism.

3.5.2 Non-Equilibrium Products and Homogeneous Chemistry

Homogeneous chemistry has been used to explain the production of olefins from the CPO of alkanes.[35] This is consistent with the high selectivity to ethylene and acetaldehyde observed in the blank foam temperature controlled experiments with ethyl propionate and ethyl lactate as fuels, suggesting that homogeneous chemistry could also be responsible for olefin formation from oxygenates. Furthermore, esters are known to decompose to olefins and acids as described in the introduction to this chapter. This reaction has been established to proceed through a unimolecular six-membered transition state shown in Figure 3.16.[83, 127]

The amount of ethylene differed considerably between the two esters as shown in Figures 3.14 and summarized in Figure 3.17. Selectivity to ethylene (and acetylene, which can

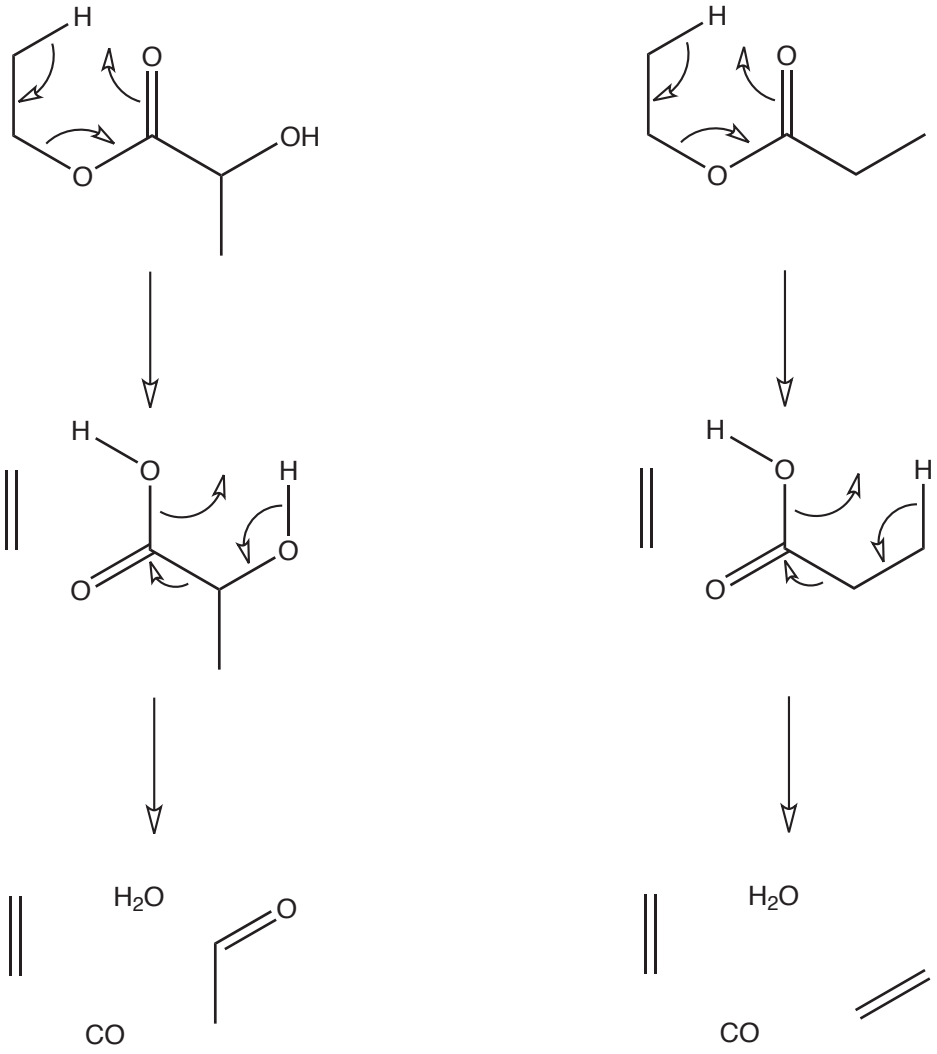

Ethylene + Acetaldehyde

2 x Ethylene

Figure 3.16: Possible mechanism of the decomposition of ethyl lactate and ethyl propionate to olefins via the acid. First, the esters break into ethylene and an acid via a 6-membered transition state. The acid then decarbonylates (perhaps through a free radical process[65]) to produce either acetaldehyde in the case of lactic acid, or ethylene in the case of propionic acid.

be a cracking product of ethylene) from ethyl propionate is nearly twice that of ethylene from ethyl lactate. By contrast, ethyl lactate forms acetaldehyde and ethylene in a nearly 1:1 ratio, while ethyl propionate shows almost no selectivity to acetaldehyde (Figure 3.17). These observations are best explained by continued cracking of propionic acid and lactic acid into ethylene and acetaldehyde, respectively. These products were also observed in experiments performed with the acids directly, described in Chapter 2. In this way, the ethyl portion of both esters can form ethylene while the acid portion decomposes to ethylene or acetaldehyde, depending on the type of acid.

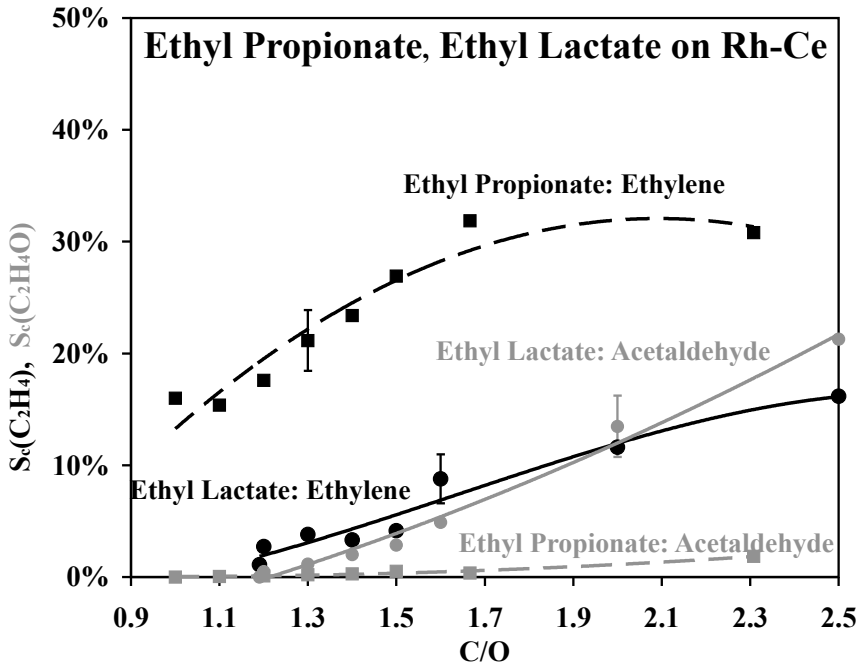

Figure 3.17: Ethyl propionate exhibits twice the selectivity to ethylene (■) as ethyl lactate, but the selectivity of ethyl lactate to acetaldehyde (●) and ethylene (●) is 1:1, whereas ethyl propionate exhibits negligible acetaldehyde (■). This difference is attributed to the hydroxyl group on ethyl lactate. The acid portion of the propionate decomposes to ethylene, while the acid portion of the lactate decomposes to acetaldehyde. The alcohol portion of both esters forms an ethylene molecule.

Gas phase decarbonylation is supported by the blank foam data (Figure 3.15). Thermally cracking ethyl lactate and ethyl propionate over uncoated alumina foams exhibited very little CO_2 but ≈20% selectivity to CO. Ethyl propionate did produce <20% selectivity to CO at low temperatures (Figure 3.15 A), but it also exhibited 10% selectivity to propionic acid which had not decarbonylated. By contrast, at high temperatures, ethyl lactate exhibited >20% selectivity to CO (Figure 3.15 B). This is accompanied by an apparent loss of acetaldehyde and an increase in methane, which suggests that acetaldehyde may be decomposing to methane and CO, a known thermal decomposition pathway.[139]

High selectivity to olefins (>40%) in the uncoated foam experiments (Figure 3.15) suggest that thermal decomposition to olefins is present in the homogeneous phase of CPO and that by tuning the C/O ratio, it is possible to eliminate olefin production or to achieve high selectivity to predictable olefins depending on the structure of the ester. Based on the stoichiometric thermal decomposition shown in Equations 3.5 and 2.7, the maximum selectivity to ethylene and acetylene from ethyl propionate is 80%. Similarly, the maximum selectivity to each ethylene and acetaldehyde from ethyl lactate is 40% (Equations 3.6 and 2.8).

While intact ester linkages were observed in the products of biodiesel reforming,[45] no ester groups were observed among the CPO products of the light ethyl esters in these experiments. However, a few differences between biodiesel and these light esters could explain the disparity. Biodiesel is a methyl ester that cannot undergo thermal decomposition via the six-membered transition state described in Figure 3.16, whereas ethyl esters readily undergo this thermal decomposition.[127] Furthermore, biodiesel contains long olefinic fatty chains that have resonance stabilization for the cleavage of C-C bonds and the resulting radicals. Neither propionate nor lactate contain such stabilizing chains, so conversion of the ester by dehydrogenation or cleavage of the carbon chain is not favored for light ethyl esters. Finally, in the biodiesel experiments, no olefinic esters were observed with fatty chains shorter than six carbons. By contrast, ethyl propionate and ethyl lactate contain three carbons in the acid chain - already too short to be observed as the stable products of biodiesel CPO.

3.6 Conclusions

Light esters such as ethyl lactate and ethyl propionate can be converted by autothermal catalytic partial oxidation at millisecond contact times over Rh and Pt catalysts. Products can be easily tuned to equilibrium synthesis gas or olefins by adjusting the C/O ratio. Rhodium based catalysts show higher selectivity to synthesis gas while Pt catalysts show higher selectivity for olefins and aldehydes. Decomposition occurs at high temperatures with nearly complete conversion over a broad range of C/O. Esters exhibit high selectivity to synthesis gas at C/O < 1.3 with few other products as predicted by equilibrium. Small organic acids such as propionic and lactic acids were also capable of autothermal reforming at these C/O. These results suggest that bio-oils and more complex biomass will be capable of autothermal CPO to synthesis gas under similar conditions.

Esters appear to decompose homogeneously to form an acid and an olefin. The acid may then continue to decarbonylate, thus forming another olefin or aldehyde, or it can react on the surface to form combustion products or synthesis gas. The types of chemicals formed by thermal decomposition of ethyl esters depend strongly on the structure of the original molecule. Ethyl lactate differs from ethyl propionate by the presence of a hydroxyl group; this hydroxyl group on the acid portion of the molecule produces acetaldehyde instead of ethylene. The ethyl portion of both esters forms another ethylene molecule. It is likely that other esters with an accessible hydrogen on the β-alcohol carbon would produce similar selectivity to olefins. In this manner, high yield of predictable olefins can be obtained from renewable feeds.

Chapter 4

CPO of Glycerol

4.1 Summary

Glycerol, a commodity byproduct of the biodiesel industry, has value as a fuel feedstock and chemical intermediate. It is also a simple prototype of sugars and carbohydrates. Through catalytic partial oxidation, glycerol can be converted to syngas without the addition of process heat. This chapter explores the CPO of glycerol using a nebulizer to mix droplets with air at room temperature for reactive flash volatilization. Introducing this mixture to a noble metal catalyst oxidizes the glycerol at temperatures >600^{o}C in 30 - 90 milleseconds. Rhodium catalysts are found to produce equilibrium selectivity to syngas, while platinum catalysts produce mainly autothermal non-equilibrium products.

The addition of water to the glycerol increases selectivity to H_2 by the water-gas shift reaction and reduces non-equilibrium products. As water is introduced at room temperature, this process represents true autothermal reforming. However, the addition of cold water also quenches the reaction, resulting in a maximum in H_2 production at a steam/carbon of 2/3 over a Rh-Ce catalyst. H_2/CO = 2.0, required for the production of methanol, can be achieved with >40% yield.

Glycerol without water produces a variety of chemicals over Pt, including methylglyoxal, hydroxyacetone, acetone, acrolein, acetaldehyde, and olefins. Decomposition by dehydration is consistent with glycerol pyrolysis and probably takes place in the gas phase, driven by heat produced at the surface of the catalyst. A surface mechanism is proposed for decomposition by dehydrogenation. Carbon selectivity to all non-equilibrium chemicals attained 55%, but no single chemical exceeded 30%.

4.2 Introduction

While biological routes for biomass processing are attractive for their low cost and mild reaction conditions, microorganisms are sensitive to molecular structure. For this reason, cellulose and lignin continue to elude biological processing technologies.

Thermochemical processing, however, is largely insensitive to chemical structure, many orders of magnitude faster, and proceeds to high conversion in a single step. A highly attractive thermal processing route for biomass involves fast, or flash pyrolysis to form an energy dense liquid, followed by refining of this "pyrolysis oil" to yield specific chemicals and fuels. As discussed in Chapter 1, Pyrolysis oils contain a variety of chemical species including acids, esters, polyols, aldehydes, alcohols, and aromatics,[2] which may have different chemistries, resulting in a variety of potential products. The study of refining pyrolysis oils is simplified by selecting model components typical of particular moeities common to the complex mixture.

Glycerol is an excellent model component for pyrolysis oil. As a carbohydrate and sugar, glycerol has the same carbon/oxygen (C/O) ratio as cellulose, about twice the oxygen content of pyrolysis oil. Furthermore, glycerol is similar to pyrolysis oil in terms of density, viscosity, and energy content.[2] These properties are listed in Table 1.1.

Due to the surplus of glycerol byproduct from biodiesel production (vegetable oil yields 10 lbs of glycerol per 100 lbs of biodiesel), research in glycerol chemistry has increased significantly in recent years.[140, 141] This research typically falls into two categories: selective chemistry with long time scales and less selective thermal processes with shorter time scales, such as pyrolysis. The latter can be used to make synthesis gas (syngas - CO and H_2), which can in turn be converted to methanol.

Methanol, a biodiesel input, is typically produced from natural gas. The conversion of glycerol to methanol represents an important niche for glycerol processing that could relieve

biodiesel producers from a dependence on high and unpredictable natural gas prices, while reducing fossil fuel needs.

Glycerol gasification has been achieved through pyrolysis to syngas and other gas products [142] and to liquid non-equilibrium products.[143, 144] Pyrolysis, gasification, and steam reforming of glycerol have been examined over noble metals.[145, 146, 147] Previous research has indicated that glycerol can be converted to syngas with high conversion over noble metal catalysts.[47] However, thermochemical glycerol research is typically conducted with a significant addition of process heat in order to vaporize the fuel (bp. 290 ^{o}C). As glycerol undergoes thermal decomposition near its boiling point, the study of preheated glycerol is intrinsically complicated by impurities. Furthermore, the resulting high temperatures can reduce selectivity to non-equilibrium thermal decomposition products, a potential source of value added chemicals.

While glycerol has potential as a chemical feedstock, its unstable price reduces the acceptable margin for processing. High input energies and subsequent dependence on conventional fuels further destabilize the economics of glycerol-related chemistry. For these reasons, a low energy or autothermal method of converting glycerol to needed chemicals is highly desirable.

4.2.1 Catalytic Partial Oxidation

Catalytic partial oxidation can be broadly broken into two regimes of interest: equilibrium conversion and the production of non-equilibrium products. Chapters 2 and 3 generally, rhodium-based catalysts tend to produce equilibrium products with high conversion. Improvements have been realized with the addition of washcoated alumina and cerium to the catalyst. It is believed that the washcoat increases the surface area, while Ce increases the distribution of Rh on the surface of the catalyst.[148] By contrast, Pt based catalysts tend to produce more combustion products and heat.[48] Pt catalysts can be used to select for non-equilibrium products, especially those produced by thermal decomposition, such as dehydrogenation routes.[137]

CPO occurs at high flow rates and millisecond contact times. As a result, transport effects can also be exploited.[48] It has been observed that more conversion to equilibrium products occurs at a greater pore density (smaller pores), whereas non-equilibrium products are favored for larger pores.

This chapter will explore these two regimes, the first using 80 ppi Rh-Ce washcoated catalysts and the second using 65 ppi Pt catalysts. This choice of catalysts maximizes equilibrium

production on the one hand, and intermediate, non-equilibrium products on the other. On Rh, equilibrium conversion of glycerol to syngas is achieved at millisecond contact times via autothermal steam reforming. Pt catalysts exhibit 55% selectivity to non-equilibrium products, many of which are likely formed in the gas phase, though a surface mechanism is proposed for the formation of methylglyoxal.

Furthermore, in order to develop techniques for the CPO of bio oil, these experiments make use of reactive flash volatilization (RFV).[49] Glycerol is not prevaporized. As discussed in Chapters 2 and 3, oxygenated fuels thermally decompose in high temperature CPO reactors. To ensure the feed of pure glycerol without intermediates, cold liquid droplets are sprayed onto the catalyst using an entrained flow nebulizer. The nebulizer allowed high velocity gas to agitate incoming liquid droplets, producing a fine aerosol on the order of 10-100 μm. These droplets contact the hot catalyst and boil / flash react to syngas and other products. An image of the reactor is depicted in Figure 4.1. As bio oil cannot vaporize, it is essential to understand the effects of RFV on model compounds and compare their performance with[47] and without prevaporization.

4.2.2 Synthesis Gas

For the production of methanol, syngas in a ratio of H_2/CO = 2/1 is required. However, the decomposition of liquid glycerol to stoichiometric syngas without any additional species proceeds by equation 4.1:

$$C_3H_8O_3 \rightarrow 3CO + 4H_2 \qquad \Delta H^o \approx 340\frac{kJ}{mol} \tag{4.1}$$

This decomposition results in H_2/CO = 4/3. Because the internal C/O atomic ratio for glycerol is 1, steam reforming to CO and H_2 is not possible without the production of other species, notably CO_2. Equivalently, the addition of water to increase H_2 consumes CO according to the weakly exothermic water-gas shift reaction (WGS - equation 4.2).

$$CO + H_2O \rightarrow CO_2 + H_2 \qquad \Delta H^o \approx -40\frac{kJ}{mol} \tag{4.2}$$

Complete selectivity to H_2 at the expense of CO takes the form of equation 4.3, yielding 7 molecules of H_2. With reactants at room temperature, this requires about the same heat input as equation 4.1 because the WGS (4.2) provides just enough heat to vaporize one mole of water.

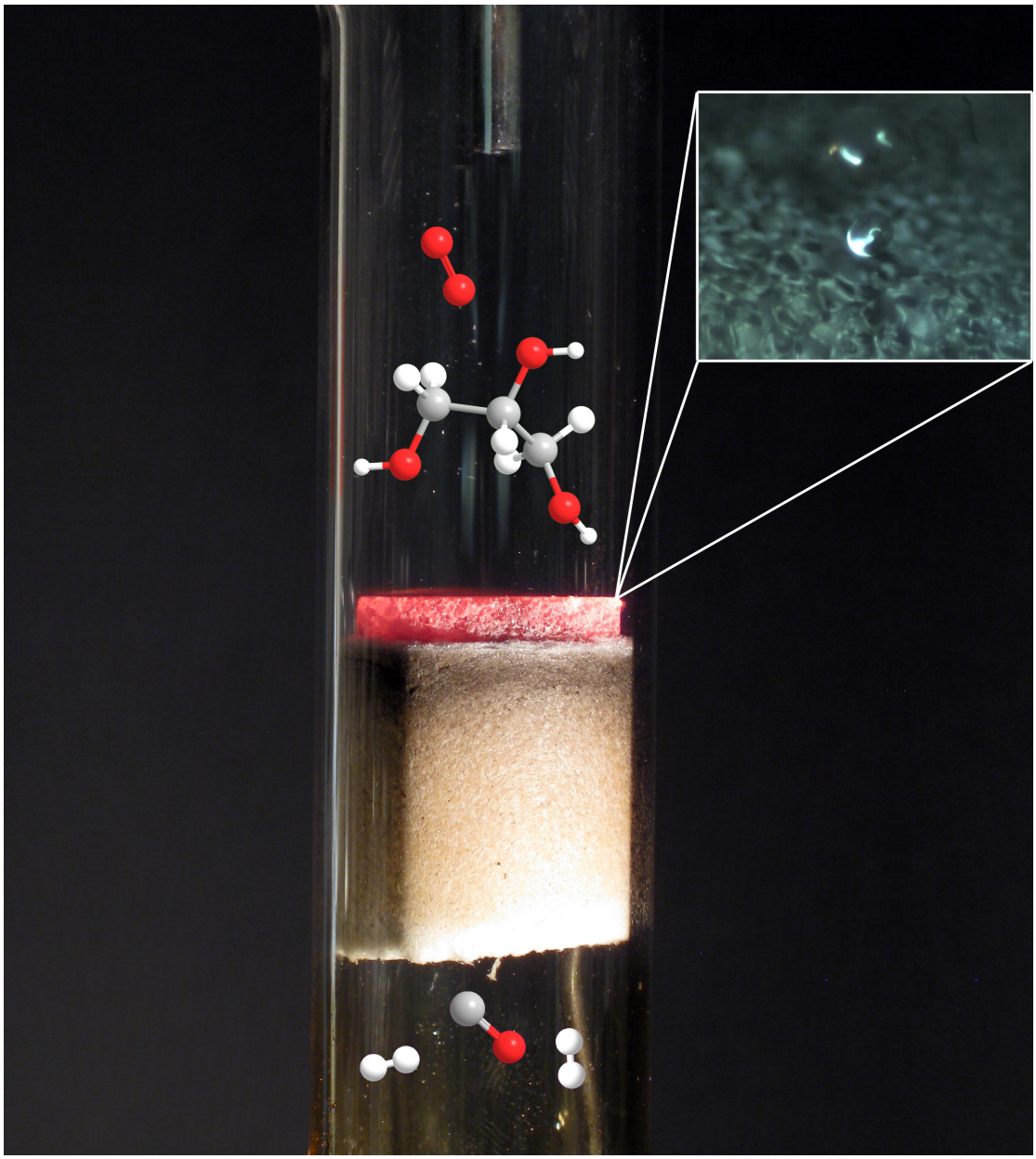

Figure 4.1: Photo-diagram of the catalytic partial oxidation of glycerol via reactive flash volatilization. Glycerol and O_2 flow in from the nebulizer, shown as a 1/8" stainless steel tube at the top. They react over the catalyst autothermally in 30 ms to produce H_2 and CO which flow out of the bottom of the catalyst. The inset shows glycerol droplets, which film-boil over the hot catalyst, exhibiting the catalytic Leidenfrost effect.

$$C_3H_8O_3 + 3H_2O \rightarrow 3CO_2 + 7H_2 \qquad \Delta H^o \approx 350\frac{kJ}{mol} \tag{4.3}$$

The production of syngas requires significant process heat. A potential increase in efficiency occurs if glycerol itself can be partially combusted, rendering the process autothermal.[21] According to equation 4.4, 1 mol of glycerol yields about twice the enthalpy of combustion as 1 mol of methane, but uses three times as much carbon.

$$C_3H_8O_3 + 3.5O_2 \rightarrow 3CO_2 + 4H_2O \qquad \Delta H^o \approx -1500\frac{kJ}{mol} \tag{4.4}$$

Therefore, in an adiabatic reactor, the combustion of one mole of glycerol provides enough heat to drive 4.5 moles of glycerol to syngas. Up to 3 moles of liquid water per mole of glycerol can be added to adjust the syngas ratio without affecting the energy input significantly. Put another way, the steam/carbon (S/C) ratio for partial oxidation and reforming of room temperature glycerol can reach S/C = 1, but additional water will quench the reaction. These considerations indicate that it is possible to achieve autothermal steam reforming through partial oxidation of glycerol with tunable syngas ratios without the addition of any process heat.

4.2.3 Non-Equilibrium Products

As shown in Chapters 3 and 3, the high temperatures associated with partial oxidation, especially on Pt, also allow for thermal decomposition.[56, 45] Steep temperature gradients, as those measured in profile measurements of methane CPO,[48] allow for non-equilibrium products to be produced and quenched before they can further decompose.

With sufficient O_2, glycerol oxidation proceeds to equilibrium products: C_1 gases, H_2, and water. In oxygen lean conditions, conversion to these equilibrium products declines, and some glycerol can be converted to other products. Two main reactions are possible: dehydration and dehydrogenation. The dehydration of a polyol is exothermic. Dehydration of glycerol can occur in several ways, the most likely resulting in hydroxypropionaldehyde or hydroxyacetone as depicted in equation 4.5. A secondary dehydration results in acrolein.

$$C_3H_8O_3 \rightarrow C_3H_6O_2 + H_2O \qquad \Delta H^o \approx -80\frac{kJ}{mol} \tag{4.5}$$

Dehydration has an activation energy of between 270 kJ/mol and 300 kJ/mol, compared with 60-90 kJ/mol activation energy of glycerol to syngas on Pt.[149, 150]

Dehydrogenation to glyceraldehyde or dihydroxyacetone is another thermal decomposition mechanism and proceeds according to equation 4.6.

$$C_3H_8O_3 \rightarrow C_3H_6O_3 + H_2 \qquad \Delta H^o \approx 40\frac{kJ}{mol} \tag{4.6}$$

Dehydration is exothermic, whereas dehydrogenation is weakly endothermic. Ignoring kinetics, at high temperatures, it is expected that glycerol will form aldehydes more than it will dehydrate to olefins. This is consistent with observed ethanol decomposition to acetaldehyde rather than ethylene under similar circumstances.[64] Nevertheless, reported selectivity to acrolein as a pyrolysis product of glycerol indicates that the kinetics for dehydration and dehydrogenation are competitive.[143, 144]

4.3 Experimental

4.3.1 Catalyst Preparation

Catalysts were prepared by coating noble metals on d=17 mm x h=10 mm cylindrical ceramic foam monoliths (99% α-Al_2O_3, 1% SiO_2) weighing ≈2.2 g before metal loading. Monolith foam density was 80 pores per linear inch (ppi) for Rh-Ce catalysts and 65 ppi for Pt catalysts.

Two different metal loadings were examined: rhodium and cerium (Rh-Ce 2.5 wt% each) with a γ-alumina washcoat (5 wt%), and platinum (Pt 5 wt%) without washcoat. All coatings were applied using the incipient wetness impregnation technique. For Rh catalysts, washcoat was added first as γ-alumina slurry in water and drop coated onto the 80 ppi foams. After drying, the foams were calcined at 600 ^{o}C. Then Rh was deposited in solutions of $Rh(NO_3)_3$ salt in water, Ce as $Ce(NO_3)_3{\cdot}6H_2O$, and Pt as PtH_2Cl_6. Foams were then allowed to dry in air over night before calcination in a furnace for six hours in air at 600 ^{o}C. Pt catalysts were reduced under N_2 and H_2 at 600 ^{o}C for six hours.

4.3.2 Reactor Design and Conditions

For Rh-Ce experiments, two catalytic foams were mounted on top of an uncoated α-alumina foam. This uncoated foam had a channel cut into the top face to allow a chromel-alumel thermocouple which measured the temperatures at the back face of the catalyst bed. All three monoliths were wrapped in ceramic paper and placed in the quartz reactor tube. Experiments

over Pt had a similar setup, except that three Pt monoliths were used instead of two. It was observed that single catalysts were insufficient to fully consume O_2. The number of catalytic foams as well as the flow rate were chosen to eliminate oxygen breakthrough. Due to the lack of upstream preheat, cold droplets impinging on the top face of the catalyst bed have the effect of quenching the reaction. To provide sufficient catalyst downstream of this cold zone, two Rh catalysts and three Pt catalysts were employed.

A schematic of the reactor is depicted in Figure 4.2. Liquid glycerol was metered by syringe pump through an entrained flow SS-50 nebulizer provided by Burgener Research, with cofed N_2, which reached pressures of 20 psi to 80 psi, depending on the flow rate. The nebulizer emitted droplets on the order of 10-100 μm which provided excellent mixing of fuel and air, greatly increasing the range of allowable C/O ratio (defined as carbon in the fuel to oxygen in air) for autothermal operation without the need for any upstream heat or mixers.

For experiments with steam addition, water was introduced as a water-glycerol mixture which was delivered by syringe pump. The tip of the nebulizer was positioned about 5 cm above the front face of the catalyst bed. A flow rate of fuel and water was fixed and N_2 and O_2 were adjusted for various C/O ratios. With the addition of water to the fuel mix, gas flow rates were reduced to maintain appropriate C/O ratios. Liquid flow rates were ≈100 g/hr for Rh-Ce experiments and ≈60 g/hr for Pt experiments.

Air stoichiometry was maintained by independently metering N_2 and O_2 by mass flow controllers (Brooks 5850i, accurate to within ±5%). O_2 circumvented the nebulizer and entered the reactor through an annulus surrounding the nebulizer. Total air flow varied between 0.9 and 3 SLPM (standard liters per minute, 18 ^{o}C, 1 atm), depending on the fuel mixture and C/O ratio. Under these conditions, contact times at 600 ^{o}C over Rh-Ce catalysts were ≈30 ms. Contact times over Pt were ≈90 ms.

Temperatures ranged from 300 ^{o}C to 1000 ^{o}C. In the cold regime, low conversion and the quenching of the reaction limited C/O. Higher temperatures were limited by the potential for sintering of the catalyst. The reactor system experienced several start-ups and shut-downs over the course of an experiment.

Steam addition was performed on the same set of Rh-Ce catalysts. Experiments with glycerol without water addition were repeated on a fresh set of catalysts, both for Rh and Pt data. While significant challenges in analysis presented themselves at C/O > 1.8 over Pt, it is noteworthy that the reactor continued to function without obvious detriment.

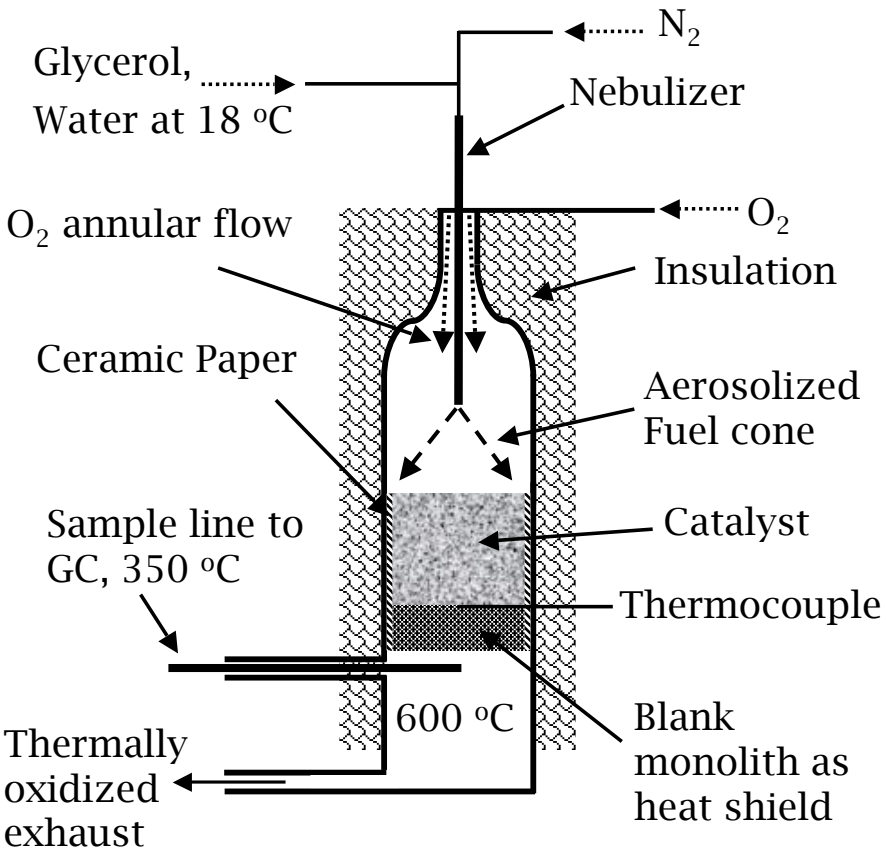

Figure 4.2: Diagram of reactor setup. Fuel and N_2 are fed at room temperature into the top of a quartz reactor by a nebulizer. Oxygen is added through an annulus around the nebulizer. The entire reactor is thermally insulated, and no heat is added. Product samples are collected immediately downstream of the catalyst bed through a heated sample line.

Samples were obtained through a port immediately downstream of the uncoated monolith. A vacuum pump drew the samples through a stainless steel sample line heated to about 350 ^{o}C. Excess effluent was piped to a condenser flask and gases were thermally oxidized.

4.3.3 Isothermal Decomposition over Uncoated Foams

In a reactor setup identical to that used for the Pt experiments, alumina monoliths without Pt replaced the catalyst bed. The reactor was placed in a tube furnace and the temperature was varied between 400 and 700 ^{o}C. N_2 flowrates were specified to be identical to flowrates at temperatures equivalent to the Pt data. Experiments were conducted without the addition of O_2; a separate set of experiments was conducted with O_2 at a C/O = 1.8. Due to the length of the furnace, contact times for these experiments were $\approx$1 second. Observed major products included 1-propanol, acrolein, acetaldehyde and CO_2; minor products included polyols, acids, hydroxyacetone and methylglyoxal.

4.3.4 Product Analysis

Analysis was performed with an HP 5890 GC equipped with TCD and FID using N_2 as an internal standard. An HP-Plot Q precolumn separated permanent gases from liquids and delivered the former through a HayeSep D packed column to the TCD, the latter through a capillary DB1 to the FID. Coking of the sample line and Plot Q column at high C/O complicated analysis of non-equilibrium products. As a result, species data obtained at C/O $\geq$ 1.9 are not included in the analysis.

All reported products and unreacted glycerol were directly observed except for water, which was derived by balancing oxygenated species: the amount of oxygen in the exit stream was compared with that known to be entering the reactor, and the remainder attributed to water. The most likely glycerol decomposition products can be found in Table 4.1. Glycol species peaked at similar times, so these species were jointly summed as "glycols" in the plots. Acrolein and propionaldehyde also overlapped strongly. As acrolein is a known glycerol thermal decomposition product, it was chosen as the most likely candidate. Other minor products, such as C_3 acids, also overlapped. Retention times sometimes shifted with varying species concentrations in calibration samples. However, the peaks identified in the plots were typically single peaks and were consistent throughout several chromatograms.

Species	Prob. Product	GC Capable	In Analysis	Comments
H_2	√	√	√	
H_2O	√		√	Closed Balance on O
CO	√	√	√	
CO_2	√	√	√	
CH_4	√	√	√	
Methanol	√	√	√	
Formaldehyde	√			peaks erratic
Formic Acid				
C_2H_2	√	√	√	
C_2H_4	√	√	√	
C_2H_6	√	√	√	
Acetaldehyde	√	√	√	
Ethanol		√	√	overlap with acrolein
Hydroxyacetaldehyde	√			sample is dimer
Glyoxal	√			Decomposes in GC
Ethylene Glycol		√	√	peak overlap, glycols
Acetic Acid		√	√	peak overlaps, aromatics
Oxalic Acid				decomposes in GC
Ethylene Oxide		√	√	peak overlap, methanol
C_3H_6	√	√	√	
C_3H_8	√	√	√	
Acetone	√	√	√	
Propionaldehyde	√	√	√	peak overlap, acrolein
Isopropanol	√	√	√	
Propanol	√	√	√	
Propionic Acid	√	√	√	
Propylene Oxide		√	√	
Acrolein	√	√	√	
Methylglyoxal	√	√	√	characteristic odor
Lactic Acid	√	√	√	overlap, hydroxyacetone
Pyruvic Acid	√	√	√	overlap, hydroxyacetone
Acrylic Acid	√	√	√	overlap, hydroxyacetone
hydroxyacetone	√	√	√	
1-3 propane-diol	√	√	√	peak overlap, glycols
1-2 propane-diol	√	√	√	peak overlap, glycols
1-3 dihydroxyacetone	√			dimer is sugar; cokes
Glycerol	√	√	√	peak overlap, glycols
Benzene	√	√	√	coke decomp product

Table 4.1: Most likely glycerol decomposition species and probability of occurring. Not all species are capable of being observed in the GC. Those that are and are most probable were analyzed for.

GC runs took 25 minutes and were left to bake out for several minutes at the end of each run. Carbon balances typically closed within 15%. Data from the highest C/O of a particular data set was accepted with carbon balances outside of this range, with slight deviations likely due to condensation and carbon deposition in the sampling system from heavy products or unconverted glycerol.

4.3.5 Data Analysis and Equilibrium Calculation

Data is presented in terms of conversion and atomic product selectivities for carbonaceous species (the ratio of the carbons in species *i* to the total carbon in all products) and hydrogen species (analagously defined for H_2 and H_2O). Points are averages of several runs, typically at least three per data point per catalyst. Variance from these averages were pooled among all C/O or S/C, depending on the abscissa, to calculate error bars which represent one standard deviation. Trend lines are typically based on polynomial fits for the data. In a few cases with a paucity of data, trend lines are hand drawn to best reflect trends suggested by the data.

Equilibrium data was calculated using the software package ChemKin 4.2. Thermodynamic data was obtained from the Burcat database.[151] Initial attempts to model the reactor as adiabatic met with the difficulty of processing a phase change in the software program. Circumventing this problem revealed that predicted temperatures were somewhat higher than observed, possibly due to heat loss from upstream convection of nebulized fuel in the reactor. Equilibrium was recalculated isothermally using the averaged back-face thermocouple data for a given C/O and S/C ratio; this temperature and atmospheric pressure were held constant while species inputs varied. Inputs included glycerol, H_2O, N_2, O_2. Equilibrium products considered were CO, CO_2, H, HO, H_2, H_2O, CH_4, O_2 and N_2. These calculated equilibrium products and quantities are depicted as dashed lines in the data.

4.4 Results

4.4.1 Rhodium Ceria

Products of CPO of glycerol over Rh-Ce are C_1 gases which track very close to equilibrium for S/C < 4/3. Figure 4.3A depicts carbon selectivity to CO and CO_2 and hydrogen selectivity to H_2 and H_2O for S/C = 0. These products represent almost all of the observed species; as

a result, a mirror plane is apparent in the data. Minor products for S/C = 0 are depicted in Figure 4.3B. Methane, another equilibrium product, increases from 0% at C/O = 0.9 to ≈4% at C/O = 1.6. Selectivity to acrolein increases slightly over the C/O range but is always <2%. A peak is apparent in the selectivity to ethylene at C/O = 1.2 of 0.6%.

Figure 4.3C & D show temperature and conversion for autothermal steam reforming of glycerol over Rh-Ce. Figure 4.3C depicts temperature with C/O as the independent axis. The addition of liquid water decreases temperature in a predictable fashion. For C/O = 0.9, temperature decreases from ≈970 ^{o}C for undiluted glycerol to 513 ^{o}C for S/C = 5/3. Figure 4.3D illustrates data with steam to carbon as the independent variable. Conversion is depicted at the top of the graph, overlapping at ≈100% for all data. Conversion decreases to 99% for C/O = 1.1 at S/C = 4/3. The temperature decreases with an increase in C/O, and this relationship is preserved at all S/C.

Figure 4.4 depicts reforming over Rh-Ce as a function of water addition to the glycerol feed. Experimental data are shown in solid lines and equilibrium predictions in dashed lines. Figure 4.4A illustrates hydrogen selectivity to H_2. As C/O increases from 0.8 to 1.1, the peak in H_2 formation increases and moves toward lower S/C.

Panel B in Figure 4.4 depicts carbon selectivity to CO, which decreases from 60% to 25% for all C/O with an increase in S/C. Figure 4.4C illustrates an opposite trend in carbon selectivity to CO_2: an increase from 35% to 70% occurs over the S/C range. For both CO and CO_2, the trend in S/C dominates trends in C/O. Stacked data reflect the insensitivity to changes in C/O for CO and CO_2.

Figure 4.4D depicts the H_2/CO ratio. The H_2/CO ratio approaches 1.0 in glycerol without water; it increases slightly with C/O. Production of H_2 with respect to CO increases with the addition of water to the glycerol feed for S/C ≤ 2/3. At greater S/C, H_2/CO decreases most dramatically for C/O = 1.1 and 1.0. At C/O = 0.8, a slight increase is observed until S/C = 5/3, reaching ≈4.0. As C/O decreases, the increase in O_2 results in a higher temperature which allows for more water to be added. Thus H_2 production increases at increased S/C.

At the end of experimentation, it was observed that some of the Rh catalysts lost mechanical stability. This behavior has been observed before[47, 64] but the cause is unknown. The loss of mechanical stability does not appear to affect catalysis or chemistry, and is believed to be a failure of the foam substrate. Photos of such mechanical loss are described in Appendix C.

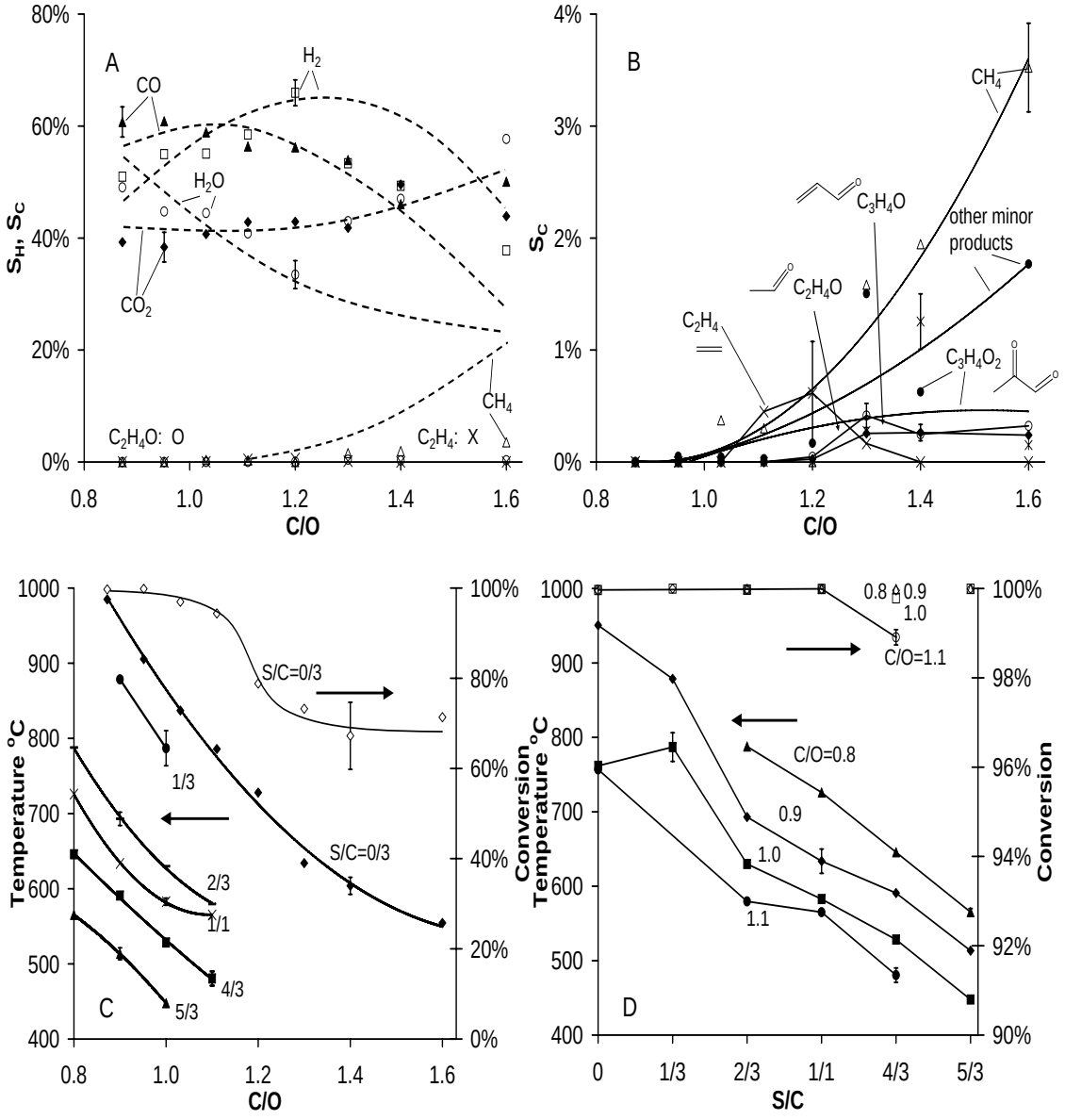

Figure 4.3: Product species (A and B), conversion, and temperature (C and D) for CPO of glycerol over Rh-Ce wash-coated catalysts. At S/C = 0, data for CO (▲), H_2 (□), H_2O (○), CO_2 (◆), and CH_4 (△) are depicted along with equilibrium lines (dashes) in Panel A. Almost all species are syngas and combustion products. At S/C = 0, for C/O ≥ 1.2, CH_4 and other minor products appear from CPO of undiluted glycerol (B). Conversion also drops at C/O ≥ 1.2 (C - top curve). The addition of water decreases temperature as shown in C and D. Reactants at room temperature convert autothermally in 30 ms. Error bars denote data within one standard deviation of the mean using pooled averages over all C/O (A, B and C) or S/C (D).

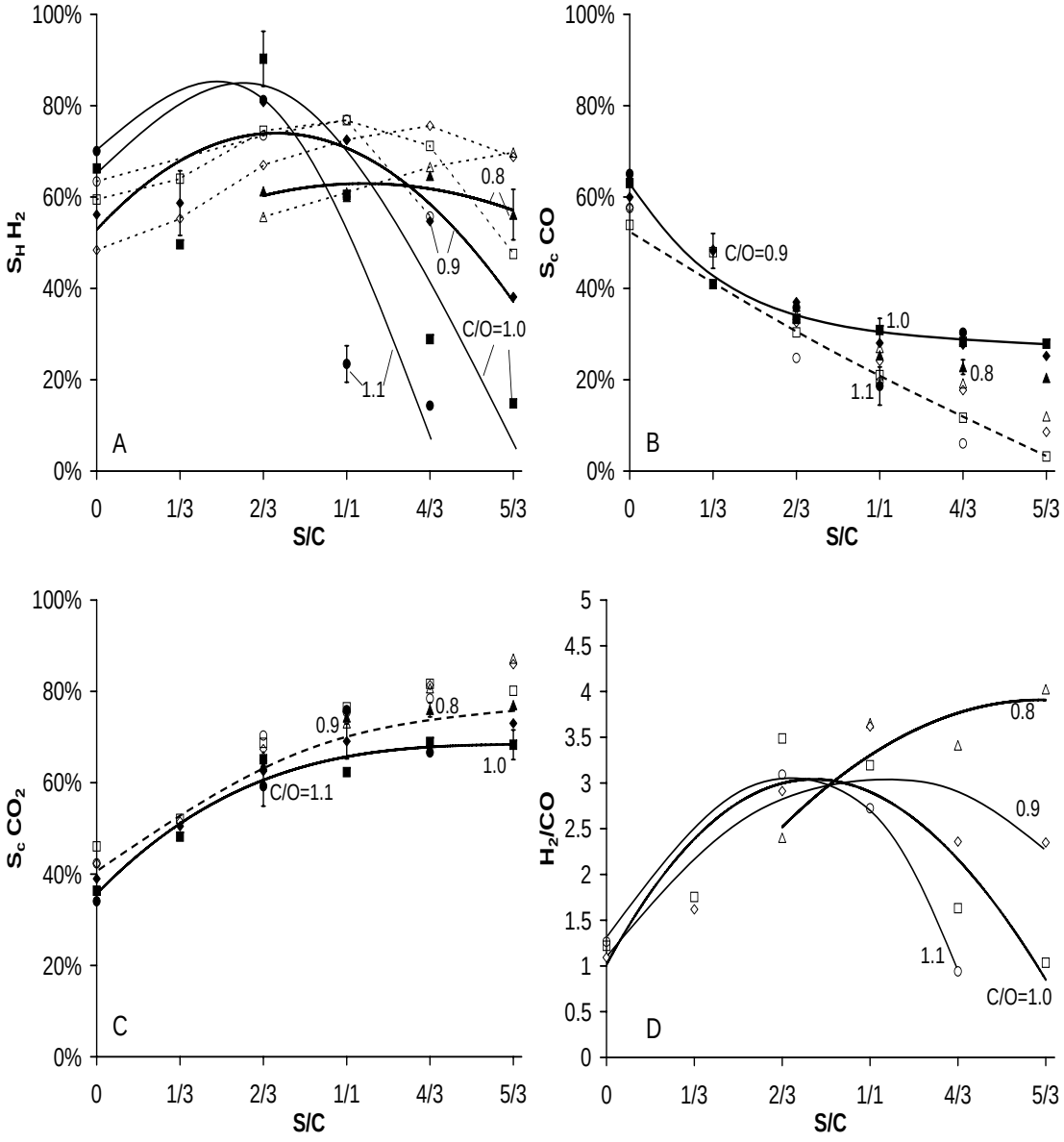

Figure 4.4: Product species of steam addition to glycerol CPO on Rh-Ce washcoated catalysts with varied C/O: C/O = 0.8 (▲), 0.9 (◆), 1.0 (■), 1.1 (●). Equilibrium data based on exit temperatures are depicted in open symbols and dashed lines. Panel A depicts selectivity to H_2; Panel B to CO, and Panel C to CO_2. Water is derived by closing the balance on O and mirrors H_2, as shown in Figure 4.3A. A maximum in H_2 selectivity generally shifts upward and left with increasing C/O in Panel A. In Panels B and C data are almost stacked; lines represent C/O = 1.0 as CO and CO_2 are relatively unaffected by changes in C/O, but follow equilibrium closely for S/C ≤ 1. Panel D depicts the H_2/CO ratio for all S/C and C/O. Error bars depict one standard deviation using pooled averages over all S/C.

4.4.2 Platinum

At C/O > 1.1, a decrease in conversion of glycerol to syngas over Rh catalysts was observed. Thermal decomposition products increased in the form of C_2 and C_3 species, as well as unconverted glycerol. To further decrease syngas production and increase selectivity to non-equilibrium products, experiments were carried out at $1.4 \leq C/O \leq 2.0$ over Pt coated alumina foams.

The product spectrum for experiments carried out over Pt coated foams is depicted in Figure 4.5. While the reactor exhibited no obvious deactivation at C/O > 1.8, the sample line to the GC and Plot Q precolumn coked significantly due to the vast quantity of unsaturated hydrocarbons injected over several days, rendering data at $C/O \geq 1.9$ erratic. Consequently, with the exception of temperature, data is only included for $C/O \leq 1.8$ shown in Figure 4.5.

Figure 4.5A depicts conversion and temperature for the entire C/O range. Conversion is >90% for all C/O but decreases with an increase in C/O. Temperature is also depicted in Panel A. Data curves for temperature and conversion are approximately parallel. Temperature decreases from 700 ^{o}C at C/O = 1.4 to 480 ^{o}C at C/O = 2.0.

Figure 4.5B illustrates the main products of glycerol CPO on Pt: CO, CO_2, H_2, and H_2O. Carbon selectivity to CO decreases monotonically from 45% to 14%. Hydrogen selectivity to H_2 similarly decreases from 22% to 5%. Selectivity to CO_2 remains relatively constant over the entire C/O range, with a slight increase from 25% to 33%. The sum of all other products is also displayed in the plot ("other products"). Selectivity to non-equilibrium products reaches 55% at C/O = 1.7.

Figure 4.5C shows carbon selectivity to species between 3% and 20%. These species include methylglyoxal, acrolein, acetaldehyde, hydroxyacetone (acetol), and ethylene, and are the main non-equilibrium products observed. Selectivity to methylglyoxal increases monotonically from 1% at C/O = 1.4 to 15% at C/O = 1.8. Selectivity to acetaldehyde is nearly identical to acrolein. On a mol basis, acrolein to acetaldehyde maintain a nearly 2/3 ratio. Selectivity to these products peaks between C/O = 1.6 and C/O = 1.7 at 13%. Selectivity to these products at C/O = 1.4 is 5%; at C/O = 1.8, 11%. Selectivity to ethylene decreases with C/O, likely due to the decrease in heat available for thermal decomposition, and is never >5%. The sum of all minor species (selectivity to carbon <3%) is also depicted, representing 6% - 8% of carbon.

Figure 4.5D depicts minor products from CPO of glycerol on Pt. Selectivity to glycols

increases slightly from 1% to 2%. Selectivities to acetone, acetic acid, and benzene were relatively consistent between 1% and 2%. Selectivity to methane decreases from 2% at C/O =1.4. The sum of all other products representing <1% of carbon is also depicted. These products account for no more than 3% of the carbonaceous products.

4.5 Discussion

4.5.1 Syngas Production and Steam Reforming

CPO of glycerol over Rh-Ce-WC catalysts proceeds to equilibrium with >99% conversion. These results are consistent with previous research in the CPO of ethanol[18] and polyols.[47] The elimination of process heat indicates that the system is robust for millisecond autothermal steam reforming of oxygenated hydrocarbons: the introduction of a significant heat sink such as vaporization of glycerol upstream of the oxidation zone does not impede catalyst performance. This indicates that CPO can be carried out without the addition of another fuel or heat source, and that a significant water load can be introduced to adjust the H_2/CO ratio without quenching the reaction.

It is anticipated that increasing the reactor size will further increase the amount of water that can be added for steam addition due to increased heat retention. However, this reactor configuration differs from previous polyol research: in order to avoid upstream reactions, no front-face heat shield is employed. Reintroducing this heat shield would likely reduce heat loss. The recirculation of hot droplets from the top face of the catalyst upstream likely accounts for some heat loss as well.

The decrease in CO production with increasing S/C, accompanied by an increase in selectivity to CO_2, indicate an increased importance of WGS. As anticipated by the thermodynamics, this effect decreases at S/C > 1.0, most likely due to quenching. These observations also explain the shifting maximum in H_2 production depicted in Figure 4.4. For S/C $\geq$ 4/3, C/O $\leq$ 0.8 is required to produce enough heat to maintain reaction kinetics. Increased C/O suffers dramatic reduction in hydrogen selectivity to H_2. As less water is added to the fuel, less oxygen is required to support the reaction, and H_2 production increases. H_2 production reaches a maximum because some water addition promotes the WGS reaction without the quenching effect of a reduction in temperature. This trend is consistent with thermodynamic analysis, which indicates that the addition of water up to a S/C = 3/1 increases production of H_2 provided that

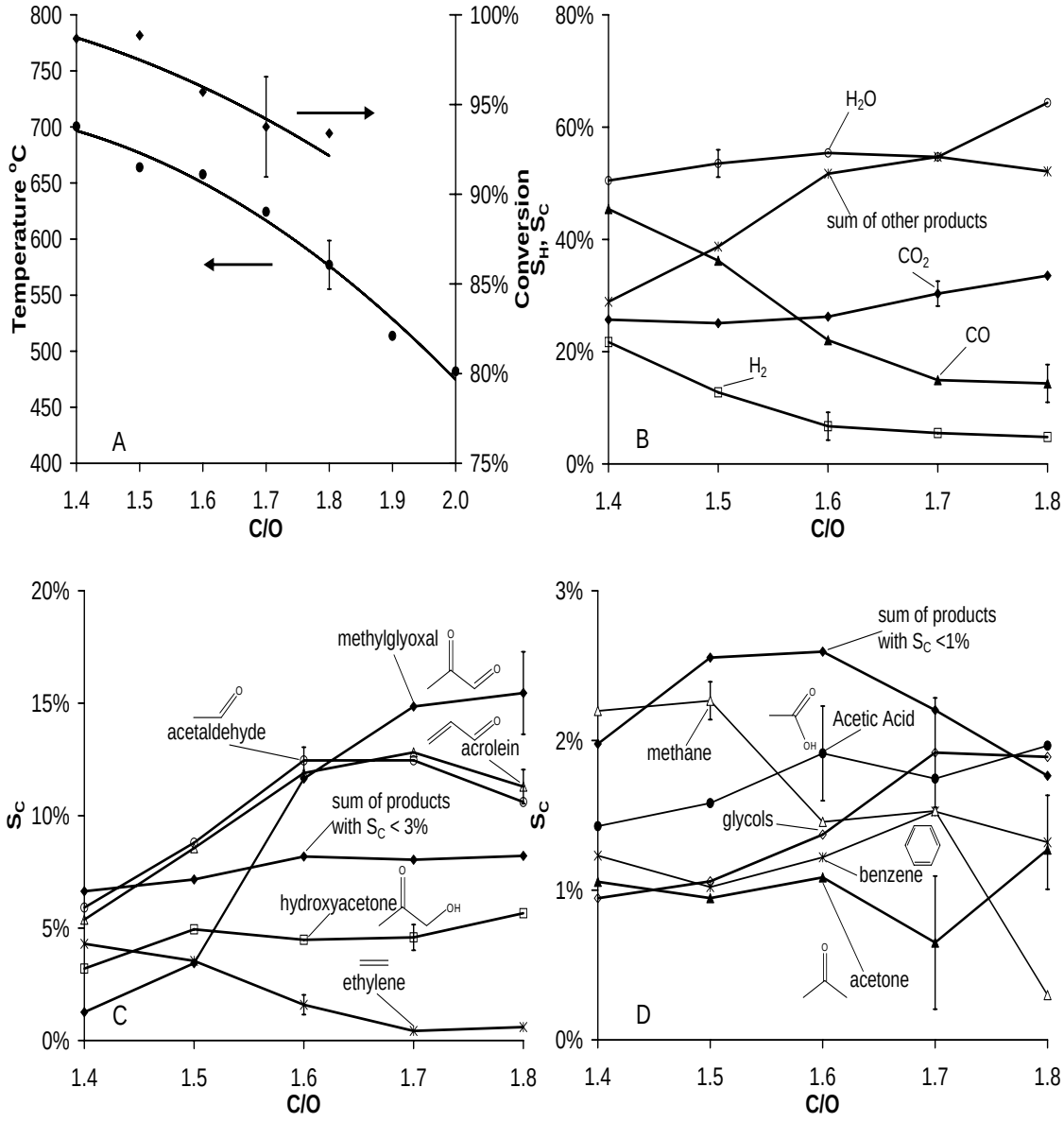

Figure 4.5: Conversion, temperature (A) and product species (B, C and D) of CPO on Pt. Conversion and temperature show a strong correlation. Major products (B) include syngas and combustion products. At C/O > 1.5, selectivity to the sum of all other species surpasses both CO_2 and CO. Panel C depicts a relationship between acrolein and acetaldehyde. Minor species include ethylene, acetic acid, and glycols, as shown in Panel D. Reactants at room temperature convert autothermally in 90 ms. Error bars depict one standard deviation using pooled averages over all C/O.

temperatures can be maintained above 630 ^{o}C.[152]

The thermodynamics of WGS and water vaporization make steam addition up to S/C = 1.0 possible in this reactor configuration without dramatically quenching the reaction. Further steam addition does appear to introduce deviations from equilibrium, especially for C/O $\geq$ 1.0. This range allows for flexibility in H_2/CO. This ratio appears to have a maximum between 2/3 < S/C < 1 and varies between 1 and 4. These results also indicate that H_2/CO = 2.0 can be achieved with >40% conversion of carbon to CO.

4.5.2 Thermal Decomposition and Non-Equilibrium Chemicals

A Pt catalyst was chosen because it has been demonstrated that increased selectivities to non-equilibrium products occur on Pt compared to other noble metal CPO catalysts.[56] It is believed that these non-equilibrium products are produced in the gas-phase, in the void space of the catalyst, driven by heat given off by oxidation reactions taking place on the catalyst surface. As a result, non-equilibrium products are expected to be similar to products observed in pyrolysis.

To probe this relationship as well as the functionality of the alumina substrate, glycerol was passed over uncoated alumina foam monoliths in a reactor heated externally. Although contact times differ by an order of magnitude and the temperature gradient is quite different from Pt experiments, the product spectrum is informative. Main products included 1-propanol, acrolein, acetaldehyde and CO_2. Only trace amounts of hydroxyacetone and methylglyoxal were observed. With the addition of oxygen, CO_2 and CO increased; however, the furnace is required to maintain operation. The formation of propanol, which is not observed in great quantity under catalytic conditions, requires further study. The other products are consistent with thermal decomposition of glycerol observed in pyrolysis experiments.[143, 144, 150, 153] Perhaps due to the great quantity of products that can form from glycerol, and an even greater number that can form under oxidative conditions, such studies are typically limited to two or three product species, such as acrolein, acetaldehyde,[143] and formaldehyde.[144].

Selectivity to acrolein and acetaldehyde display high correlations over Pt, consistent with observations by Stein et al.[143] These products are likely due to dehydration reactions observed in glycerol pyrolysis.[144] Nimlos et al. modeled the thermal decomposition of glycerol, suggesting that acetaldehyde and acrolein occur as unimolecular dehydrations involving concerted cyclic reactions.[150] In particular, acetaldehyde is formed by a single concerted unimolecular

reaction involving the 1,3-hydroxy groups. Other products of this reaction include water and formaldehyde, which likely decomposes to CO and H_2 under the high temperatures of CPO. This mechanism is depicted in Figure 4.6A.

The Nimlos mechanism also proposes that acrolein is formed by a double dehydration.[150] The first step involves a four-centered dehydration of the 2-hydroxy to form an unstable intermediate. This molecule can then undergo a unimolecular 6-centered reaction to form acrolein and a second water molecule as depicted in Figure 4.6B.

Nimlos also predicted the formation of hydroxyacetone by a competing dehydration mechanism (Figure 4.6C), but observed that previous authors have not made much mention of this species, perhaps because hydroxyacetone is unstable. In this work, hydroxyacetone is present at ≈5% selectivity. A trace amount of hydroxyacetone is reported by Antal et al.[153] and, under different reaction conditions, is observed by Corma et al.[154]

Methylglyoxal is a major product and is not observed under pyrolysis-only conditions,[144, 143] nor in great quantity in the presence of an uncoated alumina substrate. Selectivity to methylglyoxal and CO exhibit a correlation of -0.94. The increase in non-equilibrium products at the expense of syngas production is anticipated under oxygen lean conditions. However, the correlation may indicate that pathways for methylglyoxal and CO are directly competing. As CO is likely formed on the catalytic surface, a heterogeneous mechanism might explain methylgloxyal formation.

A possible mechanism for the production of methylglyoxal includes a surface reaction to form an aldehyde before or after dehydration. Mavrikakis and Barteau have observed that alcohols decompose on a Pt surface via an alkoxide intermediate to form an aldehyde through the removal of two H atoms.[155] They show that in the η^2 conformation, the aldehyde bond is parallel to the surface and continues to decompose by breaking other C-C bonds to form CO. However, in the η^1 conformation, the aldehyde is adsorbed at the oxygen only, and can desorb easily as an aldehyde species.

As C/O increases, it may be that the η^1 conformation is preferred for glycerol CPO, resulting in an increase in methylglyoxal as a surface product in competition with CO. This could be due to adsorbed C species which occupy some catalytic sites and prohibit a large molecule from occupying several sites at once, thereby preventing further decomposition. The proposed mechanism for dehydrogenation of glycerol is depicted in Figure 4.7.

Several authors have explored low temperature glycerol oxidation to glyceraldehyde and

dyhydroxyacetone on Pt.[156, 157] In particular, Kimura observed a strong effect of promoting Pt catalysts with bismuth.[156] The additional metal assisted by blocking Pt sites, effectively decreasing the opportunities for glycerol to adsorb and decompose. With limited sites available, selectivity to dehydrogenation to form an aldehyde or ketone increases dramatically. Combining these observations with dehydration may explain the high selectivity to methylglyoxal.

4.6 Conclusion

Autothermal steam reforming through catalytic partial oxidation of glycerol was demonstrated with high conversion over Rh-Ce catalysts and Pt catalysts. On Rh-Ce, liquid water can be added to the fuel up to a steam/carbon = 2/3 to increase H_2 production through WGS without quenching the reaction. A variety of H_2/CO ratios are possible by adjusting the C/O and S/C. For methanol production, H_2/CO = 2.0 can be achieved with >40% yields in a micro-reactor; increases to this yield are very likely achievable.

On a Pt catalyst, large amounts of non-equilibrium chemicals are observed for C/O $\geq$ 1.4. Acrolein, acetaldehyde, and hydroxyacetone are major pyrolysis products powered by heat produced at the surface, while methylglyoxal may be produced heterogeneously.

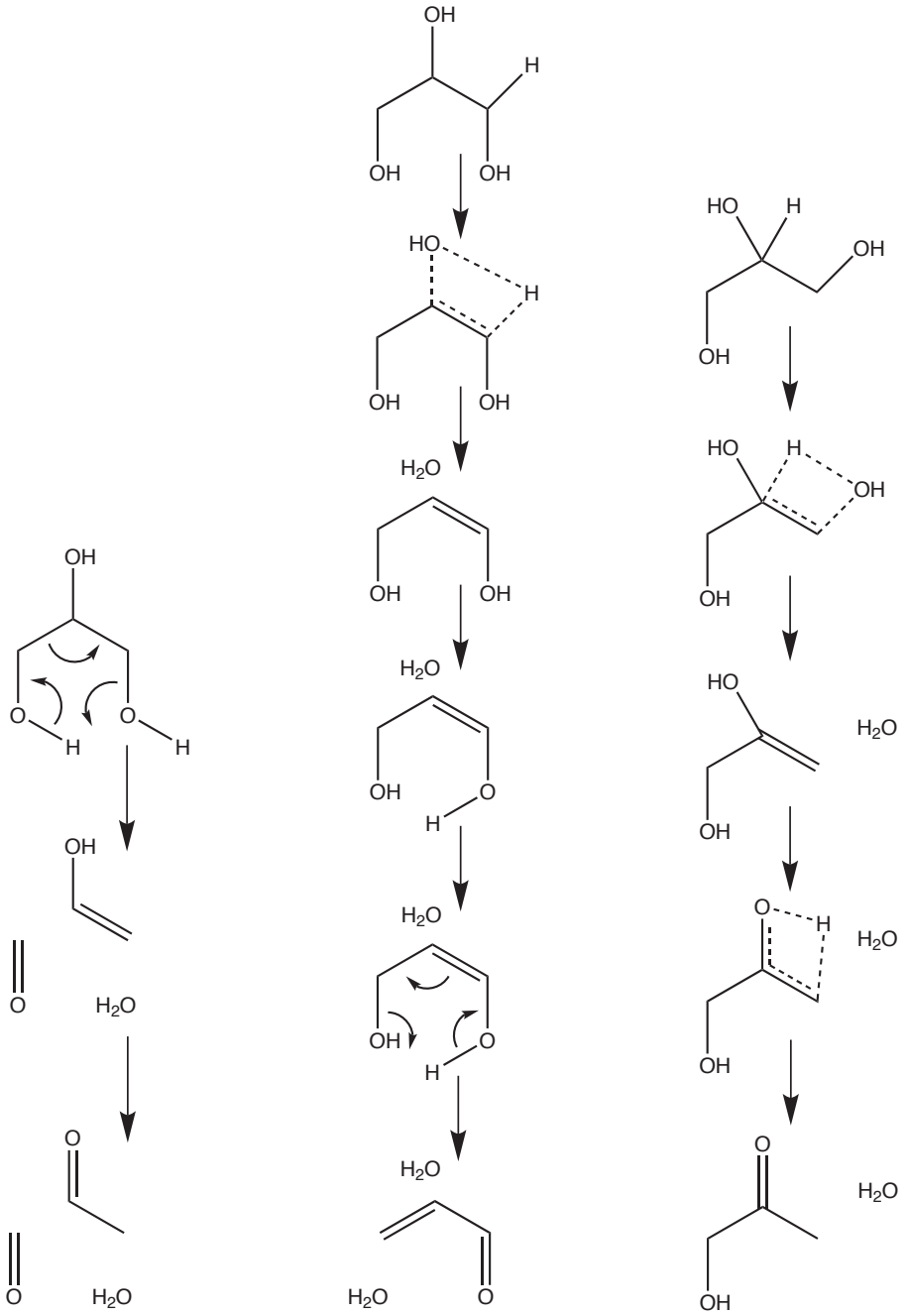

Formaldehyde & Acetaldehyde

Acrolein

Hydroxyacetone

A

B

C

Figure 4.6: Gas phase dehydration mechanisms explain several of the most abundant non-equilibrium products. Acetaldehyde and formaldehyde may form from a six-membered ring transition state; the formaldehyde likely dehydrogenates to CO and H_2. Acrolein and hydroxyacetone likely result from dehydration via four-membered transition states. The acrolein intermediate dehydrates again to form acrolein, while the hydroxyacetone intermediate undergoes a keto-enol isomerism.[150]

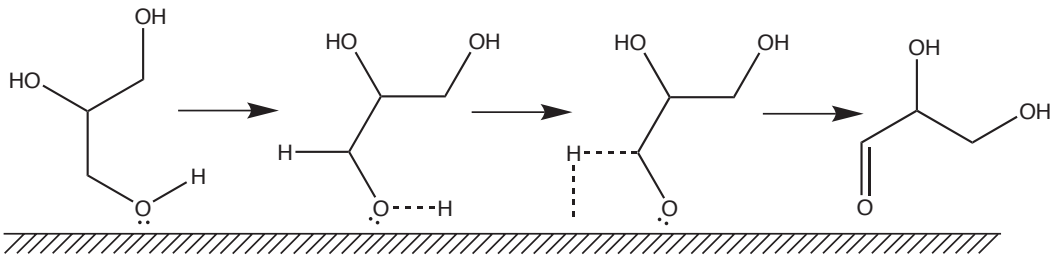

Figure 4.7: Proposed mechanism for the dehydrogenation of poly-ols. Glycerol or perhaps hydroxyacetone adsorbs in the η^1 conformation. The molecule dehydrogenates on the catalyst and desorbs as an aldehyde or ketone.

Chapter 5

CPO of Glycerol: Time On Stream

5.1 Summary

Two time on stream studies of the autothermal reforming of glycerol show deactivation of the catalyst over 375 hours and 450 hours. Liquid glycerol and water were introduced to a quartz reactor at room temperature and mixed with air in a nebulizer. The aerosol reacted to H_2, H_2O, CO, and CO_2 over a Rh-Ce/Ce/Al_2O_3 sphere bed. Catalyst deactivation was exhibited by a decrease in product H_2 and CO_2, and an increase in CO and temperature. The product changes suggest failure of the water-gas shift reaction, which is typically promoted by Ce. SEM analysis show sintering of the catalyst due to high reaction temperatures, and EDS shows inorganic deposits on the walls of the quartz reactor and on the catalyst spheres. Etching of the quartz reactor is also observed.

5.2 Introduction

Biodiesel production is a demonstrated technology that is increasing worldwide, driven by fuel prices and government policy. The EU has a 5.75% renewable fuels target for by 2010, two-thirds of which would be met by biodiesel; the US has a 1 billion gallon production Renewable Fuel Standard by 2012.[158] Biodiesel fits seemlessly into existing infrastructure and represents much greater energy benefit than ethanol. Chemically, biodiesel requires a fatty acid and an alcohol for esterification. This is often accomplished using vegetable oils as the source of the fatty acids, and methanol derived from methane as the alcohol. Transesterification of vegetable

oil produces 10 wt% glycerol as a byproduct, consuming about 10 wt% methanol in the process. Thus, biodiesel production requires methanol, which is typically derived from non-renewable fuels, and produces a byproduct which must be sold at market prices, glycerol.

One option for enhancing efficiency is to convert glycerol to methanol, and recycle it as a reactant. This conversion would reduce the dependency on fossil fuels as inputs and stabilize the price of biodiesel: methane spot prices are volatile and likely to increase with demand, and glycerol prices are increasing in volatility. It would also consume a byproduct locally, thereby avoiding transportation costs and the necessity to discover new markets for an ever increasing glycerol production.

Conversion of glycerol to methanol can be achieved by catalytic partial oxidation (CPO) of glycerol to H_2 and CO (syngas) and subsequent methanol synthesis over a CuZnO catalyst. Autothermal CPO of glycerol has been demonstrated over noble metal (Rh and Pt) catalysts at millisecond contact times, with and without preheat.[47, 159] These studies in a lab scale micro reactor demonstrate that as much as 40% of methanol demand can be offset at a biodiesel plant using local glycerol without the addition of any process heat. With proper heat management and scaling, larger yields are highly likely. However, the duration of these experiments, tens of hours onstream, has not revealed the industrial feasibility of CPO of glycerol to syngas. In particular, effects of catalyst aging have not been studied for this application.

Several aging studies for CPO catalysts have been implemented, mostly using methane or natural gas.[160, 161, 162, 163, 164] These studies are an essential step in establishing catalyst life for industrial application, and can yield valuable kinetics for deactivation. Ding et al. showed a deactivation in steam reforming due to sintering in the oxidation zone over the course of 1000 hours on stream.[161] This is consistent with accelerated aging studies which suggest sintering in the oxidation zone, where temperatures can exceed 1000 ^{o}C, can decrease surface sites and reforming rates.[165] Basini has conducted several time-on-stream studies of the CPO of methane over 500, 1000, and 20,000 hours, suggesting robustness for impurities like sulfur and aromatics.[162, 163, 164] Although these tests indicated some clustering of noble metals, deactivation in terms of product spectrum is not reported.

Although several studies have explored the aging effects of steam reforming of preheated liquid fuels,[166, 167] no long term aging studies of CPO of liquid fuels, and no studies of the aging effects of reactive flash volatilization (RFV), in which liquid fuels are introduced directly to the catalytic reactor,[49] have been reported. RFV of glycerol is advantageous in that no

preheat or prevaporization of the fuel is necessary, but RFV also has broader implications for nonvolatile fuels such as pyrolysis liquids. Thus, a catalyst aging study of glycerol RFV and CPO is also relevant for other biofuel applications.

Two aging studies of RFV to examine catalyst stability over an extended time period are reported. In both cases, loss of catalytic activity is observed, likely due to poisoning and sintering.

5.3 Experimental

This experiment required the construction of a new reactor system. A dedicated computer, LabView software, and a National Instruments CompactDAQ system were set up to monitor and control the experiment. In order to allow product analysis using a dedicated method, a GPIB interface was added to the HP 5890 Gas Chromatograph. The GC was equipped with two heated sample lines and a six-way valve allowed either sample line to pull vacuum and introduce a sample to the GC. In this way, the GC could be easily switched between multiple projects with different GC methods.

Dedicated fuel and gas lines that allowed for continuous flow without interruption of the experiment were designed and constructed according to Figure 5.1. To allow for the introduction of process gases at different pressures (eg, the nebulizer requires a significant pressure drop, and input gases were set at 100 psi), mass flow controllers and regulators were required for each gas inlet. Mass flow controllers have a typical pressure drop of 15-30 psi; outside of this range they do not function optimally. As a result, gases were fed to the mass flow controllers at pressures suitable to their inlet to the system, making use of line regulators as shown in Figure 5.1. Several other system-specific designs, as well as a full system safety revew are described in Appendix B.

Glycerol (USP grade), deionized water, N_2 (high purity, grade 9), and O_2 (UHP, grade 0) were contacted over a Rh-Ce/CeO_2/Al_2O_3 sphere bed where they reacted autothermally with contact times of $\tau \approx 10$ ms. A Rh catalyst was chosen for its high stability, and Ce was added for its increase in dispersion, reduction of sintering, and promotion of oxygen transfer.[148, 168] Although γ-Al_2O_3 washcoats are known to decrease sintering and enhance syngas yields[34, 148], no washcoat was utilized because γ-Al_2O_3 is susceptible to attrition on alumina spheres and can undergo phase change to α- and δ-Al_2O_3 that can occur at relevant temperatures. Instead, a CeO_2 washcoat was applied prior to final metal loading of Rh and Ce.

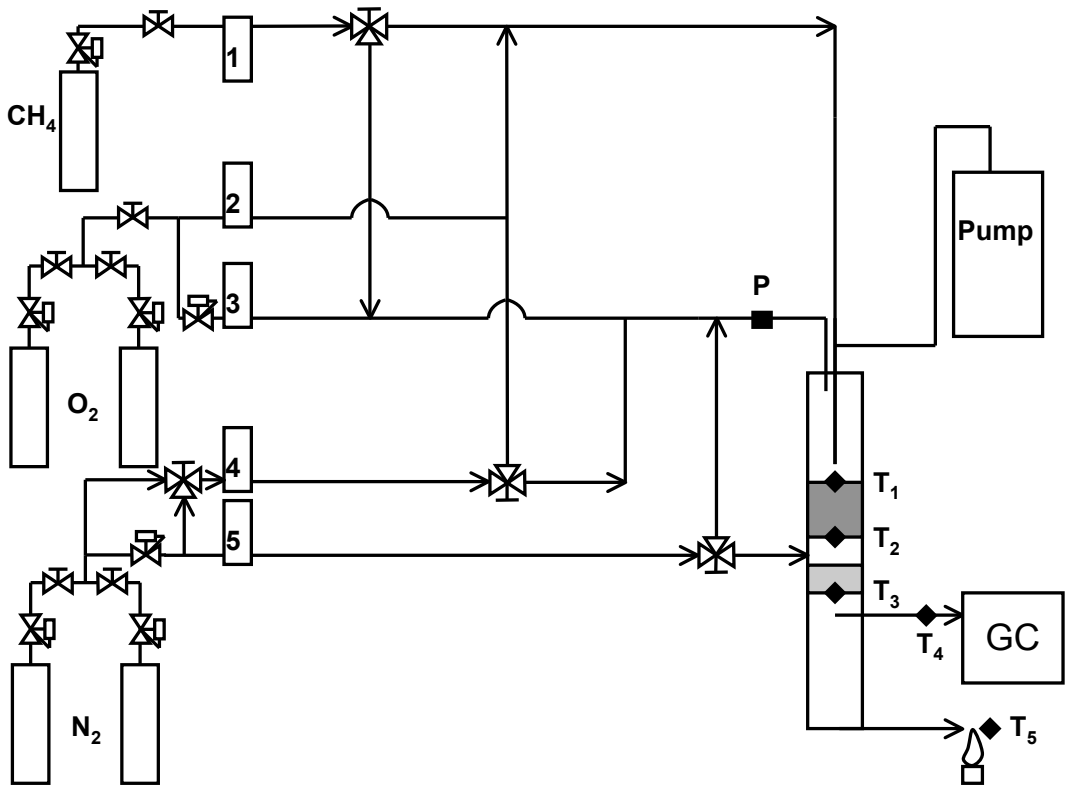

Figure 5.1: Configuration of the reactor system for the time-on-stream experiment. All gas flows, temperatures (T) and pressure (P) are monitored and controlled by the LabView interace.

Alumina spheres (diameter = 1.3 mm) were loaded with catalyst using incipient wetness impregnation. The α-alumina spheres were coated with 2.5 wt% Ce as $Ce(NO_3)_3{\cdot}6H_2O$ and calcined in a furnace for 6 hours at 600 ^{o}C. A solution of 1.2 wt% Rh, 1 wt% Ce was applied, dried, and calcined for 6 hours at 600 ^{o}C. Rh was applied in the form of $Rh(NO_3)_3$ salt in water.

The spheres were loaded into a quartz reactor to create a 3.5 cm bed on top of an alumina foam monolith, (L = 10 mm x D = 17 mm). The spheres and foam monolith were wrapped in ceramic paper insulation. In the first experiment, this insulation was FiberFrax; the second iteration added a second monolith downstream of the catalyst bed wrapped in Interam 100 (3M).

Conditions for the two experiments are listed in Table 5.1. C/O is calculated using carbon in the fuel and O_2 in the air. S/C and C/O were selected to yield maximum syngas and minimize byproduct.[159] Air stoichiometry N_2 and O_2 were controlled by four mass flow controllers: some of the gas was fed through the nebulizer and some was fed directly into the reactor, bypassing the nebulizer, as depicted in Figure 5.2. This variable allowed nominal control over droplet size by adjusting the pressure drop of gases through the nebulizer while minimizing gas outlet velocity to avoid fluidizing the spherebed. Droplet sizes were on the order of 10-100 microns. Experiments performed with less than air stoichiometry N_2 had the remainder added through a side port in the reactor to make up the internal standard for analysis.

A premixed solution of glycerol and water was pumped through a Vici M-50 positive displacement pump. The pump could be operated continuously but the controlling software required occasional user input. Liquids entered the reactor at room temperature and were sprayed through a Burgener SS-50 nebulizer to achieve small droplet size and enhanced mixing.

Samples of the effluent gases were obtained through a stainless steel tube at the base of the reactor bed. The samples were analyzed by gas chromatograph according to the method of Rennard et al.[159] Results are depicted in selectivity to carbon species or, in the case of H_2, selectivity to hydrogen species based on the stoichiometric C or H in glycerol. Balances on H and C typically closed within 10%, though a few points at the start of the 450 hour experiment exceeded this. Excess effluent was thermally oxidized.

Thermocouples were placed within the reactor at the top of the sphere bed, at the bottom of the sphere bed, at the sampling location and downstream of the sampling location. Thermocouples also monitored the sample line and the methane flame used for oxidizing the effluent. A pressure transducer monitored the pressure upstream of the catalyst bed. A pressure gauge depicted the gas pressure in the nebulizer.

All flow rates, temperatures, and the pressure transducer were controlled and monitored through LabView.

Table 5.1: Conditions for CPO of glycerol. The inclusion of N_2 was necessary to reduce the availability of O_2 for better CPO of fuel. C/O = 0.8 is chosen to decrease selectivity to nonequilibrium species. Metal loading is chosen to mitigate sintering and increase dispersion, as well as facilitate O_2 migration.

Parameter	Value
Steam / Carbon	S/C = 2/3
Carbon / Oxygen	C/O = 0.8
Nitrogen / Oxygen	3.76
Sphere Size	1.3 mm
Metal Loading	1.2 Rh%-1% Ce/2.5% Ce
Liquid Flowrate	71.44 mL / hr
Total Gas Flowrate	3.1 SLPM
Contact Time	$\tau = 10\ ms$
GHSV	$10^6\ hr^{-1}$

SEM images were obtained with a JEOL 6500 Scanning Electron Microscope with secondary electron detection. Energy Dispersive Spectroscopy (EDS) was performed on the same instrument.

Equilibrium calculations were made using Chemkin 4.1.1. $C_3H_8O_3$, N_2, O_2, H_2O, H_2, and C_1 and C_2 permanent gases were used as possible species. Gas phase equilibria were used to simulate reactor conditions by calculating the enthalpy of vaporization for the liquid water and glycerol feeds and converting an equivalent amount of glycerol to CO_2 and H_2O. Adiabatic, constant pressure conditions were implemented. Results from these calculations appear at the end of the experimental runs in open symbols. Isothermal equilibria were calculated in the same way, holding temperature and pressure constant.

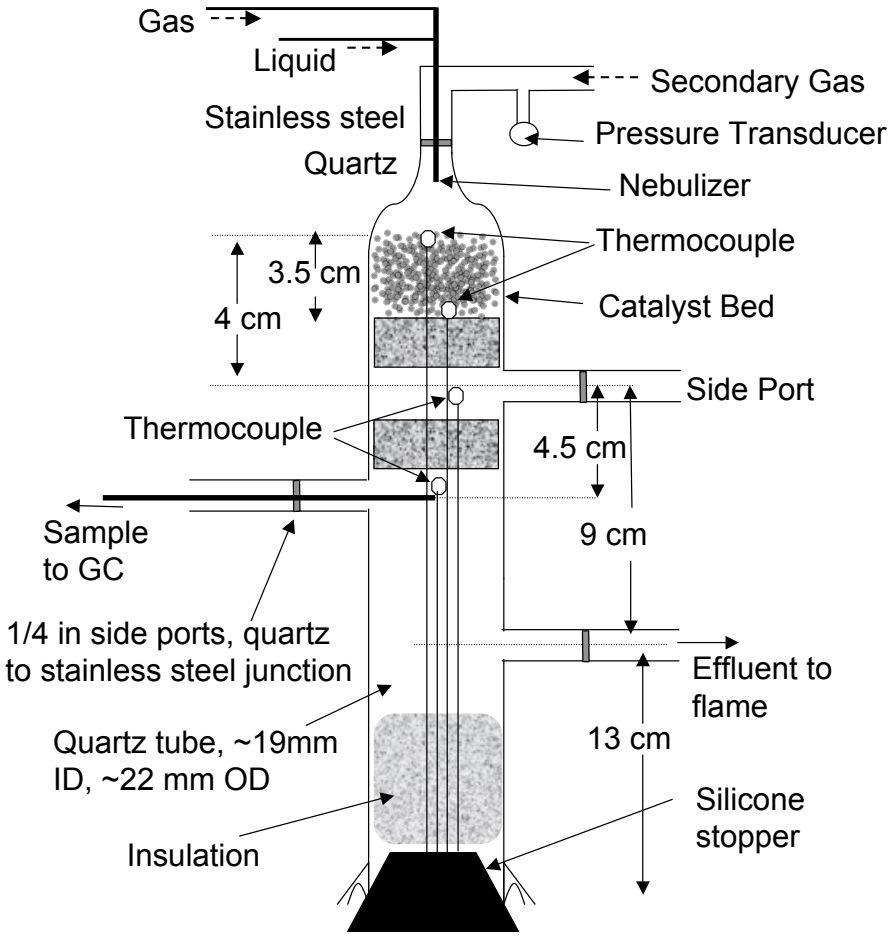

Figure 5.2: CPO Reactor. Flow was from the top through and around the nebulizer, through the catalyst bed. A side port allowed for introduction of diluent as a reference gas after the catalyst bed. Samples were obtained downstream of the bed through a sample line. Effluent was burned off through a downstream port in the side of the reactor; the bottom of the reactor was sealed with a stopper, allowing for overpressure release. The quartz reactor was placed within an aluminum box packed with insulation.

5.4 Data Analysis

5.4.1 Transient Analysis via Accelerated Aging Experiment

An accelerated aging experiment was conducted exploring the effects of transient modes on the system and performance of the catalyst. The experiment lasted 353 hours, consuming 21.4 kg of glycerol and 8.3 kg of water.

Temperature data from the accelerated aging run is depicted in Figure 5.3. The frontface temperature spiked during transient tests, some of which resulted in the translation of the catalyst bed with respect to the thermocouple. All thermocouples were placed axially with respect to the reactor and slide within a drilled hole in the monolith supports. These supports were wrapped in FiberFrax ceramic paper to hold them in place. However, aging and thinning of the ceramic paper weakened the tension holding the catalyst in place. The pressure of impinging gases on the catalyst bed, in addition to thermal events above the bed, resulted in the translation of the catalyst relative to the reactor. As the thermocouples were bound to the reactor and not the bed, the sliding catalyst bed resulted in thermocouple measurements at different positions than those at the outset of the experiment.

Figure 5.4 depicts the product spectrum over time. A decrease in CO_2 and increase in CO, in addition to the decrease in H_2, indicate a loss in water-gas-shift activity in the catalyst over time.

In order to explore catalyst aging under extreme conditions, several transient tests were conducted on the operating reactor, five of which involved full reactor shut down. These tests included hot transients: elimination of fuel to the reactor, resulting in a brief but controlled sudden decrease in C/O, traversing the combustion limits and raising the temperature of the bed; and the elimination of diluent, resulting in an aerosol carried by O_2 which also raised the bed temperature. Cold transients were simulated with the shut down of O_2 so that C/O increased until the reaction extinguished.

Besides these experimental transients, one spontaneous event resulted in a transient at 75 hours, likely due to a mechanical issue such as the relocation of several catalytic spheres due to impinging high velocity gases. These events are flagged in the plot in Figure 5.3. "N_2 Trans" events indicate a lack of diluent that caused temperatures to spike in the oxidation zone. As such, these events exposed the oxidation zone to short-duration high temperatures which likely resulted in sintering of the catalyst. "Fuel Trans" events simulated a fuel-first shutdown, and

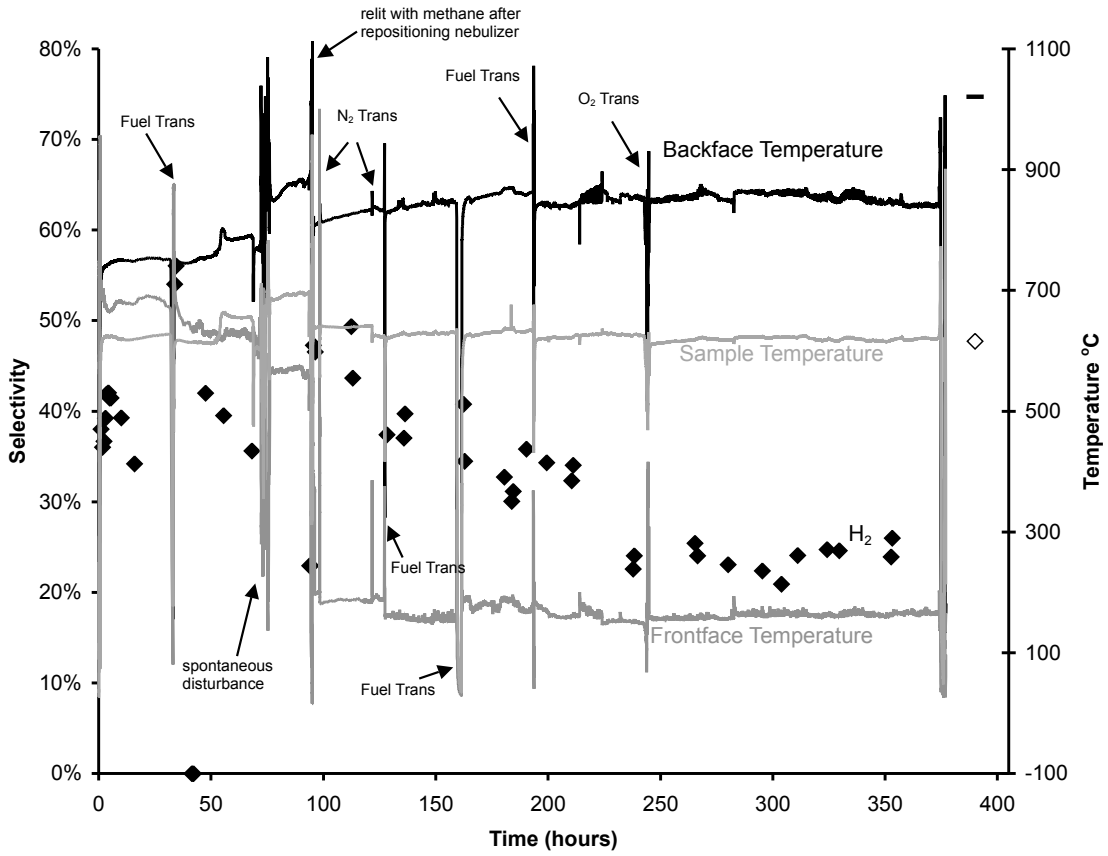

Figure 5.3: Temperature data and selectivity to H_2 from the 375 hour the time-on-stream experiment. The temperatures depicted include the frontface temperature at the top of the catalyst bed, the backface temperature at the bottom of the catalyst bed, and the sample temperature near the sampling port. During the experiment, several events and the decomposition of fiberfrax ceramic paper resulted in the translation of the catalyst bed relative to the thermocouples. As a result, the frontface thermocouple, which was initially positioned at the top of the catalyst bed, emerged above the bed by 5mm at the end of the experiment. Transient experiments are flagged: for example, "Fuel Trans" refers to removal of fuel. Adiabatic equilibrium data are depicted at 390 hours with an open symbol for H_2 and a hash for temperature.

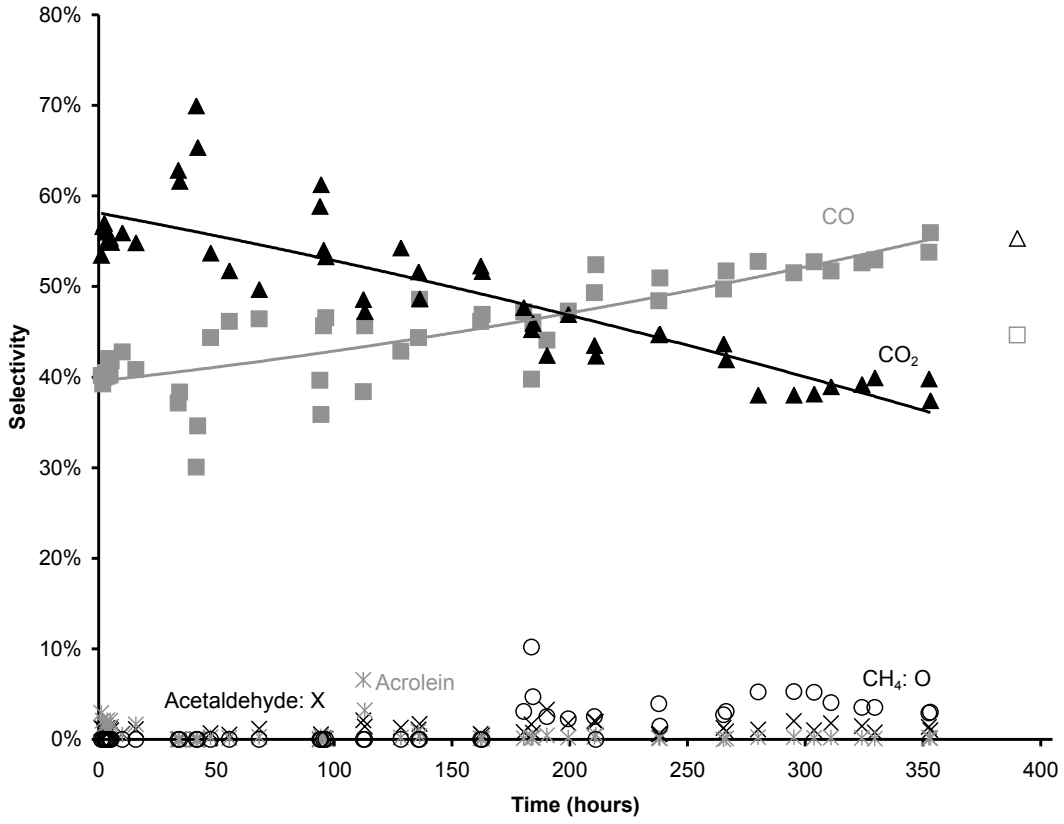

Figure 5.4: Carbon selectivity from the accelerated aging experiment. Main products are CO and CO_2. Some acrolein and acetaldehyde are reported, but typically represent < 1% carbon. Adiabatic equilibrium data are depicted at 390 hours in open symbols.

"O_2 Trans" tested cold shutdown behavior on the catalyst bed by eliminating the oxidation source.

5.4.2 Aging Experiment

The time-on-stream test was repeated with a second reactor over 450 hours, consuming 27.6 kg of glycerol and 10.8 kg of water. To further anticipate spontaneous events as occured at 75 hours in the accelerated aging experiment, in this iteration, safety protocols were implemented via LabView to avoid high temperature excursions greater than 1050 ^{o}C. Temperature data and selectivity to H_2 are depicted in Figure 5.5.

Four thermal excursions resulted in higher temperatures; two of these were sufficient to shut down the reactor automatically. These thermal events were apparently spontaneous: no fault in pump activity or gas availability was found. The events are flagged on Figure 5.5. In one case, a thermal excursion was ameliorated by switching from glycerol to methane for ten minutes. It is theorized that these thermal excursions could be a result of cycles in coke deposition and burn off, poor solution quality, impurities from the feed or the reactor, or physical relocation of catalyst spheres within the bed due to the impinging of high velocity gases over time. However, evidence is insufficient to make any but circumstantial speculation on causes at present. A test was performed to measure the homogeneity of the glycerol solution, and it was determined that once mixed, the solution does not separate over the time frame of the experiment.

Selectivity to carbon species is depicted in Figure 5.6. Selectivity to CO increases slightly over time, with a corresponding decrease in selectivity to CO_2. Selectivity to minor species increases slightly from negligible to $\approx$5%.

Over the course of the experiment, H_2 production steadily decreased. Two major decreases are observable in the data, coinciding with temperature excursion 1 and 2. However, it is worth noting that in the case of both the first and the second thermal excursion, a decrease in selectivity to H_2 *precedes* temperature increase.

Four shutoffs occurred over the course of the experiment. In the first case, the reactor was shut off automatically due to the second spontaneous temperature excursion, and after a data point was collected, a second, manual shut off was necessary to fix a leak upstream of the catalyst. A third manual shutoff occured to clean the effluent line, which had plugged as a result of the first shutoff (the sample line was also necessarily cleaned as a result of the first shutoff, which resulted in glycerol clogging sample and effluent lines downstream of the catalyst bed).

The fourth shutoff was automatically triggered by hot backface temperatures, and resulted in the discovery of a leak in the quartz reactor tube that ended the experiment.

Molar flowrates of major dry product gases are depicted in Figure 5.7.

5.5 Discussion

It is theorized that the several thermal events may be avoided by a reactor design that positions the nebulizer tip closer to the catalyst front face. The accumulation of some of the fuel on the wall of the reactor resulted in a small droplet that slid toward the catalyst. In addition to decreasing mixing, this has the effect of preheating fuel which can then form coke upstream of the reactor. As most of the fuel in this droplet is likely vaporized as it enters the catalyst, conversion and selectivities were acceptable in the short term; RFV may have longer term effects that could result in necessary coke burnoffs. It is worth noting that thermal events correlate with temporary increases in selectivity to CO_2, consistent with a burn-off or complete oxidation.

The 450 hour experiment was ultimately concluded due to the discovery of a leak within the catalyst bed. It is believed that this leak was not caused by mechanical failure of the reactor, but rather by chemical failure: etching of the quartz over time resulted in several holes appearing in the wall within the catalyst bed. This failure is also apparent in the first reactor which ran for 375 hours; however the etching did not penetrate the wall thickness over the course of the first experiment. The most likely explanation for quartz etching is the volatilization of silicon species. Abundant steam and H_2 may form SiH_4, silane, which is typically used in vapor phase silicon deposition. However, other CPO experiments performed in quartz tubes do not report quartz etching, so H_2 may not be the only cause of volatilization. Silicon gels such as alkyl silicates also have high vapor pressure and could leach silicone. This possibility is consistent with etching observed in other alcohol CPO reactors, as well as the destabilization of monoliths, especially those used for CPO of alcohol species.[56, 49]

Both the first and second reactors show similar trends in species evolution: temperatures steadily increase over time, perhaps indicating a slight decrease in endothermic steam reforming, though this is inconsistent with the increase in selectivity to CO. Another plausible explanation is the deactivation of the front of the catalyst bed, shifting the oxidation zone deeper into the bed. Selectivity to product species H_2, CO, and CO_2 approach adiabatic equilibrium for the first 100 hours of the accelerated aging experiment and 75 hours of the time-on-stream

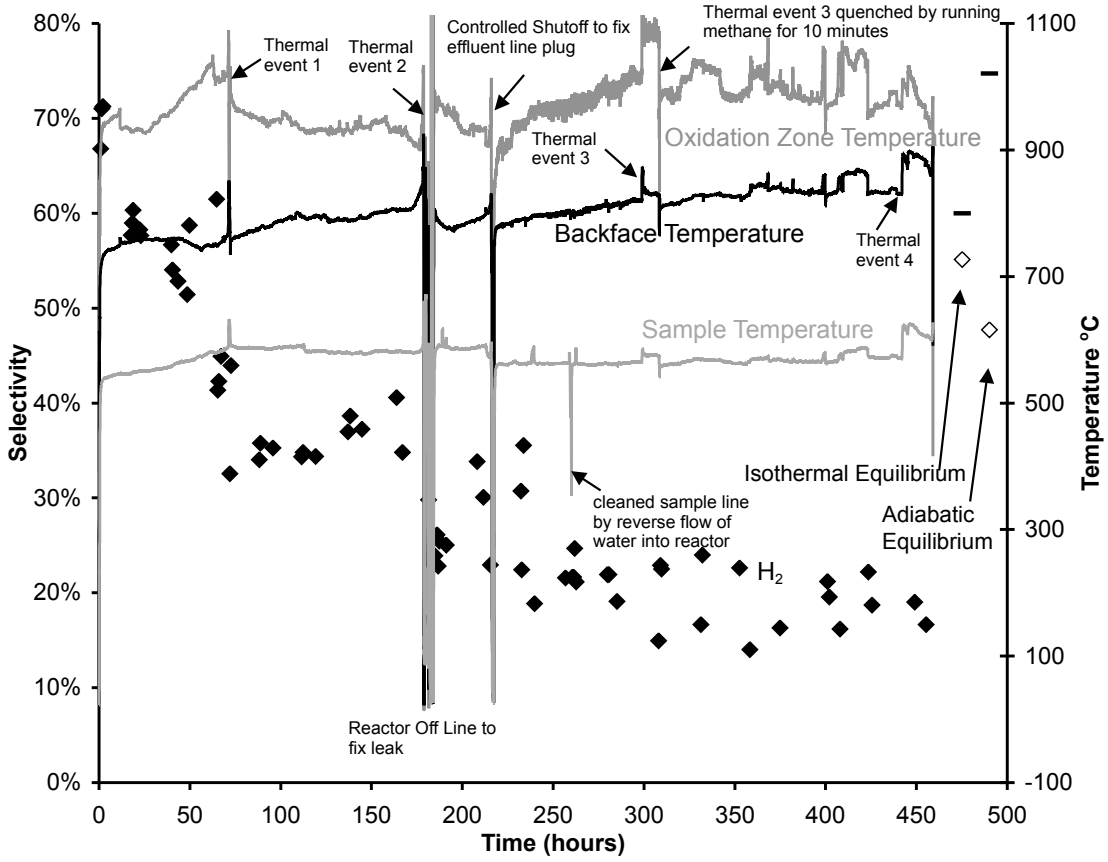

Figure 5.5: Temperatures for 450 hr test. The oxidation zone temperature (gray) is read from a thermocouple three mm below the top of the catalyst bed. Backface temperatures are shown in black. Sample temperatures in light grey represent the temperature in the reactor at the inlet of the sampling system. Selectivity to H_2 drops off after 75 hours. Equilibrium calculations are depicted at 475 hours(isothermal for T = 800 ^{o}C and 490 hours (adiabatic) in open symbols. Equilibrium temperature is depicted with a solid hash. $\tau = 10ms$.

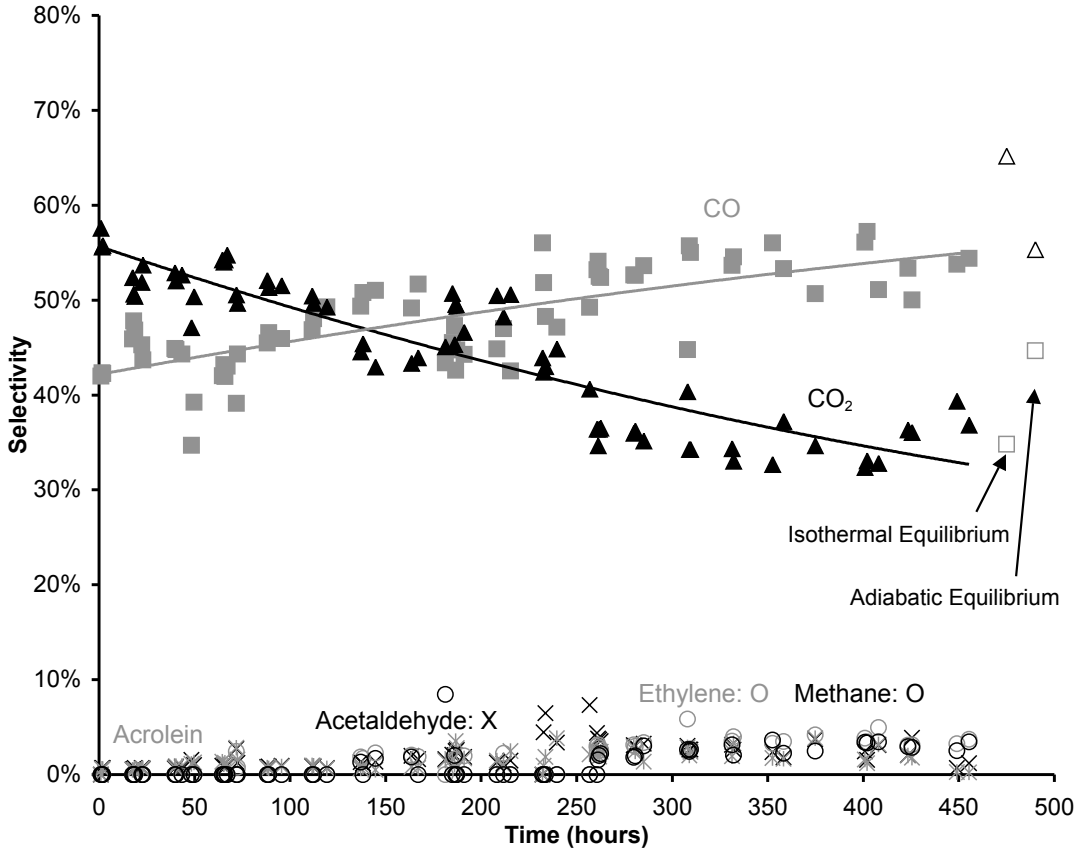

Figure 5.6: Carbon selectivities from second experiment. Major products include CO, CO_2. Minor products include acetaldehyde, ethylene, acrolein, and methane. Equilibrium calculations are depicted at 475 hours(isothermal for T = 800 ^{o}C and 490 hours (adiabatic) in open symbols.

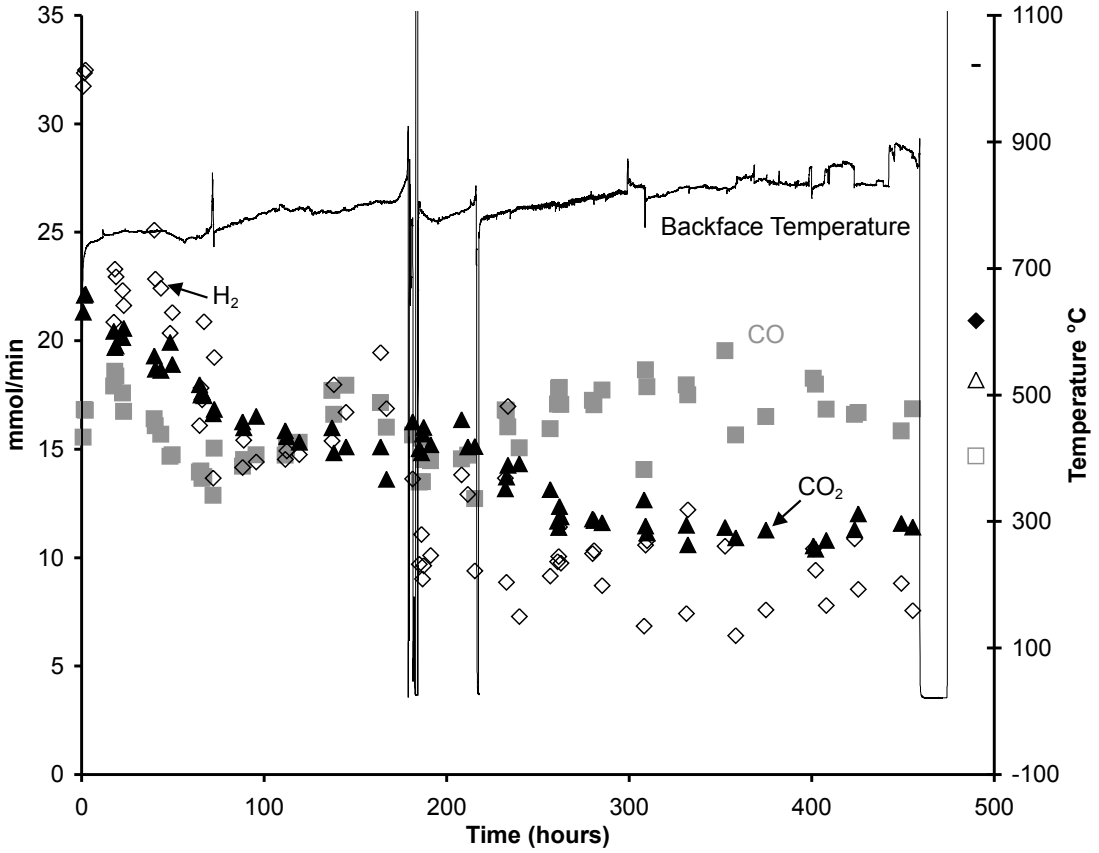

Figure 5.7: Molar flowrates of CO, CO_2 and H_2 show the product relationship in the decay of catalytic activity. Adiabatic equilibrium calculations are depicted at 490 hours.

experiment.

Temperatures at the backface are lower than equilibrium prediction by about 200 ^{o}C, likely due to heat conduction through the quartz and through ports in the reactor. Production of H_2 decreases in the first 100 hours and is related to thermal excursions within the catalyst. The H_2/CO ratio decreases from ≈1.5-2 to 0.5. The changes in product species depicted in Figure 5.7 suggest a failure in the water-gas-shift reaction over time, and are similar to results reported on steam reforming of the aqueous fraction of bio oil.[169]

A profile study of methane CPO suggests that a central contribution of Ce in the formulation of similar catalysts is the promotion of water-gas shift.[148, 170] In the absence of Ce and H_2O or CO_2 cofeed, water-gas shift does not contribute meaningfully to CPO.[75, 171] Although Ce is used in high temperature automotive oxidation catalysts, thin Ce films may sinter at lower temperature.[172] Thus, the change in catalyst performance may be partially due to Ce reformulation.

Catalyst deactivation is typically grouped into four categories: sintering due to high temperature surface changes, poisoning due to the introduction of impurities to active surface sites, coking, and phase transformation.[173, 174] Of these, studies suggest that, though it is a stable catalyst formulation, Rh/Al_2O_3 may be prone to coking from CO_2 adsorption and sintering at reaction temperatures.[175] However, as Zhang et al. mainly focused on dry reforming, the coke deposition may be less relevant in a CPO environment (See Appendix C for more discussion on deactivation, including coking). Indeed, the presence of 10% O_2 was sufficient to eliminate all coke. Similarly, coke deposited during ethanol steam reforming was unstable at higher temperatures and was rapidly eliminated by introducing dilute O_2.[166, 175] The main routes for deactivation in this experiment are likely thermal sintering and poisoning.

5.5.1 Thermal Deactivation: Sintering

Sintering, however, may play an important role in catalyst deactivation, and was observed in several studies as a significant contributing source of catalyst deactivation at similar reaction conditions.[165, 161, 34] SEM images of the catalyst, both used and fresh, are depicted in Figure 5.8. The unused catalyst has high surface area "ribbons." The used catalyst exhibits boulders with crystallites on top. This suggests sintering has reduced surface area in this example.

Two types of sintering likely occur: initial sintering during the first few hours in which the catalyst achieves operating conditions, and long term sintering which took place over the whole

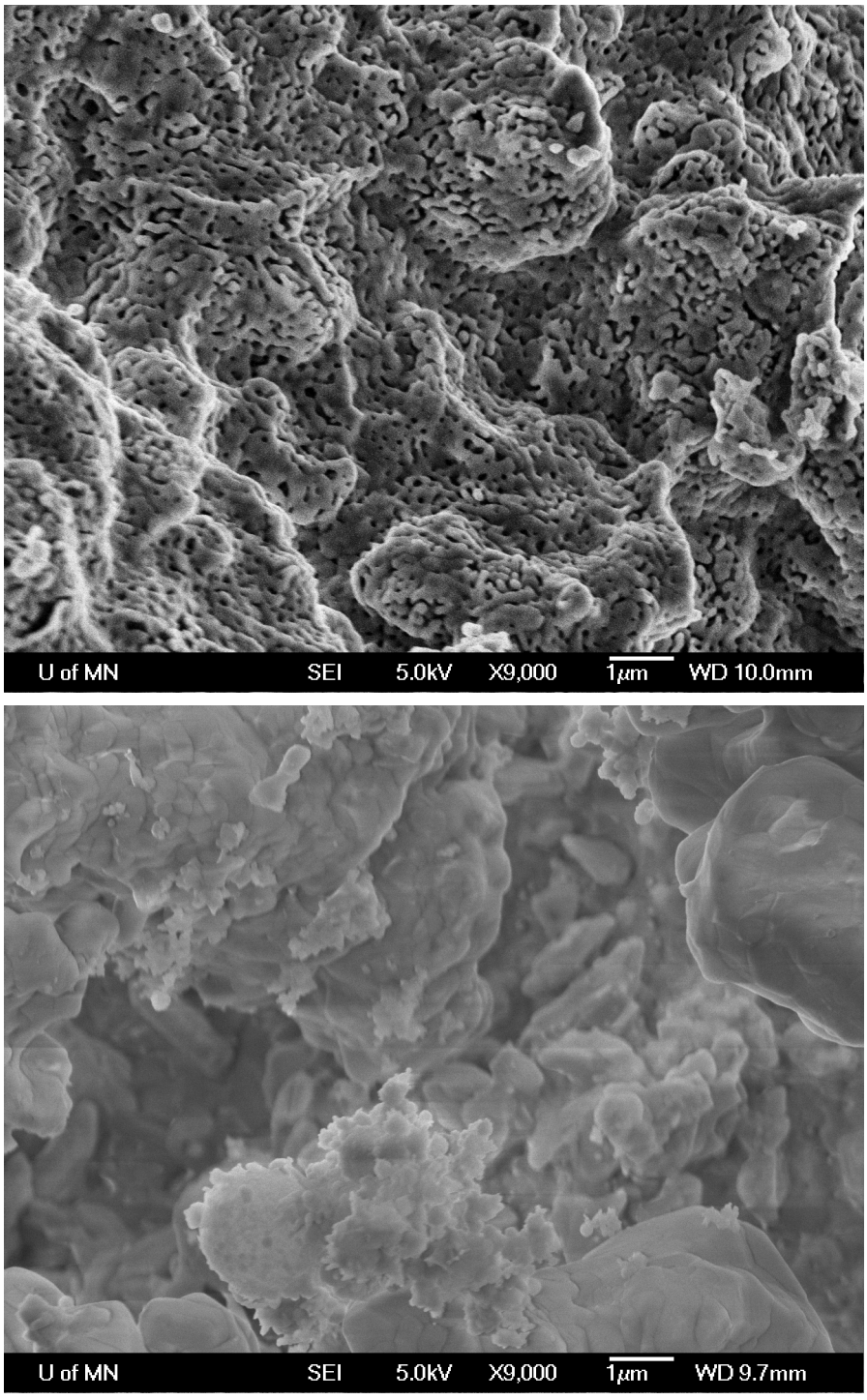

Figure 5.8: SEM images of fresh catalyst (top) and used catalyst (bottom) from the 450 hour experiment. The image of the unused catalyst reveals high surface area films of Rh and Ce. The second image shows boulders with crystallites, suggesting sintering and a loss of active metal surface sites.

time frame of the experiments, causing a slow but steady deactivation of the catalyst.

5.5.2 Poisoning

Poisoning is also a likely vector for catalyst deactivation in this study. Both reactors show deposition of an orange/red material upstream of the catalyst bed. This deposit is also found on the catalytic spheres (Figure 5.10). It is unclear what caused the deposit. Impurities in the feed gases, water cofeed, or glycerol are likely candidates for carrying an impurity into the reactor and depositing it upstream of the bed. The vaporization of Si from the quartz suggests another source of catalyst poisoning. It is possible that individual thermal events correlate with the deposition of some form of impurity, and may be related to the quartz etching.

Figure 5.9: Red ash was deposited upstream of the reactors for both the 375 hr (left) and 450 hr (right) experiments. Etching is also apparent in the quartz swirls below the ash deposit for both reactors.

An assay from the glycerol manufacturer indicates low impurities in the particular USP grade glycerol batch in Table 5.2. For instance, 20 kg of glycerol will contain ≈0.1 g of heavy metals. For comparison, the approximately 8 g of catalyst used in the reactor were loaded with 1.2 wt% Rh, or 0.096 g Rh catalyst. Poisoning is certainly a possible mechanism for catalyst deactivation in this study.

Table 5.2: Impurities in USP glycerol batch as determined by the manufacturer

Impurity	Maximum Amount
chlorides	10 ppm
arsenic	1.2 ppm
heavy metals	5 ppm
chlorinated compounds	30 ppm

A sample of catalyst and a sample of the red powder deposited upstream of the reactor were examined with EDS. The powder comprised C, O, S, Ca, Fe, Si, Mg, Ti, Na, Al. Besides expected elements, the catalyst revealed Fe, Si, Ca, Mg, as well as trace amounts of Ti and P. As noted above, several of the catalytic pellets were red upon removal from the reactor, the color matching that of the powdered deposition upstream of the catalyst bed, depicted in Figure 5.10. These results indicate that inorganic species have been deposited in the reactor - mostly upstream, but in some cases directly onto the catalyst. As recirculated aerosol droplets can condense on the surface of the reactor upstream of the catalyst bed, they are a likely candidate for the introduction of these inorganics. As such, a prevaporizaton / filtering module upstream of the reactor may be sufficient to eliminate many of these species.

Several studies show poisoning from S results in a decrease in steam reforming, characterized by an increase in temperature and a decrease in H_2 production.[176, 177] O'Connor et al studied CPO of gasoline over 10 hours and found that catalyst poisoning (S, Fe, V, Mg, Ti in the fuel) reduced production of syngas and led to O_2 breakthrough.[178] O_2 breakthrough is consistent with progression of the oxidation zone through the catalyst bed.

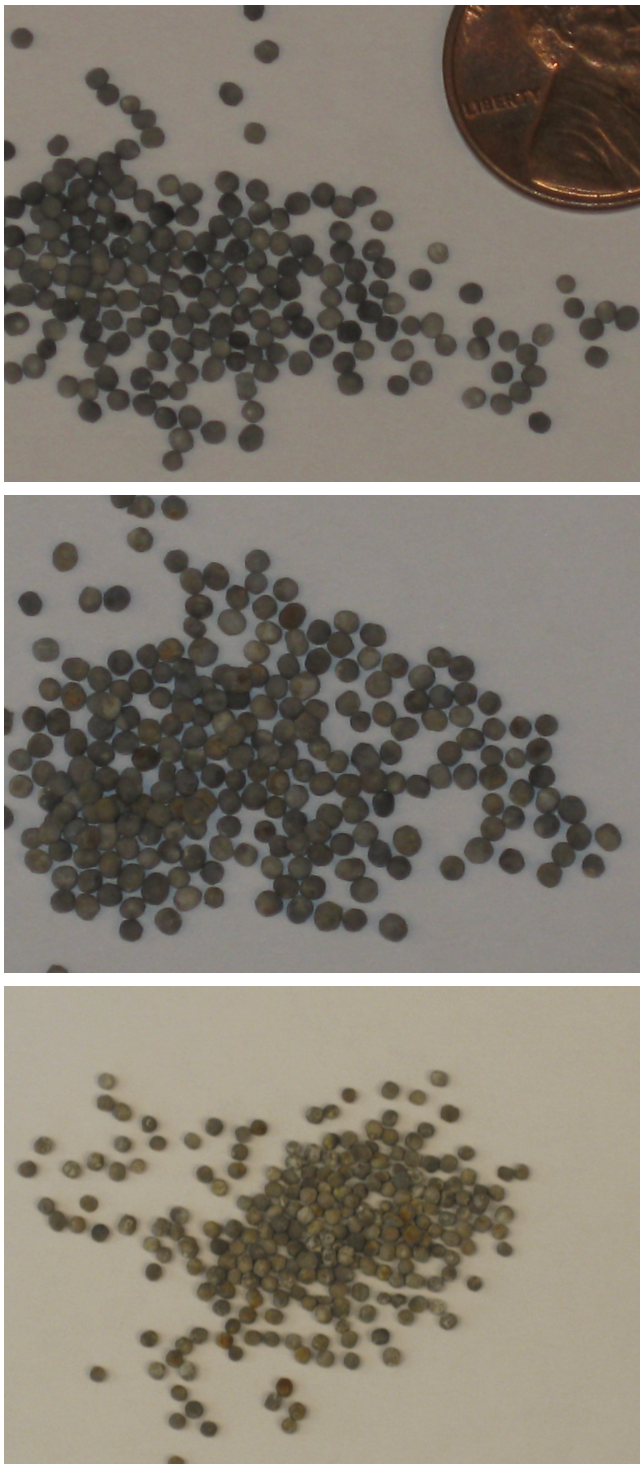

Figure 5.10: Catalyst for the CPO of glycerol. The top image shows unused catalysts: all are grey. The middle image shows catalysts used in the 375 hour RFV of glycerol experiment, and the bottom image depicts catalysts used for 450 hours. Red and brown deposits are visible on the used catalysts, the color matching that of the deposit on the walls of the reactor.

5.5.3 System Management

Transient tests conducted in the first experiment show that increases in temperature simulating shutdowns or loss of diluent or fuel can result in slight acceleration of the aging of the catalyst. However, the gradual but steady change in product spectrum suggests that transients and temperature excursions are less significant in catalyst deactivation for the RFV of glycerol. The most significant drop in H_2 selectivity appears at about 230 hours and does not correlate to any of the transient tests (Figure 5.3). By contrast, spontaneous events appear to have some relationship to a change in product selectivity (Figure 5.5).

Shifting fuel from glycerol to methane during the third thermal transient in the 450 hour experiment resulted in a return to normal temperatures. Similarly, careful management after the spontaneous transient in the 375 hour test returned temperatures to normal at ≈100 hours. With more sophisticated management protocol, it is possible temperatures could be maintained below critical sintering values even during spontaneous burnoff-type events.

5.5.4 Effect of Diluent on Reactive Flash Volatilization

A range of tests was conducted on new and on used catalysts to arrive at the optimal parameters for Table 5.1. Flowrates, N_2/O_2, S/C, and C/O were considered, though once air stoichiometry was chosen, choices of other parameters were substantially informed from previous work.[159]

Attempts were made to eliminate the diluent, and the side port was used for the addition of N_2 as an internal standard during these experiments. Eliminating the diluent can be beneficial for industrial application, as smaller reactors can be built and no N_2 separation from syngas must be considered. In addition, hotter temperatures improve equilibrium syngas yields, favoring steam reforming and improving kinetics for water-gas shift. However, experiments conducted without N_2 revealed that fuel transport difficulties inhibit optimal reactor performance. Glycerol has low volatility; droplets of glycerol and water sprayed into the reactor could not effectively disperse and mix as well as a gas. As a result, oxidation, which is typically limited by O_2 transport in methane CPO,[48], was instead limited by fuel transport. Local hotspots developed where fuel impacted and was fully oxidized, consuming all of the O_2 in the stream. Unconverted fuel cracked into byproducts in the reactor, and high temperatures promoted catalyst deactivation via sintering. This effect was eliminated with the introduction of a diluent, and as increases in N_2 improved conversion to syngas, air stoichiometry was chosen.

It is hypothesized that prevaporization to promote mixing could achieve some of the benefits of reduced diluent by improving fuel-O_2 mixing. Alternatively, the use of steam rather than liquid water could act as a suitable medium for O_2 diffusion.

5.6 Conclusion

Catalytic partial oxidation of glycerol to syngas for methanol production can reduce biodiesel production dependence on fossil fuels and offset carbon consumption in the process. A Rh-Ce catalyst tested with reactive flash volatilization of a glycerol-water solution demonstrated high yields of syngas for 75 hours, after which time catalyst deactivation reduced selectivity to H_2 and CO_2 and increased the selectivity to CO and exit temperature. Deactivation is likely due to two different modes: thermal sintering, and poisoning. The deactivation pattern suggests a failure in water-gas shift over time, possibly coupled with a progression of the oxidation zone. SEM images suggest that the catalysts have sintered due to high temperatures recorded in the oxidation zone. In addition, the accumulation of ash deposit on the reactor and on the catalyst suggests catalytic poisoning. Etching of the quartz reactor makes this material a poor choice for the RFV of liquid alcohol fuels. Several of these issues could perhaps be ameliorated by prevaporizing the fuel.

Chapter 6

CPO of Pyrolysis Oil

6.1 Summary

As carbon based liquids, pyrolysis oils represent a promising vector for biomass to fuels. However, bio oils will need to be upgraded to interface with existing infrastructure. The rapid deposition of coke in steam reforming reactors makes the conversion of bio oil to syngas difficult. The use of O_2 as a cofeed in reforming of bio oils can avoid the high energy requirements for steam production to avoid coke formation. The conversion of bio oils to syngas via catalytic partial oxidation over Rh-Ce is demonstrated. Pyrolysis oils from three sources - pine, poplar, and mixed hardwoods - are introduced directly to the catalyst via reactive flash volatilization. Coke formation is avoided on the catalyst with steam addition or by introducing the bio oil directly to the catalyst, using a water-cooled delivery system. H_2 and CO can be produced autothermally over Rh-Ce catalysts with millisecond contact times. The addition of methane or methanol to the fuel improve reactor stability. Due to the scalability of catalytic partial oxidation, on-board reforming may make use of such a reactor to produce syngas or H_2 for fuel cells in automotive applications, thereby avoiding all refining steps after pyrolysis. Alternatively, large scale syngas production using CPO can be combined with Fischer Tropsch chemistry to produce synthetic renewable fuels.

6.2 Introduction

Work presented in the previous chapters has been driven by an academic interest to understand the chemistry of various components and representative species of biomass pyrolysis oil. For a survey of bio oil components, see Table 6.1. With sufficient understanding of how each of the myriad components react in the catalytic partial oxidation environment, it should be possible to achieve CPO of bio oil directly. There are many intervening lessons that could have been presented as chapters in this work: for instance, the interactive effects of multiple species, starting with binary fuel compositions and increasing in complexity, or the chemistry of the lignin derived fraction of bio oil, which contains most of the aromatic species responsible for the formation of char. However, such exploration would be time consuming, requiring several PhDs to even scratch the surface.

Chapter 2 described the CPO of some of the most active components in boi oil, the organic acids. Chapter 3 described the importance of functionality and how a slight change in a large molecule can result in completely different chemistries in the CPO reactor. Chapter 4 demonstrated the versatility of a powerful new tool for CPO: reactive flash volatilization. With compounds like esters and polyols, which decompose readily when heated, RFV allows the investigation of individual chemistries by forcing them to interact with the catalyst. Even more importantly, it provides a means by which liquids can be converted to syngas without any preheat for vaporization. As bio oils are known to form coke with the addition of heat, this technology is essential for any application of CPO. Chapter 5 and Chapter 7 detail the deactivation of catalysts and how this can result from RFV. These lessons will have to be addressed sooner or later for high yields of syngas to be achieved, but in the near term it is still of interest to discover whether bio oil can, in fact, undergo CPO.

All of the fuels examined in the previous chapters have represented the aqueous fraction of pyrolysis oil, but the technologies derived from these experiments can be applied more widely. This chapter will focus on the CPO of whole pyrolysis oils.

6.2.1 Catalytic Gasification

Low ash pyrolysis oils can be upgraded by catalytic steam reforming. Nickel is the typical catalyst of choice for the steam reforming of several bio oil model compounds and pyrolysis oil constituents.[24, 59, 169, 179] In addition, whole bio oils or the aqueous phase of bio oils have

Table 6.1: A rough survey of the major contents of bio oil. Adapted from [23]. Bio oils vary, but include a great number of acids, esters, alcohols, carbonyls, polyols, and phenols. For this reason research in Chapters 2-4 focused on the CPO of various components in bio oil. In general, the left side of the table lists the water-soluble fraction, derived from cellulose and hemicellulose; on the right is the water-insoluble lignin derived fraction. Bio oil separates with the addition of water.

Species	wt. %	Species	wt. %
Acids	5-10	Phenolics	20-30
Formic	0.3 to 9.1	Phenol	0.1 to 3.8
Acetic	0.5 to 12	2-Ethyl phenone	0.1 to 1.3
Propanoic	0.1 to 1.8	1,4 DiOH benzene	0.1 to 1.9
Esters		Guaiacols	
Angelicalactone	0.1 to 1.2	2-Methoxy phenol (guaiacol)	0.1 to 1.1
2(5H)-Furanone, 5-methyl		4-Methyl guaiacol	0.1 to 1.9
Alcohols		Isoeugenol	0.1 to 7.2
Methanol	0.4 to 2.4	Eugenol	0.1 to 2.3
Ethanol	0.6 to 1.4	Syringols	
Ethylene glycol	0.7 to 2	2,6 DiOMe phenol (syringol)	0.7 to 4.8
Ketones & Hydroxyketones	0-10	Propyl syringol	0.1 to 1.5
Acetone	2.8	Syringaldehyde	0.1 to 1.5
Acetol (hydroxyacetone)	0.7 to 7.4	Furans	
Aldehydes & Hydroxyaldehydes	5-20	Furanone	0.1 to 1.1
Formaldehyde	0.1 to 3.3	Furfural	0.1 to 1.1
Acetaldehyde	0.1 to 8.5	Furfural alcohol	0.1 to 5.2
Ethanedial	0.9 to 4.6	5-OH-Methyl-2-furfural	0.3 to 2.2
Hydroxyacetaldehyde	0.9 to 13	Others	
Sugars		Methyl cyclopentenolone	0.1 to 1.9
Levoglucosan	0.4 to 1.4	4-OH-3-methoxybenzaldehyde	0.1 to 1.1
Glucose	0.4 to 1.3		
Fructose	0.7 to 2.9	Water	15-30
D-xylose	0.1 to 3.2		
Cellubiosan	0.6 to 3.2		
1,6 Anhydroglucofuranose	3.1		

been steam reformed over Ni in various reactor configurations.[180, 24, 181, 182] However, the reforming of pyrolysis oils presents significant challenges, most of which have to do with coke formation due to the dehydration and polymerization of pyrolysis liquids. Whole bio oils are subject to even greater coke formation due to the polymerization of aromatic and unsaturated components in the lignin-derived fraction.

Several strategies have been implemented to solve the coke problem, including catalyst choice, steam addition, fuel blending, and periodic reactivation via steam or burnoff.

Noble metals have been investigated for the steam reforming of pyrolysis liquids.[57, 183, 60] Pt and Rh especially show greater stability and resistance to coking than cheaper alternatives. Another option is to not use a catalyst at all: van Rossum reports efficient gasification of pyrolysis liquid which can then be cleaned in a second stage involving a catalyst.[180, 184]

Coke formation can also be decreased by steam / carbon feed (S/C). Production of H_2 increases with S/C, but so do heat loads as steam reforming is endothermic (Equation 6.1) and requires the production of steam.

$$C_xH_yO_z + (2x - z)H_2O \rightarrow (2x + y/2 - z)H_2 + xCO_2 \qquad \Delta H >> 0 \qquad (6.1)$$

Reforming experiments in the literature are typically carried out in excess steam, often utilizing $6 < S/C < 12$, and no examples of steady catalytic reactor operation are reported for $S/C < 3$.

Blending of pyrolysis oils can also alleviate coke formation. Mixing bio oils with methanol enhances their stability.[185, 186, 187] Czernik et al. investigated the steam reforming of the aqueous phase of pyrolysis oil over a fluidized bed of Ni catalysts with the addition of natural gas.[100] Their reactor demonstrated fuel flexibility, and the addition of natural gas promoted catalyst stability and longevity.

Solid carbon can also be eliminated using burn offs. Domine et al. demonstrated the efficacy of pyrolyzing bio oil for H_2 production over noble metal catalysts, and periodically reactivated the catalysts by feeding oxygen.[188, 189] Oxidation can occur in the presence of steam reforming. However, the presence of O_2 reduces both the experimental [183, 180, 181] and theoretical [58] yield of H_2.

If sufficient O_2 is present, partial oxidation can occur autothermally, with oxidative chemistry alleviating the heat load for the reactor according to Equations 6.2 and 6.3. Autothermal reforming of bio oil is desirable because the heat of reaction drives the chemistry, and reactors

can be scaled more easily. Stable autothermal reforming to H_2 would allow bio oil to be used as a liquid fuel for automotive fuel cell applications.

$$C_xH_yO_z + (x/2 - z/2)O_2 \rightarrow (y/2)H_2 + xCO \tag{6.2}$$

$$C_xH_yO_z + (x + y/4 - z/2)O_2 \rightarrow (y/2)H_2O + xCO_2 \qquad \Delta H << 0 \tag{6.3}$$

Depending on the the ratio x:z, Equation 6.2 can be weakly exothermic or endothermic. Some complete oxidation, Equation 6.3, provides enough energy to operate partial oxidation autothermally. Biomass and bio-oil model compounds have been converted to syngas via catalytic partial oxidation over noble metal compounds.[56, 159, 50] Additional advantages of CPO include the availability of O_2 for the removal of coke, high heat transfer rates and thermal efficiency, fast (millisecond) contact times, high conversion, and equilibrium syngas production.

This chapter presents a comprehensive exploration of catalytic gasification of pyrolysis liquids. Several reactor configurations are detailed, and numerous experiments on a variety of pyrolysis oils are considered, including the CPO of pyrolysis oils and catalytic oxidative reforming over noble metals.

6.3 Experimental

Catalysts were prepared as described in Chapter 2. Ceramic foam monoliths (99% α-Al_2O_3, 1% SiO_2) were drop-coated with an aqueous slurry of γ-Al_2O_3 powder (1 wt% of the original monolith), dried, and calcined in a furnace at 600 ^{o}C for six hours. The foams were then coated with an aqueous solution of 1 wt% each of Ce and Rh in the form of nitrate salts. After drying, catalysts were calcined at 600 ^{o}C for six hours.

Liquids were fed by a fixed volume syringe pump. In experiments with methanol addition, pyrolysis oil and methanol were premixed by weight (eg., in a 50-50 wt% solution). In each reactor scheme of the CPO experiments, liquid fuel was introduced using a stainless steel nebulizer. Air stoichiometry was maintained, though N_2 and O_2 were controlled separately. The fuel / air spray flowed into a 19 mm ID quartz tube over a 3 cm bed of alumina foam monoliths coated with Rh-Ce. In experiments with CH_4 addition, methane was added to the gas mix either through a nebulizer or directly into the reactor. A typical reactor setup is depicted in Figure 6.1. Experiments were conducted in this reactor configuration unless otherwise specified.

Temperatures were monitored at the back face of the catalyst bed in all experiments. Reactor effluent flowed through a cold-water condenser; gas phase species were sampled by syringe to GC calibrated for H_2, N_2, CH_4, CO, CO_2, C_2H_2, C_2H_4, and C_2H_6. N_2 was used as an internal standard.

In some experiments, heat was applied externally using heat tape or a furnace around the reactor tube. In these configurations, a thermocouple is included upstream of the catalyst or on the reactor wall to quantify preheat temperature.

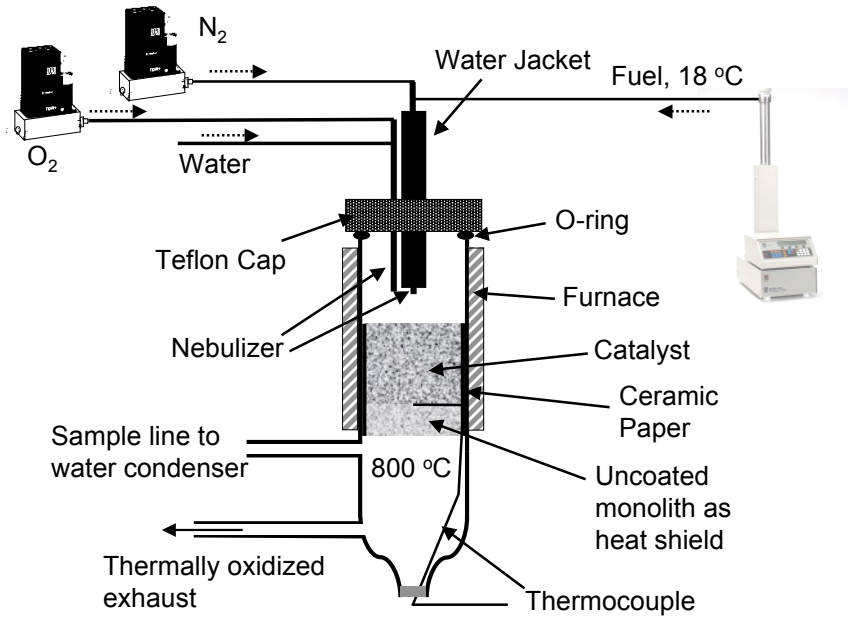

Figure 6.1: Reactor Setup. CPO experiments were conducted in a 19 mm ID quartz reactor. Fuel and air were introduced via nebulizers at the top of the reactor. The vessel was sealed with a Teflon block and an O-ring. Effluent was incinerated after being condensed by cold water. Samples were analyzed by GC. For experiments without heat addition, the clamshell furnace is replaced by insulation. When added, water is fed through a second nebulizer parallel to the first. The fuel nebulizer is clad in a 5/16 tube allowing cooling water to flow continuously to maintain low temperatures within the nebulizer, even when placed within a furnace.

A variety of experiments were conducted exploring the effects of catalyst pore size, air delivery, steam addition, the proximity of the nebulizers to the catalyst, and external heating.

The flow of O_2 and N_2 through the nebulizer results in high velocity gas and small particle sizes. Directing O_2 through another port results in greater surface diffusion of O_2 to the top face of the catalyst, thus shifting the oxidation zone. Oxygen diffusion can also be affected by adjusting the pore size of the catalyst: smaller pores result in a shorter oxidation zone. However, smaller pores also increase the pressure drop of the catalyst bed, which affects recirculation of high velocity liquid nebula and gas. Shortening the distance between the nebulizer and the catalyst increases heat transfer rates, but reduces the radius of the spray mist.

For the pyrolysis oils, which are a combination of many different chemicals, mole is defined as $C_1O_xH_y$ according to Table 6.2. Pyrolysis oils were prepared at NREL, where the elemental analysis was also performed. Over time the properties of these oils changed and some phase separation occurred due to polymerization and dehydration.[28] Bio oils were reconstituted for these experiments using vigorous mixing or methanol addition. Where phase separation persisted, the lighter fraction was used.

Table 6.2: Elemental analysis performed at NREL on the pyrolysis oils yielded these results for defining a "mole" of each oil.

	Poplar	Pine	Hardwoods
C	1.00	1.00	1.00
H	1.78	1.90	1.83
O	0.70	0.76	0.80

A thermodynamic analysis was performed using the Chemkin 4.1.1 software package. Bio oils were simulated using a combination of phenol, methanol, formic acid, and formaldehyde. Isothermal equilibrium was determined holding pressure constant based on the measured back-face temperatures. Besides reactants (also including O_2 and CH_4) and N_2, equilibrium products allowed were CO, CO_2, C_2H_2, C_2H_4, and C_2H_6.

6.4 Data Analysis

The conversion of pure pine pyrolysis oil was achieved using external heating. The effects of water addition to this configuration were examined. Figure 6.2 shows data from the partial

oxidation of pine oil in a furnace. N_2 flowed through a water cooled fuel nebulizer, positioned 1 mm above the catalyst bed comprising a 20ppi/45ppi/45ppi catalysts on top of a 45 ppi uncoated foam acting as a heat shield. O_2 flowed through a second stainless steel port also positioned 1 mm above the catalyst.

In comparison, Figure 6.3 depicts the same experiment with the addition of three moles of water per carbon atom in the fuel. Fuel (0.024 mol/min) and N_2 flowed through a nebulizer positioned 1 cm above the catalyst bed comprising 45ppi/45ppi/80ppi catalyst atop a 45 ppi ceramic monolith acting as a heat shield. Water (0.072 mol/min) and O_2 flowed through a second nebulizer also positioned 1 cm above the catalyst bed.

In both experiments, each data point represents the average of three runs at the given C/O ratio, with the exception of C/O = 1.8, which represents one data point. The addition of three moles water per carbon atom in the fuel has little effect on the product stream in this configuration: yields of CO and H_2 are comparable for C/O = 1.3 in both experiments. However, water addition increases the yield of syngas with an increase in C/O: steam reforming becomes more competitive with limited oxidation.

Oxidation is efficient at maintaining a coke free reactor; however, high O_2 addition consumes syngas product. As a result, syngas yield decreases for C/O < 1.5. With limited availability of oxidative chemistry, coke deposition compromises syngas selectivity; as a result there is a decrease in syngas yield for C/O > 1.5.

Upstream temperatures were significantly lower with the addition of water due to the heat loss to vaporization and heat capacity of steam. Backface temperatures were similar with and without water addition, consistent with similar product spectra. This suggests that under these operating conditions, steam reforming is not sufficiently fast to significantly affect the product spectrum.

An 80-20 wt% hardwood pyrolysis oil / methanol solution was converted to syngas using a furnace. Data are depicted in Figure 6.4. The first three points explore C/O = 0.9, after which the air flow rate was adjusted to yield a C/O = 1.1. To reduce coke deposition between fuel introduction and catalyst, a water cooled nebulizer was positioned 1 mm above the catalyst bed, which comprised 20 ppi / 45 ppi / 45 ppi catalysts atop a 45 ppi uncoated heat shield. N_2 flowed through the nebulizer; oxygen entered through a separate stainless steel tube positioned 0.2 mm above the catalyst bed.

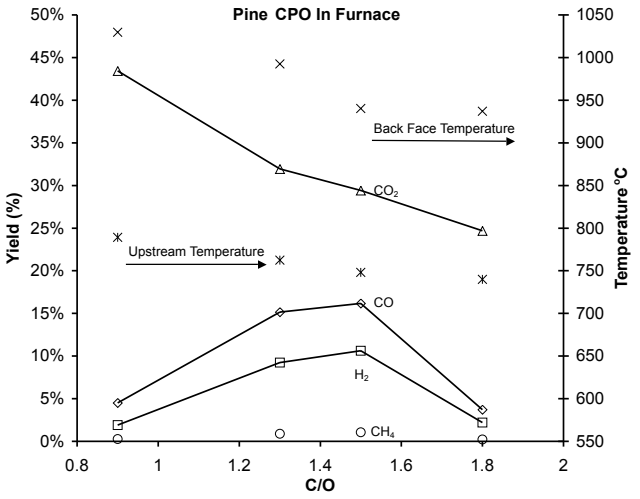

Figure 6.2: Catalytic partial oxidation of pure pine pyrolysis oil in a furnace. A maximum in syngas production is apparent due to two phenomena: as O_2 increases (lower C/O), oxidation of syngas product results in an increase in water and CO_2, consuming valuable syngas. As C/O increases, a build up of coke impairs reactor operation, resulting in inefficient conversion to syngas. Conversion $\approx 48\%$, GHSV $\approx 17000\ \text{hr}^{-1}$, $\tau \approx 53$ ms.

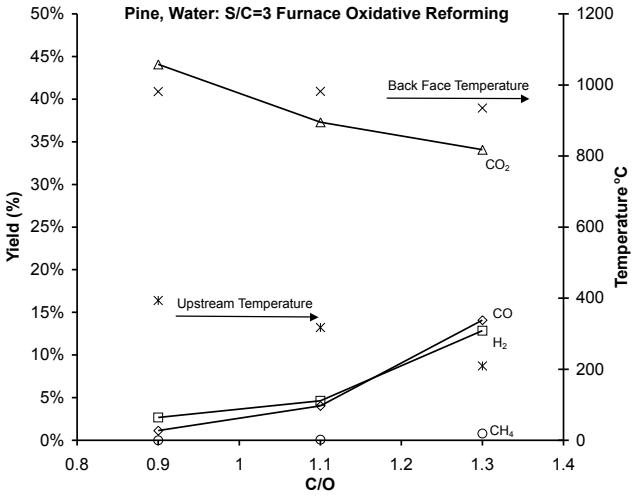

Figure 6.3: Catalytic partial oxidation of pure pine pyrolysis oil in a furnace with three moles water per carbon atom added. Water acts as a significant heat sink, decreasing upstream temperatures and hindering reaction rates even as it increases steam reforming. The effect of increasing O_2 is apparent as C/O decreases: yield of syngas decreases while CO_2 increases. Conversion $\approx 45\%$, GHSV $\approx 37000\ \text{hr}^{-1}$, $\tau \approx 24$ ms.

Under these conditions, the data in Figure 6.4 depict the steadiness of this reactor configuration. H_2 yield is relatively constant, though low, at 25%, and CO yield reasonably level at 65%. There is not an obvious change in syngas production with this small change in C/O, though the higher C/O shows some signs of possible deactivation (decreases in CO, H_2) whereas the lower C/O showed relatively constant or perhaps even increasing yields to syngas. Although the reactor ran smoothly for the entire experiment, coke buildup was noticeable in the reactor upon shutdown.

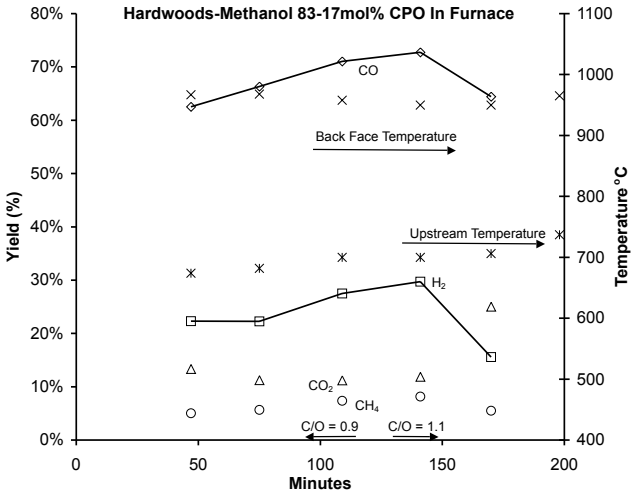

Figure 6.4: Catalytic partial oxidation of 80 wt% hardwoods, 20 wt% methanol in a furnace with 700 ^{o}C preheat. Conversion to CO is highly efficient; conversion to H_2 achieves only 15% yield. Overall conversion $\approx$ 90%. GHSV $\approx$ 18000 hr^{-1}, $\tau \approx$ 47 ms.

6.4.1 Autothermal Operation

A series of experiments were performed to explore the possibility of autothermal operation. A poplar-methanol solution was converted to syngas autothermally using a simple reactor setup, as depicted in Figure 4.2: the feed system is not water-cooled, and the air blown nebulizer is positioned 2 cm above the catalyst bed. Data for this experiment are depicted in Figure 6.5.

Although the reactor achieves autothermal operation, coke deposition upstream of the catalyst and within the fuel feed system precludes steady operation. The reactor shut down after

approximately 200 minutes of operation. Trends in CO_2, H_2, and CH_4 are consistent with a steady loss of activity, likely due to coke deposition in the reactor.

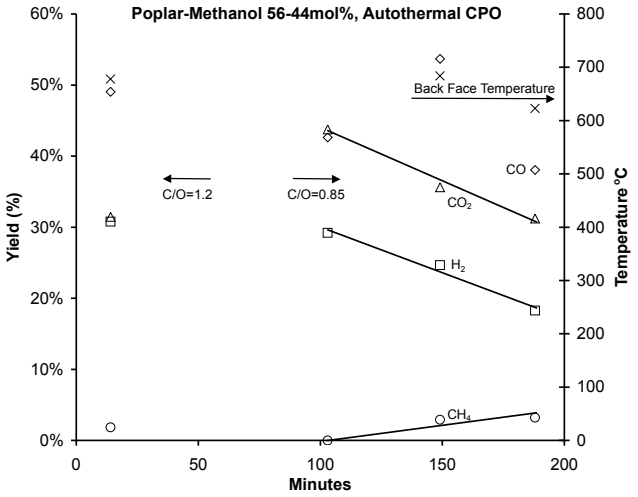

Figure 6.5: Autothermal CPO of a 50-50 wt% solution of methanol and poplar bio oil. The reactor operates for almost three hours before shutdown; deactivation due to coking is observable in the trends for H_2, CO_2, and CH_4. Lines are drawn to demonstrate these trends. Conversion $\approx$ 84%, GHSV $\approx$ 35000 hr^{-1}, $\tau \approx$ 30 ms.

Poplar pyrolysis oil and methanol in a 50-50 wt% solution were partially oxidized autothermally with the addition of methane and air. The air / fuel stoichiometry corresponds to overall C/O = 0.8. Flowrates for oil-methanol-methane are 0.012-0.009-0.004 molC/min. Liquid fuels are propelled by air through a nebulizer positioned 5 mm above the catalytic bed, comprising three 80 ppi foam monoliths loaded with noble metals and one uncoated foam monolith acting as a heat shield at the back face, also using the RFV setup described in Chapter 4 (Figure 4.2). Results are depicted in Figure 6.6.

The partial oxidation of pyrolysis oil, methanol, and methane is repeated using an upflow setup depicted in Figure 6.7. The nebulizer, a $1/8^{th}$ inch stainless steel tube, is immersed in a pool of distilled water below the catalyst, allowing the water to cool the tube as fuel sprays upwards onto the catalyst surface. Results from this configuration are depicted in Figure 6.8. Total conversion decreases with the upward spray due to the accumulation of fuel in the water

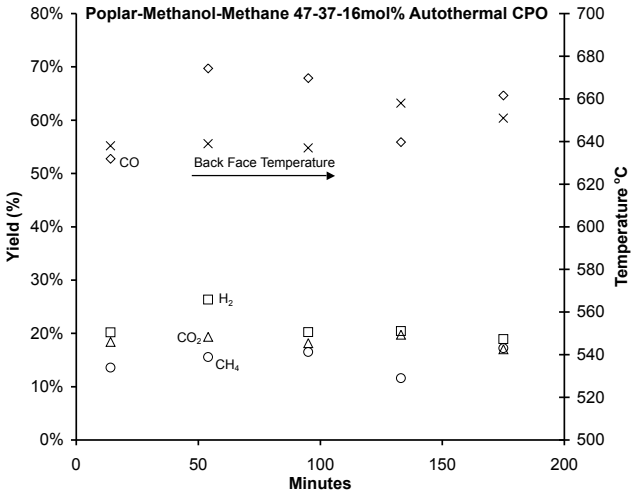

Figure 6.6: Autothermal Partial Oxidation of a 50-50 wt% poplar oil-methanol solution with 0.1 SLPM CH_4 addition. C/O = 0.97, Conversion ≈ 96%, GHSV ≈ 22000 hr^{-1}, $\tau \approx 54$ ms.

pool. However, the decrease in coke formation within the nebulizer and near the catalyst enhances stability, thereby demonstrating the need for a coolant system on the nebulizer. This was realized for the other experiments in the form of a jacketed water-cooled nebulizer.

An increase in reactor stability was observed with the addition of a small introduction methane (Figures 6.6 and 6.8) as compared to no methane introduction (Figure 6.5). A series of experiments with poplar oil were conducted to assess the requirement for methane addition.

Pure pine pyrolysis oil is converted to syngas autothermally with the addition of methane and air as depicted in Figure 6.9 (here, rather than yields, dry effluent molar concentrations omitting N_2, are plotted). Pine pyrolysis oil and N_2 enter the reactor through a nebulizer positioned 1 mm above the catalyst front face; O_2 enters through a separate stainless steel tube positioned 3 mm above the front face of the catalyst bed - three 45 ppi catalysts atop a 45 ppi heat shield. Production of C_1 species and H_2 are relatively constant over the time frame observed.

The 21 mol% methane addition shown in Figure 6.9 represents the best combination of steady activity and minimal cofeed for pine pyrolysis oil reforming. Experiments carried out with 15 mol% methane ceased operating autothermally after one hour; those with 25 mol%

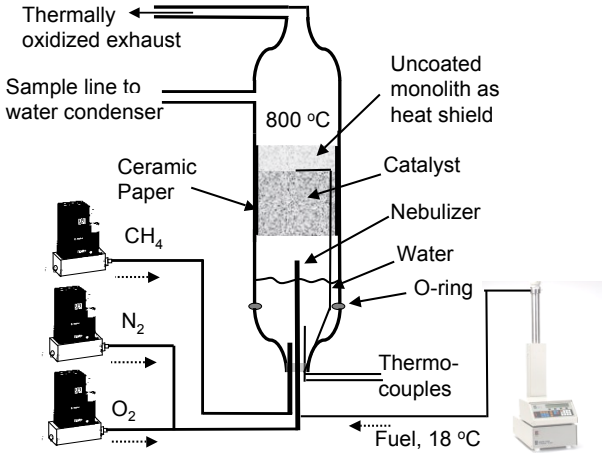

Figure 6.7: Water Cooled Test. Flow was upward, allowing the nebulizer to sit in a pool of distilled water, maintaining temperatures below 40 ^{o}C. Unreacted bio oil convected back into the water pool, but increased stability from the cooled nebulizer demonstrated the need for a water-cooling system.

methane did not show a benefit in product stability and, like the experiment depicted in Figure 6.9, also ran until the fixed volume syringe pump was empty. These data are depicted in Figure 6.10. It is worth noting that in almost all of these experiments, the methane effluent is approximately equal to the inflow.

6.4.2 Thermodynamic Calculations

Selected results are depicted in Table 6.3 along with thermodynamically predicted product concentrations and yields. Contact time (τ) and gas hourly space velocity (GHSV) assuming C_1 equivalents are depicted. Concentrations reported are dry and without N_2. Bio Oil in Mix and related categories depict carbon percent derived from bio oil, methanol, and methane

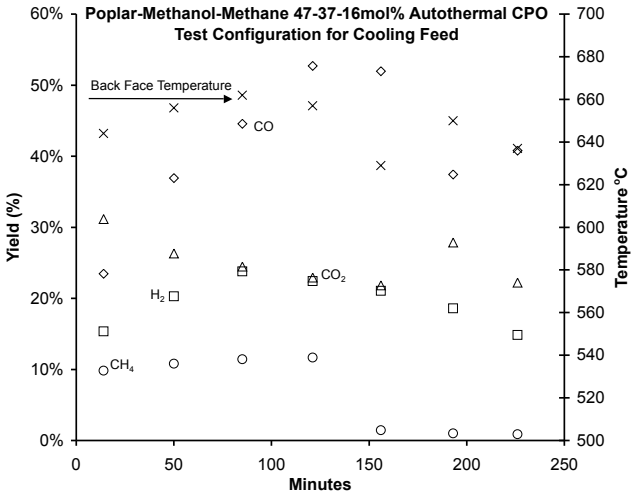

Figure 6.8: Autothermal Partial Oxidation of a 50-50 wt% poplar oil-methanol solution with 0.1 SLPM CH_4 addition at a total C/O =0.97. Carbon conversion $\approx$ 73%. In this configuration, the nebulizer sprayed upward from a pool of distilled water to maintain the temperature, as depicted in Figure 6.7. The pool of water was later replaced by a water-cooling jacket system on the nebulizer, which was used for the rest of the experiments. GHSV $\approx$ 22000 hr^{-1}, $\tau \approx 54$ ms.

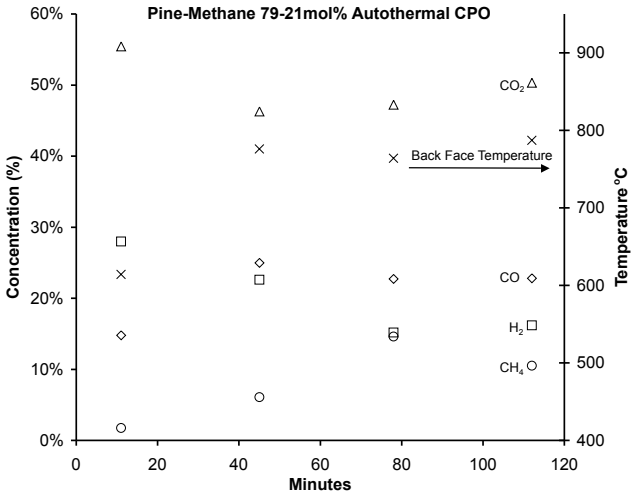

Figure 6.9: Dry effluent concentrations from the catalytic partial oxidation of pine oil with 0.15 SLPM methane (79% pyrolysis liquid by carbon content). The reactor ran autothermally and was shut down when all fuel was consumed. GHSV ≈ 25000 hr^{-1}, $\tau \approx 40$ ms.

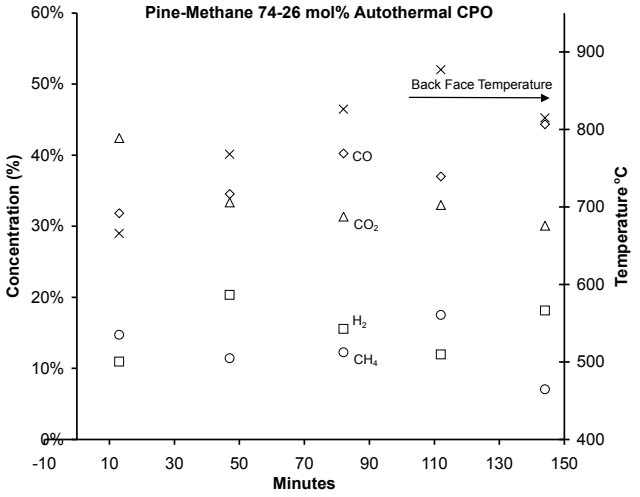

Figure 6.10: Autothermal catalytic partial oxidation of pine pyrolysis oil with a methane cofeed (74% oil, 26% CH_4 by C). Greater methane addition stabilizes the reactor, but the improvement diminishes with CH_4 increase. GHSV ≈ 27000 hr^{-1}, $\tau \approx 39$ ms.

Table 6.3: Experimental (Ex) and calculated isothermal equilibria (based on backface temperatures (Th)) yields and concentrations for selected data points. Heat sources are given under "Ht Src", Autothermal = AtoThml; "Furnace" refers to experiments conducted in a clamshell heater. Backface Temperatures (BF) and upstream temperatures (US) are listed under heat source. "% Oil in Mix" gives the carbon amount in the total feed derived from bio oil. "% CH_3OH" (methanol) and "% CH_4" are analogously defined. Conc refers to the concentration of dry gas species, ignoring N_2. X_C gives the total conversion of carbon species in the feed. GHSV gives the gas hourly space velocity in hr^-1.

FUEL	poplar		poplar		pine		pine		pine		pine		hrdwoods	
τ [sec]	0.053		0.030		0.036		0.040		0.026		0.050		0.051	
GHSV	22000		37000		27000		25000		35000		17000		17000	
Ht Src	AtoThml		AtoThml		AtoThml		AtoThml		Furnace		Furnace		Furnace	
T_{BF} [^{o}C]	651		684		826		776		935		993		950	
T_{US} [^{o}C]									209		763		700	
S/C	0		0		0		0		3		0		0	
C/O	0.97		0.85		1.00		1.00		1.30		1.30		1.10	
% Oil	47		56		74		79		100		100		83	
% CH_3OH	37		44		0		0		0		0		17	
% CH_4	16		0		26		21		0		0		0	
Conc [%]	Ex	Th	Ex	Th	Ex	Th	Ex	Th	Ex	Th	Ex	Th	Ex	Th
H_2	22	51	27	46	16	48	23	46	19	52	15	39	26	40
CO	51	28	42	26	40	39	25	38	23	17	26	47	58	41
CH_4	13	2	2	0	12	0	6	0	1	0	1	0	6	0
CO_2	13	19	28	27	31	13	46	16	57	32	58	14	9	19
X_C [%]	101	100	94	100	103	100	62	100	49	100	48	100	94	100
Yield [%]														
H_2	19	71	25	62	16	74	16	74	13	27	9	68	30	61
CO	65	57	54	49	49	75	20	70	14	34	15	77	73	69
CH_4	17	3	3	0	15	0	5	0	1	0	1	0	8	0
CO_2	17	40	36	51	38	25	37	30	34	66	32	23	12	31

6.5 Discussion

Pyrolysis oils from three different sources were converted to syngas in millisecond contact times. While varying process conditions and bio oil quality affect the stability of millisecond reforming, the addition of cofeeds such as methanol or methane can offset these issues. Autothermal operation is also possible for some oils and is more stable with the addition of methane. With the incorporation of a water-gas shift stage, CO can be consumed and H_2 produced, thereby increasing H_2 production.

The yield of H_2 from autothermal partial oxidation of pyrolysis oils is much lower than steam reforming of the same compounds. This is a natural result of the differences between oxidative Equations 6.2 + 6.3 and reforming Equation 6.1. The tradeoff, of course, is in energy demand, thermal efficiency, and coke management. For methane CPO, despite similar kinetics in dilute concentrations, oxidative chemistry is faster than steam reforming under competitive conditions.[190] The lower activation temperature for oxidation [191] underscores faster kinetics for bio oil as well. These observations suggest some oxidation can be useful for maintaining a clean reactor and catalyst; combining this with some external heating and steam addition may achieve the additional benefits of higher H_2 production. Rioche et al. introduced O_2 in sufficient quantity to examine autothermal reforming, but the high S/C = 10.8 required a large quantity of O_2 which oxidized part of the H_2 product.[183]

The addition of methane to CPO experiments also renders the catalyst more stable. However, methane is barely consumed in these experiments. That is to say, although no labeling of particular methane molecules was performed, the addition of methane to the reactants increases methane in the effluent by nearly as much.

Methane is much more stable than most of the constituents in pyrolysis oils: activation on a noble metal catalyst requires the breaking of the C-H bond for methane,[190] whereas oxygenated molecules typically adsorb via electron rich oxygen atoms.[155]. Methane is less reactive than bio oil over noble metals. However, as a gas, methane mixes well with air flowing from the nebulizer. Pyrolysis aerosols, on the other hand, must evaporate or react on the catalytic surface in the form of a liquid droplet. Thus, the transport of bio oil to the catalyst surface is inferior to that of methane. In addition, cold bio oil droplets can reduce the surface temperature of the catalyst prior to oxidation, which may inhibit reaction rates. The net effect is that cofed methane allows for more of the catalyst to stay at steady reaction temperatures, even while only

a small fraction of methane is consumed. Where bio oil is not reaching the catalyst, the addition of methane allows the catalyst to be hot and active; where bio oil is reaching the catalyst, methane merely passes through like a diluent.

The yield of H_2 is low compared to predicted equilibrium. As described above, oxidation reactions are fast with respect to reforming reactions under CPO conditions on Rh catalysts. This oxidation may preferentially occupy surface sites, reducing the effect of steam reforming. As a result, unmeasured H_2O yields are over the predicted amount. Loss in steam reforming is also observed as a consequence of deactivation, eg, due to sulfur impurities.[177]

Water-gas shift (WGS) is also responsible for H_2 production and is typically equilibrated on a healthy Rh-Ce, washcoated catalyst.[170] For experiments with poplar and hardwood, WGS is certainly not equilibrated: an abundance of CO (and implicitly, water) is reported, while a deficiency in CO_2 and H_2 are apparent. The pine data may be off for a different reason, or the analysis of $C_xH_yO_z$ may no longer be relevant due to phase separation of the oil.

Methanation can consume H atoms at the cost of H_2. In all cases where CH_4 is added to the reactor, an abundance of CH_4 is measured in the effluent. This has been discussed above. However, CH_4 is also well above equilibrium (albeit not as high) in all cases for which methane is not added as a portion of the fuel.

The loss of WGS activity, steam reforming, and an increase in methanation all indicate deactivation of the catalyst. Although the catalysts were still functional and clean of coke, they apparently do not compare in activity to those used for similar reaction of model compounds.[56, 159, 50] Maintaining healthy noble metal catalysts is an important research goal for catalytic upgrading of bio oils that sophisticated reactor design may achieve.

Two challenges affect reactor design for upgrading pyrolysis oil. As depolymerized, dehydrated plant matter, many of the constituents of pyrolysis oils have a tendency to polymerize over time.[28] This polymerization is accelerated at higher temperature (typically temperatures in excess of 80 ^oC are quoted in the literature[189]), and the dehydration of pyrolysis oils to form char is a significant consideration for thermal upgrading processes at operating temperatures. Second, while pyrolysis oils contain less ash than biomass, they do contain some ash. As a result, the deactivation of catalysts due to inorganic deposition is a major reactor design hurdle.

For the first challenge, sophisticated reactor design can alleviate char formation between pyrolysis oil introduction and catalysis. Char forms from pyrolysis oils (and from biomass) at

long exposure to low heating rates; gasification occurs at high temperature with fast heating rates.[192] Thus, extremely rapid heat transfer is essential to achieve gasification temperatures without char formation. In the case of CPO, this requires introducing the fuel at room temperature and bringing it to reaction temperature, >700 ^{o}C, within a few milliseconds. Catalytic reactors are well equipped for this task as the heat transfer from catalyst to reactant is greater than gas phase heat transfer from hot walls. Moreover, exothermic chemistries are particularly well suited to high heat transfer rates as the heat is produced directly at the catalyst site. For this reason, catalytic oxidation has much greater potential for low coke pyrolysis oil gasification than does catalytic steam reforming.

Several reactor design improvements resulted in more stable performance. The upflow reactor configuration demonstrated the improvement derived from maintaining cool bio oil as it enters the reactor. As pyrolysis oils dehydrate and coke at temperatures above 80 ^{o}C it is necessary to introduce cold liquids directly to the reactor. With the lessons of reactive flash volatilization described in Chapters 1 and 4, impinging cold liquid directly onto the catalyst can be achieved. Applying a water-cooling jacket system to the nebulizer enabled the use of a high temperature furnace for subsequent experiments. It also allowed for a second improvement in reactor design that resulted in greater performance: moving the nebulizer very close to the catalyst. To avoid the polymerization of bio oils at low heating rates, bio oils cannot move slowly in a furnace or above a hot catalyst. They must immediately contact the active hot zone where they can be decomposed to syngas, and thus be introduced (at room temperature) very near to the catalyst (within 1 mm) which is at high temperature (>600 ^{o}C).

However, on a lab scale, an additional problem must be considered: Leidenfrost film boiling. On a hot catalytic surface, liquid droplets of bio oil form a vapor phase barrier between the droplet and the catalyst that buoys up the liquid droplet. This is especially pronounced on porous surfaces, which exhibit longer droplet residence times.[193] Liquid then bounces to areas of lower temperature which, in a small reactor, include the quartz walls at the edge of the hot catalyst. Here the liquid finally achieves good thermal contact with the cooler (300-400 ^{o}C) wall. However, due to low heat transfer rates and the absence of catalyst at the wall, the liquid chars rather than breaking down to C_1 products. A furnace to heat the walls higher than the catalyst front face temperature can avoid this problem. Scaling the reactor up will likely also ameliorate this problem, though perhaps a spouting or fluidized bed would be a more direct solution.

Another solution to the formation of char is the introduction of steam. Steam requires higher temperature than O_2 to react with coke, but can be more effective.[191] Significant quantities of water are necessary to achieve steam reforming rates on par with coke formation, and this represents a thermal drag on the system. If sufficient heat is available to offset this thermal cost, steam reforming can achieve much higher H_2 production and greater conversion of pyrolysis oil to C_1 products. Insufficient heat addition eliminates these benefits of water addition, and results in extremely comparable product spectra, as depicted in Figures 6.2 and 6.3.

The second challenge, that of ash build up, appears non-detrimental to the catalyst. Ash accumulates upstream and on the frontface of the catalyst as depicted in Figure 7.5 and can be brushed off periodically, allowing the catalyst to be reused. Many of the above-described experiments occurred on catalysts reused in this manner without ill result. However, the time frame for the total life of these catalysts, several tens of hours, is too short to draw meaningful conclusions about the resilience of noble metal catalysts to inorganic impurities. Research into this question is ongoing, and is described further in Chapter 7.

Another experimental parameter in the reactor design for the above described experiments is pore diameter. Conventional wisdom and experimental evidence with bio-oil proxies indicate that smaller pores result in greater conversion to equilibrium syngas products.[53, 34] However, the velocity of droplets impinging on 80 ppi catalysts requires a pressure drop that results in recirculation of the aerosol. For model compounds, this recirculation is not a major issue: the small fraction of recirculated fuel eventually deposits on the walls and slides down into the catalyst, or vaporizes on the walls and enters as a gas. However, pyrolysis oil cannot vaporize and, given the low rate of heat transfer on the wall, readily polymerizes in such a setup. As a result, recirculation must be minimized or, at least, deposited pyrolysis oil must not form char in such a way that it clogs the reactor vessel.

One solution to this problem is to increase the proximity of the nebulizer to the catalyst, such that little or no open area exists to support the formation of coke from low heat transfer at the walls, thereby blocking the nebulizer. A second solution is to decrease the pressure drop or the velocity of the spray. Given the mechanism of a gas-blown nebulizer, it is difficult to decrease the velocity of the spray, though other atomizer setups may circumvent this problem. Increasing the pore diameter, on the other hand, reduces the pressure drop. A series of experiments on 20 ppi, 45 ppi, and 80 ppi foams indicate that a 20ppi/45ppi/45ppi bed is most effective at achieving high conversion and low rates of coke formation due to upstream recirculation.

As this reactor is autothermal and scalable, it is conceivable to use bio oil as a H_2 source with an on-board reformer for automotive fuel cell applications. For instance, using the second column in Table 2, the poplar blend, and assuming a top power consumption rate of 1kg H_2/hr for a light duty automobile,[194] a reactor would require 3.7 kg of catalyst, or 37 g Rh. With improvements in WGS performance and reactor design, 14 g Rh may be sufficient. Further improvements in Rh loading and catalyst design may render the on-board reforming of bio oil practical in automotive applications.

6.6 Conclusions

Pyrolysis oils can be catalytically converted to syngas for upgrading to liquid fuels. Noble metal catalysts achieve high conversion to H_2 and CO. The reaction can proceed autothermally or higher yields can be achieved with the addition of process heat. With the incorporation of a WGS reactor, bio oil can be used as a H_2 source for on-board reforming of H_2 for automotive fuel cell applications. Coke formation is a major hurdle for reactor design, though solutions are possible with high rates of heat transfer or the addition of steam. Ash handling may remain a problem for catalytic partial oxidation, though an upstream freeboard design may eliminate this issue.

Chapter 7

Future Work

The investigation of the catalytic partial oxidation of pyrolysis oils presented in this document indicates that biomass can be upgraded to synthetic fuels through a two-step thermochemical route. Just as improvements in the pyrolysis of biomass have resulted in more stable, consistent, higher energy bio oils,[195] future developments in the reactive flash volatilization and catalytic partial oxidation can increase production of syngas and enhance reactor stability. Several research projects are planned to target these improvements.

7.1 Fast Photography of CPO of Liquid Fuels

One advantage of using quartz as a reactor material is that it is translucent. This thesis has several pictures of operating reactors; the ability to see within the reaction zone is an enormous aid to experimentation. With sight, one can observe whether the reactor is operating and in what transients; one can determine where reaction is taking place and where it is quenched, and gather an enormous amount of data that is difficult to quantify or describe, but that nevertheless improves reactor design.

Some of this data can be quantified utilizing high speed photography. A camera capable of shooting thousands of frames per second (fps) pointing at a catalytic surface can reveal quantitative information about how droplets break apart, diminish in size, and affect the surface. To this end, research is currently underway in photographing and examining various liquids dropping onto porous catalytic surfaces. Figure 7.1 demonstrates a setup used for these experiments. In the place of foam catalysts, flat alumina disks can be coated with noble metals; alternatively

foams can be used, or uncoated surfaces for comparison.

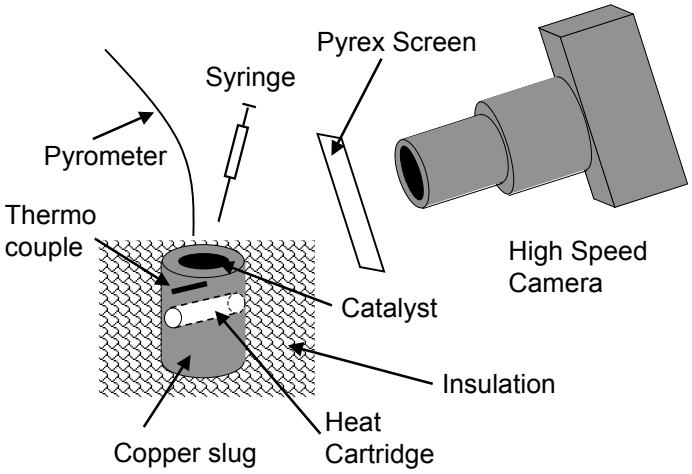

Figure 7.1: Setup for temperature-controlled fast photography experiments. A copper slug acts as a thermal mass with high heat transfer. A heat cartridge attached to a VariAC maintains temperature, monitored by a thermocouple near the surface of the slug. A flat catalyst rests on top of the slug, where liquids can be delivered by syringe or nebulizer. The catalyst surface temperature is monitored by optical pyrometer.

The copper slug is used as a large thermal mass with high heat transfer, so that the temperature of the hot surface will be independent of impinging liquid droplets. A thermocouple monitors the temperature in the copper slug; a pyrometer measures the surface temperature of the catalyst. Adjusting the voltage delivered to the cartridge results in temperature control. Liquid can be delivered by syringe, nebulizer, or spray. The slug apparatus can be replaced by a conventional reactor.

Figure 7.2 depicts a droplet of glycerol impacting an 80 ppi Rh-Ce coated foam. The RFV of the droplet is physically observable in the film boiling the occurs. The surface, over 500 ^{o}C, breaks down glycerol by CPO and rapidly heats it to boiling, causing the ejection of gases at the surface. These gases buoy up the droplet, which skitters across the foam despite the pores. This whole sequence is filmed at 1000 fps; represented are choice frames over a series containing 44 frames. Contact times in the CPO of gases are on the order of ms, but for RFV, boiling takes time. Though total flowrates are comparable, droplets spend a significantly greater portion of

time at the front surface boiling.

However, if the droplets can establish good thermal contact, heat transfer rates improve significantly. Rather than vaporize the liquid on the very exterior of a droplet, boiling can heat the whole droplet with direct heat transfer. This takes place at lower temperatures, suggesting that, contrary to intuition, higher heat rates can be achieved at lower temperature!

A series of such videos at various temperatures indicate that film boiling begins at a given temperature on these porous media, and a transition to complete Leidenfrost Effect takes place over about 100 ^{o}C. At the lower end of this range, droplets will skitter over smooth surfaces, but will stop at surface defects and boil. At the upper end of this range, droplets will ignore surface defects and skitter across. The glycerol droplet is above this range and. demonstrates Leidenfrost film boiling.

Bio oil, which cannot be revaporized, can film boil in RFV. Figure 7.3 depicts poplar bio oil on a Rh-Ce coated Al_2O_3 flat disk at 420 ^{o}C. This temperature, in the middle of the Leidenfrost range for poplar oil, allows the droplet to skitter across the surface from its point of impact to deposited coke (a remainder from a previous droplet at lower temperature). When the bio oil impacts the coke, the surface abnormality holds it while it boils. Then the droplet, having heated up due to oxidation near the surface, achieves film boiling and skitters off of the frame. Some remainder of the bio oil is left behind amongst the coke and rapidly disappears as it is oxidized. Remarkably, the droplet absorbed some of the coke, proving that hot Rh surfaces can be considered "self-cleaning" for coke.

More experiments of this kind are underway. Furthermore, the analysis of the experiments conducted to-date is in progress. As such, this work represents one of the near-term products of this thesis. These studies will show the effects of heat transfer, temperature, and surface abnormalities on liquid droplets as they impact a porous, catalytic media.

7.2 Spatially Resolved CPO of Pyrolysis Oil Model Compounds

Data discussed in previous chapters was obtained by analyzing product effluent. Comparisons with reactor inlet conditions resulted in metrics such as conversion, yield, and selectivity. This sort of integral data, while instructive of chemistry and catalyst performance under certain conditions, essentially treats the catalyst as a black box.

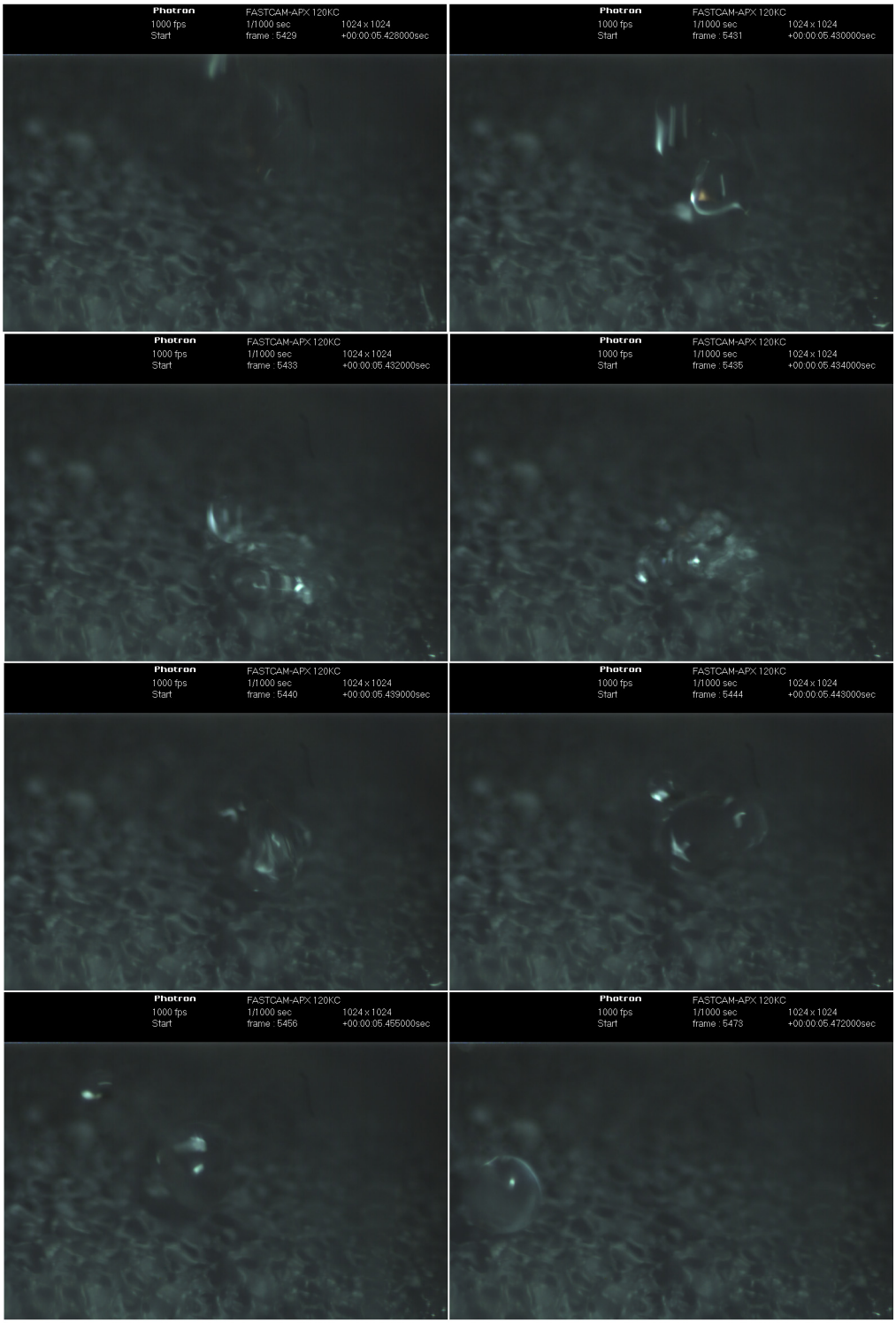

Figure 7.2: A droplet of glycerol introduced to an 80 ppi Rh-Ce catalyst at >500 ^{o}C film-boils, causing it to skitter across the foam. This series of images takes place over 44 ms. The droplet falls, spreads, recombines, and rolls across the surface.

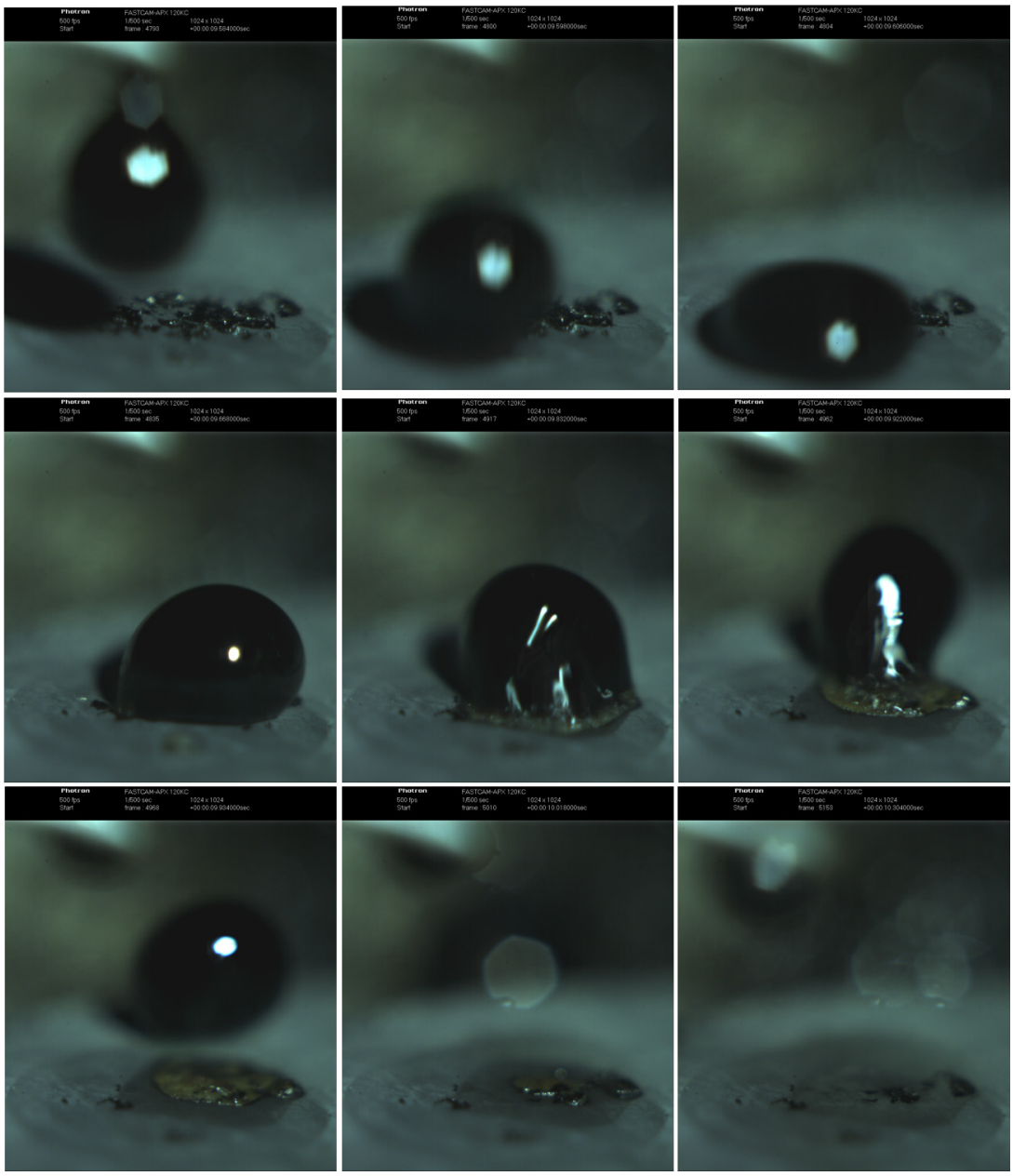

Figure 7.3: A droplet of poplar pyrolysis oil on a flat Rh-Ce coated Al_2O_3 disk demonstrates the self-cleaning nature of a Rh-Ce catalyst. The droplet falls onto the surface and rolls across, buoyed up by film boiling at 420 ^oC. The droplet, approximately 1-2mm in diameter, rolls to previously deposited coke and removes it as it rolls off. Some of the bio oil is left behind in a puddle and vanishes as it is oxidized. This sequence takes 720 ms.

To add compelling evidence in terms of reaction kinetics, product intermediates, and transport phenomena, spatially resolved data are essential. A spatial profiling technique has been developed in recent years in the Schmidt group, starting with the work by Horn et al.[171] This technique reveals reaction intermediates and shows the evolution of products within the catalyst bed, thus revealing the important reactions and their kinetics in CPO. The technique involves drilling a hole in the catalytic monolith smaller than the characteristic pore size of the catalyst, and inserting a fused silica capillary. With a $\approx$100 μm hole bored into the capillary, products can be drawn by vacuum from within the reactor, essentially quenching them as they flow through the catalyst. In addition, a thermocouple or pyrometer can be inserted into the capillary to obtain temperature data from the flowing gas or surface of the catalyst, respectively. A reactor schematic similar to that used in these experiments is depicted on the right half of Figure 7.4.

For millisecond reactors in which products are rapidly produced and quenched, an understanding of product development over the length of the catalyst bed is extremely revealing. For methane CPO, the evolution of product intermediates shows the relative effects of oxidation and steam reforming, revealing that H_2 is produced in two zones. In the first zone, oxygen is consumed, producing syngas in a direct mechanism (Equation 7.1)

$$CH_4 + O_2 \rightarrow CO + H_2 \tag{7.1}$$

as well as producing combustion products. In the second zone, steam reforming (Equation 7.2) dominates, producing yet more H_2 with steam produced in the first zone.

$$CH_4 + H_2O \rightarrow CO + 3H_2 \tag{7.2}$$

The spatial resolution technique has also been very revealing about transport phenomena for reactants in methane CPO, indicating, for instance, that rates are transport limited in O_2 over Rh, but kinetically limited over Pt.[75]

Recent research with this technique focuses on the oxidative dehydrogenation of ethane to ethylene and, as such, examines non-syngas chemistry. This demonstrates the versatility of the technique, which can also be applied to liquid oxygenated fuels and, thus, to model compounds of pyrolysis oil.

Initial work in this area will study acetaldehyde, C_2H_4O. Acetaldehyde is highly volatile and reasonably stable in the gas phase. As a result, feeding fuel vapor should render the experiment

minimally different from previous experiments, and thermal decomposition of products in the heated sample lines can be reduced to a minimum. A schematic of this apparatus is depicted in Figure 7.4.

Acetaldehyde vapor will equilibrate with bubbled argon in an isothermal flask maintained in an ice bath. The remainder of the reactants can be added to the Ar-fuel stream and mixed in the reactor upstream of the catalyst. A stopper is added for safety reasons because acetaldehyde is much more reactive than methane or ethane. The capillary for sampling will be controlled by a stepper motor in much the same way as in previous experiments. 45 ppi catalysts will be used because the pore size is much larger than the OD of the sampling capillary. A drilled 45 ppi Rh-Ce catlayst for this experiment is depicted in Figure 1.2. Products will be monitored by mass spectrometry and gas chromatograph.

With the lessons learned from this first departure from non-oxygenated fuels, future work in this area can build, exploring higher order functional groups and more model compounds. In particular, as a stable dehydrogenation product, acetaldehyde is often produced in the CPO of other bio oil model compounds (see Chapters 2, 3, 4). Acetaldehyde is also the main non-equilibrium product in the CPO of ethanol.[64, 18] Thus, the spatial resolution of the CPO of ethanol will require the addition of only one species: ethanol.

In this way, spatially resolved data can be "built up," beginning with the simplest of model compounds and working toward larger chemicals of increasing complexity. Along the way, important differences in fuel handling, vaporization, and product analysis can be learned one step at a time.

7.3 Investigation of the Effect of Inorganic Impurities on Noble Metal Catalysts in a CPO Reactor

Inorganic impurities can be detrimental to noble metal catalysts in a CPO reactor. In the time on stream experiment in Chapter 5, ppm levels of inorganic impurities, over hundreds of hours, severely deactivated catalyst performance and deposited visible residue on the catalyst and reactor surface. In the bio oil experiments described in Chapter 6, ash buildup on the surface of the catalyst was observed after reactor burnoff. The H_2 production in these experiments was significantly lower than equilibrium, which is atypical of CPO over Rh-Ce catalysts.

A qualitative study of the effects of typical biomass ash constituents (Na, K, Cl, N, P) was

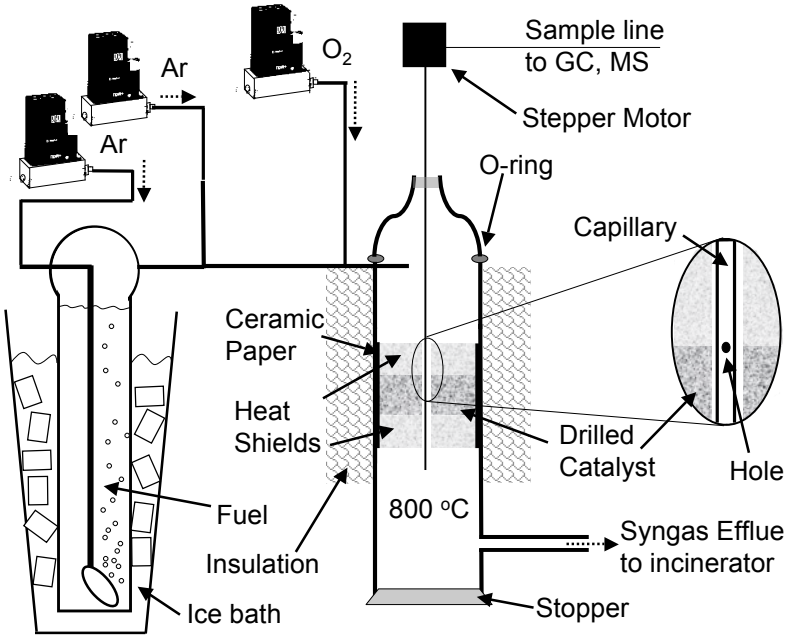

Figure 7.4: Diagram of reactor setup for the spatial resolution of product and temperature data in the CPO of model compounds of biomass pyrolysis liquids. Ar is fed through two mass flow controllers: one bubbles up through a temperature controlled (ice bath) liquid, achieving equilibrium vapor pressure for fuel delivery, while the other flows the compensatory Ar, mixing with O_2. A capillary with a micron hole samples chemical species; the capillary can be replaced with an optical pyrometer or a thermocouple for temperature measurements of the surface or gas, respectively. Product samples are analyzed continuously by mass spectrometer and GC. Sample lines are heated to avoid condensation; the reactor is insulated to simulate adiabatic conditions. A stopper allows for safety precautions with highly volatile, reactive fuels, such as acetaldehyde. A stepper motor moves the capillary up and down with 0.3 mm precision.

conducted by dissolving salts into an ethanol-water mixture. These solutions contained high ash content on the order of 1% in order to accelerate the effects of the impurity. RFV of the solution was performed, ensuring molecular introduction of inorganic impurities to the catalyst. In every case except N, introduced impurities deactivated the catalyst, as observed by O_2 breakthrough, downstream flames, and an increase in upstream pressure. These experiments are summarized in Table 7.1.

Table 7.1: Inorganic impurities ("Elmnt)" introduced to noble metal catalyst via reactive flash volatilization in a qualitative study.[196] Impurities were introduced in the form of "Molecule," except in the reference case "none" which was a clean ethanol-water mix. "t" refers to the duration of the experiment in hours. Max P describes the pressure observed over the course of the experiment. "DnStrmFlm" indicates the presence of a downstream flame; "Accum" the accumulation of ash and carbon above the catalyst, and "FlmClr" the color of the effluent flame when impurities were introduced. Burnoffs, ("BrnOf") were attempted by running clean methane for a period of time, extending the lifetime of the Na experiment slightly, for example.

Elmnt	Molecule	t [hr]	Max P [psi]	DnStrmFlm	Accum	FlmClr	BrnOf
K	KOH	3.75	7	√	√	lilac	√
Na	NaOH	2.5	6	√	√	orange	√
N	NH_4NO_3	4	2.7	√		blue	
P	H_3PO_4	0.75	2.5	√		white	√
Cl	HCl	1	4.4	√	√	pink	
none		4	2.5			blue	

Impurities were dissolved in the form of acids and bases in order to study only the effects of one element at a time. Experiments were conducted for up to 4 hours to determine whether deactivation was occurring and by what means. Experiments were terminated when they no longer operated autothermally or when the pressure drop over the catalyst exceeded 15 psi. Pressure upstream of the catalyst bed, monitored by a pressure guage, increased in some of the experiments due to the accumulation of ash and carbon on the front face (Figure 7.5 Top). This type of accumulation was observed with bio oil in Chapter 6 (Figure 7.5 Bottom) and with solid biomass.[50] CPO was still possible on these catalysts, however.

Figure 7.5: Ash accumulates on top of the catalyst. In the top image,[196] KOH doped ethanol-water CPO resulted in ash and coke build up above the front face during controlled impurity experiments. In the bottom image, ash accumulation is exhibited from the CPO of pine bio oil after coke burnoff.

In all cases of introduced impurities, a downstream flame (DnFlm) was observed, indicating incomplete oxidation. This suggests impurities can compete with O_2 for active sites, thus shifting the oxidation zone and compromising the catalyst.

Every impurity except N deactivated the catalyst and had to be terminated prior to 4 hours. However, some impurities passed through the catalyst bed in the gas stream, as observed in the effluent flame, which changed color as metals oxidized. Of all of these forms of deactivation, P presented perhaps the most insidious, as no ash accumulation was observed. It is presumed that P competitively occupies active sites to rapidly deactivate the catalyst.

These experiments underscore the need for more analysis. In particular, the experiments highlight the following observations:

1. As catalysts did not deactivate immediately due to ash accumulation upstream, a fluidized bed or moving bed may be sufficient to avoid the pressure drop observed in these experiments.

2. Some impurities were volatilized under CPO conditions. Burnoffs with clean fuel such as CH_4 reinvigorated some catalyst performance. This suggests high temperatures and the proper reaction conditions could be successful in cleaning the catalyst of impurities.

3. These experiments were performed under accelerated deactivation conditions, with high inorganic addition. Although biomass can contain high fractions of impurities, bio oils typically contain less than a fraction of 1%.[23, 28, 1]. Under more experimentally relevant conditions, ash may be less of a problem.

4. These experiments were conducted using RFV, just like the time on stream experiment in Chapter 5. However, prevaporization, where possible, may avoid ash accumulation on the catalyst surface.

To this end, future work in the CPO of bio oils will require a more quantitative study of the effects of ash content in liquid feed.

Such a study is under way. In order to ensure impurities interact directly with the catalyst, RFV of an ethanol-water mixture will be reexamined. However, to avoid the harsh conditions caused by caustic solutions, basic salts are replaced by organic salts in this iteration. Effluent will be continually monitored by MS and periodically measured by GC. Pressure upstream and the backface temperature will similarly be monitored continuously. Imaging of catalyst

deactivation will be performed by XRD and SEM. To this end, the catalysts have been cut into thin slices to allow imagining of the catalyst before and after use.

Depending on the outcome of these experiments, reactor design improvements are imagined. For ash deactivation which occurs by solids accumulation, a CPO experiment in a fluidized bed or rotating bed will explore efforts at continuous ash removal.

In addition, another time on stream experiment can be explored using prevaporized fuel to discover whether impurities can be eliminated in the feed system prior to contacting the catalyst.

7.4 Analysis of Chemistry of CPO Model Compounds

7.4.1 Organic Functional Groups

This study examined the CPO of C_3 acids, ethyl esters, and glycerol in detail. As noted in Chapter 1, previous work has also explored several functional groups. However, a comprehensive exploration of the effects of functional group chemistry in CPO is underway. This study explores the effects of each individual oxygenated functional group for C_2 species, including acetaldehyde, acetic acid, ethanol, ethylene glycol, dimethyl ether, and methyl formate. Multiple functionalities are only included in the context of ethylene glycol: the high cost of hydroxyacetaldehyde prohibits an exploration of this compound, and glyoxal and oxalic acid are too unstable to examine meaninfully in a GC, let alone in a CPO reactor.

Initial results from the study of CPO of C_2 functional groups over Pt will be completed shortly. These results will be compared to homogeneous chemistry in and out of the presence of O_2. The inclusion of O_2 is an essential parameter as it can promote radical formation and thus initiate gas phase decomposition. The results will be further compared over Rh-Ce to verify that RFV can produce equilibrium syngas from each of the C_2 functional groups.

With a thorough understanding of the decomposition of functional group chemistry for small molecules, the CPO of individual species representing the carbohydrate fraction of pyrolysis oil will be well understood.

7.4.2 Anisole and Phenol: Effect of Aromatics

Several model compounds can be used to study the lignin fraction of pyrolysis oil, including vanillin and syringol. However, these species are highly functionalized, complicating the study

of their decomposition. An alternative is to build up an understanding of individual functionalized aromatics. As such, phenol and anisole will be considered in CPO.

Phenol is the simplest oxygenated aromatic and, as such, is a likely intermediate in the decomposition of more complicated lignin species. It is anticipated that phenol will lose its acidic H relatively easily; the next step, destruction of aromaticity, will be the rate limiting step. Phenol is likely to fractionate into a variety of species after this point, or perhaps to oxidize fully to C_1 products.

Anisole is an interesting model compound for lignin because of the C-O-C bond common in the complex polymer (see Figure 3.3). If CPO of anisole can separate phenol from anisole with high selectivity, valuable aromatic oxygenated chemicals can be derived from lignin using CPO. This would open a very promising niche for CPO as a lucrative process step in a biorefinery.

References

[1] Zhang Qi, Chang Jie, Wang Tiejun, and Xu Ying. Review of biomass pyrolysis oil properties and upgrading research. *Energy Conversion and Management*, 48:87–92, 2007.

[2] S. Czernik and A. V. Bridgwater. Overview of applications of biomass fast pyrolysis oil. *Energy Fuels*, 18:590–598, 2004.

[3] President George W. Bush. State of the union address. Delivered to the Nation and Joint Houses of Congress, January 2006.

[4] Daniel Moran and James A. Russel. The militarization of energy security. *Strategic Insights*, 7(1), 2008.

[5] Kenneth S. Deffeyes. *Hubbert's Peak: The Impending World Oil Shortage*. Princeton University Press, 2001.

[6] S. H. Mohr and G. M. Evans. Peak oil: Testing hubbert's curve via theoretical modeling. *Natural Resources Research*, 17:1–11, 2008.

[7] *International Energy Outlook 2009*, chapter 2: Liquid Fuels. `http://www.eia.doe.gov/oiaf/ieo/liquid_fuels.html`, 2009.

[8] *Chair's Summary of G8 Summit at L'Aquila*, 2009.

[9] R. K. Pachauri and A. Reisinger, editors. *Climate Change 2007: Synthesis Report Summary for Policymakers*. Intergovernmental Panel on Climate Change, 4 edition, 2007.

[10] A. B. Frank, J. D. Berdahl, J. D. Hanson, M. A. Liebig, and H. A. Johnson. Biomass and carbon partitioning in switchgrass. *Crop Science*, 44:1391–1396, 2004.

[11] Synfuel success. *Time*, June 1980.

[12] J. Raloff. Congress kills the U.S. synfuels corp. *Science News*, 129(2):22, 1986.

[13] Randall Swisher and Kevin Porter. *Renewable Energy Policy and Politics: a Handbook for Decision-Making*, chapter 7: Renewable Policy Lessons from the US: The Need for Consistent and Stable Policies, page 185. London; Sterling, VA: Earthscan, 2006.

[14] *New Energy Tax Credits for Hybrids*. `http://www.fueleconomy.gov/Feg/tax_hybrid.shtml`, 2009.

[15] US Department of Transportation. *Car Allowance Rebate System*. `http://www.cars.gov/`, 2009.

[16] *HR 2454 Summary*. Committee on Energy and Commerce: US House of Representatives, 2009.

[17] *Energy Secretary Chu Announces $1.2 Billion in Recovery Act Funding for Science*. `http://www.energy.gov/news2009/7083.htm`, 2009.

[18] G. A. Deluga, J. R. Salge, L. D. Schmidt, and X. E. Verykios. Renewable hydrogen from ethanol by autothermal reforming. *Science*, 303:993–997, 2004.

[19] V. Fierro, V. Klouz, O. Akdim, and C. Mirodatos. Oxidative reforming of biomass derived ethanol for hydrogen production in fuel cell applications. *Catalysis Today*, 75:141–144, 2002.

[20] M. Krumpelt, T. R. Krause, J. D. Carter, J. P. Kopasz, and S. Ahmed. Fuel processing for fuel cell systems in transportation and portable power applications. *Catalysis Today*, 77:3–16, 2002.

[21] S. Ahmed and M. Krumpelt. Hydrogen from hydrocarbon fuels for fuel cells. *Int. J. Hydrogen Energy*, 26:291–301, 2001.

[22] Robert D. Perlack, Lynn L. Wright, Anthony F. Turhollow, Robin L. Graham, Bryce J. Stokes, and Donald C. Erbach. Biomass as feedstock for a bioenergy and bioproducts industry: The technical feasibility of a billion-ton annual supply. Technical report, US Department of Energy and US Department of Agriculture, 2005.

[23] A V Bridgwater, editor. *Fast Pyrolysis of Biomass: A Handbook*. CPL Press, 2008.

[24] Dingneng Wang, Stefan Czernik, and Esteban Chornet. Production of hydrogen from biomass by catalytic steam reforming of fast pyrolysis oils. *Energy and Fuels*, 12:12–24, 1998.

[25] A. V. Bridgwater, D. Meier, and D. Radlein. An overview of fast pyrolysis of biomass. *Organic Geochemistry*, 30:1479–1493, 1999.

[26] Mark M. Wright, Robert C. Brown, and Akwasi A. Boateng. Distributed processing of biomass to bio-oil for subsequent production of fischer-tropsch liquids. *Biofuels, Bioproducts, and Biorefining*, 2:229–238, 2008.

[27] D. Wang, S. Czernik, D. Montane, M. Mann, and E. Chornet. Biomass to hydrogen via fast pyrolysis and catalytic steam reforming of the pyrolysis oil or its fractions. *Industrial and Engineering Chemical Research*, 36:1507–1518, 1997.

[28] George W. Huber, Sara Iborra, and Avelino Corma. Synthesis of transportation fuels from biomass: Chemistry, catalysts, and engineering. *Chemical Review*, 106:4044–4098, 2006.

[29] *Dakota Gasification Company*. `http://www.dakotagas.com/About_Us/index.html`.

[30] *GreatPoint Energy*. `http://www.greatpointenergy.com/`, 2008-9.

[31] *Rialto Project*. `http://www.rentechinc.com/rialto.php`, 2009.

[32] Daniel A. Hickman and Lanny D. Schmidt. Syngas production by direct oxidation of methane on monoliths. *J. Catal.*, 138:267–282, 1992.

[33] M. Huff and L. D. Schmidt. Olefin and syngas formation by direct catalytic oxidation of ethane at short contact times. *Journal of Physical Chemistry*, 97:11815–11822, 1993.

[34] N. J. Degenstein, Ramanathan Subramanian, and L. D. Schmidt. Partial oxidation of n-hexadecane at short contact times: Catalyst & washcoat loading and catalyst morphology. *Appl. Catal., A*, 61:4207–4219, 2006.

[35] G. J. Panuccio, K. A. Williams, and L. D. Schmidt. Contributions of heterogeneous and homogeneous chemistry in the catalytic partial oxidation of octane isomers and mixtures on rhodium coated foams. *Chemical Engineering Science*, 61:4207–4219, 2006.

[36] pfrengineering.com. *REFORM-3PC Steam Hydrocarbon Reforming Simulation Program*. `http://www.pfrengineering.com/new_page_3.htm`, March 2007.

[37] C. T. Goralski Jr. and L. D. Schmidt. Catalytic incineration of volatile organic compounds at millisecond contact times. *AIChE Journal*, 44:1880–1888, 1998.

[38] R. P. O'Connor and L. D. Schmidt. Partial oxidation of cyclohexane in a single gauze reactor. *Journal of Catalysis*, 191:245–256, 2000.

[39] Jakob J. Krummenacher, Kevin N. West, and Lanny D. Schmidt. Partial oxidation of higher hydrocarbons at millesecond contact times: Decane, hexadecane, and diesel. *J. Catal.*, 215(332–343), 2003.

[40] B. J. Dreyer, I. Lee, J. J. Krummenacher, and L. D. Schmidt. Autothermal steam reforming of higher hydrocarbons: n-decane, n-hexadecnae, and JP-8. *Appl. Catal., A*, 307:184–194, 2006.

[41] Jiazhan Xu, Xiping Zhang, Renato Zenobi, Jun Yoshinobu, Zhi Xu, and John T. Yates Jr. Ethanol decomposition on Ni(111) observation of ethoxy formation by IRAS and other methods. *Surface Science*, 256:288–300, 1991.

[42] Manos Mavrikakis, D. J. Doren, and Mark A Barteau. Density functional theory calculations for simple oxametallacycles: Trends across the periodic table. *Journal of Physical Chemistry B*, 102:394–399, 1998.

[43] Manos Mavrikakis and Mark A Barteau. Oxygenate reaction pathways on transition metal surfaces. *J. Mol. Catal. A: Chem.*, 131:135–147, 1998.

[44] G. Scott. Jones, Manos Mavrikakis, Mark A Barteau, and John M. Vohs. First synthesis, experimental and theoretical vibrational spectra of an oxametallacycle on metal surface. *Journal of American Chemical Society*, 120:3196–3204, 1998.

[45] Ramanathan Subramanian and L. D. Schmidt. Renewable olefins from biodiesel by autothermal reforming. *Angew. Chem., Int. Ed.*, 44:302–305, 2005.

[46] Jakob J. Krummenacher, Kevin N. West, and Lanny D. Schmidt. Partial oxidation of higher hydrocarbons at millesecond contact times: Decane, hexadecane, and diesel. *J. Catal.*, 215(332–343), 2003.

[47] P. J. Dauenhauer, J. R. Salge, and L. D. Schmidt. Renewable hydrogen by autothermal steam reforming of volatile carbohydrates. *J. Catal.*, 244:238–247, 2006.

[48] Raimund Horn, Ken A. Williams, Nick J. Degenstein, Anders Bitsch-Larsen, Daniella Dalle Nogare, Sarah A. Tupy, and Lanny D. Schmidt. Methane catalytic partial oxidation on autothermal Rh and Pt foam catalysts: Oxidation and reforming zones, transport effects, and approach to thermodynamic equilibrium. *J. Catal.*, 249(378-391), 2007.

[49] J. R. Salge, B. J. Dreyer, P. J. Dauenhauer, and L. D. Schmidt. Renewable hydrogen from nonvolatile fuels by reactive flash volatalization. *Science*, 244:238–247, 2006.

[50] Paul J. Dauenhauer, Bradon J. Dreyer, Nick J. Degenstein, and Lanny D. Schmidt. Millisecond reforming of solid biomass for sustainable fuels. *Angewandte Chemie International Edition*, 46:5864–5867, 2007.

[51] Joshua L. Colby, Paul J. Dauenhauer, and Lanny D. Schmidt. Millisecond autothermal steam reforming of cellulose for synthetic biofuels by reactive flash volatilization. *Green Chem.*, pages 773–783, 2008.

[52] G. W. Huber and A. Corma. Synergies between bio- and oil refineries for the production of fuels from biomass. *Angewandte Chemie*, 38:7320–7338, 2007.

[53] E. Wanat, B. Suman, and L. D. Schmidt. Partial oxidation of alcohols to produce hydrogen and chemicals in millisecond reactors. *Journal of Catalysis*, (18-27), 2005.

[54] S. Wang, T. Ishihara, and Y. Takita. Partial oxidation of dimethyl ether over various supported metal catalysts. *Applied Catalysis A: General*, 228:167–176, 2002.

[55] Bradon J. Dreyer. *Synthesis Gas and Olefins from the Catalytic Autothermal Reforming of Volatile and Non-volatile Liquids*. PhD thesis, University of Minnesota, 2007.

[56] David C. Rennard, Paul J. Dauenhauer, Sarah A. Tupy, and Lanny D. Schmidt. Autothermal catalytic partial oxidation of bio-oil functional groups: Esters and acids. *Energy Fuels*, 22:1318–1327, 2008.

[57] Kazuhiro Takanabe, Ken ichi Aika, K. Seshan, and Leon Lefferts. Sustainable hydrogen from bio-oil – steam reforming of acetic acid as a model oxygenate. *Journal of Catalysis*, 227:101–108, 2004.

[58] Ekaterini Ch. Vagia and Angeliki A. Lemonidou. Thermodynamic analysis of hydrogen production via autothermal steam reforming of selected components of aqueous bio-oil fraction. *International Journal of Hydrogen Energy*, 33:2489–2500, 2008.

[59] Maximiliano Marquevich, Stefan Czernik, Esteban Chornet, and Daniel Montane. Hydrogen from biomass: Steam reforming of model compounds of fast-pyrolysis oil. *Energy and Fuels*, 13:1160–1166, 1999.

[60] Aristides C. Basagiannis and Xenophon E. Verykios. Steam reforming of the aqueous fraction of bio-oil over structured Ru/Mgo/Al2O3 catalysts. *Catalysis Today*, 127:256–264, 2007.

[61] Gustave Bryant and Eastman Kodak Company Howard A. Tanner. Decomposition of esters. US Patent 2304872, December 1942.

[62] Ingrid K. Meier and Jeffrey Schwartz. Olefin synthesis by vanadium(v)-induced oxidative decarboxylation-deoxygenation of 3-hydroxy carboxylic acids. *Joural of Organic Chemistry*, 55:5619–5624, 1990.

[63] Joseph A Miller, Jeffrey A Nelson, and Mike Byrne. Process for making olefins. US Patent 5077477, December 1991.

[64] J. R. Salge, G. A. Deluga, and L. D. Schmidt. Catalytic partial oxidation of ethanol over noble metal catalysts. *J. Catal.*, 235:69–78, 2005.

[65] K. R. Doolan, J. C. Mackie, and C. R. Reid. High temperature kinetics of the thermal decomposition of the lower alkanoic acids. *International Journal of Chemical Kinetics*, 18(5):575–596, 1986.

[66] Gabriel Chuchani, Ignacio Martin, Alexandra Rotinov, and Rosa M. Dominguez. Elimination kinetics and mechanism of primary, secondary and tertiary α-hydroxycarboxylic acids in the gas phase. *Journal of Physical Organic Chemistry*, 6:54–58, 1993.

[67] L. R. Domingo, J. Andres, V. Moliner, and V. S. Safont. Theoretical study of the gas phase decomposition of glycolic, lactic, and 2-hydroxyisobutyric acids. *Journal of American Chemical Society*, 119:6415–6422, 1997.

[68] A. Golomb and P. D. Ritchie. Studies in pyrolysis. part xvii. the acyl derivatives and lactides of some α-hydroxy acids. *unknown*, pages 838–847, 1962.

[69] Gonzalo Blay, Isabel Fernandez, Pilar Formentin, Jose R. Pedro, Antonio L. Rosello, Rafael Ruiz, and Yves Journaux. Catalytic aerobic oxidative decarboxylation of α-hydroxy-acids. methyl mandelate as a benzoyl anion equivalent. *Tetrahedron Letters*, pages 3327–3330, 1998.

[70] J. R. Jones, William A. Waters, and J. S. Littler. Oxidations of organic compounds with quinquevalent vanadium. part viii. the kinetic resemblance between the oxidations of some α-hydroxy-acids and that of pinacol and of its monomethyl ether. *Journal of the Chemical Society*, pages 630–633, 1961.

[71] Eva Melzer and Hanns-Ludwig Schmidt. Carbon isotope effects on the decarboxylation of carboxylic acids. *Biochemistry Journal*, 252:913–915, 1988.

[72] R. Alan Aitken and Andrew W. Thomas. Ethyl mandelate as a convenient new benzoyl anion equivalent. *Synlett*, 3:293–294, 1997.

[73] Nouria A. Al-Awadi and Osman M. E. El-Dusouqui. Pyrolysis of β-hydroxyketones and α-ketoesters: Gas-phase elimination kinetics of 3-hydroxy-3-methyl-2-butanon and methyl benzoylformate. *unknown*, unknown:295–298, 1997.

[74] Roger Taylor. The mechanism of thermal eliminations part xxiii: [1] the thermal decomposition of pyruvic acid. *International Journal of Chemical Kinetics*, 19:709–713, 1987.

[75] R. Horn, K. A. Williams, N. J. Degenstein, and L. D. Schmidt. Mechanism of H2 and CO formation in the catalytic partial oxidation of CH4 on Rh probed by steady-state spatial

profiles and spatially resolved transients. *Chemical Engineering Science*, 62:1298–1307, 2007.

[76] J. L. Davis and Mark A Barteau. Reactions of carboxylic acids on the Pd(111)-(2x2)O surface: multiple roles of surface oxygen atoms. *Surface Science*, 256:50–56, 1991.

[77] Carl Houtman and Mark A Barteau. Reactions of formic acid and formaldehyde on Rh(111) and Rh(111)-(2x2)o surfaces. *Surface Science*, 248:57–76, 1991.

[78] M. A. Barteau, M. Bowker, and R. J. Madix. Acid-base reactions on solid surfaces: The reactions of HCOOH, H_2CO, and $HCOOCH_3$ with oxygen on Ag(110). *Surface Science*, 94:303–322, 1980.

[79] C. Wheeler, A. Jhalani, E. J. Klein, S. Tummala, and L. D. Schmidt. The water-gas-shift reaction at short contact times. *J. Catal.*, 223:191–199, 2004.

[80] J. L. Davis and M. A. Barteau. Hydrogen bonding in carboxylic acid adlayers on Pd(111): Evidence for catemer formation. *Langmuir*, 5:1299–1309, 1989.

[81] Yoshiro Yasaka, ken Yoshida, Chihiro Wakai, Nobuyuki Matubayasi, and Masaru Nakahara. Kinetic and equilibrium study on formic acid decomposition in relation to the water-gas-shift reaction. *Journal of Physical Chemistry A*, 110:11082–11090, 2006.

[82] D. Sitamanikyam and E. V. Sundaram. Kinetics of thermal decarboxylation of ortho- and para- substituted benzoic acids in glycerol. *Indian Journal of Chemistry*, 10:1011–1013, 1972.

[83] Saul Patai, editor. *The Chemistry of Acid Derivatives Part 2*, volume Supplement B-2. John Wiley and Sons, 1979.

[84] C. H. Bamford and M. J. S. Dewar. The thermal decomposition of acetic acid. *Journal of the Chemical Society*, pages 2877–2882, 1949.

[85] Eric J. Hintsa, Alec M. Wodtke, and Yuan T. Lee. Infrared multiphoton dissociation of ethyl and methyl acetate. *Journal of Physical Chemistry*, 92:5379–5387, 1988.

[86] Minh Tho Nguyen, Debasis Sengupta, Greet Raspoet, and Luc G. Vanquickenborne. Theoretical study of the thermal decomposition of acetic acid: Decarboxylation versus dehydration. *Journal of Physical Chemistry*, 99:11883–11888, 1995.

[87] Edmund N. Ndip Moses, Manoj K. Shukla, Jerzy Leszcynski, and Richard L. Redington. Theoretical study of the ground-state gas-phase unimolecular decomposition channels of propynoic acid. *Journal of Quantum Chemistry*, 100:779–787, 2004.

[88] Rosana C. L. Pereira and Paulo C. Isolani. Multiphoton gas phase dissociation of methyl and ethyl formates. *Journal of Photochemistry and Photobiology, A: Chemistry*, 42:51–61, 1988.

[89] Arthur T. Blades. The kinetics of the pyrolysis of ethy- and isopropyl formates and acetates. *Canadian Journal of Chemistry*, 32:366–372, 1954.

[90] K. Siplia, E. Kuoppala, L. Fagernas, and A. Oasmaa. Characterization of biomass-based flash pyrolysis oils. *Biomass and Bioenergy*, 14:103–113, 1998.

[91] Jiliang Zuo. Purification of black liquor from papermaking pulp. CN Patent 96-115935, 1998.

[92] Ulrike Tschirner. Lignocellulosics and the wood based biorefinery. Technical report, University of Minnesota CE5595, September 2006.

[93] Wikipedia. *Esters*. `http://en.wikipedia.org/wiki/Ester`, March 2007.

[94] Masanori Kuroda, Akihisa Fukuda, Kinya Sakanishi, Tomoaki minowa, Yoshiyuki Sasaki, and Akira Yabe. Manufacture of industrial raw materials such as methanol, methyl formate, lactic acid, etc., from wood with good heat recycling. JP Patent 2006111593.

[95] World Health Organization. *FAO Nutrition Meetings*, number Resort Series 44A: WHO/Food Add/68.33, Geneva, 1967.

[96] Anne Marie Helmenstine. *List of Additives and What They Do*. `http://chemistry.about.com/od/foodcookingchemistry/a/eadditives.htm`, December 2006.

[97] Marc G. Loudon. *Organic Chemistry*. The Benjamin/Cummings Publishing Company, Inc., 3 edition, 1998.

[98] Navinchandra Asthana, Aspi Kolah, Dung T. Vu, Carl T. Lira, and Dennis Miller. A continuous reactive separation process for ethyl lactate formation. *Organic Process Research and Development*, 9(5):599–607, 2005.

[99] Argonne National Laboratory. *Frequently Asked Questions about Ethyl Lactate*. http://www.anl.gov/techtransfer/Available_Technologies/Environmental_Research/faq_ethyl_lactate.html, December 2006.

[100] Stefan Czernik, Richard French, Calvin Feik, and Esteban Chornet. Hydrogen by catalytic steam reforming of liquid byproduts from biomass thermoconversion process. *Industrial and Engineering Chemical Research*, 41:4209–4215, 2002.

[101] Jemma Vickery. *Green Chemistry: What are Green Solvents?* http://www.chemsoc.org/ExemplarChem/entries/2004/bristol_vickery/green_solvents.htm, December 2006.

[102] David E. Henton, P. Gruber, J. Lunt, and J. Randall. *Polylactic Acid Technology, Natural Fibers, Biopolymers, and Biocomposites*. CRC Press LLC, Boca Raton, 2005.

[103] Patric R. Gruber, Eric S. Hall, Jeffrey J. Kolstad, Matthew L. Iwen, Richard D. Benson, and Cargill Ronald L. Borchardt. Continuous process for manufacture of lactide polymers with controlled optical purity. US Patent 5142023 and family, August 1992.

[104] University of Nebraska Lincoln. *Polylactic Acid Research*. http://agproducts.unl.edu/pla.htm, December 2006.

[105] *Natureworksllc.com*. http://www.natureworksllc.com/, 2009.

[106] *Press Release*. http://www.bglactic.com/UK/news_old.htm, 2005.

[107] Mary Bellis. *Polyester - PET*. http://inventors.about.com/library/inventors/blpolyester.htm, March 2007.

[108] biodiesel.org. *Biodiesel Basics*. http://www.biodiesel.org/resources/biodiesel_basics/default.shtm, December 2006.

[109] Jan Van Breugel and Purac Biochem B.V. Gerrit Leendert Nanninga. Fuel composition. US Patent 6719815, April 2004.

[110] Carl Houtman and Mark A Barteau. Adsorbed states of acetone and their reactions on Rh(111) and Rh(111)-(2x2)o surfaces. *Journal of Physical Chemistry*, 95:3755–3764, 1991.

[111] M. M. Walczak, P. K. Leavitt, and P. A. Thiel. Oxygenated fluorocarbons adsorbed at metal surfaces: Chemisorption bond strengths and decomposition. *Journal of American Chemical Society*, 109:5621–5627, 1987.

[112] Stephane Lavoie and Peter H. McBreen. Evidence for C–H - O=C bonding in coadsorbed aromatic-carbonyl systems on Pt(111). *Journal of Physical Chemistry B*, 109:11986–11990, 2005.

[113] E. Zahidi, M. Castonguay, and P. McBreen. RAIRS and TPD study of methyl formate, ethyl formate, and methyl acetate on Ni(111). *Journal of American Chemical Society*, 116:5847–5856, 1994.

[114] Mark A Barteau. Organic reactions at well-defined oxide surfaces. *Chemical Review*, 96:1413–1430, 1996.

[115] Carl Houtman and Mark A Barteau. Reactions of methanol on Rh(111) and Rh(111)-(2x2)o surfaces: Spectroscopic identification of adsorbed methoxide and η^1-formaldehyde. *Langmuir*, 6:1558–1566, 1990.

[116] J. Will Medlin, Manos Mavrikakis, and Mark A Barteau. Stabilities of substituted oxametallacycle intermediates: Implications for regioselectivity of epoxide ring opening and olefin epoxidation. *Journal of Physical Chemistry B*, 103:11169–11175, 1999.

[117] W. Erley and D. Sander. The adsorption and decomposition of formic acid on ni(111): The identification of formic anhydride by vibrational spectroscopy. *Journal of Vacuum Science Technology A*, pages 2238–2244, 1989.

[118] Jianyi Shen, Weijie Ji, Yuwang Han, and Yi Chen. Method for preparing pyruvic acid ethyl ester by gas-phase catalytic oxidation of lactic acid ethyl ester. CN Patent 1359893, 2002.

[119] Nicholas F. Dummer, Robert Jenkins, Xiabao Li, Salem M. Bawaked, Paul McMorn, Andrew Burrows, Christopher J. Kiely, Richard P. K. Wells, David J. Willcock, and Graham J. Hutchings. Inversion of enantioselectivity for the hydrogenation of ethyl pyruvate in the gas-phase over Pt/SiO_2 modified with derivatives of hydroquinidine. *J. Catal.*, 243:165–170, 2006.

[120] Pierre A. Glaude, William J. Pitz, and Murray J. Thomon. Chemical kinetic modeling of dimethyl carbonate in an opposed-flow diffusion flame. In *30th International Symposium on Combustion*, pages 1–22. Lawrence Livermore National Laboratory, 2004.

[121] A. T. Blades and H. S. Sanhu. The arrhenius factors for some six-center unimolecular reactions. *International Journal of Kinetics*, III:187–193, 1971.

[122] Ikchoon Lee, Ok Ja Cha, and Bon-Su Lee. Theoretical studies on the gas-phase pyrolysis of esters. *Journal of Physical Chemistry*, 94:3926–3930, 1990.

[123] Earl M. Bilger and Harold Hibbert. Mechanism of organic reactions. iv. pyrolysis of esters and acetals. *Journal of the American Chemical Society*, 58:823–826, 1936.

[124] R. Taylor. The kinetic isotope effect in the pyrolysis of esters and the nature of the transition state. *Journal of the Chemical Society Perkins Transactions 2*, pages 165–168, 1972.

[125] Roger Taylor. The mechanism of the gas-phase pyrolysis of esters. Part 7. The effects of substituents at the acyl carbon. *J. C. S. Perkin II*, pages 1255–1258, 1978.

[126] Roger Taylor. The transition state in ester pyrolysis. Part 9. On the surface-catalyzed mechanism for the elimination. *Journal of the Chemical Society Perkins Transactions 2*, pages 1730–1737, 1979.

[127] Richard T. Arnold, Grant Gill Smith, and R. M. Dodson. Mechanism of the pyrolysis of esters. *Journal of Organic Chemistry*, pages 1256–1260, 1950.

[128] W. K. Metcalfe, S. Dooley, H. J. Curran, J. M. Simmie, A. M. El-Nahas, and A. M. Navarro. Experimental and modeling study of $C_5H_{10}O_2$ ethyl and methyl esters. *Journal of Physical Chemistry*, unknown:unknown, 2007.

[129] E. M. Fisher, W. J. Pitz, H. J. Curran, and C. K. Westbrook. Detailed chemical kinetic mechanisms for combustion of oxygenated fuels. *Colloquium: Reaction Kinetics of Combustion*, 2000.

[130] Robert Alexander, Paul G. Kralert, and Robert I. Kagi. Kintics and mechanism of the thermal decomposition of esters in sediments. *Advances in Organic Geochemistry*, 19(1-3):133–140, 1991.

[131] B. L. Yates, A. Ramirez, and O. Velasquez. The thermal decomposition of β-hydroxy esters. *Joural of Organic Chemistry*, 36(23):3579–3582, 1971.

[132] Rafael Notario, Jairo Quijano, J. Camilo Quijano, Luisa P. Gutierrez, Wilmar A. Suarez, Claudia Sanchez, Luis A. Leon, and Eduardo Chamorro. Theoretical study of the thermolysis reaction of ethyl β-hydroxycarboxylates in the gas phase. *Journal of Physical Chemistry A*, 106(17):4377–4383, 2002.

[133] Ikchoon Lee, Ok Ja Cha, and Bon-Su Lee. Theoretical studies on the gas-phase pyrolysis of carbonate esters, hydroxy-esters and -ketones. *Bulletin of the Korean Chemical Society*, 12(1):97–101, 1991.

[134] Nobuo Mori, Satoshi Omura, Noihiko Kobayashi, and Yojiro Tsuzuki. Intromolecular hydrogen bonds. v. aliphatic hydroxy-carboxylates. *Bulletin of the Chemical Society of Japan*, 38(12):2149–2155, 1965.

[135] Nicole Borho, Martin A. Suhm, Katia Le Barbu-Debus, and Anne Zehnacker. Intra- vs intermolecular hydrogen bonding: dimers of α-hydroxyesters with methanol. *Physical Chemistry Chemical Physics*, 8:4449–4460, 2006.

[136] A. T. Ashcroft, A. K. Cheetham, J. S. Foord, M. L. H. Green, C. P. Grey, A. J. Murrell, and P. D. F. Vernon. Selective oxidation of methane to synthesis gas using transition metal catalysts. *Nature*, 344:319–321, 1990.

[137] A. S. Bodke, D. A. Oschki, L. D. Schmidt, and E. Ranzi. High selectivities to ethylene by partial oxidation of ethane. *Science*, 285:712–715, July 1999.

[138] A. S. Bodke, S. S. Bharadwaj, and L. D. Schmidt. The effect of ceramic supports on partial oxidation of hydrocarbons over noble metal coated monoliths. *Journal of Catalysis*, 179:138–149, 1998.

[139] C. N. Hinshelwood and W. K. Hutchinson. A comparison between unimolecular and bimolecular gaseous reactions. the thermal decomposition of gaseous acetaldehyde. *Proc. Royal Society*, 111(A):380–385, 1926.

[140] Francois Jerome, Yannick Pouilloux, and Joel Barrault. Rational design of solid catalysts for the selective use of glycerol as a natural organic building block. *ChemSusChem*, 1:586–613, 2008.

[141] Chun-Hui (Clayton) Zhou, Jorge N. Beltramini, Yong-Xian Fan, and G. Q. (Max) Lu. Chemoselective catalytic conversion of glycerol as a biorenewable source to valuable commodity chemicals. *Chem. Soc. Rev.*, 37(3):527–549, 2008.

[142] T. Valliyappan, N. N. Bakhshi, and A. K. Dalai. Pyrolysis of glycerol for the production of hydrogen or syn gas. *Bioresour. Technol.*, 99:4476–4483, 2008.

[143] Yolanda S. Stein and Michael Jerry Antal Jr. A study of the gas-phase pyrolysis of glycerol. *J. Anal. Appl. Pyrolysis*, 4:283–296, 1983.

[144] John B. Paine III, Yezdi B. Pithawalla, John D. Naworal, and Charles E. Thomas Jr. Carbohydrate pyrolysis mechanisms from isotopic labeling part 1: The pyrolysis of glycerin: Discovery of competing fragmentation mechanisms affording acetaldehyde and formaldehyde and the implications for carbohydrate pyrolysis. *J. Anal. Appl. Pyrolysis*, 80:297–311, 2007.

[145] Axel Behrens, Peter Bender, Nicole Schodel, and Hubertus Winkler. Process and device for producing hydrogen from organic oxygen compounds. US Patent 2007286797, DE102006017888, December 2007.

[146] R. D. Cortright, R. R. Davda, and J. A. Dumesic. Hydrogen from catalytic reformign of biomass-derived hydrocarbons in liquid water. *Nature*, 418:964–967, 2002.

[147] S. Adhikari, S. D. Fernando, and A. Haryanto. Glycerin steam reforming for hydrogen production. *Transactions of the American Society of Agricultural and Biological Engineers*, 50(2):591–595, 2007.

[148] Alessandro Donazzi, Brian C. Michael, and Lanny D. Schmidt. Chemical and geometric effects of Ce and washcoat addition on catalytic partial oxidation of CH4 on rh probed by spatially resolved measurements. *J. Catal.*, doi:10.1016/j.jcat.2008.09.028, 2008.

[149] D. A. Simonetti, E. L. Kunkes, and J. A. Dumesic. Gas-phase conversion of glycerol to synthesis gas over carbon-supported platinum and platinum-rhenium catalysts. *J. Catal.*, 247:298–306, 2007.

[150] Mark R. Nimlos, Stephen J. Blanksby, Xianghong Qian, Michael E. Himmel, and David K. Johnson. Mechanisms of glycerol dehydration. *J. Phys. Chem. A*, 110:6145–6156, 2006.

[151] Alexander Burcat. Prof. Burcat's thermodynamic data. *http://garfield.chem.elte.hu/Burcat/burcat.html*, last checked August 13, 2008.

[152] Sushil Adhikari, Sandun Fernando, and Agus Haryanto. A comparative thermodynamic and experimental analysis on hydrogen production by steam reforming of glycerin. *Energy Fuels*, 21:2306–2310, 2007.

[153] M. J. Antal Jr., W. S. L. Mok, J. C. Roy, and A. T-Raissi. Pyrolytic sources of hydrocarbons from biomass. *J. Anal. Appl. Pyrolysis*, 8:291–303, 1985.

[154] Avelino Corma, George W. Huber, Laurent Sauvanaud, and Paul O'Connor. Biomass to chemicals: Catalytic conversion of glycerol/water mixtures into acrolein, reaction network. *J. Catal.*, 257:163–171, 2008.

[155] Manos Mavrikakis and Mark A Barteau. Oxygenate reaction pathways on transition metal surfaces. *J. Mol. Catal. A: Chem.*, 131:135–147, 1998.

[156] Hiroshi Kimura and Keiichi Tsuto. Selective oxidation of glycerol on a platinum-bismuth catalyst. *Appl. Catal., A*, 96:217–228, 1993.

[157] Regis Garcia, Michele Besson, and Pierre Gallezot. Chemoselective catalytic oxidation of glycerol with air on platinum metals. *Appl. Catal., A*, 127:165–176, 1995.

[158] Paul Westcott, Ronald Trostle, and Edwin Young. *Agricultural Baseline Projections: Baseline Presentation, 2008-2017*. http://www.ers.usda.gov/briefing/Baseline/present2008.htm, February 2008.

[159] David C. Rennard, Jacob S. Kruger, and Lanny D. Schmidt. Autothermal catalytic partial oxidation of glycerol to syngas and to non-equilibrium products. *ChemSusChem*, 2(89-98), 2009.

[160] Sauri Gudlavalleti, Tijmen Ros, and Dick Lieftnik. Thermal sintering studies of an autothermal reforming catalyst. *Applied Catalysis B: Environmental*, 74:251–260, 2007.

[161] Shi Ding, Yiyang Yang, Yong Jin, and Yi Cheng. Catalyst deactivation of rh-coated foam monolith for catalytic partial oxidation of methane. *Industrial and Engineering Chemical Research*, 48:2878–2885, 2009.

[162] L. Basini. Fuel rich catalytic combustion: Principles and technological developments in short contact time (sct) catalytic processes. *Catalysis Today*, 117:384–393, 2006.

[163] Luca Basini. Issues in H2 and synthesis gas technologies for refinery, GTL and small and distributed industrial needs. *Catalysis Today*, 106:34–40, 2005.

[164] L. Basini, K. Aasberg-Petersen, A. Guarinoni, and M. Ostberg. Catalytic partial oxidation of natural gas at elevated pressure and low residence time. *Catalysis Today*, 64:9–20, 2001.

[165] I. Tavazzi, A. Beretta, G. Groppi, M. Maestri, E. Tronconi, and P. Forzatti. Experimental and modeling analysis of the effect of catalyst aging on the performance of a short contact time adiabatic CH4-CPO reactor. *Catalysis Today*, 129:372–379, 2007.

[166] Alex Platon, Hyun-Seog Roh, David L. King, and Yong Wang. Deactivation studies of Rh/Ce0.8Zr0.2O2 catalysts in low temperature ethanol steam reforming. *Topics in Catalysis*, 46:374–379, 2007.

[167] D. G. Loffler, S. D. McDermott, and C. N. Renn. Activity and durability of water-gas shift catalysts used for the steam reforming of methanol. *Journal of Power Sources*, 114:15–20, 2003.

[168] S. Eriksson, M. Wolf, A. Schneider, J. Mantzaras, F. Raimondi, M. Boutonnet, and S. Jaeras. Fuel-rich catalytic combustion of methane in zero emissions power generation processes. *Catalysis Today*, 117:447–453, 2006.

[169] Lucia Garcia, Richard French, Stefan Czernik, and Esteban Chornet. Catalytic steam reforming of bio-oils for the production of hydrogen: effects of catalyst composition. *Applied Catalysis A: General*, 201:225–239, 2000.

[170] Brian C. Michael, Alessandro Donazzi, and Lanny D. Schmidt. Effects of H2O and CO2 addition in catalytic partial oxidation of methane on Rh. *Journal of Catalysis*, 265:117–129, 2009.

[171] R. Horn, K. A. Williams, N. J. Degenstein, and L. D. Schmidt. Syngas by catalytic partial oxidation of methane over rhodium: Mechanistic conclusions from spatially resolved measurements and numerical simulations. *J. Catal.*, 242:92–102, 2006.

[172] Yanchun Zhou and Mohamed N Rahaman. Effect of redox reaction on the sintering behavior of cerium oxide. *Acta Mater*, 45(9):3635–3639, 1997.

[173] Pio Forzatti and Luca Lietti. Catalyst deactivation. *Catalysis Today*, 52:165–181, 1999.

[174] P. O. Thevenin, A. G. Ersson, H. M. J. Kusar, P. G. Menon, and S. G. Jaras. Deactivation of high temperature combustion catalysts. *Applied Catalysis A: General*, 212:189–197, 2001.

[175] Z. L. Zhang, V. A. Tsipouriari, A. M. Efstathiou, and X. E. Verykios. Reforming of methane with carbon dioxide to synthesis gas over supported rhodium catalysts. *Journal of Catalysis*, 158:51–63, 1996.

[176] Dushyant Shekhawat, Todd H. Gardner, David A. Berry, Maria Salazar, Daniel J. Haynes, and James J. Spivey. Catalytic partial oxidation of n-tetradecane in the presence of sulfur or polynuclear aromatics: Effects of support and metal. *Applied Catalysis A: General*, 311:8–16, 2006.

[177] Anders Bitsch-Larsen, Nick J. Degenstein, and Lanny D. Schmidt. Effect of sulfur in catalytic partial oxidation of methane over Rh-Ce coated foam monoliths. *Applied Catalysis B: Environmental*, 78(3-4):364–370, 2008.

[178] R. P. O'Connor, E. Klein, and L. D. Schmidt. High yields of synthesis gas by millisecond partial oxidation of higher hydrocarbons. *Catalysis Letters*, 70:99–108, 2000.

[179] Zhaoxiang Wang, Yue Pan, Ting Dong, Xifeng Zhu, Tau Kan, Lixia Yuan, Youshifumi Torimoto, Masayoshi Sadakata, and Quanxin Li. Production of hydrogen from catalytic steam reforming of bio-oil using C12A7-O–based catalysts. *Applied Catalysis A: General*, 320:24–34, 2007.

[180] Guus van Rossum, Sascha R. A. Kersten, and Wim P. M. van Swaaij. Catalytic and noncatalytic gasification of pyrolysis oil. *Industrial and Engineering Chemical Research*, 46:3959–3967, 2007.

[181] Panagiotis N. Kechagiopoulos, Spyros S. Voutetakis, Angeliki A. Lemonidou, and Iacovos A. Vasalos. Hydrogen production via reforming of the aqueous phase of bio-oil over ni/olivine catalysts in a spouted bed reactor. *Industrial and Engineering Chemical Research*, 45:1400–1408, 2009.

[182] Panagiotis N. Kechagiopoulos, Spyros S. Voutetakis, Angeliki A. Lemonidou, and Iacovos A. Vasalos. Hydrogen production via steam reforming of the aqueous phase of bio-oil in a fixed bed reactor. *Energy and Fuels*, 20:2155–2163, 2006.

[183] Cyrille Rioche, Shrikant Kulkarni, Frederic C. Meunier, John P. Breen, and Robbie Burch. Steam reforming of model compounds and fast pyrolysis bio-oils on supported noble metal catalysts. *Applied Catalysis B: Environmental*, 61:130–139, 2005.

[184] Guus van Rossum, Sascha R. A. Kersten, and Wim P. M. van Swaaij. Staged catalytic gasification/steam reforming of pyrolysis oil. *Industrial and Engineering Chemical Research*, 48:5857–5866, 2009.

[185] Luc Moens, Stuart K. Black, Michele D. Myers, and Stefan Czernik. Study of the neutralization and stabilization of a mixed hardwood bio-oil. *Energy and Fuels*, 23:2695–2699, 2009.

[186] M. E. Boucher, A. Chaala, and C. Roy. Bio-oils obtained by vacuum pyrolysis of softwood bark as a liquid fuel for gas turbines. part i: Properties of bio-oil and its blends with methanol and a pyrolytic aqueous phase. *Biomass and Bioenergy*, 19(5):337–350, 2000.

[187] Anja Oasmaa, Kai Sipila, Yrjo Solantausta, and Eeva Kuoppala. Quality improvements of pyrolysis liquid: Effect of light volatiles on the stability of pyrolysis liquids. *Energy and Fuels*, 19:2556–2561, 2005.

[188] Marcelo Eduardo Domine, Eduard Emil Iojoiu, Thomas Davidian, Nolven Guilhaume, and Claude Mirodatos. Hydrogen production from biomass-derived oil over monolithic

Pt- and Rh-based catalysts using steam reforming and sequential cracking processes. *Catalysis Today*, 133-135:565–573, 2008.

[189] Eduard Emil Iojoiu, Marcelo Eduardo Domine, Thomas Davidian, Nolven Guilhaume, and Claude Mirodatos. Hydrogen production by sequential cracking of biomass-derived pyrolysis oil over noble metal catalysts supported on ceria-zirconia. *Applied Catalysis A: General*, 323:147–161, 2007.

[190] Alessandro Donazzi, Alessandra Beretta, Gianpiero Groppi, and Pio Forzatti. Catalytic partial oxidation of methane over a 4% rh/α-Al2O3 catalyst part i: Kinetic study in annular reactor. *Journal of Catalysis*, 255:241–258, 2008.

[191] K. Polychronopoulou, C. N. Costa, and A. M. Efstathiou. The steam reforming of phenol reaction over supported-Rh catalysts. *Applied Catalysis A: General*, 272:37–52, 2004.

[192] B. V. Babu and A. S. Chaurasia. Heat transfer and kinetics in the pyrolysis of shrinking biomass particle. *Chemical Engineering Science*, 59:1999–2012, 2004.

[193] Zhao Yu, Fei Wang, and L. S. Fan. Experimental and numerical studies of water droplet impact on a porous surface in the film-boiling regime. *Industrial and Engineering Chemical Research*, 47:9174–9182, 2008.

[194] *Hydrogen and Our Energy Future*. US Department of Energy, 2006.

[195] M. Ringer, V. Putsche, and J. Scahill. Large-scale pyrolysis oil production: A technology assessment and economic analysis. Technical Report NREL TP-510-37779, National Renewable Energy Laboratory, November 2006.

[196] Sarah Ann Tupy. Partial oxidation of biofuels: The ash problem. Master's thesis, University of Minnesota, 2008.

Appendix A

Glossary and Acronyms

Care has been taken in this thesis to minimize the use of jargon and acronyms, but this cannot always be achieved. This appendix defines common terms in a glossary, and contains a table of acronyms and their meaning.

A.1 Glossary

- **Autothermal Reforming** (**ATR**) – Partial oxidation of a fuel with the addition of steam to enhance H_2 production. The oxidation releases energy so that no firebox or external heat source is required.
- **Backface** (**BF**) – The position at the junction of the end of the catalyst bed and the heat shield downstream of the catalyst bed.
- **Backface Heat Shield** – The monolith downstream of the catalyst, used to insulate the catalyst.
- **Biomass Pyrolysis Oil** (**Bio Oil or Pyrolysis Oil**) – A liquid phase, sometimes referred to as "tar," produced when biomass is rapidly heated in an inert environment.
- **Carbon to Oxygen Ratio** (**C/O**) – A description of the amount of oxidation for a particular reaction. "Carbon" refers to the number of carbon atoms in the fuel relative to O, the number of oxygen atoms in the oxidant. Oxygen atoms in the fuel are not counted in this fraction because they cannot release energy: the fuel is already oxidized by those atoms.

- **Catalytic Partial Oxidation** (**CPO**) – The use of a catalyst, such as a noble metal, to release some, but not all, of the energy in an organic fuel. Typically, partial oxidation results in the production of syngas.

- **Combustion** – The strongly exothermic reaction wherein oxygen and fuel react to form H_2O and CO_2 according to Equation A.1

$$C_xH_yO_z + (x + y/4 - z/2)O_2 \rightarrow xCO_2 + y/2H_2O \qquad \Delta H^o << 0\frac{kJ}{mol} \tag{A.1}$$

- **Contact Time** (τ) – The time that a flowing packet of vaporized reactants at reaction temperature can interact with a catalyst. See also GHSV.

$$\tau = \frac{\epsilon \times V}{\left(\frac{T_{rxn}(K)}{291K}\right) Q} \tag{A.2}$$

where T_{rxn} refers to the reaction temperature in Kelvin measured at the backface thermocouple.

- **Conversion** (**X**) – The fraction of reactants converted to products according to Equation A.3

$$X = 100\% \times \frac{F_{in} - F_{out}}{F_{in}} \tag{A.3}$$

for F_{in} as the molar flow rate of a reactant into the reactor and F_{out} is the molar flow rate of the unconverted reactant out of the reactor. An equivalent definition is often used in this work, wherein the sum of carbon in all products replaces the difference of F_{in} - F_{out}, and F_{in} represents the total carbon introduced to the reactor, as depicted in Equation A.4. In this case, conversion refers to the carbon conversion; to obtain conversion of other species requires correcting by the stoichiometric coefficient. These definitions will differ by carbon error.

$$X = 100\% \times \frac{\sum C_i \times F_i}{C_{fuel} \times F_{in}} \tag{A.4}$$

Where F_i is the molar flow of species i containing C_i atomic carbons.

- **Frontface** (**FF**) – The position at the junction of the top of the catalyst bed.
- **Frontface Heat Shield** – The monolith upstream of the catalyst, used to insulate the catalyst.
- **Gas Hourly Space Velocity** (**GHSV**) – The flowrate of gas in inverse hours under standard conditions (1 atm, 25 ^{o}C) through a catalyst.

$$GHSV = \frac{Q}{\epsilon V} \tag{A.5}$$

Q is the volumetric flow rate of reactants; ϵ is the void fraction of the catalyst (eg, where gas can flow), and V is the total volume of the catalyst.

- **Incipient Wetness Impregnation** – A method of coating a substrate with an active catalytic phase, wherein the catalyst precursor, a salt solution or powder slurry, is drop-coated onto the substrate, dried, and heated to decompose the salt.
- **Internal C/O** – The ratio of carbon atoms in the fuel to oxygen atoms in the fuel.
- **Reactive Flash Volatilization** (**RFV**) – A method of CPO in which room temperature liquid droplets are introduced directly onto the front face of the catalyst without any preheat.
- **Selectivity** ($\mathbf{S}_i$) – The ratio of a given atom in species i to the total number of those atoms in converted fuel. Selectivity for carbon-containing species is defined by Equation A.6:

$$S_C(i) = \frac{C_i \times F_i}{C_{fuel} \times (F_{in} - F_{out})} \tag{A.6}$$

Where F_i is the molar flowrate of species i. Products containing no carbon (H_2 and H_2O) are analogously described by hydrogen selectivity to j: $S_H(j)$, defined in Equation A.7.

$$S_H(j) = \frac{H_j \times F_j}{H_{fuel} \times \left(F^{in}_{fuel} - F^{out}_{fuel}\right)} \tag{A.7}$$

where H_j indicates the number of hydrogen atoms in species j.

In both cases, if the alternate definition for conversion is used (that of total products counted rather than unconverted fuel), then the difference F_{in} - F_{out} is replaced by the sum of all carbon containing products, according to Equation A.8,

$$S_C(i) = \frac{C_i \times F_i}{\sum C_i \times F_i} \tag{A.8}$$

and S_H can be found by $\frac{H_j}{F_{in}-F_{out}} \times \theta$, the ratio of H to C in the fuel, as described in Equation A.9

$$S_H(j) = \frac{H_j \times F_j}{\sum C_i \times F_i \times \theta} \tag{A.9}$$

- **Static Mixer** – A monolith upstream of the catalyst bed and separated by at least 1 cm, used to ensure gases are well mixed prior to contacting the catalyst. Also serves as a thermal bed to vaporize reactants.

- **Steam Reforming** (**SR**) – The endothermic reaction wherein water and fuel react to form H_2 and CO according to Equation A.10.

$$C_xH_yO_z + (x-z)H_2O \rightarrow xCO + (y/2 + x - z)H_2 \qquad \Delta H^o >> 0\frac{kJ}{mol} \tag{A.10}$$

- **Substrate** – The ceramic material coated with an active material, such as a noble metal, to form a catalyst. Typical substrates in this work are α-Al_2O_3 or mixtures of α-Al_2O_3 and SiO_2. Substrates may have a variety of geometries, such as spheres or foam monoliths.

- **Synthesis Gas** (**Syngas**) – A mixture of H_2 and CO resulting from partial oxidation. Can also contain other gases, such as N_2, CO_2 and CH_4, though clean syngas refers to just CO and H_2.

- **Washcoat** (**WC**) – A ceramic deposited onto a substrate used to add some property (eg, surface area, stability) to a catalyst. Typically an γ-Al_2O_3 or CeO_2 in this work.

- **Water-Gas Shift** (**WGS**) – The weakly exothermic reaction wherein water and CO react to form H_2 and CO_2 according to Equation A.11

$$CO + H_2O \rightarrow CO_2 + H_2 \qquad \Delta H^o \approx -40\frac{kJ}{mol} \tag{A.11}$$

A.2 Acronyms

Table A.1: Acronyms

Acronym	Meaning
ATR	Autothermal Reforming
bp	Boiling Point
C/O	Carbon to Oxygen ratio
CPO	Catalytic Partial Oxidation
EDS	Electron Dispersive Spectroscopy
fps	Frames per Second
GC	Gas Chromatograph
ΔH^o	Standard heat of reaction
HHV	Higher Heating Value
ID	Inside Diameter
MS	Mass Spectrometer
OD	Outside Diameter
PLA	Polylactic acid
POx	Partial Oxidation
ppi	Pores per linear inch
ppm	parts per million
RFV	Reactive Flash Volatilization
S/C	Steam to Carbon ratio
SEM	Scanning Electron Microscope
SLPM	Standard Liters per Minute
SR	Steam Reforming
Syngas	Synthesis Gas
TPD	Temperature Programmed Desorption

Continued on next page

Table A.1 – continued from previous page

Acronym	Meaning
WC	Washcoat
WGS	Water-gas shift
XRD	X-Ray Diffraction

Appendix B

Safety Protocol for the Time on Stream Apparatus

B.1 Summary

The operation of a continuous reactor requires the application of suitable materials for durable use under reaction conditions as well as a thorough safety analysis with fail-safe mechanisms and safety protocol. This Appendix documents the materials considerations and safety protocol developed for the glycerol time on stream experiment. It includes a series of worst-case scenarios detailing the safety backup system designed into the experiment.

B.2 Introduction

Safety must be considered for all laboratory experiments. Hazards, known and potential, must be thoroughly evaluated prior to launching a new project. For the glycerol time on stream test, a significant departure from previous experiments occurred in the that the reactor design called for an unmanned system. It is less safe to have an operator sleeping in the lab over the course of days and weeks than to properly establish safety protocol and monitoring systems.

In addition, maintaining a continuous reaction on a lab scale requires significant design. System gases must be replaced periodically without disruption to the reactor. Materials must be chosen to withstand reaction conditions over the entire duration of the experiment. As the experiment was not to dominate an entire work area, it must be isolated from other events, including,

for instance, fluctuations in power and mechanical disturbance from proximate experiments.

For these reasons, system design was carefully considered to promote safety and continuous, unmanned operation. Several safety analyses were conducted prior to the initiation of this experiment. Materials were chosen for their stability over time, and the entire system, including input gases, flow controls, reactor, effluent, and monitoring, were designed for optimal performance under every predictable scenario.

B.3 Materials Considerations

High temperature partial oxidation reactions subject materials to both oxidative and reducing environments at temperatures in excess of 800 ^{o}C. Mechanical failure of many materials typically used in such an environment is unacceptable for a prolonged study. For example, reactors are typically sealed with O-rings, and ports are sealed with NMR septa. While these materials can hold up for a period of hours for the duration of a day-long experiment, they are treated as consumables and frequently replaced. Furthermore, the failure of unstable polymers or metals does not only cause a leak, but may introduce impurities into the reactor system.

This reactor was sealed with Swagelok stainless steel fittings, capable of handling reaction temperatures and much higher pressures than subjected to the reactor. To seal the quartz reactor to Swagelok stainless steel fittings required a specially crafted quartz-stainless steel tube union, made by Larson Electronic Glass. The quartz end of the unions was fixed to the reactor by a professional glass blower.

Extreme care was administered in the connection of steel unions to the Swagelok part of the reactor fittings because quartz is much less resistant to the torque required to open and close such unions. To reduce stress on the reactor ports, 1/8" stainless steel inlet flow tubes were coiled several times to make them more flexible. Teflon tubing was used where acceptable, and the 1/4" exhaust tubing was connected via heated flexible tubing. This last was chosen to be metal because significant heating of the exhaust is required to keep products from condensing.

Noble metals are applied to ceramic foams or spheres via incipient wetness impregnation. Spheres were chosen in this case for two reasons. In the first place, spheres are more resistant to mechanical failure. A weakened strut in a foam can cause the foam to collapse (see Appendix C), whereas a weakened sphere in a sphere bed is merely compacted slightly. Second, small spheres can be introduced through the 1/4" tube at the top of the reactor, and can be taken

out through the same hole.

By contrast, 17 mm OD foams can only be introduced through the reactor bottom and must be pushed out from the top using a thin tube. The application of pressure with such a thin tube can frequently result in mechanical failure of the monolith. This is unacceptable for a catalyst. However, to support the catalyst bed requires a foam plug, and damaging this uncoated ceramic foam is not as problematic.

The backface heat shield, that is, the ceramic foam supporting the sphere bed within the reactor, is held in place by friction using a wrapping of ceramic paper. In a typical CPO reactor, this paper is composed of FiberFrax and shrinks slightly upon heating. As a result, catalysts frequently require less force to remove than to install. The weakening of the friction supporting the catalyst bed is unacceptable for an experiment that is to last any significant length of time. As a result, FiberFrax was replaced with the 3M product, Interam 100.

Thermocouples are typically used to measure point temperatures in reactor environments. Thin thermocouples have rapid response times but are also fragile and prone to mechanical failure after long term use. While single installation subjects them to less opportunity for mechanical failure, the particular nature in which thermocouples tend to fail - by reading a false temperature far outside of the acceptable limits of working conditions - renders this particular failure particularly noisome. Two thermocouples were used to monitor the backface temperature and initiate shutdown procedures. Both thermocouples had to read above or below a particular value in order to trigger the safety protocol; in this way, if one of the thermocouples malfunctioned, it would not shut down the reactor.

B.4 Regular Precaution and Typical Dangers

Aside from the specific dangers listed below, a series of conventional hazards requires standard precaution. This reactor system involves the following types of danger:

- Pressurized gases
- Toxic chemicals
- High amperage power consumption
- Mechanical pumps

- Hot vessels
- Open flame
- Combustible liquids and gases.

As such, proper safety gear should be warn when operating and especially when managing hardware in the system. Proper attire includes:

- safety glasses; goggles when opening gas lines
- nitrile gloves when working with conventional chemicals; rubber gloves for more potent chemicals
- lab coat and sleeves when working with chemicals
- flame retardant clothing when working with combustible liquids and gases
- thermal gloves for hot surfaces
- particular care for live electrical wires

B.5 Safety Mechanisms

Several system safety mechanisms have been implemented into the design of this system. They can be broken into two categories: software and hardware.

B.5.1 Software Safety

The Visual Interface (VI) written in LabView incorporates several safety mechanisms in addition to the normal gathering of data. Temperatures and pressure are recorded regularly to a separate file. Alarms triggered by several events result in the activation of a secondary record each time the alarm sounds. The alarms are established with the following parameters:

Temperature Range Six different thermocouples within a specified range.

Pressure Range Pressure measured above the catalyst bed must be within a specified range.

Mass Flow Controller Flow The actual monitored flow for each of five MFCs must be within a specified range.

Each of the alarms can be linked to a separate set of instructions. For example, oxygen flow rate through two MFCs is shut down upon the temperature exceeding a certain range on the thermocouples in the catalyst bed. Shut off events can be overridden but still trigger the alarm. In the event that oxygen is shut off, for instance, the low O_2 flowrate can trigger an alarm to alert the user.

Because the gases are metered at high and low pressure, alarms can detect when the cylinders are close to running out. The high pressure inlets decrease first as the pressure in the cylinder drops. If these flows are very small compared to the low pressure flows, high pressure inlets can serve as an advance alarm to alert the user of the need to open a new gas cylinder.

B.5.2 Hardware Safety

In addition to the above software protocols, the following describe the system design and its safety features.

Emergency Shut-off Valves All three gases (N_2, O_2 and CH_4) can be closed by a valve on the control panel.

Weak Point A silicone stopper at the base of the reactor allows for pressure relief to avoid accumulation of gases or destruction of the reactor.

Hood Vent The entire system is stored in a lab hood.

Air Circulation The hood is stored in a chemical lab equipped with a ventilation system.

Effluent Oxidation The effluent from the system is burned in a methane flame.

Carbon Monoxide Alarms Two CO detectors are stationed in the lab to alert users of any leaks.

Reactor Containment The quartz reactor is stored within a sturdy 1/8" aluminum box and packed with insulation.

Backup Battery Power A backup power supply allows the reactor to continue running in case of a power outage of up to 90 minutes.

B.6 Conceived Errors and Safety Scenarios

The following represent a series of possible events and the expected evolution of the scenario given the safety protocol in place.

B.6.1 Catalyst Deactivates: CPO Unsteady

In the case of unsteady catalysis, temperatures should vary as the oxidation zone fluctuates in the catalyst bed.

1. If the fluctuation is small, it should be observable in the temperature and pressure data available on the LabView interface or in the recorded file. The user can adjust conditions within the reactor using the VI.

2. If the fluctuation is within operating range but the oxidation zone has moved down the bed, it will be observable in the product sample as unreacted O_2. The user can adjust the conditions in the reactor using the VI.

3. If the fluctuation is large, it will cause the temperature measurements to exceed their boundaries. An alarm will sound and shut off the oxygen flow to the reactor. The reactor will cool; liquid glycerol, water, and N_2 will continue to cool the reactor.

B.6.2 Catalyst Deactivates: Catalyst Support Disintegrates

Should the spheres become crushed or otherwise impaired, or should impurity within the fuel accumulate within the catalyst, the pressure over the catalyst bed should increase.

1. Slight pressure increase may induce the user to modify the conditions of flow within the reactor by adjusting flowrates in the VI.

2. Sudden pressure increase may induce the user to shut down gases using the safety valves controlling flow.

3. If the pressure slowly increases to the point where it exceeds the pressure threshold of the transducer, an alarm will sound, the O_2 will be shut down and the reactor will cool. Moments later, N_2 will also shut down. Liquid glycerol and water will continue to accumulate in the reactor.

4. If the explosion causes temperatures or the pressure to exceed their limits, the alarm will sound. O_2 will be shut down by the VI; then N_2 will be shut down. Liquid will continue to flow. Further increase in pressure will cause the weak point to blow: the silicone stopper will pass out of the reactor and pressure will be relieved.

5. If the pressure increases exceedingly fast it is conceivable that the reactor ports can be ruptured. In this instance the reactor has been positioned to allow the ports to break laterally with respect to the hood.

B.6.3 Reactor Explosion

A potential problem with any CPO reactor is explosion. Explosions are typically caused by an excess of O_2 in the presence of volatile fuel. While glycerol and water are not highly volatile and thus not prone to explosions, the event is nonetheless possible.

1. An explosion within the reactor may be confined within the reactor itself with no damage to the surrounding system. If the temperatures and pressures do not exceed their limits, the reactor may stabilize and continue operation.

2. If a user is present, he may cut the O_2 using the VI or with the valve control to the O_2.

3. If the reactor temperatures or pressures exceed their limits, the O_2 will be shut down by the VI. An alarm will sound.

4. If the explosion results in a build up of pressure, the transducer may exceed its set value. An alarm will sound and the O_2 will be cut, followed by the N_2 after a short while. The liquid glycerol and water will still enter the reactor and cool it down.

5. If the explosion results in a high pressure, it may blow the silicone stopper out of the bottom of the reactor, relieving pressure. Exit gases will flow out of the bottom of the reactor. The methane flame will no longer be combusting the effluent. Effluent will be exhausted into the hood.

6. If the explosion is particularly violent, it may blow a port off of the reactor. The reactor has a lateral configuration to direct the ports away from the front of the hood. Effluent may not all be combusted by the methane flame. Some may exhaust into the hood.

7. If the explosion ruptures the reactor, the reactor is contained within a 1/8" aluminum box packed with soft insulation. Exhaust gas may flow into the aluminum box. The accumulation of syngas within the box represents a potential danger. However, the tight packing of the insulation restricts the quantity of gas that can accumulate, and the lack of electronics within the box reduce the hazard of an explosion. As a precaution, the box has been tested with a leaky reactor. Even in the presence of sparks and flames, no explosions have resulted.

B.6.4 Power Outage

The LabView VI, the process equipment, the vacuum of the hood, and the data acquisition system are all subject to the supply of electricity. In the past 5 years, approximately 5 power outages have occurred, usually lasting no more than 90 minutes. In one case, power was cut for much longer time. If the power is cut, the following protocol should protect the system and the user.

1. Power outage deactivates the hood. The reactor process equipment are on a backup uninterruptible power supply (UPS) which was calculated to last for 90 minutes. Effluent of the reactor is burned in the methane flame. No carbon monoxide is released into the room.

2. Power outage deactivates the hood and the methane flame is out. The reactor continues to operate for 90 minutes. Effluent is not burned in the flame and carbon monoxide is produced which can enter the room. Calculations show that the reactor should produce enough carbon monoxide to fill the room to 70 ppm of CO, within the tolerable limit. Two battery operated carbon monoxide detectors will alert the user of the situation.

3. Power stays off for more than 90 minutes. The methane flame is out. In this case, the backup power supply will be consumed. Electricity is not delivered to the MFCs or the pump; all immediately cease operation. The reactor slowly cools. Upon reestablishing power, the reactor remains shut off. If the carbon monoxide reaches a critical level, two battery operated detectors will warn users.

B.7 Catastrophic Failure

The following scenarios illustrate the required failures to result in a catastrophic failure, being defined as one that could result in potential danger to a user.

B.7.1 CO Poisoning

1. The electricity to the hood is cut.
2. The electricity to the reactor system remains intact.
3. The methane flame is extinguished.
4. The continuous flow of air through the room is arrested or slowed.
5. The batteries in the first carbon monoxide alarm require replacement.
6. The batteries in the second carbon monoxide alarm require replacement.

B.7.2 Dangerous Explosion

1. The reactor fractures.
2. The experiment continues without triggering any of the system alarms.
3. The insulation within the box is significantly reduced in volume due to extended use.
4. The aluminum box is structurally weakened.
5. A source of O_2 such as ambient air or flow from the reactor enters the box.
6. A flame or spark enters the box.

B.7.3 Chemical Hazard

1. The catalyst deactivates and does not fully oxidize the fuel.
2. Fuel is thermally converted to acrolein.
3. Acrolein accumulates in the exhaust line and in the reactor.

4. The user does not use proper safety precautions when maintaining the apparatus OR the hood deactivates and the carbon monoxide alarms do not function.

B.8 False Positive

A potential danger can occur when an alarm defectively triggers a shut-off event. To avoid false positives, two thermocouples are placed downstream of the catalyst bed. If these thermocouples simultaneously exceed 1200 ^{o}C, or if they both register below 300 ^{o}C, such that the reactor is no longer oxidizing fuel, the oxygen MFCs will be set to zero. If just one thermocouple triggers the alarm, the alarm is sounded and the user is notified, but no event occurs automatically. Only these thermocouples can shut down O_2 flow. All other thermocouple events trigger an alarm and alert the user.

B.9 Standard Operating Procedure

The following procedures should be used for this apparatus.

B.9.1 Fuel Maintenance

The catalytic partial oxidation of glycerol requires glycerol and water, the fuel, to be mixed in a ratio of 1 $mol_{glycerol}/2\ mol_{water}$. This corresponds to 71.878 wt% glycerol, 28.122 wt% water. Liquids should be mixed on a balance into a properly labeled container. The container should be shaken vigorously to induce mixing, and should be stirred with a magnetic stir bar for at least one hour. The mixed fuel is then added through a Buchner Funnel or proper filter to the fuel tank. The fuel tank should be checked on a regular basis to ensure sufficient supply. The fuel tank should be covered to avoid the introduction of dust or impurities into the system.

B.9.2 Gas Maintenance

Air is introduced into the system through four MFCs. To provide continuous supply, each process gas, N_2 and O_2, have two cylinders stored near the door to Amundson 436. These cylinders are connected in parallel to a single gas line. Each cylinder has a regulator with a needle valve. The needle valve and cylinder should both be closed on one cylinder, and both open on the other. When a gas cylinder is running low, the following should be performed:

1. Open the other gas cylinder. Ensure that there is gas in the cylinder.
2. If there is not gas in the cylinder, close it. Then swap out the cylinder. See below.
3. If there is gas in the cylinder, close the needle valve on the cylinder that is running low.
4. Open the needle valve on the fresh cylinder.
5. Close the cylinder that is running low. Replace it with a fresh cylinder. See below.

As per usual, cylinders should be changed in the following manner:

1. Ensure the needle valve is closed on the empty cylinder.
2. Ensure the valve on the cylinder itself is closed.
3. Using a properly sized wrench, take the regulator off of the cylinder.
4. Cap the empty cylinder.
5. Write "Empty" on the cylinder's information card.
6. Open the chain and remove the cylinder. Replace it with a fresh cylinder.
7. Rechain the cylinder storage area to secure them to the wall.
8. When the cylinder is ready to be removed to the shed, log it out on the clip board.
9. Open the cap on the fresh cylinder.
10. Gently rotate the cylinder into position with respect to the regulator.
11. Fix the regulator to the cylinder.
12. Open the cylinder valve.
13. Snoop the cylinder to check for leaks. Tighten if necessary.
14. If the cylinder is not to be used immediately, close the cylinder valve.

At reactor flowrates, Nitrogen cylinders last approximately 60 hours. Oxygen cylinders last approximately 9 days.

Appendix C

Deactivation Pictures

Photos of experimental apparatus reveal some of the mechanisms in which they are consumed. This sort of evidence can be crucial in determining how to improve materials for a given experiment - whether by construction or by initial materials selection. This appendix provides several photos of consumed CPO equipment.

One mechanism by which equipment can fail is through loss of mechanical stability. Figure C.1 depicts three catalysts that have lost rigidity. This disintegration has been observed previously (Chapter 4, [159, 64, 47]). The cause is as yet unknown, but is thought to be due to silica leaching from the support. These catalysts are still active, but due to support failures, cannot be easily loaded into the reactor or ensure as high tortuousity as they did when fresh.

Support loss can cause catalysts to be unuseful, though it is not necessarily a form of deactivation, which results in the catalyst losing chemical performance rather than mechanical performance. Catalyst deactivation is typically broken down into four categories: phase transformation, coking, poisoning, and sintering.

In a CPO reactor, coke deposition is rarely observed, despite being an equilibrium product, and despite high throughputs and short contact times. Bio oil, comprised of depolymerized lignocellulose, differs from model compounds in this regard. Whereas mild heat rates increase the partial pressure of model compounds, they are sufficient to dehydrate bio oil to coke. Figure C.2 depicts a bio oil reactor completely shut down due to coke accumulation.

However, the accumulation of coke in this image is upstream of the catalyst, where graphitic deposits are shiny. The catalyst itself is black, but not graphitic. Rh based catalysts are very difficult to coke: Rh is an excellent reforming and oxidation catalyst, so heat is typically sufficient

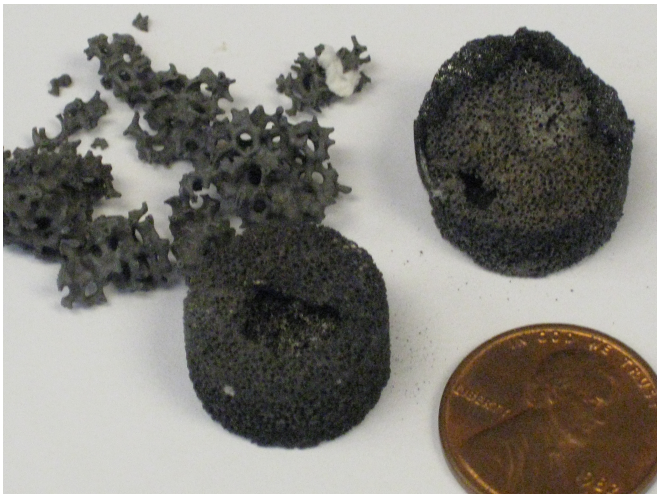

Figure C.1: Photo of monoliths which have lost mechanical stability. In this image, a 20 ppi catalyst has crumbled after use in the CPO of bio oils. Two 80 ppi catalysts are also shown with holes punched into the monoliths after CPO of bio oils. It has been observed previously that the CPO of oxygenated functional groups can result in catalyst disintegration (Chapter 4, [159, 64, 47]). The cause is as yet unknown, but is thought to be due to silica leaching from the support. Incidentally, the top right monolith also shows coke deposition - the black fringe at top - and slagging, the white patch near at the 2 o'clock position.

Figure C.2: Photo of a coked reactor after the CPO of 50-50 wt% poplar pyrolysis oil and methanol, which ran autothermally for a short while before shutting down due to coke formation. A finger is resting on the position where the catalyst bed is, and the difference in color may indicate that the catalyst is not as coked as the rest of the reactor.

to burn off coke or steam it off faster than it can accumulate. Coke is rarely observed on Rh, as it is in Figure C.3, a 20 ppi Rh catalyst used on the top of the bed for pyrolysis CPO with the addition of water (S/C = 3). However, due to the large pore size, homogeneous decomposition can apparently compete favorably with surface coke elimination, resulting in a net accumulation.

Figure C.3: Photo depicting a 20 ppi catalyst used for the CPO and reforming of pyrolysis oil. This catalyst was at the front of the bed and its pore size was too large for the noble metal to react this coke, which visibly accumulated in the pores. Water was added in this experiment in the amount S/C = 3.0, resulting in cooler temperatures that can promote coke deposition.

Water addition in this case has the effect of quenching the catalyst and absorbing the heat required to decoke the catalyst. By contrast, bio oil CPO can proceed under the same conditions without the addition of water. A used reactor is depicted in Figure C.4. This reactor was employed in the CPO of pine pyrolysis oil without any methanol stabilization. The reactor ran stably for the entire test and was found to be free of coke upon shutdown. The combination of heat, proximity of the nebulizer to the catalyst, and controlled air flow maintained a coke free environment.

Coke deposition can thus be controlled with reactor design and careful reaction conditions, but other deactivation mechanisms must be considered. Fly ash can be deposited over time and

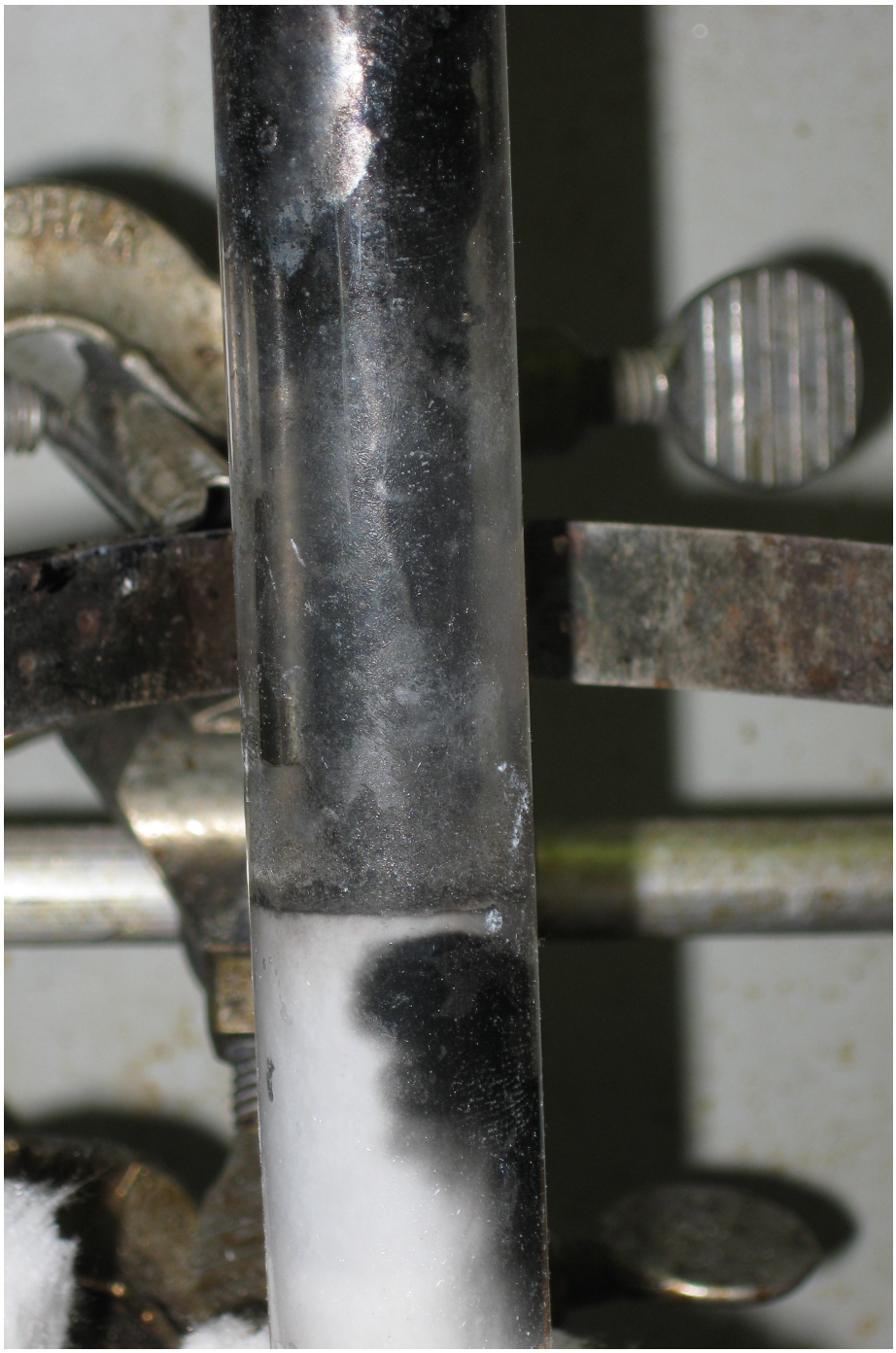

Figure C.4: Photo depicting the lack of carbon deposition near the inlets and catalyst. This reactor was used in the partial oxidation of pure pine pyrolysis oil assisted by a furnace. Coke is apparent far upstream of the catalyst at the top of the image, deposited by recirculation of pyrolysis oil aerosol. However, near the catalyst a 1/8" tube can clearly be distinguished, as can the 5/16" jacket of the water-cooled nebulizer.

accumulate on the catalyst (See Figure 7.5). This type of ash can be collected elsewhere in the reactor, as shown in Figure C.5. This indicates that reactor design such as fluidized beds or moving bed catalysts may be sufficient to avoid ash deposition.

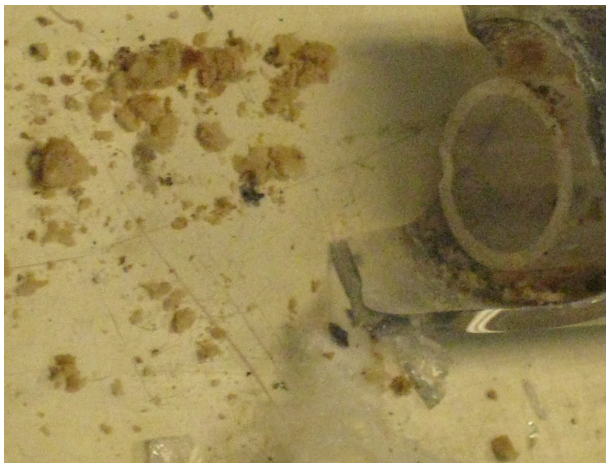

Figure C.5: Ash accumulation from pyrolysis oil is apparent in this reactor. The pyrex annulus is used to insulate the jacketed nebulizer from the hot furnace, shown here from the CPO of 50 wt% pine pyrolysis oil, 50 wt% methanol. All of this ash is upstream of the catalyst, suggesting that this type of ash accumulation can be eliminated with reactor design.

However, some ash accumulates on the catalyst specifically or, when accumulating, is difficult to eliminate. Slagging of impurities in a high temperature oxidation reactor is very likely. Figure C.6 depicts an image of a catalyst that has accumulated ash in the form of a glassy deposit. This catalyst was used in the CPO of a 50-50 wt% mix of poplar and methanol, and was the topmost catalyst in the bed.

Impurities can be derived from the fuel, in this case, bio oil, or from the reactor itself. In Figure C.7, a reactor is depicted after use for the CPO of pine pyrolysis oil and methanol in a 50-50 wt% solution. The reactor ran stably but, during coke burnoff in which air was introduced to the reactor in situ while a torch provided heat from outside, an unusually bright light indicated highly exothermic chemistry local to the torch. The FiberFrax appeared to "burn off" but was likely melted to form the glassy beads apparent on the side of the exposed catalyst bed. This glass may also be responsible for the bubbling on the reactor, which occurred simultaneously.

The bubbling on the reactor is reminiscent of the quartz etching observed in the time on

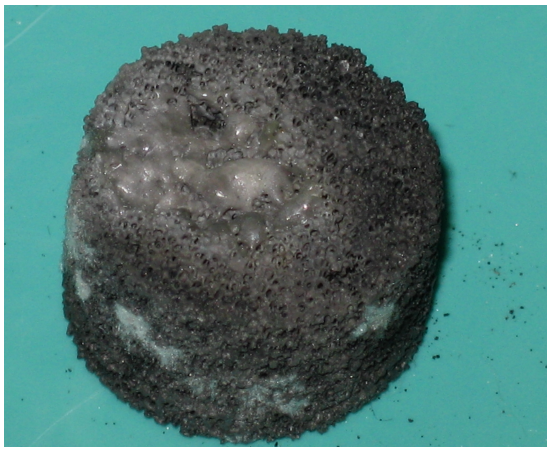

Figure C.6: Rh-Ce catalyst used in the CPO of 50 wt% poplar pyrolysis oil with methanol shows the deposition of a glass due to introduced impurities.

Figure C.7: Photo depicting a catalyst bed near its used reactor. The reactor, used for the CPO of 50 wt% pine pyrolysis oil, 50 wt% methanol, began leaking before breaking on disassembly. The catalyst is exposed where there should be FiberFrax ceramic paper; a similar shape is burned into the quartz reactor. The ceramic paper exothermically melted onto the catalyst, producing glassy bulbs appearing on the side of the exposed bed.

stream experiment with glycerol. A picture of this etching is shown in Figure C.8.

Figure C.8: Close-up of the quartz etching in the reactor from the 450 hour time on stream test of the RFV of glycerol. Red ash deposit is visible above the smoky bubbling of the reactor.

This etching may also have occurred in short exothermic bursts, coincident with the spontaneous thermal events described in Chapter 5. As such, the thermal events may have been due to exothermic chemistry related to the leaching of silica from quartz or the FiberFrax paper.